THE UNIVERSITY
of EDINBURGH

DECODING INFORMATION FROM NEURAL POPULATIONS IN THE VISUAL CORTEX

SCOTT C. LOWE

Doctor of Philosophy
School of Informatics
University of Edinburgh

2017

Scott C. Lowe:
Decoding information from neural populations in the visual cortex
Doctor of Philosophy, 2017

SUPERVISORS:
Prof. Mark van Rossum, University of Edinburgh
Prof. Stefano Panzeri, Istituto Italiano di Technologia
Prof. Alex Thiele, Newcastle University

DECLARATION

I declare that this thesis was composed by myself, that the work contained herein is my own except where explicitly stated otherwise in the text, and that this work has not been submitted for any other degree or professional qualification except as specified.

Edinburgh, 2017

Scott C. Lowe,
October 16, 2017

LAY SUMMARY

The most complicated system known to man is that of his own brain. It's often said that the human mind is the most powerful supercomputer on Earth, though this comparison can seem contrived as the two, brains and computers, clearly work in very different ways. However, brains are, fundamentally, systems which process information about the world experienced through the senses (sight, hearing, touch, taste, smell, and others besides) and do computations so that we can extract meaning from this data — distinguish the smell of a rose, tell the difference between a cat and a dog, recognise the face of a loved one. As we progress through the regions of the brain, moving from the parts directly connected to the sensory organs (eyes, ears, and so on), to the deeper recesses of the mind, representations within the brain become increasingly abstract. Eventually the information about the world, now processed by other parts of the brain to pick out the really important bits, reach the regions of the brain involved in planning and decision making.

Since brains are information processing systems, we can study them using the tools of information theory to try to better understand how they function. In this thesis, we study how the parts of the brain which process visual information work and allow us to see. When babies are born, their brains don't know how to handle the information from their eyes; they have to learn how to see. Even as an adult, you can train your brain to form better representations of the things that you see. If you repeatedly look at similar images and try to distinguish between them, you will get better with practice (though not forever — at some point your performance will stop improving). However, we don't know exactly what changes in the brain to enable you to do this.

We investigated this by tasking monkeys to distinguish between similar stimuli — one image but presented with many different contrasts — and recording the activity in their brains as they learnt to get better at this task. We found that the first part of the brain which processes vision (known as V_1) was already very good at encoding the differences between the stimuli. In fact, it was so good that it didn't need to get better than it was to begin with. Another part of the brain (known as V_4), which analyses more abstract properties of the shapes of visual stimuli, initially didn't distinguish between the contrast of the stimuli. But it got better with training, and the increase in information in this bit of the brain was the same as the increase in the performance of the monkey. This suggests that the parts of the monkey's brain which make the decision about how to respond to the stimulus have to use the information

in the latter part of the brain (V4) and don't get to use the information which is in the first part (V1). One hypothesis is that this happens because V1 only has lots of information about these stimuli due to a quirk related to them being different contrasts. Stimuli in the real world vary in more important ways, and identifying the contrast of what you're seeing doesn't really help you to tell the difference between a bear and tree if you're out in the woods. Only by training yourself on the task of contrast discrimination does your brain learn to focus on this, presumably less important, feature.

We then turned our attention to the oscillatory activity occurring in the part of the brain which first processes vision (V1). In the brain, the activity of neurons neighbouring each other within local regions fluctuate together in rhythmic harmony. Importantly, the activity of the population can oscillate at more than one frequency at once. To offer up an analogy, the neurons are like the players in an orchestra with violin, cello, and double bass sections. The instruments play simultaneously and the high frequency oscillations of the violin (the high pitched notes) sit on top of the medium and slower oscillations of the cello and double bass (both lower pitched notes). Except in the brain, every neuron can play multiple instruments at once. Since there are lots of neurons, you can only hear one of the notes when the activity of many of the neurons are synchronised for the same note, otherwise its all just random noise. The amplitude of these oscillations — how loud the different notes are — varies over time, and some of them are created by the neurons in response to the sensory input (i. e. whatever the individual is looking at).

We studied how the amplitudes of the oscillations were triggered by different properties of natural stimuli by showing monkeys a clip from a Hollywood movie and recording the activity in their primary visual cortex (V1). The outside of your brain, which includes V1, is made up of 6 layers stacked on top of each other, with each layer the thickness of a sheet of card. We worked out which of the layers and which of the frequencies of oscillations contained information about the movie. There are two different oscillations which encode information about the visual stimulus, and they correspond to different properties of the movie. In particular, the low frequency oscillations relate to sudden, coarse, changes in the movie, which occur whenever there is a scene transition or jump cut. This sort of change in stimulus is also like what happens when your eyes dart from one thing to another, so this signal may reflect how your brain copes with such sudden changes in visual stimulus. The higher frequency oscillations relate to the finer details in the movie, like the edges of objects moving around. Although the amplitude of the oscillations is, on average, the same in all the layers, only particular layers have oscillations which relate to the stimulus. If we return to our orchestra analogy, this is like splitting our bassists into groups and

observing that each group plays loudly and quietly some of the time. All the groups play loudly as often as each other, but only one of the groups plays loudly when the movie they are accompanying moves from one scene to another. Consequently, you can tell a when scene transition occurs just by listening to that group play together. We don't know what causes the other groups to play loudly (or quietly), but we do know it isn't systematically related to the movie they're accompanying.

ABSTRACT

Visual perception in mammals is made possible by the visual system and the visual cortex. However, precisely how visual information is coded in the brain and how training can improve this encoding is unclear.

The ability to see and process visual information is not an innate property of the visual cortex. Instead, it is learnt from exposure to visual stimuli. We first considered how visual perception is learnt, by studying the perceptual learning of contrast discrimination in macaques. We investigated how changes in population activity in the visual cortices V1 and V4 correlate with the changes in behavioural response during training on this task. Our results indicate that changes in the learnt neural and behavioural responses are directed toward optimising the performance on the training task, rather than a general improvement in perception of the presented stimulus type. We report that the most informative signal about the contrast of the stimulus within V1 and V4 is the transient stimulus-onset response in V1, 50 ms after the stimulus presentation begins. However, this signal does not become more informative with training, suggesting it is an innate and untrainable property of the system, on these timescales at least. Using a linear decoder to classify the stimulus based on the population activity, we find that information in the V4 population is closely related to the information available to the higher cortical regions involved with decision making, since the performance of the decoder is similar to the performance of the animal throughout training. These findings suggest that training the subject on this task directs V4 to improve its read out of contrast information contained in V1, and cortical regions responsible for decision making use this to improve the performance with training. The structure of noise correlations between the recorded neurons changes with training, but this does not appear to cause the increase in behavioural performance. Furthermore, our results suggest there is feedback of information about the stimulus into the visual cortex after 300 ms of stimulus presentation, which may be related to the high-level percept of the stimulus within the brain. After training on the task, but not before, information about the stimulus persists in the activity of both V1 and V4 at least 400 ms after the stimulus is removed.

In the second part, we explore how information is distributed across the anatomical layers of the visual cortex. Cortical oscillations in the local field potential (LFP) and current source density (CSD) within V1, driven by population-level activity, are known to contain information about visual stimulation. However the purpose of these oscil-

lations, the sites where they originate, and what properties of the stimulus is encoded within them is still unknown. By recording the LFP at multiple recording sites along the cortical depth of macaque V1 during presentation of a natural movie stimulus, we investigated the structure of visual information encoded in cortical oscillations. We found that despite a homogeneous distribution of the power of oscillations across the cortical depth, information was compartmentalised into the oscillations of the 4 Hz to 16 Hz range at the granular (G, layer 4) depths and the 60 Hz to 170 Hz range at the supragranular (SG, layers 1–3) depths, the latter of which is redundant with the population-level firing rate. These two frequency ranges contain independent information about the stimulus, which we identify as related to two spatiotemporal aspects of the visual stimulus. Oscillations in the visual cortex with frequencies $<$40 Hz contain information about fast changes in low spatial frequency. Frequencies $>$40 Hz and multi-unit firing rates contain information about properties of the stimulus related to changes, both slow and fast, at finer-grained spatial scales. The spatiotemporal domains encoded in each are complementary. In particular, both the power and phase of oscillations in the 7 Hz to 20 Hz range contain information about scene transitions in the presented movie stimulus. Such changes in the stimulus are similar to saccades in natural behaviour, and this may be indicative of predictive coding within the cortex.

ACKNOWLEDGEMENTS

There are many people who have helped me on this journey and it would be remiss to deny this opportunity to thank each of them.

First and foremost, thank you to both Mark van Rossum and Stefano Panzeri, for their advice and supervision throughout all the work described in this thesis. I surely could not have done this without either of you.

My thanks also go to Alex Thiele, for his advice concerning my work on perceptual learning (described in Chapter 2). On that note, thank you to Xing Chen, for collecting the electrophysiological data described in Chapter 2 and, along with Mehdi Sanayei, for helping me to understand it.

Next, thank you to Daniel Zaldivar and Yusuke Murayama, for collecting the electrophysiological data, described in Chapters 3 and 4, and for helping me to understand it. Thank you to Nikos Logothetis, for supervising the collection of this data and enabling the access of resources at the Max Planck Institute. Also, thank you to Cesare Magri, for laying the foundations for the analysis described in Chapter 3.

To everybody at the University of Edinburgh's Neuroinformatics Doctoral Training Centre, thank you for being such an all-round great community. There are many of you for whom I have the honourable privilege of calling friends, and I am sure this will not be the last we see of each other.

And finally, last but not certainly not least, thank you to my parents and my sister for offering their continual support and encouragement throughout the last few years, before that, and beyond.

CONTENTS

INITIALISMS AND ABBREVIATIONS

2AFC	two-alternative forced-choice
ACh	acetylcholine
AUROC	area under receiver operating characteristic (ROC) curve
BOLD	blood oxygen-level dependent contrast imaging
CI	confidence interval
cpd	cycles per degree
CRT	cathode ray tube
CSD	current source density
dva	degrees of visual angle
EEG	electroencephalography
FFT	fast Fourier transform
FIR	finite impulse response filter
G	granular compartment of V1, equivalent to L4
IG	infragranular compartment of V1, equivalent to L5/6
IIR	infinite impulse response filter
IT	inferior temporal cortex (Brodmann's Areas 20 and 21)
KL	Kullback-Leibler divergence
L	long ("red") cone
L1	layer 1 of V1
L2/3	layer 2/3 of V1
L4	layer 4 of V1, equivalent to G
L4Cα	layer 4Cα of V1
L4Cβ	layer 4Cβ of V1

L5	layer 5 of V1
L5A	layer 5A of V1
L5B	layer 5B of V1
L5/6	layers 5 and 6 of V1, equivalent to IG
L6	layer 6 of V1
LFP	local field potential
LGN	lateral geniculate nucleus
M	medium ("green") cone
M1	monkey 1
M2	monkey 2
MEA	multi-electrode array
MSTd	dorsal medial superior temporal area
MT	middle temporal cortex, also known as V5
MUA	multi-unit activity
NaCl	sodium chloride
NH	null hypothesis
NSB	Nemenman-Shafee-Bialek entropy estimation method
PFC	prefrontal cortex
PSTH	peristimulus time histogram
PT	Panzeri-Treves bias correction method
QE	Quadratic Extrapolation bias correction method
R	rod cell
RF	receptive field
RGC	retinal ganglion cell
ROC	receiver operating characteristic
S	short ("blue") cone

SG	supragranular compartment of V1, equivalent to L1 and L2/3
SNR	signal-to-noise ratio
V1	primary visual cortex (Brodmann's Area 17)
V2	visual area 2 (Brodmann's Area 18)
V3	visual area 3
V4	visual area 4
V5	visual area 5, also known as middle temporal cortex (MT)
V6	visual area 6, also known as dorsomedial area

1 INTRODUCTION

In this chapter, we present background information which the reader is required to know in order to understand the original research material which follows in the remainder of the thesis. Here, we will introduce and discuss the fundamental properties of the mammalian visual system, information theory, and neuronal correlations.

1.1 NEURONS AND THE BRAIN

The central nervous system consists of the brain, spinal cord, and retina. Within each, there are specialised biological cells called **neurons**, whose properties allow them to encode information about the external world gleamed through the body's sensory organs, manipulate this information and perform computations with it in order to control the behaviour of the body.[1] The peripheral nervous system and the retina together provide a stream of data about the environment within which the subject resides, known as the **senses** (sight, sound, touch, smell, taste, temperature, pressure, *etc.*). The computations performed by the central nervous system allow it to extract features from this stream of sensory information, store properties of it for later computational use, and decide which behavioural actions to perform in order to move its body and influence the environment within which it resides (arguably the only important function of a brain; Wolpert, 2011).

Information transmission between neurons is principally mediated by changes in the voltage, or potential difference, between the inside and the outside of the neuron (Purves et al., 2008, Chapter 2). A change in this membrane potential within one neuron will propagate along its cell body, and in doing so will affect other neurons which make direct conductive connections with it. However, the majority of connections between neurons are indirect, involving a synaptic junction in which chemicals, referred to as neurotransmitters, are released by one neuron and sensed by another where it induces an electrochemical change.

In order to be able to transmit electrical signals over long distances (longer than 1 mm), neurons digitise their information as **action potentials**. At rest, the membrane potential of a neuron is typically negative, around $-70\,\mathrm{mV}$. For an action potential to

1 Neurons are common across all species of animals, though the architecture of their nervous systems vary greatly. Plants are also able to infer properties of their environment and respond accordingly using chemical and electrical signals, despite their lack of neurons (Barlow, 2008; Brenner et al., 2006).

be elicited by a neuron, its membrane potential must depolarise, becoming less negative. Once the membrane voltage passes above a certain threshold (typically around $-55\,\text{mV}$, but the specific value depends on the neuron in question) a temporary change occurs in the dynamics of the ion channels which allow ionised chemicals to pass between the inside and outside of the cell. Sodium ions suddenly flow into the neuron, then potassium ions flow out just as suddenly, causing the membrane potential to rapidly increase to around $+40\,\text{mV}$ and then fall back to a voltage a little below its value at rest. The sharp rise and fall of the voltage across the membrane is known as an action potential, or *spike*, and has a duration of only around 1 ms to 2 ms (Dayan and Abbott, 2001, Chapter 1). Following a spike, there is a recovery period (refractory period) of another few milliseconds during which further spikes cannot be elicited; following this the system is returned to its original resting state.

We can consider an occurrence of action potential event to be the output of a neuron. Aided by an insulating covering of myelin and repeating stations (known as Nodes of Ranvier), an action potential can travel along its **axon** for long distances.[2] At the terminus of the axon, synaptic connections are formed with the dendrites of other neurons. Upon the arrival of an action potential at the synapse, neurotransmitters are released which can either increase or decrease the membrane potential of the recipient neuron.

Learning occurs principally by the strengthening and weakening of these synaptic connections between neurons such that more or fewer neurotransmitters are transferred into the recipient upon the arrival of a single action potential (Dayan and Abbott, 2001, Chapter 8; Purves et al., 2008, Chapter 23).

1.2 MAMMALIAN VISUAL SYSTEM

Sensitivity to the visual spectrum is an important survival trait for almost all land animals. Whether predator or prey, the ability to see allows an individual organism to receive and perceive information about their environment over large distances. Such a trait has obvious survival implications, and therefore confers an evolutionary advantage.

Across all mammals, the visual system is composed of several processing stages, illustrated in Figure 1.1. Light enters the eye (if possible, focused into a clear image by the lens), and is encoded as electrical signals in the retina at the back of the eye. This information is transmitted to the brain through the optic nerve, where it

2 The longest axon in the human body is the that of the dorsal root ganglion, which extends from the big toe to the primary sensory cortex in the brain. The equivalent nerve in the blue whale can have an uninterrupted axon 25 m in length (Smith, 2009; Voytek, 2012).

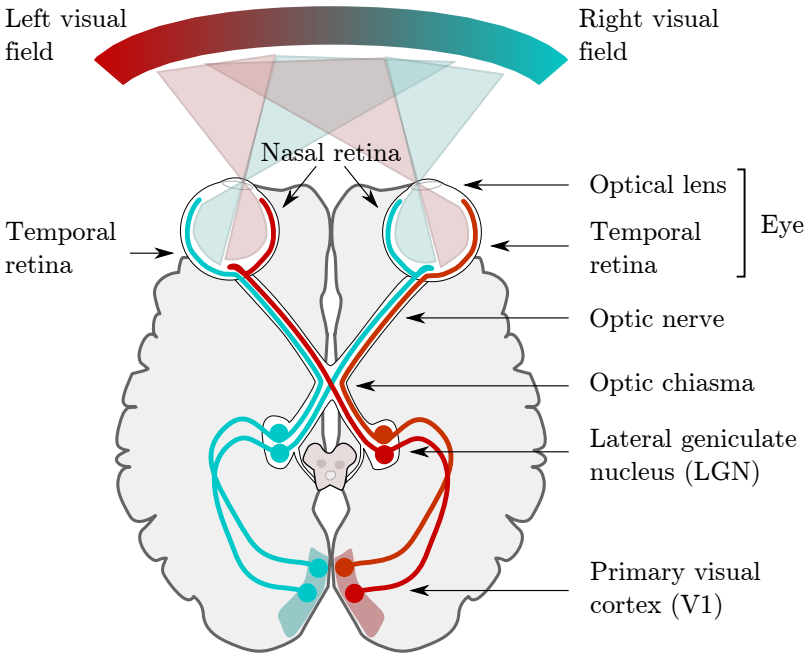

FIGURE 1.1. *Human visual pathway.* Visual information enters the eye, is encoded in the retina and progresses to the visual cortex, via the LGN. Reproduced (with modifications) from Wikimedia Commons under the CC BY-SA 4.0 license.

reaches the LGN. From here, the visual information is propagated to the primary visual cortex (V1), which feeds its outputs to the rest of the visual (and non-visual) cortical regions. For humans and other primates, vision is our dominant sense, and a large fraction of our brains (sometimes estimated as around half the brain, excluding the cerebellum) is devoted to processing visual information.

1.2.1 *The eye*

The story of visual perception begins with the eye. Eyes have evolved multiple times throughout the history of life on Earth. Noting that other animals have eyes which are structured differently, in this section we describe the properties of the eye as they are for humans and other mammals.

1.2.1.1 *Rods and cones*

For any visual system, the most fundamental component is a set of cells which are sensitive to electromagnetic radiation. In mammals the light-sensitive cells, or *photoreceptors*, come in two types: **rods** and **cones** (Purves et al., 2008, Chapter 11).[3] Rods and

3 There are also intrinsically photosensitive retinal ganglion cells, however these cells are not directly involved in forming an image of the visual stimulus. Instead, they mediate the circadian rhythm, and influence pupil dilation (Berson et al., 2002; Ecker et al., 2010; Wong et al., 2005).

cones are subtypes of neurons which contain photosensitive proteins, rhodopsin and photopsin, respectively. When photons of light collide with a photopigment protein, it changes state and shape, causing a cascade of biochemical changes resulting in the closing of ion channels in the cell membrane of the neuron. Since the energy in the photon[4] (which is indivisibly quantised) must closely match the difference in energy levels of the photopigment, each photopigment is only sensitive to a particular range of wavelengths of light. The spectral absorption curves for photopigments used in the rods and cones of humans are shown in Figure 1.2.

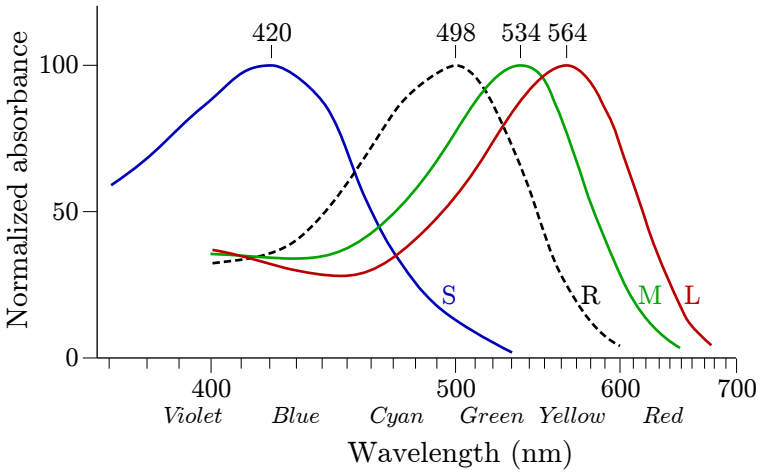

FIGURE 1.2. *Spectral absorption curves for pigments found in cone and rod cells.* The normalised response curves for rods (R) and long (L), medium (M), and short (S) cones typical of humans with normal colour vision. Note the x-axis scales linearly with frequency, and hence is non-linear with respect to wavelength. Beneath, the common names of the visible colours are indicated at their respective frequencies. Reproduced (with modifications) from Wikimedia Commons under the CC BY-SA 3.0 license, showing data appearing in Bowmaker and Dartnall (1980).

Rod photoreceptor cells are very sensitive to light, making them ideal for seeing in dark and low-lighting conditions. However, in well-lit scenes, rods quickly become saturated, at which point they offer no information about the external world other than the fact that it is "quite bright right now".

Cone photoreceptors come in several different types, each using a different photopigment to detect different ranges of the electromagnetic spectrum. In humans, there are three types[5] of cones: long, medium, and short (L, M, and S) cones. These can be approximately considered sensitive to red, green, and blue light respectively — however, it should be noted that there is a broad range of wavelengths which each

4 The amount of energy within a photon is related to its wavelength according to the Planck–Einstein relation, $E = hf$, where E denotes the energy of a photon, f, the frequency associated with it, and h is Planck's constant.

5 With the exception of colour-blind individuals, who may have only two or fewer types of cones, and tetrachromats (Jameson et al., 2001; Jordan and Mollon, 1993; Nagy et al., 1981) who have four.

is sensitive to (see Figure 1.2), and this range is very similar for the L and M cells. Possessing three cones makes humans (along with other apes and Old World monkeys) the exception instead of the norm within the mammal class — most mammals, including cats, dogs, and the New World monkeys, are dichromatic with only two types of cones (M and S).

The presence of photoreceptors with different spectral sensitivities enables *colour vision*. When light of a given frequency meets the retina, we can compare the relative responses of the different types of cone to determine which frequency it was. From the absolute intensity of the responses, we can determine the intensity or brightness of the light.

The distribution of rods and cones within the eye is not uniform. Across most of the eye, the density of rods is twenty times higher than that of cones; however, there is a small region of 1.2 mm diameter, called the **fovea**, within which the cone density is 200 times higher (Purves et al., 2008, Chapter 11). The extremely high cone density within the fovea, which covers the central 5° of the visual field, provides this part of the retina with the highest visual acuity. To preserve the high resolution of foveal vision, in this small part of the retina there is a one-to-one mapping from cones to bipolar cells, and 3 to 4 times more ganglion cells than cones (Wässle et al., 1990).

The very highest level of visual acuity is in the foveola — the central part of the fovea where the cone density is greatest — which covers eccentricities less than 0.5° from the line-of-sight (Hendrickson, 2005). Surrounding the fovea, is the parafovea which includes eccentricities from 2.5° to 4°. This, in turn, is encomposed by the perifovea, extending out to 9° of eccentricity. The rest of the visual field is referred to as peripheral, and has coarser acuity. Visual acuity decreases greatly away from the fovea; with an eccentricity of just 6° from the line of sight, acuity falls to 25 % of its peak (Purves et al., 2008, Chapter 11). Consequently, humans move their eyes (and heads) frequently to ensure they can see the subject of their attention as clearly as possible even as their attention shifts between subjects.

Throughout the rest of the eye, the high density of rods ensures that the few photons which are present in low-lighting conditions have as a high chance of meeting a rod cell as possible. Even so, only 10 % of the photons which reach the eye are absorbed by a rod (Hecht et al., 1942).

The ratio of the three types of cones is also neither balanced nor homogeneous across the surface of the retina. Although the proportion of M and L cones are roughly equal, S cones constitute only 5 % to 10 % of the total, and even less within the fovea (Purves et al., 2008, Chapter 11). This provides humans with excellent ability to distinguish between shades of red, orange, yellow, and green, and is thought to have

been evolutionarily selected for in order to enhance the ability to spot fruit in bushes (Bompas et al., 2013).

1.2.1.2 *Retinal processing*

Since there are about 130 million photoreceptors in the human eye, but only 1.5 million axons which send information from the retina to the brain (Nassi and Callaway, 2009), the information collected from the photoreceptors must be compressed. This compression is lossy, but the processing performed in the retina allows the important properties of natural stimuli to be preserved and unimportant properties discarded. The important feature of natural stimuli which must be preserved is the spatial variations in luminance (Purves et al., 2008, Chapter 11). Indeed this is the reason why there are so many photoreceptors in the first place — to capture spatial changes at high resolution. One unimportant feature of the stimuli is the absolute intensity of the light; consequently the output from the retina to the brain is local spatial contrast and how this varies over time. Furthermore, the colour of stimuli tends to vary coarsely within stimuli, and so this is downsampled. There is also decorrelation of the output from the retina, reducing the redundancy in the information sent to the brain.

This functionality is achieved by the circuitry within the retina. In particular, **bipolar cells** connect to the rods and cones and filter their outputs, with some bipolar cells inverting the output of the photoreceptors. **Retinal ganglion cells** (RGCs) connect to a group of these bipolar cells, connected such that each RGC has a small, localised, circular receptive field (RF) to which it is sensitive. Each RGC is wired such that they are sensitive to the difference in intensity between the centre of their RF and the rest of the RF. Consequently there are two complementary flavours of RGCs. The first responds strongly when the centre of the RF is more illuminated than the surrounding (an **on-centre** ganglion), and the second responds strongly when the surrounding is more illuminated than the centre (an **off-centre** ganglion). The axons of the RGCs constitute the optic nerve, and their outputs are the source of visual information received by the brain.

Invariance to the changes in absolute illumination is produced partly by the centre-surround selectivity of the RGCs, and partly by **horizontal cells**. Horizontal cells receive inputs both from several cones and from other horizontal cells, such that each has a wide RF and represents the average illumination over a large area (Purves et al., 2008, Chapter 11). The output of horizontal cells is fed back to the cones, suppressing their changes in activity driven by illumination. In doing so, horizontal cells effectively subtract from each cone the average activity of all neighbouring cones, providing light adaptation.

There are known to be many types of RGCs (at least 17), most of which are not well studied and poorly understood, but the three most common types are well characterised and constitute around 88 % of all the RGCs (Nassi and Callaway, 2009).

Midget ganglion cells have small receptive fields with low contrast sensitivity and consequently sensitivity to high spatial and low temporal frequencies (Nassi and Callaway, 2009). They are red-green colour opponent, with either an M or L cone in the centre and a mixture of M and L cones surrounding it. Approximately 70 % of retinal cells which project to the LGN are midget cells, making them by far the most common class of RGCs.

Parasol ganglion cells have larger receptive fields, resulting in higher contrast sensitivity which is achromatic, and a preference for high temporal, low spatial frequencies (Nassi and Callaway, 2009). The axon conductivities for parasol ganglion cells are higher than those of midget ganglions, and output of the parasols provides the first visual response within the visual cortex.

The third most common RGC type is the bistratified ganglion cells, which convey blue-on yellow-off colour-opponent signals.

1.2.2 *The lateral geniculate nucleus*

The optic nerve sends visual information from the retina to the lateral geniculate nucleus (LGN). The LGN is banded, with layers of cells of several types, as illustrated in Figure 1.3.

The outputs of midget RGCs are directed to parvocellular layers in the LGN, which is then directed to layer 4Cβ within V1 (L4Cβ). Because the signal passes through the parvocellular layers, this is known as the P-pathway. Parasol RGCs target the magnocellular LGN layers, which subsequently target L4Cα of V1 (the M-pathway). Bistratified RGCs project to the koniocellular layers of LGN, which then target cytochrome oxidase-expressing patches (blob cells) in layer 2/3 of V1 (L2/3; the K-pathway).

The tuning properties of LGN cells are very similar to RGCs. Each of these three streams progresses simultaneously and in parallel, conveying different information about the stimulus but sampling from the same spatial locations within the visual field.

1.2.3 *The primary visual cortex*

The primary visual cortex (V1) is constituted of several **layers** stacked on top of each other, with total thickness around 2 mm in primates. Each of these layers contains a different distribution of the many types of cortical neurons, and each layer has

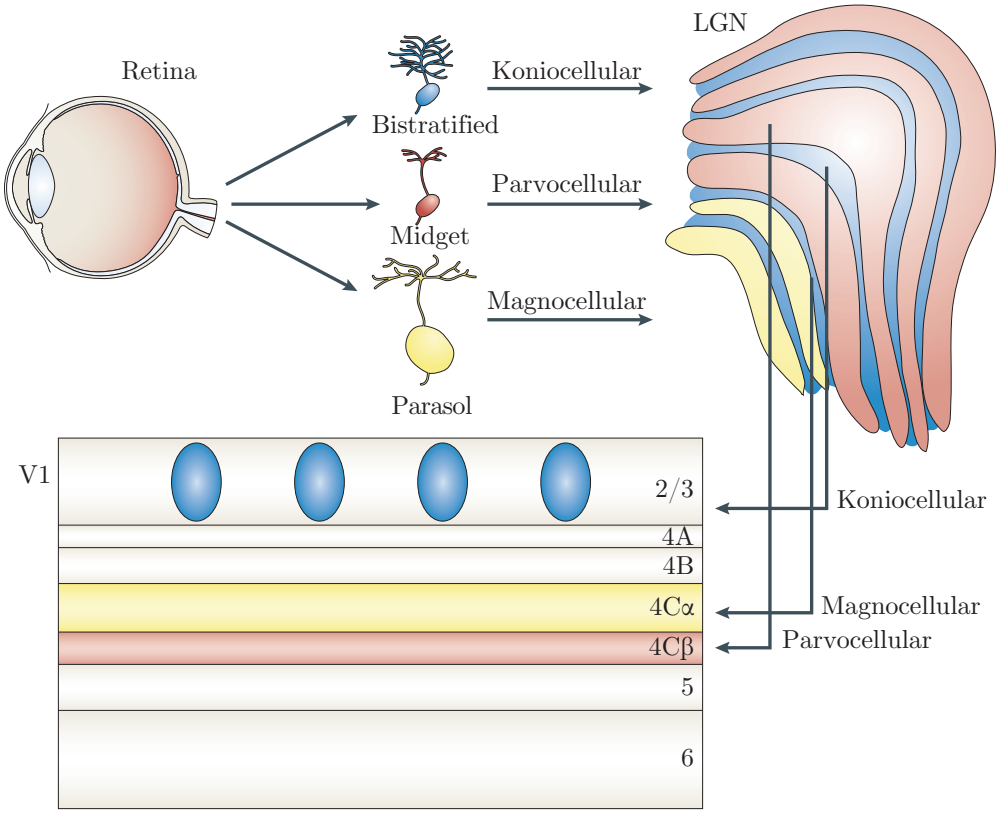

FIGURE 1.3. *Parallel pathways from the retina to the cortex.* Midget (red), parasol (yellow), and bistratified (blue) ganglion cells are well characterized and have been linked to parallel pathways that remain anatomically separate through the LGN and into the V1. Although these ganglion cell types are numerically dominant in the retina, many more types are known to exist and are likely to provide other important pathways yet to be identified. Adapted by permission from Macmillan Publishers Ltd: *Nature Reviews Neuroscience* (Nassi and Callaway, 2009), copyright 2009.

inputs and outputs directed to different brain regions (Harris and Mrsic-Flogel, 2013). Classically, we refer to 6 anatomically-defined layers which together make up V1 — however as knowledge about the cortical structure has increased, these have been subdivided further.

Fixing our location within the cortical plane and examining the properties of neurons as we move along the cortical depth reveals that these neurons have the same visual RF (Hubel and Wiesel, 1962; Hubel and Wiesel, 1963), and this extends for a planar radius of around 500 µm (Mountcastle, 1997). Furthermore, the neurons within a cylindrical column of the cortex preferentially to oriented edges with the same angle (Hubel and Wiesel, 1962). The structure of the cortex (the constitution of each of the 6 layers) is similar across all its planar surface (not just within the confines of area V1), suggesting there is a fundamental columnar processing unit which is replicated across the surface of the cortex (Binzegger et al., 2009; Douglas and Martin, 1991, 2004; Douglas et al., 1989; Mountcastle, 1957). It has been hypothesised that the circuitry of the cortical column has structural and functional similarities across all sensory modalities, serving as a generic cortical processing unit.

Cortical columns (and their constituent neurons) within V1 have been observed to be tuned to bars or edges with specific spatial frequency, orientation, direction of motion, and colour. Neighbouring cortical columns compete with each other due to the horizontal inhibition within L2/3 of V1. As a consequence, topological maps self-organise across the surface of V1, together providing an efficient representation of the space of stimuli native to the individual's sensory environment (Miikkulainen et al., 2005; Stevens et al., 2013; Wilson and Bednar, 2015). As we traverse the cortical plane, neurons change in RF location, preferred orientation, and spatial frequency, such that there is good coverage over the full distribution of possible stimuli.

However, it should be noted that the rate of change of RF location is not constant as we traverse across the surface of V1. The very high density of cones within the fovea, and the one-to-one correspondence of cones to RGCs exclusively within the fovea, result in a disproportionately high fraction of the visual information reaching V1 originating at the fovea.[6] Correspondingly, a larger fraction of cortical computation is expended on this region of the visual field, and the amount of cortical material devoted to processing foveal stimuli is higher than that devoted to peripheral stimuli. The relationship between the eccentricity of an area within the visual field and the area within the visual cortex which is sensitive to this space is referred to as **cortical magnification**. The amount of cortical magnification of the visual field is inversely proportional to the eccentricity from the foveola (Strasburger et al., 2011).

6 Approximately half the fibres in the optic nerve carry information from the fovea, despite the fact it only covers 0.1 % of the eye's total field of view.

1.2.4 *The rest of the visual cortex*

From V1, the flow of visual information within the brain forks, progressing down two parallel streams (Goodale and Milner, 1992; Mishkin and Ungerleider, 1982). Beginning with V1 and visual area 2 (V2), the dorsal stream progresses to visual area 5 (V5) and visual area 6 (V6). Brain regions within this stream are involved in spatial attention. They communicate with other regions which control eye movements and hand movements, and hence it is nicknamed the "where" pathway.

The ventral stream also begins with V1 and V2, but then progresses to V4 and the inferior temporal cortex (IT). Involved in the recognition, identification, and categorization of visual stimuli, it is referred to as the "what" pathway. Whilst V1 responds strongly to oriented bars, neurons in V2 and V4 have been found to respond to increasingly more abstract shapes. At the higher end of the visual stream, IT contains cells which have been identified to respond to high-level objects, such as faces.

These visual cortical regions are connected to other cortical regions higher up the cortical processing hierarchy. Some of these are associative cortical regions, which integrate information across different sensory modalities. The visual and associative cortices are also connected to regions related to planning and decision making, such as the prefrontal cortex (PFC).

1.3 Information theory, and its applications within neuroscience

A common experimental methodology used in neuroscience is to record the extracellular activity of individual neurons under different conditions. From this, we can compare the activity of the neuron under different conditions to examine whether it is dependent on this set of conditions, and if so investigate the nature of the relationship between the two.

Frequently, the approach used is to take many recordings of the same neuron for the same condition, and then take the average across these repetitions (*trials*) to reduce the effects of neuronal variability, producing a peristimulus time histogram (PSTH), for instance. This neuronal variability is often referred to as *noise*, however it is debatable as to whether differences in the behaviour of individual neurons between trials are due to noise within the system or are in fact due to non-stationarity within the system due to changes in neural state or unknown latent variables within the system (see Section 1.4.2 for further discussion).

Such a simple treatment of the data — averaging the response over repetitions — is fundamentally flawed, since this is not the manner in which brains process stimuli. At any moment in time, the brain has access to the activity of many neurons

simultaneously (not a single neuron in isolation), but only has a single sample of each one (not multiple instantiations of the same neuron).

If we instead use information theory to study the neuronal activity, we can consider how much information there is across a system containing multiple neurons during an isolated period of time, for instance a single trial. By using an information theoretic technique, we can overcome the limitations of the more simple methods; but no method is perfect and there are other limitations which arise when using information theory instead. In this section, I will first outline the analytic procedure through which information theoretic analysis is applied to neuroscientific data, some of the problems which arise, and how to try to overcome them.

1.3.1 *Neuroscientific context*

In the context of trying to experimentally investigate properties of the sensory cortex of the brain, one typically uses an experimental set-up with a finite collection of discrete experimental stimuli. These stimuli are then repeatedly presented to the sensory organ in an appropriate fashion, and the responses during each presentation are recorded.

For such an experimental set-up, let us assume that on each trial some stimulus s is selected at random, with probability $p(s)$, from a set of discrete stimuli $\mathbf{S}$. The random variable S denotes this selection of a stimulus, with some arbitrary probability distribution across the elements of $\mathbf{S}$. Even if our stimuli come from a continuous stimulus space, parametrically varying in orientation or frequency, say, it is important to discretise this down to a finite subset of stimuli from which samples will be drawn. This is because we must estimate either $p(s, r)$, $p(r|s)$, or $p(s|r)$ from the data for each stimulus s and response r in order to compute the mutual information, which is only possible if we have at least one presentation of every stimulus within our collection of stimuli.

The neuronal response could be one (or more than one) of several data types, such as a spike train from one or more neurons, the local field potential (LFP), current source density (CSD), blood oxygen-level dependent (BOLD) signal, a calcium indicator, electroencephalography (EEG), or others (Magri et al., 2009; Quiroga and Panzeri, 2009). The principles of information theory can be applied whichever neural signal recorded from and taken to be a measure of the neural response. In Chapter 2, we will work with information encoded in multi-unit activity (MUA) and spike trains, whilst in Chapters 3 and 4 we will be considering the LFP and CSD.

With regards to the analysis of sensory recordings (with which this thesis will be concerned), the different conditions used on the trial are typically different stimuli,

and the extracellular recordings provide us with the neuron's response to the stimuli. When applying information theory to neuronal data, we treat the brain as a communication channel, transmitting information about sensory input. We are hence interested in how much information the response in the brain contains about which stimulus was presented to it.

However, it should be noted that we frame the problem in the context of a **communication channel** simply because this is the framework around which Shannon information is formulated (MacKay, 2003, Chapter 2). Within information theory, systems are modelled with information passing between a transmitter and receiver through a communication channel. The message passing between them is modified as it passes through the channel, and the receiver must attempt to decipher which message was originally sent.

In some ways, some functions of the brain are similar to the process of a compression algorithm. The initial encoding of the stimulus as transcribed by the appropriate sensory organ contains a large amount of information about the precise input stimulus — for example the individual pixel values with an image stimulus — which has a large amount of redundancy if one is interested only in detecting, classifying, and reacting to stimuli. A binary image of only 17×17 pixels can express 9.9×10^{86} different states — a value ten million times larger than the number of atoms in the visible universe, thought to be around 10^{80}. However the vast majority of these images (for this, and equally true for a larger image with more intensity levels and colours) resemble unstructured random noise. The set of images which are of interest for interacting with a real world environment is vastly smaller; with an appropriate high-level statistical model, the subset of stimuli which are of interest can be compressed down to a much smaller number of bytes. For instance, we can take large image and compress this down to a binary value indicating whether this visual stimulus contains the face of familiar person.

After a stimulus has been processed by the brain, information about the exact intensities of individual pixels is lost, but salient information about the environment is preserved. We can hence investigate how stimuli are encoded within the brain by considering certain properties of the stimulus and computing the amount of information about them which is contained within the neural recordings. Here, we make the following assumption: if the neuronal activity is observed to contain information about the stimulus, we can assume this information is present due to the manner within which information is encoded by the brain, and that this information can be drawn upon to inform decisions taken with regard to the stimulus. We rationalise this assumption on the basis that we know the brain contains information about stimuli (otherwise it would be functionally blind/deaf), and it would be wasteful to expend

resources encoding stimuli accurately but in a non-functional manner. Such waste would run contrary to the evolutionary pressures for energy efficiency within the neuronal architecture (Laughlin, 2001; Niven and Laughlin, 2008).

The neural data which can be collected with modern experimental equipment is very dense and rich in content. For instance, individual spikes can be recorded with the precision of fraction of a millisecond, and broadband LFPs allow for many frequency components to be analysed from the same recording. Typically, it is not possible to compute the information about the stimulus contained in the entire data stream all at once when such a large quantity of neural activity is recorded simultaneously. This is because our analysis is limited by the relatively small number of trials which can be collected for any given dataset.

In order to study information encoded within neural recordings, we must compare the activity across many repetitions of the same stimulus. Furthermore, to be able to compare the activity across trials, we must ensure we are making our recordings in precisely the same manner throughout all trials. Given the large number of neurons within the brain and the natural movement of brain tissue over time, it is not possible to set-up multiple experiments with the same subject and record precisely the same neurons each time. Consequently, the maximum number of repetitions we can achieve for any recording stream is limited to the number of repetitions which can be recorded over the course of a single recording session of at most a few hours in duration. With trials whose duration are in the order of a minute, we can only expect to record in the order of 100 trials in any dataset with consistent and comparable neural recordings across all the trials.

Using information theory, we can investigate the nature of the neural code used by individual neurons and populations of neurons (Optican and Richmond, 1987). For example, if our dataset consists of recordings of neuronal spiking activity, we can consider the amount of information contained in the spike train coincident with a 40 ms stimulus, say. First, we can consider our response vector to be the total number of spikes over the 40 ms window and compute the information contained in these about the identity of the presented stimulus. Second, we can consider our response vector to be the number of spikes in each quarter of the stimulus presentation period (four 10 ms windows). This step could equally be performed with more windows of finer granularity, so in general we would have a response vector $r = [r_1, \ldots, r_L]$, with L windows each of length T/L and r_i the number of spikes during the i-th window[7]. Since the information contained in single 40 ms window approach is, by construction, fully contained in the vector of responses within the shorter windows, we can investigate amount of information contained within the timing of the spikes. If there

7 In our example, $T = 40$ ms.

is no significant difference between the amount of information about the stimulus contained in the two vectors, it seems reasonable to conclude that the stimulus, or some attributes which distinguish it, are encoded in the firing rate, whilst the exact timing of the spikes is unimportant.

In general, we will choose some framework through which the raw data is reduced to a manageable finite ensemble of possible states, **R**. Having constrained both our encoding of the stimulus and the response to a finite set of states, we can investigate the relationship between them using Shannon information (Shannon, 1948).

1.3.2 *Theoretical background to information theory*

Within the understanding of Shannon information, information is quantified in a manner analogous to how "surprised" a receiver would be if they were to reveal the contents of a message sent by the transmitter. Unless there is only one possible message, there is uncertainty over what will be sent, potentially with some messages more likely than others. If an *a priori* likely message is received, this confirms the expectations of the receiver, so they are less "surprised". If an unlikely message is received, the receiver is more "surprised". Intuitively, the amount of information gained on receipt of the message is related to how much the uncertainty in the message was reduced upon its arrival.

Rigorously, we define the **Shannon information** content of an outcome or result x to be

$$\mathrm{h}(x) = \log_2 \frac{1}{p(x)}. \tag{1.1}$$

This corresponds to how "surprised" we would be to observe the result x being produced by the system in question. Note that $h(x) = 0$ if $p(x) = 1$ (if an event is certain, we are never surprised and gain no information observing it), and $h(x) \to \infty$ as $p(x) \to 0^+$ (we gain more information — we are increasingly surprised — when a diminishingly unlikely event occurs).

The **entropy** of a system is a measure of amount of the uncertainty we have about its state. We define this as the expected amount of Shannon information we will gain when we observe the state of the system,

$$\begin{aligned} \mathrm{H}(X) &= \mathop{\mathbb{E}}_{x\sim X}\left[\log_2 \frac{1}{p(x)}\right] \\ &= \sum_{x\in\mathbf{X}} p(x)\log_2 \frac{1}{p(x)} \\ &= -\sum_{x\in\mathbf{X}} p(x)\log_2 p(x), \end{aligned} \tag{1.2}$$

where X is the ensemble of possible states of the system in question.

When studying neural recordings using information theory, we will need to take note of the uncertainty in which stimulus is presented, $\mathrm{H}(S)$, and the uncertainty in the response, $\mathrm{H}(R)$. In particular, the amount of information about the stimulus contained in the response is equivalent to their **mutual information**, $\mathrm{I}(S;R)$. The mutual information is the amount by which our uncertainty in the stimulus is reduced when we discover the identity of the response to that stimulus — which, by symmetry, is equivalent to the amount by which our uncertainty in the response decreases when we discover the identity of the stimulus. In general, we can express the mutual information between two random variables, X and Y, as

$$\begin{aligned} \mathrm{I}(X;Y) &= \mathop{\mathbb{E}}_{x\sim X,\, y\sim Y}\left[\log_2 \frac{p(x,y)}{p(x)p(y)}\right] \\ &= \sum_{x\in\mathbf{X},\, y\in\mathbf{Y}} p(x,y)\,\log_2 \frac{p(x,y)}{p(x)p(y)} \\ &= \mathrm{H}(X) - \mathrm{H}(X|Y) \\ &= \mathrm{H}(Y) - \mathrm{H}(Y|X). \end{aligned} \tag{1.3}$$

For brevity, throughout this thesis we will use the term *information* to refer to the mutual information between two random variables (instead of the self-information defined in Equation 1.1).

In Equation 1.3, we made use of the conditional entropy, $\mathrm{H}(X|Y)$. This is so named because it is the entropy of one variable when conditioned on the state of another.[8] Analogously to Equation 1.1, conditional entropy is defined as

$$\begin{aligned}\mathrm{H}(X|Y) &= \mathop{\mathbb{E}}_{x\sim X, y\sim Y}\left[\log_2 \frac{1}{p(x|y)}\right] \\ &= \sum_{x\in\mathbf{X}, y\in\mathbf{Y}} p(x,y)\log_2 \frac{1}{p(x|y)} \\ &= \sum_{y\in\mathbf{Y}} p(y) \sum_{x\in\mathbf{X}} p(x|y)\log_2 \frac{1}{p(x|y)} \\ &= -\sum_{y\in\mathbf{Y}} p(y) \sum_{x\in\mathbf{X}} p(x|y)\log_2 p(x|y). \end{aligned} \tag{1.4}$$

The Venn diagram shown in Figure 1.4 illustrates the relationship between the entropies of X and Y, their joint entropy, conditional entropies, and mutual information, which may assist the reader in conceptualising the relationship between these terms.

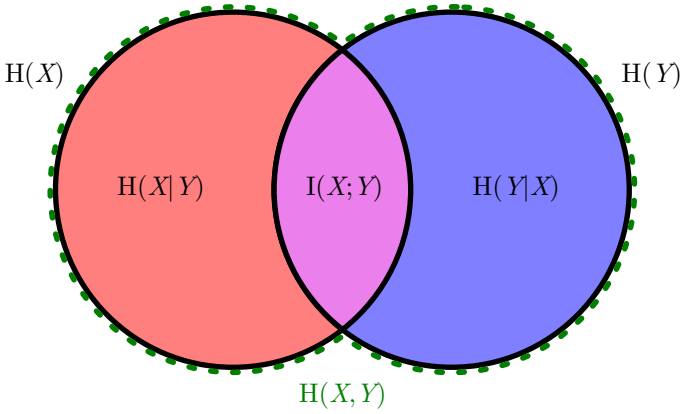

FIGURE 1.4. *Venn diagram of mutual information between X and Y.* The two black circles represent the entropies of X and Y, $\mathrm{H}(X)$ and $\mathrm{H}(Y)$, and their total area (outlined in green) is the total joint uncertainty, $\mathrm{H}(X,Y)$. In the scenario depicted, $\mathrm{H}(X)$ and $\mathrm{H}(Y)$ are partially but incompletely redundant. Consequently, the uncertainty of X is reduced (but not expected to be zero) when Y is known: the conditional entropy $\mathrm{H}(X|Y)$ (red region) is smaller than $\mathrm{H}(X)$, but is not empty. The amount by which our expected uncertainty in X is reduced, $\mathrm{H}(X) - \mathrm{H}(X|Y)$, is equivalent to the mutual information between X and Y, denoted $\mathrm{I}(X;Y)$ and represented by the magenta region. We can reason similarly about the other conditional entropy, $\mathrm{H}(Y|X)$ (blue region).

8 It is also referred to as the noise entropy, particularly when we consider the entropy of the response conditioned on the stimulus, $\mathrm{H}(R|S)$.

1.3.3 *Applying information theory in practice*

Computing the mutual information between stimulus and response requires us to estimate $p(s)$, $p(r)$, and either $p(s|r)$ or $p(r|s)$ for every possible stimulus, s, and response, r. The requirement to know $p(s)$ renders applying mutual information outside of a controlled environment all-but impossible. If the subject is free moving, a prior over the set of potential stimuli it could be exposed to is very challenging to define. However, within an experimental setting we can control the stimulus presentation such that there is only a finite set of unique stimuli, and the probability of each of them, $p(s)$, is defined by our experimental protocol. In practice, $p(r|s)$ is much easier to derive than $p(s|r)$, and so we estimate $p(r)$ and $p(r|s)$. As mentioned earlier, we must repeatedly present each stimulus so it is possible to estimate the response distribution $p(r|s)$ for each stimulus condition.

However, estimating these probabilities from the data can cause problems with our estimated mutual information. Since we have only a finite number of samples, there will inevitably be inaccuracies in our probability estimates (the *limited sampling* problem). Should we repeat the experiment, the natural variation in the samples we collect will result in statistical variance in our measured mutual information. Moreover, the variation due to finite sampling may cause our response distributions to appear different for different stimuli, even when the underlying response generation process is the same for each stimulus. Such problems produce an *over-estimation bias* in the computed mutual information compared with the ground truth. For instance, if a particular response never occurs for a given stimulus presentation, a naïve frequentist estimate of its probability would be 0. This would lead us to mistakenly conclude that it is impossible that a certain stimulus was presented if we observe this response, even if we could in fact have observed this combination of stimulus and response had we collected more samples.

Of even greater concern, the bias to the estimated mutual information can vary greatly depending on the choice of experiment or analysis framework. One cannot draw comparisons between naïvely estimated mutual information values under different experimental criteria because the changes in the bias can completely dwarf the changes in the ground truth information value. It is therefore necessary to estimate the bias on the naïve mutual information value and make a correction to counteract it.

1.3.4 *Bias correction*

A number of techniques exist to correct for the bias in the mutual information estimation. The simplest of these is to shuffle the data so that responses are paired with stimuli at random (Optican et al., 1991). Unfortunately, this will often be a poor estimate of the bias (Panzeri and Treves, 1996), because there may be responses which never occur with certain stimuli. Pairing stimuli and responses together at random inflates the set of unique responses to each stimulus above what is possible in practice, and as a consequence an estimate of the bias determined in this manner will be a pessimistic overestimate.

However, for a multi-dimensional response (where each stimulus presentation produces a response vector), shuffling provides an invaluable bias-correction technique. Using the methodology of Montemurro et al. (2007), we add an additional step to compute the noise entropy under the simplifying assumption that each dimension of r is independent of the others. Exploiting this, we have

$$p_{\text{ind}}([r_1, r_2, r_3, \cdots]|s) = p(r_1|s)\, p(r_2|s)\, p(r_3|s)\, \cdots \tag{1.5}$$

and can compute $\mathrm{H}_{\text{ind}}(R|S)$, the entropy under the independence assumption, directly from estimates of each $p(r_i|s)$ derived from the data. This has very little bias compared with $\mathrm{H}(R|S)$ since there are so many more samples — the ratio of samples for unique response vectors to individual response elements rises exponentially with the dimension of the response vector. One can alternatively estimate this entropy, $\mathrm{H}_{\text{ind}}(R|S)$, from pseudo-response arrays by shuffling each element in the response vector conditioned on the stimulus, producing $\mathrm{H}_{\text{sh}}(R|S)$. Since this shuffling destroys information contained in the dependencies between elements in the response vector, this is an estimate of the same entropy value as $\mathrm{H}_{\text{ind}}(R|S)$. Except the bias on $\mathrm{H}_{\text{sh}}(R|S)$ will be similar to the bias of $\mathrm{H}(R|S)$ because each computation uses the same number of samples. Consequently, we can estimate the mutual information between S and R using

$$\begin{aligned}\mathrm{I}_{\text{sh}}(S;R) &= \mathrm{H}(R) - (\mathrm{H}(R|S) - (\mathrm{H}_{\text{sh}}(R|S) - \mathrm{H}_{\text{ind}}(R|S))) \\ &= \mathrm{H}(R) - \mathrm{H}(R|S) + \mathrm{H}_{\text{sh}}(R|S) - \mathrm{H}_{\text{ind}}(R|S),\end{aligned} \tag{1.6}$$

which has a much smaller bias than $\mathrm{I}_{\text{uncorrected}}(S;R)$.

An alternative method to correct for the bias is to decompose the measured mutual information as a power series in terms of $1/N$, where N is the number of trials recorded. The $1/N$ coefficient in the expansion depends only on the number of stimuli and number of possible responses (Miller, 1955; Treves and Panzeri, 1995). This

dominant term is a good estimate of the bias, and subtracting it from our uncorrected information value greatly improves its accuracy (Treves and Panzeri, 1995). This works for a single-dimensional or multi-dimensional response, and is more accurate than shuffling for a single-dimensional response (Panzeri and Treves, 1996). However, this term is dependent on the total number of potential responses for each stimulus. Since some stimuli may not be able to elicit every response, this is smaller than the number of theoretically possible responses. However as described above, some responses may be possible to produce but unobserved in the limited set of samples. Consequently, the Panzeri-Treves (PT) bias-correction method of Panzeri and Treves (1996) uses Bayesian statistics to estimate the actual number of potential responses. This method was observed to be accurate provided there are at least 4 times as many repetitions of each stimulus as there are possible responses (Panzeri et al., 2007).

A second method of correcting the bias which uses a power series expansion is the Quadratic Extrapolation (QE) method of Strong et al. (1998). Here, the bias on the mutual information is assumed to be well approximated by a second order $1/N$ expression,

$$\mathrm{I}_{\text{uncorrected}}(S;R) = \mathrm{I}_{\text{true}}(S;R) + \frac{a}{N} + \frac{b}{N^2}, \tag{1.7}$$

and the two free parameters, a and b, are found by computing the information content with fractions of the full available dataset (i. e. using $N/2$ and $N/4$ trials). Since the two are built on the same assumptions QE gives similar performance to PT, but QE requires more computational processing as it is fit empirically instead of derived analytically.

The Nemenman-Shafee-Bialek (NSB) entropy estimation method (Nemenman et al., 2004) provides an alternative framework through which the bias can be minimised. This method begins with a uniform prior and uses Bayesian inference to update the probability distribution given each sample in turn. The result has less residual bias than the PT or QE methods, but at higher computational cost (Panzeri et al., 2007).

Each of these bias correction methods make a trade off between variability and bias. Introducing more terms in order to reduce the bias invariably increases variability, but this is a price worth paying since the uncorrected bias is so prominent in the results. Unless indicated otherwise, we will be using the PT bias correction method when computing mutual information with a single dimensional response, and I_{sh} with PT when using a multi-dimensional response vector. In addition to this, we will repeat the mutual information calculation with shuffled stimulus-response pairing multiple times (typically 20 different shuffled pairings) with bias correction and use the average of the bootstraps to estimate the residual bias uncorrected by PT.

The estimated residual bias is also removed from our reported mutual information between stimulus and response.

1.4 NEURAL CORRELATIONS

When an individual is repeatedly presented with the same stimulus, a representation of the stimulus is formed within the brain of the individual. One might expect that, should we eliminate variations in the environment such that an external stimulus is precisely the same — an identical audio track is played without any background stimulus or a visual image is presented with the eyes held in place, for instance — the activity within the associated sensory cortex would be identical on each repetition of the stimulus presentation. However this is not the case. Firstly, some stimuli, such as optical illusions and multistable perceptual phenomena induce unstable high-level representations in the brain (Lumer et al., 1998; Sterzer et al., 2009; Watanabe et al., 2014). But this aside, for more classical typical stimuli (with only a single perceptual interpretation) the high-level representations of stimuli are stable, but the activity of each individual neuron is not. On each successive presentation of a stimulus, the number of spikes elicited in response to the stimulus and the time at which each occurs may vary. Precisely how a stable internal representation of a stimulus is constructed from the collection of unstable responses from individual neurons remains an open question actively researched within the theoretical neuroscience community.

Since neurons function in harmony and not in isolation, and the neural code is distributed across the population of many neurons, it is often important to consider how the behaviour of multiple neurons relate to one-another. A simple way to do this is to measure the correlation between the outputs of pairs of neurons.

Although this is a less nuanced technique than using Shannon information to study the relationship between the neurons, measuring the correlation provides us with a much easier to use metric. In particular, the amount of data needed to measure the mutual information between stimulus and response increases exponentially in the dimensionality of the response, which means it is impossible to compute the amount of information conveyed by the response of more than a handful of neurons. In comparison, a simplistic interpretation of the correlation between the neurons can be performed with fewer trials. However, as we discuss below, one must take into account the relationship between the signal and the noise correlation to correctly understand the impact of the neural correlations on the information contained by a collection of neurons.

1.4.1 *Signal correlations*

All other things being held constant, the response to a stimulus from an individual neuron will come from a fixed distribution. Studying the average firing rate evoked in a single neuron in response to a collection of stimuli allows us to investigate the response profile of the neuron. When the collection of stimuli vary parametrically, the distribution of responses for a given neuron with respect to this parameter is known as its **tuning curve**.

We can evaluate how similar the response profiles are for two neurons by computing their signal correlation. To do so, we first find the average response from each neuron for a set of stimuli, S. Next, we calculate the Pearson correlation coefficient between the two sets of responses. In doing so, we treat each unique stimulus in S as an independent sample of the relationship between the two neurons. Some neurons behave similarly to each other in response to stimulation across a range of potential stimuli, and these pairs of neurons have correlated responses with respect to the input stimuli.

From an information theoretic perspective, neurons with high signal correlation will have high redundancy. Of course, a redundant neural code is potentially useful as a method of error correction (MacKay, 2003, Chapter 1), providing robustness against neuron death. Having multiple neurons encoding the same information can improve accuracy by considering the population activity (the total or average of each neuron) instead of the individuals, and this may also permit a faster response time within the brain. However, the prospective gain in performance when considering the responses from a set of neurons (redundant or not) depends on their noise correlations, and the relationship between the signal and noise correlation for the pair.

1.4.2 *Noise response correlations*

Previously we noted that the response from a single neuron to a fixed stimulus is not fixed but effectively sampled from some stochastic distribution. This internally-generated fluctuation in the neuronal response is referred to as noise. When we consider a pair of neurons, the responses from each may vary independently over their two distributions; alternatively their responses may co-vary. If the simultaneously measured responses from the pair of neurons are both higher than average on the same trials, and lower than average on the same trials, their noise is positively correlated. Should the response from one neuron be consistently higher than average when the other is lower than average, we say their noise is negatively correlated.

To a certain extent, positive noise correlations between neighbouring neurons are inevitable, because they have correlated inputs. Firstly, the path length (in the graphical sense of the number of separating nodes) between any given pair is likely to be short because neurons are preferentially connected to other neurons within their local vicinity. Secondly, since there are more neurons in V1 than in the LGN (Kanitscheider et al., 2015), the upscaling of the afferent sensory input makes noise correlations within V1 inevitable.

Intuitively, one can see that such noise correlations between pairs of neurons can inhibit the accuracy with which the stimulus is encoded in their activities. Suppose that two neurons both respond monotonically more to stimuli of higher contrast. Knowing their tuning curves and their current activity, we can decode the contrast of the current stimulus with some level of accuracy. If the two neurons are independent of one another, knowing the activity of both will give us a more accurate and more precise estimate of the actual contrast of the stimulus. But if the activity between the pair of neurons is positively correlated, the information conveyed from the pair of neurons is reduced — when one gives an overestimate of the contrast from a by-chance elevated activity level, so does the other. In contrast, negative correlations would enhance our decoding accuracy, for an overestimate from one neuron would more frequently be mitigated by an underestimate from the other.

However, this line of thinking only holds for a homogeneous population of neurons, where every neuron has its response drawn from the same distribution. As illustrated in Figure 1.5a, if a pair of neurons have positive signal correlation, then a positive noise correlation points in the direction distinguishing between the two stimuli, reducing the amount of information encoded by the pair of neurons. If the pair of neurons have negatively correlated responses with respect to the stimuli, a positive noise correlation increases the amount of information encoded instead (Figure 1.5b).

A similar line of reasoning can be considered for two neurons with offset tuning curves (Franke et al., 2016). As shown in Figure 1.6, when the two tuning curves are considered together we traverse a manifold in $2d$ space. Noise correlations are a hindrance (information-limiting correlations, Moreno-Bote et al., 2014) only when the direction of noise correlation points in the same direction as the derivative of the tuning manifold, since this change is easily confused with a change in the parameter describing the manifold. Whereas noise correlations which are orthogonal to the manifold are beneficial to the neural code, since the result has lower variability when projected onto the manifold than that of independently generated noise. However, when the manifold forms a closed loop (as is the case with orientation tuning, shown in Figure 1.6) the derivative of the tuning manifold processes through a full 360°, and

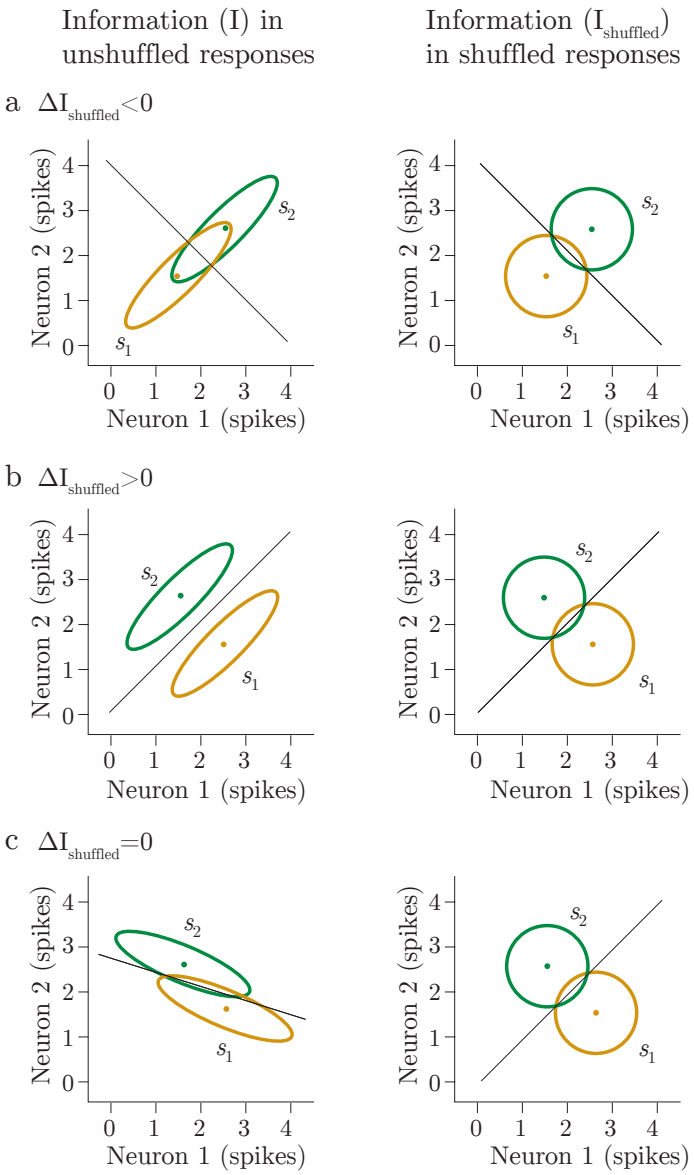

FIGURE 1.5. *Effects of correlations on information encoding.* We show the effect of positive noise correlations on the information encoded by two neurons that respond to two different stimuli in three scenarios. The panels on the left show the original unshuffled responses, those on the right show the effect of shuffling the responses over trials to destroy the noise correlations. Each ellipse indicates the 95 % confidence interval (CI) for the responses. Each diagonal line shows the optimal decision boundary — responses falling above the line are classified as stimulus 2 and responses below the line are classified as stimulus 1. (a): A larger fraction of the ellipses lie on the "wrong" side of the decision boundary for the true, correlated responses than for the independent responses, so $I - I_{\text{shuffled}} = \Delta I_{\text{shuffled}} < 0$. (b): A smaller fraction of the ellipses lie on the wrong side of the decision boundary for the correlated responses, so $\Delta I_{\text{shuffled}} > 0$. (c): The same fraction of the ellipses lies on the wrong side of the decision boundary for both the correlated and independent responses, so $\Delta I_{\text{shuffled}} = 0$. Adapted by permission from Macmillan Publishers Ltd: *Nature Reviews Neuroscience* (Averbeck et al., 2006), copyright 2006.

the ideal noise correlation varies depending upon which stimulus signal is under consideration.

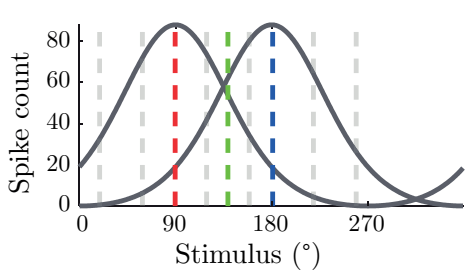

(a) Tuning curves for two model neurons.

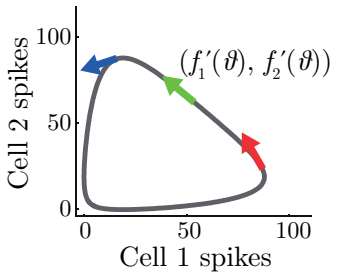

(b) Pairwise responses traverse a manifold within $2d$ space.

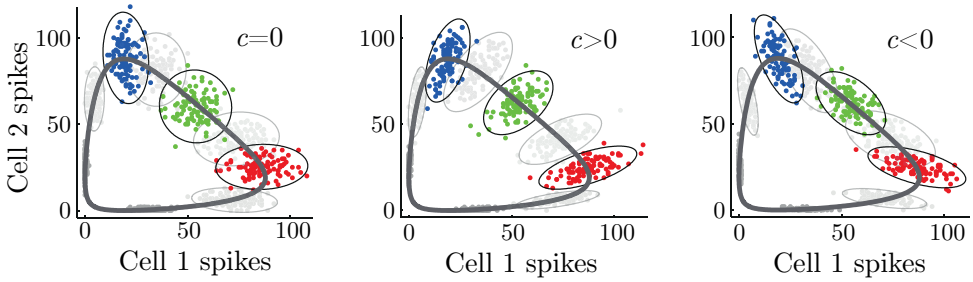

(c) The effect of noise correlations on decoding from the tuning manifold.

FIGURE 1.6. *Impact of different structures of noise correlation upon population coding.* (a): Two model direction-selective neurons respond to different stimuli (dashed lines) according to tuning curves (solid grey curves), $f_1(\theta)$ and $f_2(\theta)$, with two direction preferences that differ by 90°. (b): The two tuning curves are represented as a solid grey line parametrized by the stimulus direction, θ. In the space of the two-neuron output, this grey line forms an informative subspace: the location of the pair response along the grey line yields information about the stimulus presented. More precisely, for each stimulus, θ, the tangent vector, $(f_1'(\theta), f_2'(\theta))$, defines the informative direction (arrows in colours corresponding to the stimulus values in the left panel). (c): For each stimulus presented, noise correlation distorts the cloud of two-neuron responses about the mean over trials; depending upon the geometry of this distortion with respect to the informative direction, it can either benefit or harm the coding accuracy. Positive correlation in the pair ($c > 0$) favours the reliability of coding with respect to the independent case ($c = 0$), while negative correlation ($c < 0$) is detrimental. Specifically, when $c > 0$, the responses for nearby stimulus directions overlap less, and, hence, coding is more reliable. (Conversely, if the two tuning curves have similar preference, $c < 0$ is favourable whereas $c > 0$ is detrimental.) More precisely, coding is favoured if the eigenvector of the covariance matrix parallel to the tangent vector, $(f_1'(\theta), f_2'(\theta))$, comes with a small eigenvalue; correlation then relegates the noise in the orthogonal, uninformative direction. Ellipses are contours of equal probability, drawn at 2.5 standard deviations. Reprinted from *Neuron*, Franke et al. (2016), Copyright (2016), with permission from Elsevier.

2

PERCEPTUAL LEARNING IN V1 AND V4

In this chapter, we investigate the neural correlates of perceptual learning within two visual cortical regions, the primary visual cortex (V1) and the extrastriate visual cortex area V4. This work builds on the Master's thesis of Lowe (2012), which served as a preliminary study for the work presented here.

Perceptual learning is the phenomena in which an individual becomes more adept at fine-grain discrimination of stimuli through repetitive stimulation with the particular stimulus class. Clearly, such changes in perceptual ability are mediated by changes within the brain, but it is not currently known which neural changes drive the increase of such perceptual abilities.

A long-standing question within the field of perceptual learning has been whether cortical changes are driven through bottom-up or top-down developments. Under the bottom-up hypothesis, repetitive stimulation of similar stimuli causes V1 to change its self-organisation such that its representations of these stimuli are more prominent. This change within V1, simply from increased exposure to the stimulus class, will naturally result in a more accurate encoding of the properties of the stimulus salient to the task. Since the higher-level cortical regions will have better information available to them from which to make their classification decisions, their performance will increase.

With the top-down hypothesis, demand for better classification performance from high-level (output) cortical regions triggers an increase in cortical feedback, and the release of neurotransmitters such as acetylcholine (ACh), dopamine, or norepinephrine in multiple cortical regions, including primary sensory regions. These neurotransmitters are associated with an increase in the rate of change in synaptic connection strengths within the cortical region where they are present. The combined effect of this electrochemical feedback triggered by the higher-level cortical regions facilitates a change in the lower cortical regions, such as the sensory corticies: the neurotransmitters accelerate the rate of change of synaptic connections, whilst direct feedback steers the network to strengthen particular connections corresponding to the current stimulus.

Using multi-unit spiking data recorded from macaque V1 and V4, recorded by Xing Chen within the lab of Alex Thiele, Newcastle University, I investigated these hy-

potheses by decoding the information about the sensory stimulus encoded in V1 and V4 and comparing the rate of change of this over the course of experimental training.

2.1 BACKGROUND

When an individual repeatedly performs a sensory perception task they will, over time, demonstrate an improvement in performance. If the task is repeated — frequently and over the course of several weeks — until performance finally saturates, the effect can persist for months. This phenomenon is known as perceptual learning, and its duration sets it apart from shorter term effects such as sensitization (a transient increase in sensitivity following a period of stimulation) and priming (a change in perception of one stimulus immediately following a different, but related, stimulus).

For the purposes of studying perceptual learning, fine-grained discrimination tasks are appropriate; since they are intrinsically difficult, they cannot be immediately solved and there is scope for improvement. For instance, an example of a typical task chosen by neuroscientists when studying perceptual learning is that of discerning the difference between straight lines of very similar orientations, or the alignment offset between sets of straight lines, known as vernier acuity. If it is trained, perceptual learning can be exhibited across seemingly all sensory modalities (Dinse et al., 2003; Gibson and Gibson, 1955; Gilbert, 1994; Gilbert et al., 2001); other tasks which have been used for experiments include depth perception (Fendick and Westheimer, 1983; Westheimer and Truong, 1988), somatosensory spatial resolution (Godde et al., 2000; Pleger et al., 2001), estimation of weight, and discrimination of pitch (Carcagno and Plack, 2011; Demany, 1985).

However, the improvements in sensory discrimination which are made through perceptual learning are highly specific to the task at hand. For instance, training for vernier acuity only gives improvements for stimuli with the same orientation ($\pm 30°$) and spatial frequency ($\pm 1/2$ octave) (Fiorentini and Berardi, 1980; Poggio et al., 1991), and training on line separation yields no effect when the lines are later replaced with dots (Poggio et al., 1992). Moreover, results are specific to the retinotopic location of the stimulus, with translation through $<10°$ from the training spot sufficient to remove the effects (Fiorentini and Berardi, 1980; Fiorentini and Berardi, 1981; Karni and Sagi, 1991; Poggio et al., 1991). This said, some studies have found a limited amount of effect-transfer to regions in the opposite hemisphere for timing-dependent tasks (Ball and Sekuler, 1987; Berardi et al., 1987).

There is still some contention over where the physiological changes which lead to perceptual learning are situated in the brain. Consequently, there are several com-

peting models which attempt to explain how perceptual learning arises. The "early" model hypothesises that improvements principally occur at a low level in the sensory cortex (Fahle, 2005; Gilbert et al., 2001). The "late" model states that improvements are in the higher level cortical areas related to decision making (Yu et al., 2004). Whilst according to the "reverse hierarchy model", improvements are made first in higher level decision areas, and then these are propagated down the cortical hierarchy to lower levels via top-down feedback signals if the changes at higher levels are insufficient (Ahissar and Hochstein, 2004; Hochstein and Ahissar, 2002).

Perceptual learning is thought to be connected to cortical remapping and reorganisation in response to similar stimuli (Dinse et al., 2003; Pleger et al., 2003; Polley et al., 2006). In such experiments, the region of the cortex coding for the stimulus is seen to expand. Some researchers in this field have suggested that perceptual learning might be the mechanism which underpins all adult plasticity in the sensory and association cortices (Gilbert et al., 2001).

Neural changes correlated with perceptual learning have been observed at many levels of the cortical hierarchy. Studies have found changes in the orientation tuning curves of neurons in both V1 (Schoups et al., 2001) and V4 (Li et al., 2004; Raiguel et al., 2006; Yang and Maunsell, 2004), however the effects are greater in V4 than in V1 (Raiguel et al., 2006), and not all studies find neural changes in V1 and V2 which relate to perceptual learning, even when the subject has demonstrated psychometric improvement in the task (Ghose et al., 2002).

Due to the specificity of perceptual learning, only neurons in the retinotopic area where the stimulus is located are affected. When the properties of individual neurons have been observed to change during perceptual learning, their tuning curves for task-relevant features have become sharper. Under activity-based models of neural information processing, this will provide more information about the task-relevant stimulus property if it falls on the steeper slope of the tuning curve. Studies have also shown that the effect of perceptual learning is most pronounced on the most relevant neurons from the perspective of information conveyed (Raiguel et al., 2006).

Since all neurons in the visual system have contrast tuning to some degree, one might think a contrast discrimination task a good choice for a perceptual learning study. However, perceptual learning has proven unreliable for such discrimination problems, possibly because contrast sensitivity is already overtrained due to its importance in low-light conditions. Better results have sometimes been found if the contrast test stimulus is accompanied with flanking stimuli (Adini et al., 2002), a phenomenon known as context-dependent learning, though other studies have found learning occurs at the same rate both with and without flankers (Yu et al., 2004), despite nearly identical setup between the experiments with the conflicting two results.

When studying perceptual learning with information theory, an obvious expectation is for the information contained in the population spiking activity to increase over time as perceptual learning occurs. It is also likely that this increase will not be symmetric across the population, with some neurons adapting their responses to the training stimulus class more than others. In line with previous experiments (Raiguel et al., 2006), I would also expect to see more of a change in information for neurons in V4 than V1, and also a greater change in the V4 neurons which are the most informative to begin with (Raiguel et al., 2006). In keeping with the reverse hierarchy model, learning should begin in V4 first before being propagated down to V1, so one would expect to see distinct increases in the mutual information between the stimulus and V4 on a shorter timescale than between V1 and V4.

Since temporal coding, in particular response latency, has been found to be important for subtle contrast differences (Arabzadeh et al., 2006; Reich et al., 2001), I hypothesise that the amount of information in the temporal coding of the spiking data will have increased above and beyond any increase in the information contained in the firing rates alone. Furthermore, I expect to see that response latencies become more stimulus dependent, conveying an increasing amount of information about the stimulus contrast.

Additionally, since these studies (Arabzadeh et al., 2006; Reich et al., 2001) also found the information contained within firing rate alone was sufficient for gross discrimination of contrast, I hypothesise that information in the latency and temporal code will only increase significantly for test stimuli close in contrast to the sample stimulus (see Section 2.2 for an explanation of the experimental setup).

2.2 EXPERIMENTAL METHODS

The experimental data analysed in this chapter was acquired by Xing Chen, under the supervision of Alexander Thiele at the Institute of Neuroscience, Newcastle University. The experimental protocol was designed by Xing Chen and Alexander Thiele, and has been described previously (Chen, 2013; Chen et al., 2013; Chen et al., 2014). All procedures were carried out in accordance with the European Communities Council Directive RL 2010/63/EC, the US National Institutes of Health Guidelines for the Care and Use of Animals for Experimental Procedures, and the UK Animals Scientific Procedures Act. Two male macaque monkeys (5 and 14 years of age) were used in this study.

2.2.1 *Head post implantation*

During an initial surgical operation, a custom-made head post (Peek, Tecapeek) was embedded into a dental acrylic head stage. Details of the surgical procedures and post-operative care have already been published (see Thiele et al., 2006, for details).

2.2.2 *Stimuli*

Stimuli were displayed on a cathode ray tube (CRT) monitor with display dimensions 400 mm × 320 mm at a viewing distance of 0.54 m, with resolution 1280 px × 1024 px. The monitor refresh rate was 85 Hz for monkey 1 (M1) and 75 Hz for monkey 2 (M2).

2.2.3 *Initial training*

The monkeys were familiarised with the experimental set-up and structure with an initial training task otherwise unrelated to the main perceptual learning task on which the animals were later trained. In this initial task, the animals compared the colour of a circle stimulus with that of succeeding circle stimuli, while maintaining fixation on a central target. When a target stimulus appeared (a circle of a matching colour), subjects were required to release a touch bar in order to receive a fluid reward. Eye position was monitored using an infrared video tracking system.

2.2.4 *Electrode array implantation*

During surgery, animals were sedated with ketamine, and general anaesthesia was maintained using isoflurane following endotracheal intubation. A craniotomy was made to remove the bone overlying V1, V2, and dorsal V4, using a pneumatic drill. The bone was kept in sterile 0.9 % sodium chloride (NaCl) for refitting at the end of the surgery. The dura was opened up to allow access to regions V4 and V1. Microelectrode chronic Utah arrays, attached to a CerePortTM base, were implanted under sterile conditions in the cortex. For M1, two 4×5 grids of microelectrodes were implanted in area V4, and one 5×5 grid was implanted in V1. For M2, a 5×5 grid was implanted in V4, and a 5×5 grid in V1.

A minority of electrode contacts were unstable, and post-surgery were found to have excessively high impedance. These electrodes (channels) were not viable for use in electrophyisiological recordings. The number of recording channels from the multi-electrode arrays (MEAs) used in the study are shown in Table 2.1.

Subject	Region	Number of viable channels
M1	V4	30
	V1	23
M2	V4	20
	V1	25

TABLE 2.1. *Number of channels from which recordings were taken, for each of the monkeys and brain regions.*

2.2.5 *Receptive fields*

After animals had fully recovered, RFs were mapped using reverse correlation between random visual stimulation and neuronal response. For both animals, the RFs of neurons recorded from the V4 arrays were 7.5° from the centre of the visual field. For M1, the MEA in V1 was 4.6° from the centre, and for M2 it was 1.5°.

The RF locations for the implantation sites in V4 and V1 were not retinotopically congruent for either animal. Consequently, for each animal the experimental protocol was performed first in the peripheral region of the visual field corresponding to the RF of the V4 array, and then repeated in the parafoveal region corresponding to the V1 array.

Since the improvements in task-performance driven by perceptual learning are known to be specific to stimuli at the same location as the training stimuli (Fiorentini and Berardi, 1980; Fiorentini and Berardi, 1981; Karni and Sagi, 1991; Poggio et al., 1991), training the animal on the stimulus at the peripheral location should not impact its performance when the experiment is repeated at a parafoveal location.

2.2.6 *Behavioural task*

The experimental design has been described previously (see Chen et al., 2013). Training on the perceptual learning task, whilst recording from the MEA implanted in the visual cortex, proceeded over several weeks. Each day, 5 days per week, the subject had a single recording session composed of multiple trials. During each trial, the subject is tasked with identifying whether a **test** stimulus has higher or lower contrast than a preceding **sample** (or **pedestal**) stimulus of 30 % contrast (two-alternative forced-choice, 2AFC). If the subject responds correctly, they are provided with a water reward. Training continued until the subject's test performance stabilised at a plateau.

Each trial consists of 6 steps, listed below and depicted in Figure 2.1.

1. The trial begins with the appearance of a **fixation point**, on which the subject must focus their gaze.

2. A **sample stimulus** appears in the form of either a Gabor patch (V4 recordings) or a circular sinusoidal grating (V1 recordings), presented at the pedestal contrast of 30 % in the location corresponding to the RF of the MEA. The sample stimulus is presented for approximately 530 ms.

3. The fixation target persists, and the sample stimulus disappears. This period of unstimulated spontaneous neural activity is the **sample-test interval**, with either fixed or variable duration (see Table 2.2).

4. A **test stimulus** appears in the same location as the sample stimulus, but with a different contrast. The test contrast is selected randomly from a set of 14 possibilities (stimulus location dependent, see Table 2.3). This stimulus is presented for approximately 530 ms.

5. The fixation target persists, and the test stimulus disappears. This period of unstimulated spontaneous neural activity is the **test-target interval**, with duration approximately 425 ms.

6. Two **target stimuli** appear above and to the right of the fixation point (which disappears). The subject may now make a saccade to their chosen target to indicate whether they think the test stimulus had higher or lower contrast than the sample.

7. If the subject responds correctly, a water reward is dispensed.

8. After a blank inter-trial period, the fixation target reappears and a new trial begins.

All stimuli are presented over a uniform grey background. The subject must fixate on the central target throughout the sections 1 to 5 of the trial, otherwise the trial is aborted. Only completed (unaborted) trials were included in the analysis.

As mentioned in Section 2.1, previous studies have found it is necessary to present flanking stimuli around the main stimulus in order to induce perceptual learning. During our experimental study, preliminary research demonstrated flankers were not necessary for perceptual learning provided the contrast of the pedestal stimulus was held the same for every trial.

Trials were presented in blocks, with each block containing a fixed number of repetitions of each test contrast ordered at random. To ensure the subject was incentivised to attempt all the trials and not just excel at the easiest stimuli, at the end of each block any trials which received incorrect responses were repeated.

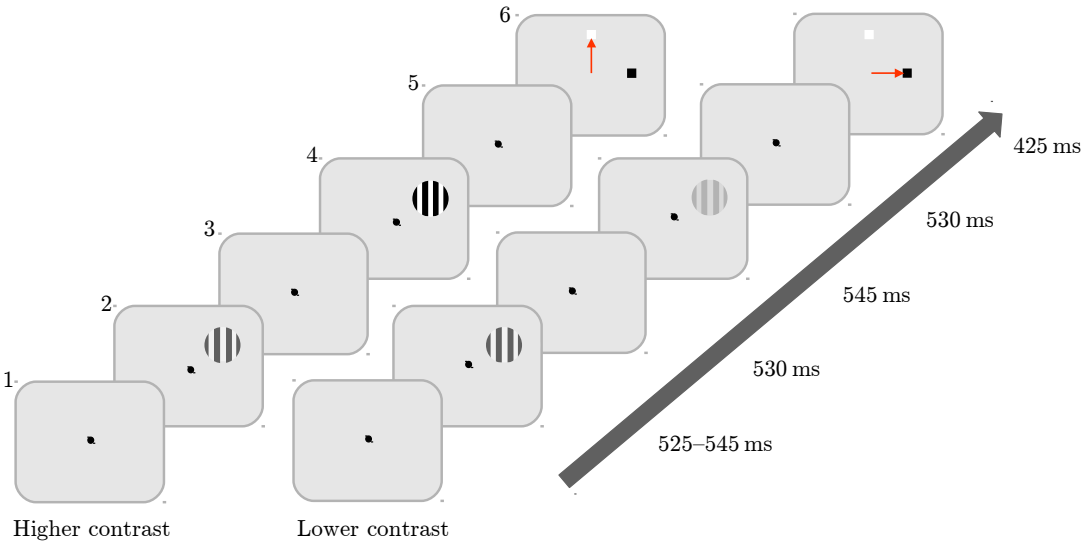

FIGURE 2.1. *Experimental procedure.* 1: The monkey fixates upon a central spot. 2: A sample stimulus, either a Gabor patch or a sinusoidal grating, is presented with 30 % contrast. 3: Blank sample-test interval. 4: Test stimulus presented with either higher or lower contrast. 5: Blank test-target interval. 6: Two target stimuli appear, and the subject makes a saccade to one to indicate its choice. Durations indicated are approximate values; see text for details and Table 2.2 for precise timing. Stimuli contrasts depicted here are not to scale and are for illustrative purposes only.

		Duration (ms)				
Subject	Region	t_1	t_2	t_3	t_4	t_5
M1	V4	[530.9, 545.5]	529.275	[539.7, 1058.7]	529.275	423.475
	V1	[525.8, 539.0]	529.275	541.164	529.275	423.475
M2	V4	[526.3, 540.6]	529.275	546.632	533.176	426.578
	V1	[525.8, 540.7]	533.176	546.570	533.176	426.640

TABLE 2.2. *Precise durations of each section of a single trial.* The durations are listed for the pre-sample delay period (t_1), sample presentation (t_2), sample-test interval (t_3), test presentation (t_4), and test-target interval (t_5). Square brackets indicate a range of possible values. Precise stimulus durations differ for the two animals due to their respective monitor refresh rates.

Subject	Region	Type	Test contrasts (%)
M1	V4	Gabor	10, 15, 20, 25, 27, 28, 29, 31, 32, 33, 35, 40, 50, 60
	V1	sinusoid	5, 10, 15, 20, 22, 25, 28, 32, 35, 40, 45, 50, 60, 90
M2	V4	Gabor	10, 15, 20, 25, 27, 28, 29, 31, 32, 33, 35, 40, 50, 60
	V1	sinusoid	5, 10, 15, 20, 22, 25, 28, 32, 35, 40, 45, 50, 60, 90

TABLE 2.3. *Stimuli parameters for each subject and recording region.* The set of test contrasts were selected so that the difficulty of the task ranged from easy to very hard. The test contrasts were set such that M1 achieved a similar initial accuracy for both peripheral and parafoveal stimuli.

	Monkey 1		Monkey 2	
	V4	V1	V4	V1
Number of channels	30	23	20	25
Number of sessions	30	17	26	22
Stimulus location	peripheral	parafoveal	peripheral	foveal
Centre co-ords (dva)	$(-5, 16)$	$(-3.5, 3)$	$(-5, 16)$	$(-0.7, -1.3)$
Eccentricity (dva)	16.8°	4.6°	16.8°	1.48°
Stimulus size (dva)	16.0°	3.0°	14.0°	0.75°
Stimulus type	Gabor	sinusoid	Gabor	sinusoid
Spatial frequency (cpd)	2	2	2	4

TABLE 2.4. *Experimental details for each animal and MEA recording region.* Stimulus co-ordinates are given in degrees of visual angle (dva). Spatial frequency is specified in cycles per degree (cpd).

The number of trials per recording session was not fixed; the recording session was terminated when the subject was no longer interested in engaging with the experiment. Consequently there was high variability in the number of trials per session, ranging from 254 to 1889.

During training, the subject's performance on the task initially increased each day. After around 20 sessions, its performance stabilised at a plateau. Once the performance level was consistent for 5 consecutive sessions, this phase of the experiment was terminated.

The subject then progressed to a roving version of the experiment, in which the pedestal contrast could be either 20 %, 30 % or 40 % contrast. In the roving task, the subject asked to respond as to whether the test contrast exceeded the variable sample contrast. However, here we will only analyse the results of the non-roving version of the experiment with a static pedestal contrast of 30 %.

2.2.7 *Data acquisition*

Raw data was acquired at a sampling frequency of 32 556 Hz using a 24 bit analog-to-digital converter. The minimum and maximum inputs were 11 µV and 136 986 µV — values outside this range were recorded at the floor or ceiling value respectively. To ensure data was collected from each channel with a good signal-to-noise ratio (SNR), digital referencing was performed prior to recording the raw data.

Raw data was subsequently bandpass filtered with a lower cutoff frequency of 600 Hz and an upper cutoff from within the range 2500 Hz to 4000 Hz. The upper cutoff frequency was manually selected for each channel and session such that it was low enough to exclude high frequency noise from the experimental equipment, but no lower than necessary.

2.2.8 *Initial spike extraction*

Spikes were extracted from the filtered data using a voltage threshold. For each recording channel and session, a threshold was selected by hand at a voltage higher than the background noise, such that both high and low amplitude spikes will exceed the threshold. For each channel, the extracted spike trains contain spikes from multiple neurons (multi-unit activity) surrounding the electrode. All the spikes from high-amplitude neurons close to the electrode will be included, but lower-amplitude spikes from further away may be detected with a peak voltage around the detection threshold. Consequently, only a subset of the spikes from more distant neurons will be detected.

After defining a detection threshold, spikes were extracted using the following algorithm.

1. Find the first sample point to exceed the threshold.
2. Find the peak of the spike by searching for next time the voltage decreases (searching forwards by at most 24 data points, spanning 0.74 ms).
3. Extract the 8 data points preceding and 23 data points succeeding the peak as the waveform of the spike, with duration 0.98 ms.
4. Skip forward to the end of the extracted waveform (24 data points after the peak) before searching for the next sample point to exceed the threshold again.

By its construction, this algorithm enforces a minimum inter-spike interval of 0.74 ms.

2.3 PREPROCESSING METHODS

This section includes general analysis methods used throughout the rest of the chapter. Additional analysis methodology is given as part of each results section. The methods described in this section were performed jointly with Xing Chen.

2.3.1 *Elimination of monitor induced artifacts*

An artifact was identified which was triggered whenever the monitor refreshed. Unfortunately, the monitor-refresh artifact had a profile very similar to that of a neural spike. Consequently, it continued to contaminate the data further down the processing pipeline post-spike extraction.

The precise shape and magnitude of the artifact signal varied depending on channel and session, however for each individual channel the timing and shape of the artifact relative to the monitor refresh was highly reliable over the course of an individual session. Therefore, this artifact was removed from the data by averaging the raw recordings between each monitor refresh to find a stereotyped artifact profile, and subtracting this template from the recordings immediately following each monitor refresh. Since the artifact signal was sharply peaked and the monitor refresh was not phase-locked with the data sampling frequency, the stereotypical template was super-resolved by binning the samples into bins with 4 times the sampling frequency. For each monitor refresh, the template subtracted from the data samples was linearly interpolated against the super-resolved template depending on the phase of the data sampling rate.

2.3.2 *Elimination of movement induced artifacts*

For a minority of trials (3.6 %, 2879 out of 80 071) physical movements by the subject generated high-amplitude artifacts across multiple recording channels. Due to the high-amplitude and unpredictability of such events, it was not possible to remove artifacts cleanly from the rest of the signal. Instead, since these problems occurred on a small proportion of the total trials, we identified trials where this artifact was present and removed them from subsequent analysis.

Since movement artifacts dominated recordings where they were present, and these artifacts were present in multiple channels simultaneously, we identified trials containing them by changes in the covariance between channels. For each trial, we computed the Pearson correlation coefficient,

$$\rho(X, Y) = \frac{\operatorname{cov}(X, Y)}{\operatorname{var}(X)\ \operatorname{var}(Y)}, \tag{2.1}$$

between the signals, X and Y respectively, from each pair of channels. Some sessions were entirely free from artifact contamination, and for these sessions the distribution of $\rho(X, Y)$ across all trials and all pairs of channels was unimodal, with centre between 0.2 and 0.4. For sessions which included trials where the motion artifact was present, the distribution was bimodal with a second smaller group whose centre was between 0.4 and 0.7. For each session, a cut-off value was manually selected which partitioned the two clusters. All trials corresponding to a pairwise correlation coefficient above the threshold were excluded from further analysis.

2.3.3 *Removal of empty trials*

During a minority of trials (0.81 %, 651 out of 80 071) failures in the recording apparatus resulted in no spikes being recorded. We identified these trials as those which had no detected spikes for any of the $\geq$20 simultaneously recorded channels[1] over the full 2.5 s duration of the trial. These "empty" trials were removed from subsequent analysis.

2.3.4 *Spontaneous activity normalisation*

The manual selection of spike detection thresholds described in Section 2.2.8 resulted in a lack of consistency across sessions of both the stimulus-evoked and spontaneous firing rates for individual channels. To resolve this problem, spiking activity was re-

1 See Table 2.1 for the exact number of recording channels in each multi-electrode array.

extracted with an automated threshold set such that the spontaneous firing rate was matched across sessions.

For each channel, a target spontaneous firing rate, f_{target}, was set by manually choosing a session from the middle of the experiment with an intermediate signal to noise ratio. Spikes from each channel had previously been sorted using computer-assisted manual clustering, and the target firing rate was set at the total multi-unit firing rate of all clusters. Unsorted spikes outside of the clusters were not included in the firing rate target. This choice should ensure the target firing rate is a sensible expectation of the true background firing rate for as many recording sessions as possible.

Due to, amongst other differences, changes in the noise level between sessions, simply using the same voltage threshold for each session would not result in extracting a consistent firing rate. To determine the appropriate spike detection threshold which would match the target spontaneous activity for each session, we searched using an iterative routine on the number of extracted spikes as a function of the threshold. On each iteration, the spontaneous firing rate was determined based on the number of spikes during the pre-trial fixation period (Step 1 in Section 2.2.6), as extracted using our algorithm described in Section 2.2.8.

To ensure the iterative algorithm had a suitable initialisation, which considerably reduced the runtime, the initial threshold was set using the following method.

1. Find the overall firing rate over all trials (including stimulus presentation as well as spontaneous activity) for the benchmark session being used to define the target spontaneous activity firing rate, $\tilde{f}_{\text{target}}$.

2. Set $\mathbf{V}_{40}$ to be the maximum voltage over every 40 consecutive samples (a duration of 1.23 ms) during the first hour of recording for the session to be matched.

3. Find the threshold T_0 such that number of values in $\mathbf{V}_{40}$ exceeding T_0 equals one hour of spikes at a rate of $\tilde{f}_{\text{target}}$.

This initialisation routine allowed us to search over all possible thresholds very rapidly, and find a suitable initial threshold which was close to the final solution for the majority of channels and sessions.

We then extracted the spikes using the algorithm described in Section 2.2.8, and compared the average firing rate during all pre-trial fixation periods in the recording session with f_{target}. If the initial threshold was too low, our second try was 3 % higher; if it was too high, our second try was 1 % lower.[2] After this, we performed an iterative search for the target threshold using a weighted combination of linear interpolation and bisection on each step (80 % linear interpolation, 20 % bisection). The weightings

2 Since the computation involved in our spike extraction routine scales linearly with the number of spikes extracted, we err on the side of over-estimating the threshold since this costs notably less time.

for this hybrid root-finding algorithm were determined empirically and chosen to give reliably fast convergence. The search was halted once a threshold was found which yielded a spontaneous firing rate within $\pm 1\,\%$ of the target.

Our choice to set the spike detection threshold in this manner assumes that the spontaneous firing rate for each recording channel is stable over the course of a month of recordings. Such an assumption is imperfect, since it is possible for small movements in the chronic implant to change which neurons are closest to the electrode. Furthermore, it is possible that rewiring of the neural synapses either due to natural changes or triggered by the perceptual learning experiment will change the baseline firing rate of the recorded neurons. However, the results of our spike sorting suggest that most of the neurons close to the electrode contact remained close through the experiment. Additionally, it is not currently known whether perceptual learning triggers changes in spontaneous activity but we anticipate that homoeostasis will counteract any changes induced by it in order to stabilise the overall firing rate. Certainly any choice of spike extraction threshold is arbitrary, and this choice yields much greater consistency in our data, rendering sessions across the duration of the experiment more directly comparable.

2.4 RASTER PLOTS

To inspect the data, we created rastergrams showing every spike detected from an individual recording contact across every trial in every recording session. Such data visualisation steps afford an overview of the dataset, and are useful to verify the integrity of the data. Artifacts, such as those whose removal we described in Section 2.3, often appear clearly in rastergrams. For instance, an artifact which occurs at fixed intervals from the stimulus onset such as the monitor-induced artifact (see Section 2.3.1) appears as a narrow vertical line (not shown). Without normalising the spontaneous activity Section 2.3.4, inter-session changes in recording properties would result in large session-to-session changes in overall firing rate, which are also clear to the eye when displayed in a rastergram (not shown).

In order to familiarise the reader with the data, exemplar rastergrams are shown in Figures 2.2, 2.3, 2.4, and 2.5. We can see that in V1 (see Figure 2.2 and Figure 2.3), there is a peak in the firing rate in response to the stimulus onset, with a delay of approximately 50 ms. Shortly after the stimulus onset response, the neural activity reduces down to a level which is sustained throughout the rest of the stimulus presentation period. With M1, the sustained firing rate is similar to the background rate (a sample of which is shown before the onset response), whereas for M2 the sustained rate is more clearly elevated versus the background rate. Although only a single channel is

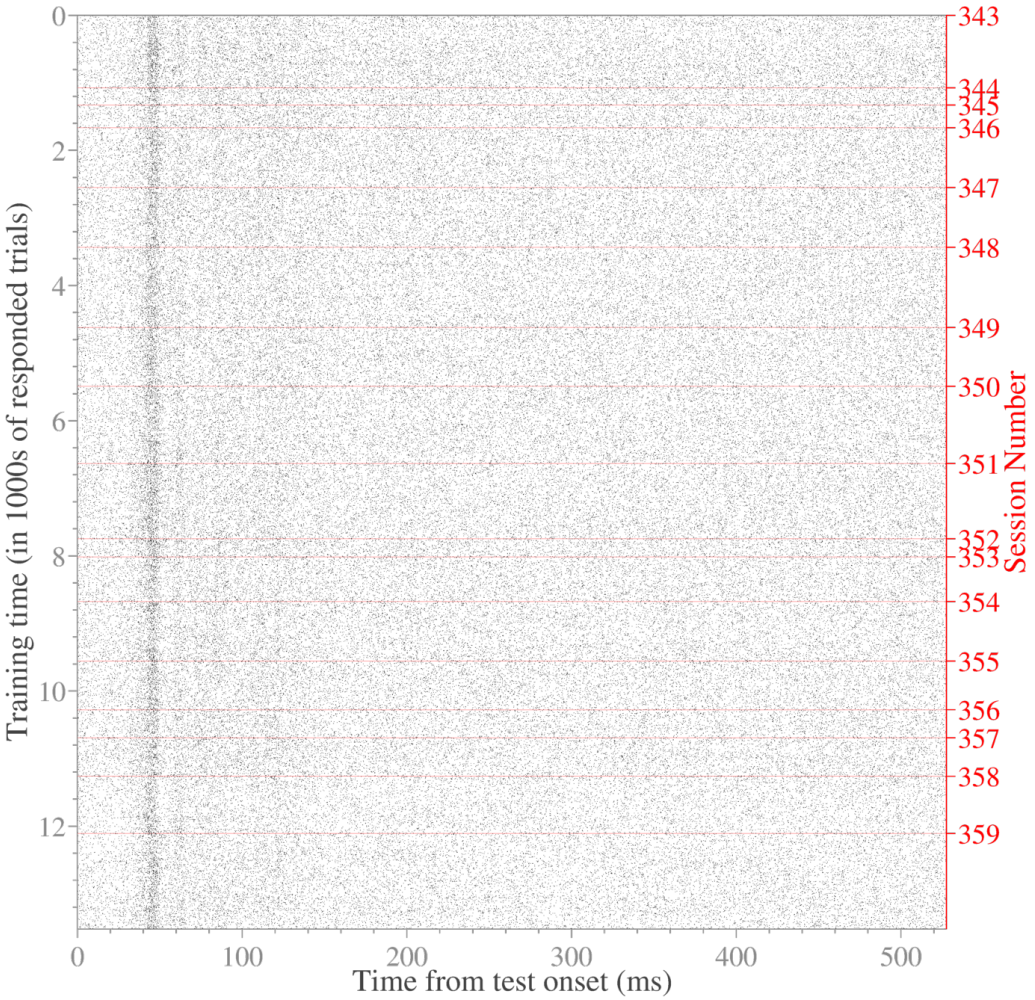

FIGURE 2.2. *Rastergram showing every spike recorded from channel* 11 *of* M1 *in* V1 *during test stimulus presentation.* Along the x-dimension, the time since stimulus onset at which the spike was recorded. Along the y-dimension, the total number of unaborted trials. Trials from all experimental sessions are concatenated along the y-dimension, with the inter-session breaks indicated by red lines.

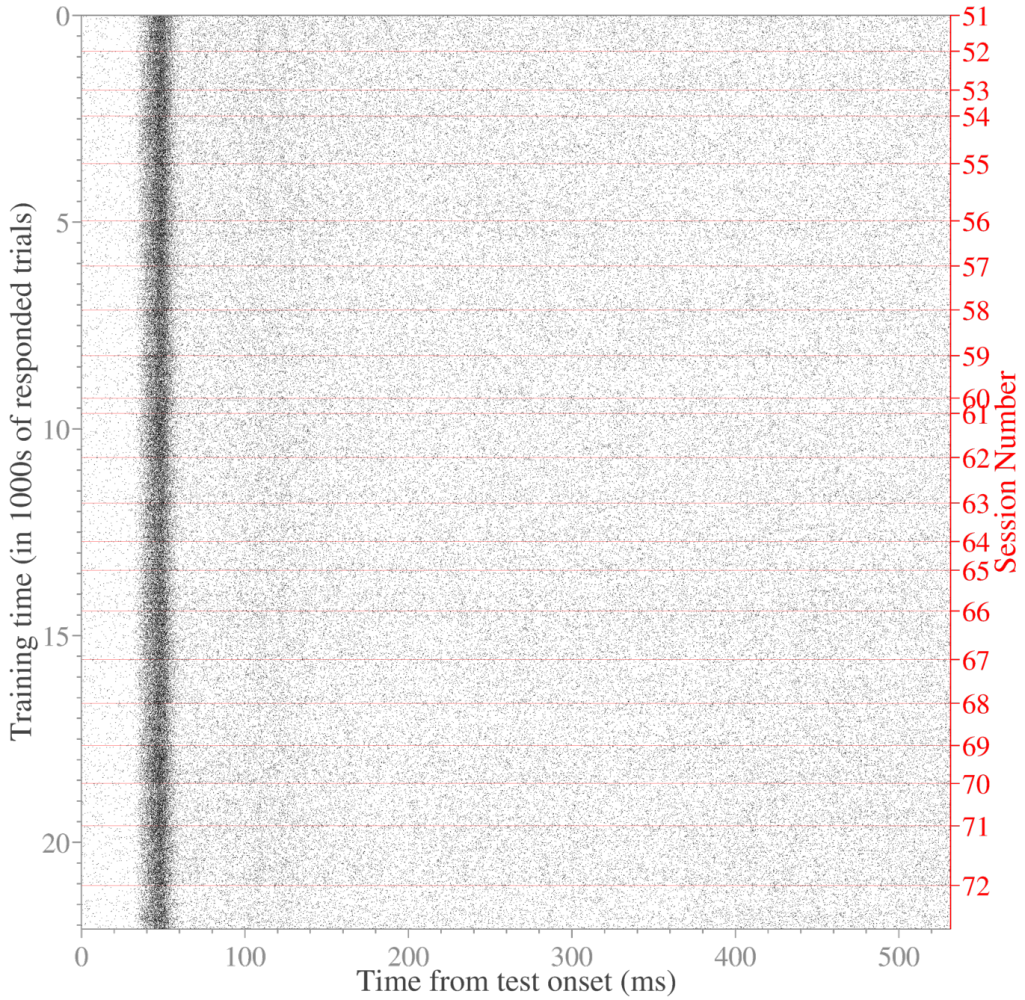

FIGURE 2.3. *Rastergram showing every spike recorded from channel* 12 *of* M2 *in* V1 *during test stimulus presentation.* Along the x-dimension, the time since stimulus onset at which the spike was recorded. Along the y-dimension, the total number of unaborted trials. Trials from all experimental sessions are concatenated along the y-dimension, with the inter-session breaks indicated by red lines.

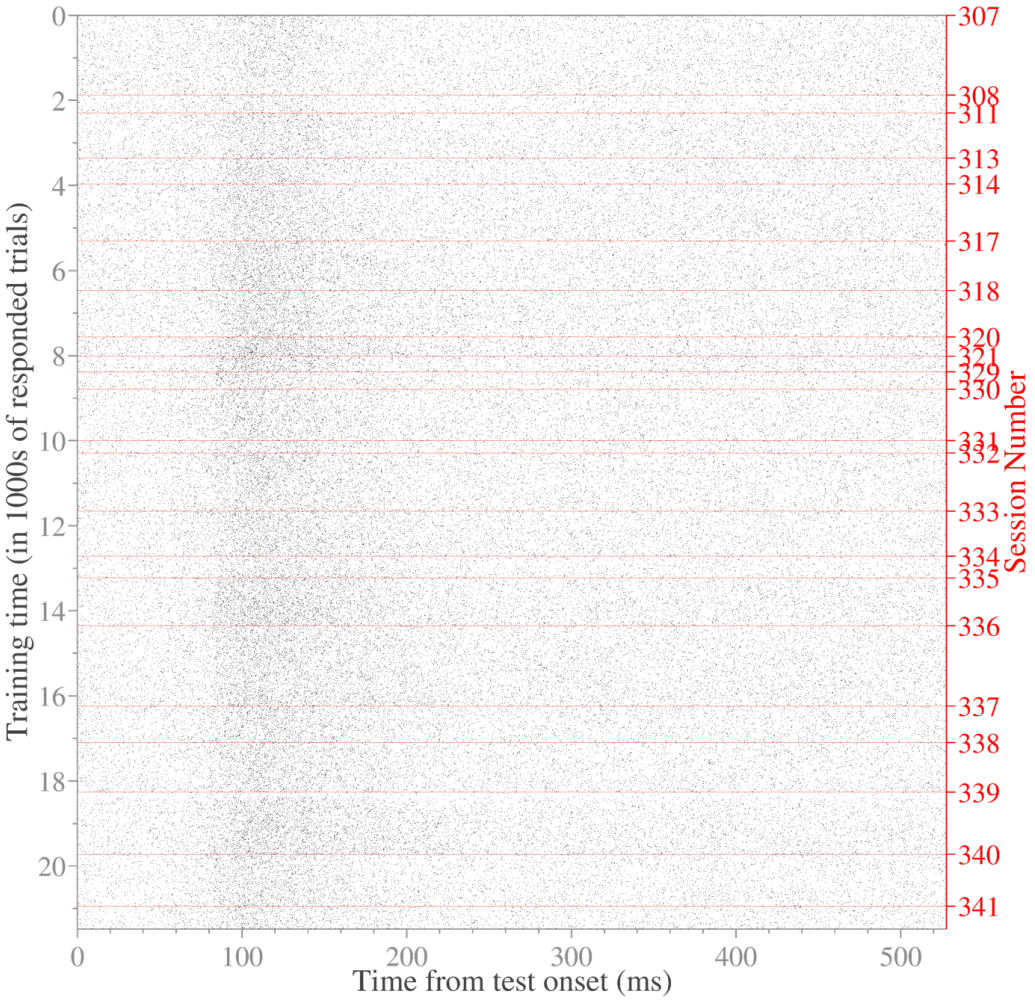

FIGURE 2.4. *Rastergram showing every spike recorded from channel* 51 *of* M1 *in* V4 *during test stimulus presentation.* Along the x-dimension, the time since stimulus onset at which the spike was recorded. Along the y-dimension, the total number of unaborted trials. Trials from all experimental sessions are concatenated along the y-dimension, with the inter-session breaks indicated by red lines.

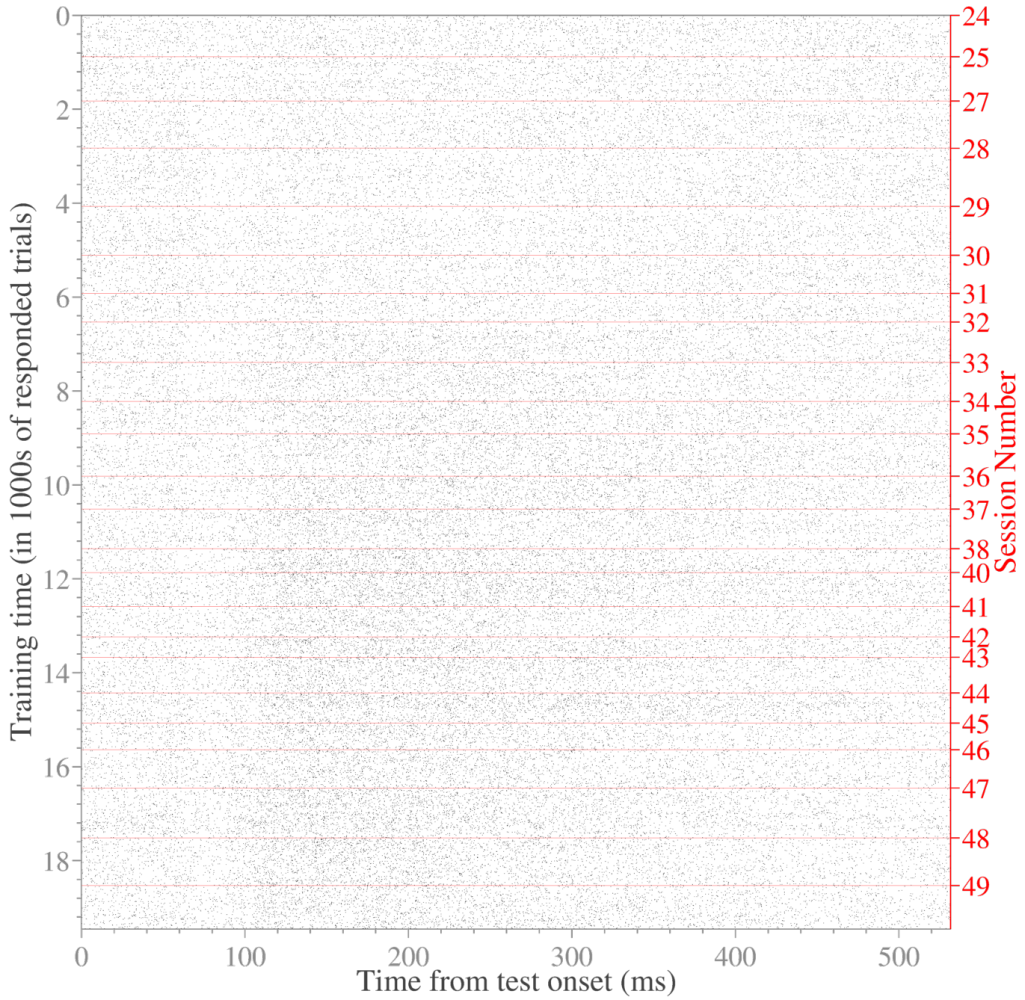

FIGURE 2.5. *Rastergram showing every spike recorded from channel* 6 *of* M2 *in* V4 *during test stimulus presentation.* Along the x-dimension, the time since stimulus onset at which the spike was recorded. Along the y-dimension, the total number of unaborted trials. Trials from all experimental sessions are concatenated along the y-dimension, with the inter-session breaks indicated by red lines.

shown for each subject, these properties were common to most of the simultaneously captured neural recordings. For V4, we observe a longer response latency of around 100 ms (Figure 2.4 and Figure 2.5). For M2, spiking appears to be inhibited before the elevated response begins.

We quantified the change in firing rate evoked by the stimulus relative to the background spontaneous activity with a sensitivity analysis, discussed in Section 2.6. Next, we will consider the how the firing rate is typically related to the contrast of the stimulus in Section 2.5.

2.5 STIMULUS RESPONSE CURVES

By comparing the contrast of the stimulus with the averaged evoked firing rate, we can investigate the relationship between stimulus and response. For some channels, the multi-unit response recorded was untuned, with the same firing rate evoked by each stimulus, on average (not shown). For most channels, there was a stimulus dependent response which increased monotonically. Some channels showed a more highly tuned response than others, indicated by a steeper response curve or reduced noise (measured as the standard deviation of the response over repetitions). Example contrast tuning curves, which are stereotypical for the tuned responses we observed, are shown in Figure 2.6.

2.6 SENSITIVITY ANALYSIS

One simple method of comparing how the encoding of stimuli changes over time is to use the sensitivity index, d'. This gives a measure of how separable the signal and the noise are, by comparing the difference in their means with the overall standard deviation. As such, it is one of several methods to measure the SNR of a communication channel.

For Gaussian distributed data, the sensitivity index is defined as

$$d' = \frac{\mu_{\text{stim}} - \mu_{\text{noise}}}{\sigma_{\text{joint}}}, \tag{2.2}$$

where the joint standard deviation is the root mean square of the standard deviation for each of two distributions,

$$\sigma_{\text{joint}} = \sqrt{\frac{\sigma^2_{\text{stim}} + \sigma^2_{\text{noise}}}{2}}. \tag{2.3}$$

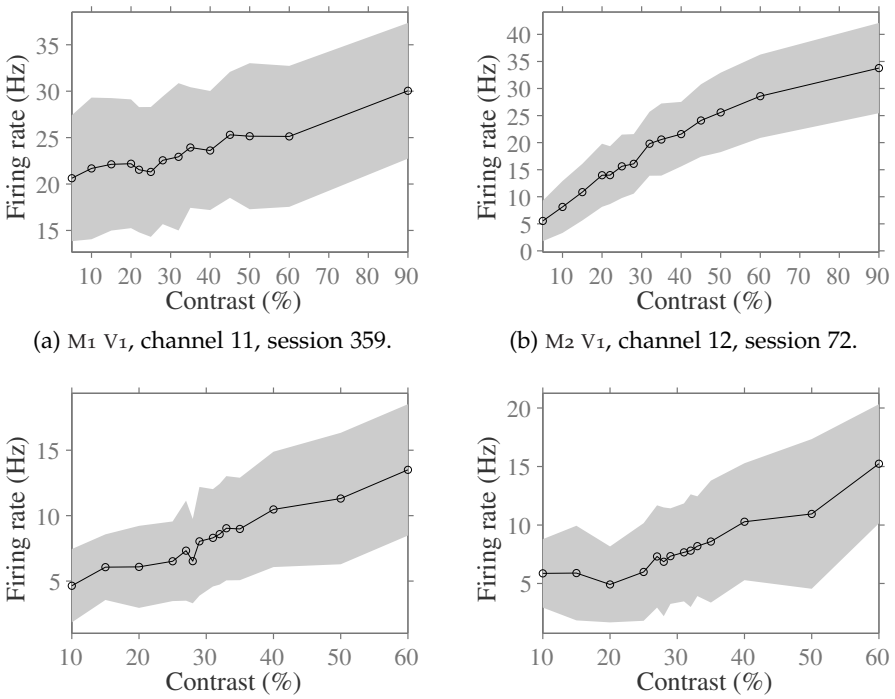

(a) M1 V1, channel 11, session 359.

(b) M2 V1, channel 12, session 72.

(c) M1 V4, channel 51, session 341.

(d) M2 V4, channel 6, session 49.

FIGURE 2.6. *Stimulus response tuning curves.* In each subfigure, we show the firing rate evoked by each test stimulus during the final recording session. The average firing rate is shown (black line), along with the standard deviation over all stimulus repetitions (shaded grey region).

For our analysis, the noise is the spiking activity during periods of spontaneous activity. With the sample stimulus and 14 test stimuli with differing contrast levels, we have 15 possible signals to choose from for each dataset. Since it has the most presentations and lies in the middle of the range of the contrasts, we will just consider d' with respect to the response signal when presenting the sample stimulus.

The number of spikes over a finite duration, which cannot be negative, is typically Poisson distributed instead of Gaussian distributed. However, the two distributions do converge for large n, and so we disregard this and use the Gaussian form of the definition of d'.

2.6.1 *Methods for sensitivity analysis*

To compute d', we used the number of spikes occurring during a 1050 ms period of activity. The spontaneous (noise) activity was defined as the number of spikes detected during the 525 ms immediately preceding the sample stimulus onset. The signal activity was the number of spikes during the 525 ms immediately following the sample stimulus onset. From this, d' was computed using Equation 2.2.

To investigate whether d' changed significantly during the course of our experiments, we compared the average d' during the first and final three experimental sessions (intervals which we denote A and B, respectively). A paired t-test (two-tailed) was used to study whether d' consistently increased or decreased for the channels.

The violin plots (see, for instance, the upper-right panel of Figure 2.7a) show the Gaussian kernel density estimation of the distribution over channels of d' before and after training (intervals A and B). This bandwidth of the Gaussian kernel was determined using the rule of thumb bandwidth estimator,

$$h = \hat{\sigma} \left(\frac{4}{3n} \right)^{\frac{1}{5}}, \tag{2.4}$$

where n is the number of samples and $\hat{\sigma}$ is the estimated standard deviation for the population determined from these samples. We applied the bandwidth estimator to the set of d' averaged over the first three sessions of training, **A**, and averaged over final three sessions, **B**, to find h_A and h_B. In each plot, the same kernel bandwidth of $H = \min(h_A, h_B)/2$ is used when estimating the density at A and at B. This ensures sufficient detail about the distribution is preserved for each, and the two are comparable with each other.

2.6.2 *Results for sensitivity analysis*

For V1, we found d' decreased with training (see Figure 2.7). A similar result was observed for each subject. The average change in the sensitivity index was $\Delta d' = -0.323$ ($p = 0.02$, paired t-test) for M1 and $\Delta d' = -0.419$ ($p < 4 \times 10^{-7}$, paired t-test) for M2.

The results for V4 contrast with our findings for V1. For M1, some V4 channels marginally increased and others marginally decreased their d' with training (Figure 2.7c). Overall, there was on average a small increase in d', with $\Delta d' = +0.052$, which was not a statistically significant change ($p = 0.46$).

For M2, many V4 channels were either indifferent to the stimulus, $d' = 0$, or were suppressed by it, $d' < 0$ (Figure 2.7d) on the first day of the experiment. There was a significant increase of $\Delta d' = +0.491$ ($p < 7 \times 10^{-8}$) over training. However the final d' for almost all channels recorded for M2 was still lower than the average d' for M1.

2.6.3 *Discussion of sensitivity*

By analysing the sensitivity index, d', we can see whether channels become more or less responsive to our stimulus class over time. Since V1 is an early step in the visual processing hierarchy, its neurons respond strongly to simple stimuli such as the sinusoidal gratings we present. Consequently, neurons have large responses to our stimuli even from the first session of the experimental training. Over time, we found a decrease in sensitivity in V1 for both subjects. We suspect this decrease in sensitivity of the neural response in V1 to the sample stimulus is due to unpreventable deterioration in the recording quality of the implanted chronic electrodes over time. Over time, the noise increases and the SNR falls, which leads to a reduction in the distinguishability of the two activity distributions.

On the other hand, V4 is higher up the visual hierarchy and in general responds to more a complex stimulus class. For M1, many of the neurons we recorded from were responsive to the primitive Gabor stimulus from the beginning of training. But for M2, this was not the case — on the contrary, many neurons were suppressed by the Gabor stimulus. With training, neurons recorded in M1 did not notably change their sensitivity to the sample stimulus, whereas d' did increase for M2.

We make particular note of the fact that d' in V4 increased for M2 from initially mostly negative values. In principle, a decrease in activity in response to a stimulus can provide as much information about the presence of the stimulus as increase in activity. However, it is difficult for neurons to increase their spontaneous activity due to the constraining effects of homeostasis, and it would be energetically inefficient

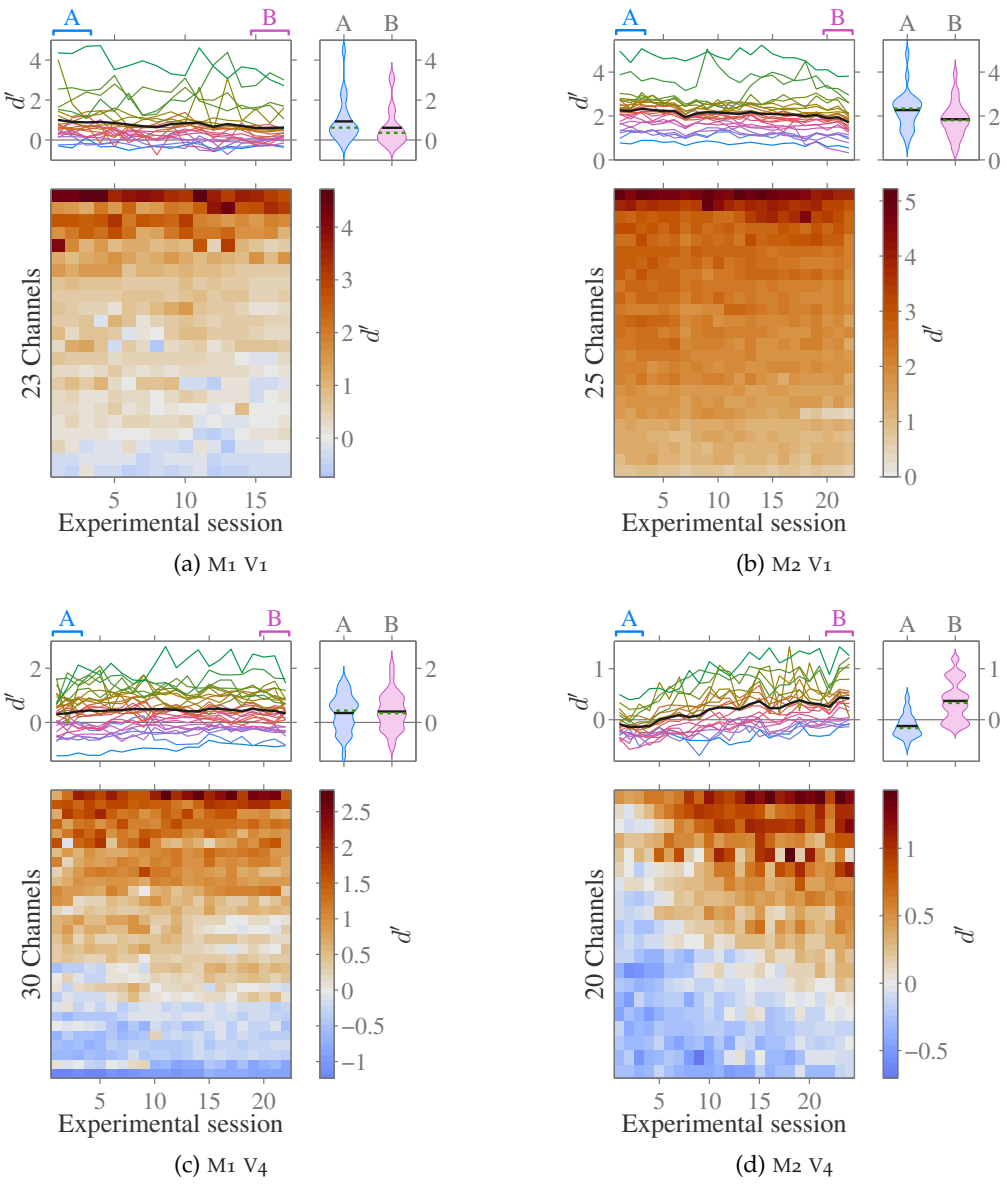

(a) M1 V1 (b) M2 V1

(c) M1 V4 (d) M2 V4

FIGURE 2.7. *Change in sensitivity index, d', over training sessions.* (a): d' for M1 V1, shown for each recording channel, with channels ordered according to average d' over all sessions. Above, traces of d' for each channel (colours), and average over channels (black). Below, heatmap showing d' for each channel. Right top, violin plots showing distribution over channels of the average d' in the first (A) and last (B) three sessions, with mean (solid black line) and median (dashed green line) over channels indicated. The violin plot shows a Gaussian kernel density using a bandwidth determined automatically as described in Section 2.6.1. (b): Same as (a), but for M2. (c) and (d): Same as (a) and (b), but for V4.

for them to do so. Therefore, since the firing rate of a neuron cannot fall below 0 there is a smaller limit to the amount by which firing rates can differ if the information about the stimulus is conveyed by a reduction in activity compared to the background rate. To provide more sensitivity for the response to our experimental stimuli, it thus makes sense for neurons which are suppressed by the stimulus class to increase their responses such that they are enhanced by its presence. In practice, the de-suppression of the responses may arise not from the need of many individual neurons to encode the stimulus, but from a small number increasing the magnitude of their responses and then the connected neurons (which are positively correlated) increase their responses also.

From these results, we hypothesise that the sensitivity of the response to the experimental stimuli increases for the local network retinotopic to the stimulus location if it is too low for the network overall. If the neurons are sufficiently sensitive to the stimulus to begin with (if d' is high enough) then the sensitivity remains the same and does not increase with training. Of course, the recorded sensitivity may decrease due to the decline in the recording quality.

With this measure, we can determine which channels contain neurons which change their relative responsiveness to the stimulus class, but we do not know how the distribution of responses change across the 14 different stimuli. It is certainly plausible for neurons which begin their training already responsive to the stimuli to change their distribution of activity with respect to the contrast of the stimulus to provide more pertinent information for the experimental task. For instance, this would be achieved if the absolute activity in response to the sample stimulus remains the same but the rate of change of activity with respect to the contrast of the stimulus increases.

2.7 NEURAL CORRELATIONS

To provide a simple measure of the similarity in the neural responses given by the recording channels, we computed the correlation in their responses. As described in Section 1.4, we can consider both the signal correlation and the noise correlation.

To measure the signal correlation, we first averaged the response (over all repetitions) elicited by each stimulus for each recording channel. Then, for each pair of channels we took the correlation in the average responses to each stimulus. Channels which respond to the set of stimuli in a similar manner will have a high signal correlation, irrespective of how the response curve is shaped.

To determine the noise correlation, we measured the correlation in responses from a pair of channels obtained over all presentations of single stimulus. This was repeated for each stimulus class, and then averaged over the stimuli. Channels whose

responses vary in a similar manner for a simultaneously recorded trial will have a high noise correlation.

In both cases, we measured the correlation between the responses from the two channels using the Pearson correlation coefficient. If we let the responses observed from our two recording channels be denoted by the random variables X and Y, their Pearson correlation coefficient is given by

$$\rho(X,Y) = \frac{\operatorname{cov}(X,Y)}{\operatorname{var}(X)\,\operatorname{var}(Y)}. \tag{2.5}$$

This provides a measure of the covariance between X and Y which is normalised again their standard deviations, meaning that $-1 \leq \rho \leq 1$ and ρ is robust against linear rescaling of either X or Y (or both). If $\rho = \pm 1$, there is a perfect linear relationship between X and Y, whereas $\rho = 0$ when X and Y are completely independent of one another.

To investigate whether the signal and noise correlations rose or fell during the experiments, we compared the average correlation over the first and last three sessions (intervals A and B). We used a paired t-test to measure whether the correlations changed significantly over all pairs of channels.

2.7.1 *Results for neural correlations*

For both brain regions, the signal correlation between pairs channels is shown in Figure 2.8. For V1, the signal correlations significantly increased for both M1 and M2 ($p < 1 \times 10^{-12}$ and $p < 3 \times 10^{-25}$, respectively). With M1, the signal correlations rose on average by 0.107 ± 0.014. The signal correlation was very high for M2 from the start of the experiment, and consequently the increase was only a tenth of the magnitude (0.0100 ± 0.0009). For V4, the signal correlations decreased for M1 ($p = 0.00054$), but there was no significant change for M2 ($p = 0.73$).

The noise correlation between pairs of channels is shown in Figure 2.9. For V1, the noise correlations increased for M1 ($p < 4 \times 10^{-6}$) but decreased for M2 ($p < 4 \times 10^{-34}$). For V4, noise correlations increased for both subjects ($p < 3 \times 10^{-22}$ and $p = 0.0020$ respectively).

2.7.2 *Discussion of neural correlations*

Signal correlation provides a measure of the heterogeneity of the responses. For M2 V1, all recording channels responded to the stimuli strongly and with a similar stimulus-

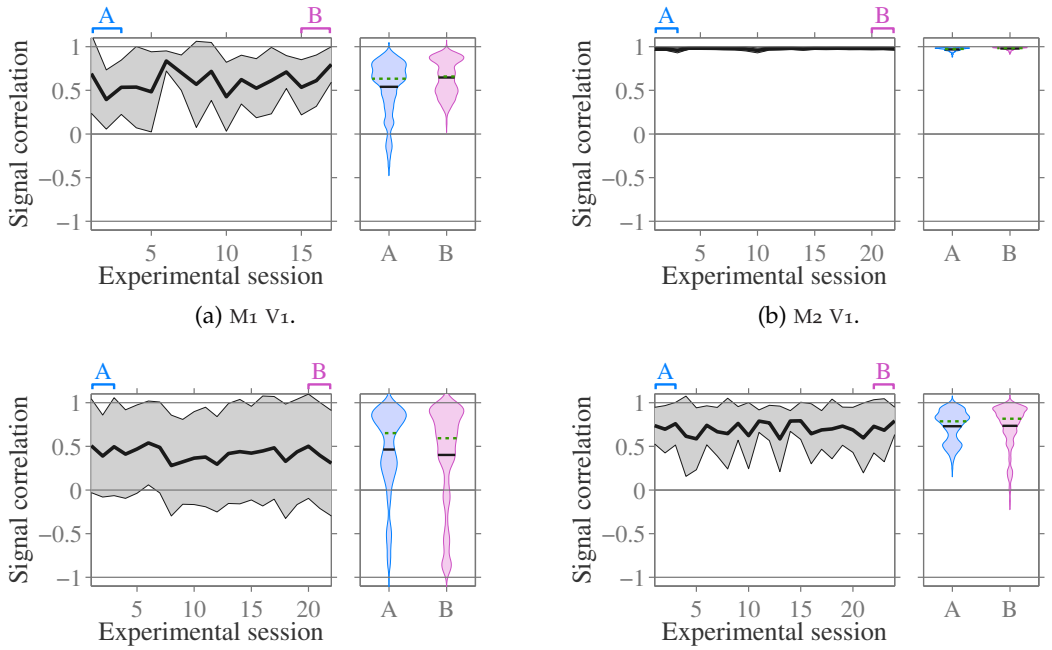

(a) M1 V1. (b) M2 V1.

(c) M1 V4. (d) M2 V4.

FIGURE 2.8. *Signal correlation between pairs of recording channels.* The correlation in the average firing rate in response to each stimulus condition was computed for each pair of channels ((a) 253 pairs of channels, (b) 300 pairs, (c) 435 pairs, (d) 190 pairs). Main panels: average across all pairs of channels, with standard deviation indicated by the shaded region. Right hand panels: the Gaussian kernel density for the distribution over channel pairs of the average signal correlation during the first (*A*) and last (*B*) three sessions, with mean (solid black line) and median (dashed green line) indicated. The bandwidth for the Gaussian kernel density estimate was determined as described in Section 2.8.1.

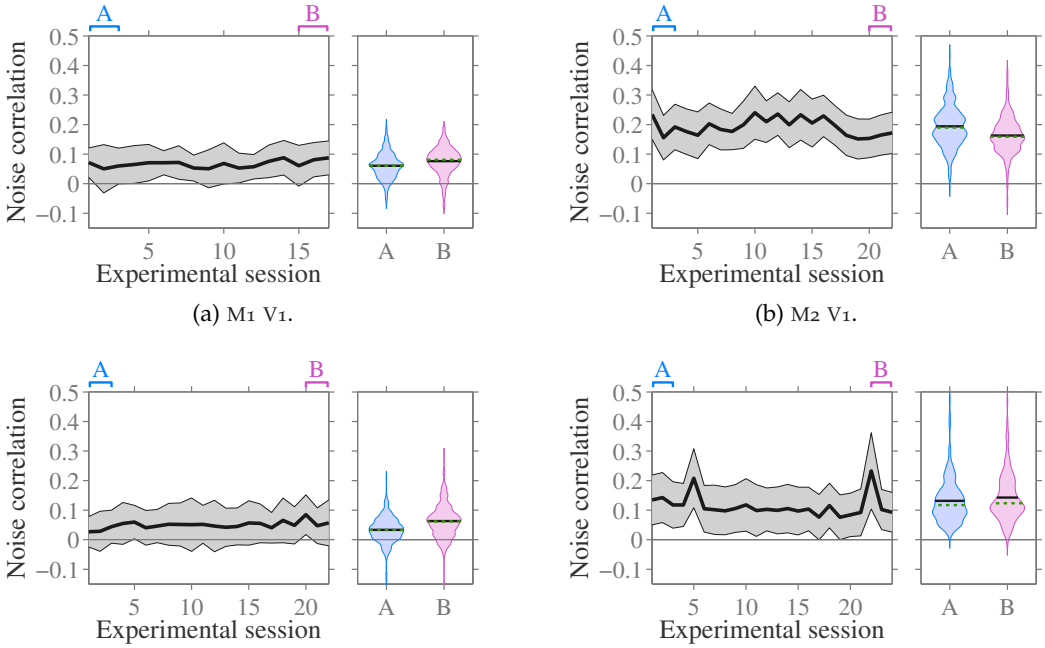

(a) M1 V1. (b) M2 V1.

(c) M1 V4. (d) M2 V4.

FIGURE 2.9. *Noise correlation between pairs of recording channels.* The correlation in the average firing rate in response to each stimulus condition was computed for each pair of channels ((a) 253 pairs of channels, (b) 300 pairs, (c) 435 pairs, (d) 190 pairs). Main panels: average across all pairs of channels, with standard deviation indicated by the shaded region. Right hand panels: the Gaussian kernel density for the distribution over channel pairs of the average noise correlation during the first (*A*) and last (*B*) three sessions, with mean (solid black line) and median (dashed green line) indicated. The bandwidth for the Gaussian kernel density estimate was determined as described in Section 2.8.1.

response tuning curve, and so the signal correlation was very high. Other data sets had a more diverse set of neurons, and hence a lower signal correlation.

As described in Section 2.5, the majority of neurons have a contrast-response curve which increases monotonically. Under such an encoding regime, the amount of information encoded by a pair of neurons will be higher if their responses are anti-correlated. (See Section 1.4.2 for discussion of this). Consequently, we might expect noise correlations to decrease with training, since this provides one potential mechanism for the performance of the network to improve. However, we instead found that noise correlations increased with training for M1 in both V1 and V4, and only decreased significantly for M2 V1.

2.8 INFORMATION IN INDIVIDUAL CHANNELS

We now apply the principles of Shannon information, as described in Section 1.3, to the perceptual learning data. We are interested in how easy it is to determine which contrast the stimulus was presented with by observing the neural activity in response to the stimulus. Since the subject's performance increases with training, we expect to find the amount of information encoded in the neural activity to increase with training. This much is trivial, since perception occurs within the neural activity of an individual. What will be interesting to uncover is *where* the neural changes take place — in V1, in V4, neither, or both?

To make its decision, the subject potentially has access to all the neurons we have recorded and all the neurons in the brain from which we have not recorded. For the best idea of how much information the brain has access to from the recordings we have available, we could evaluate how much information is contained in the vector of neuronal responses for every recording channel. However, this is problematic. As the number of data streams combined into the response vector increases, the number of possible unique response vectors increases exponentially. However, the number of trials recorded is fixed, and the number of possible response vectors must be constrained to prevent the estimated amount of information diverging to infinity (see Section 1.3).

Therefore, in this section we consider the information about the contrast of the stimulus encoded in the firing rate detected from only a single channel at once. In doing so, we will ignore the possible redundancy or synergy in the information encoded by the response of multiple channels. Later, in Section 2.12, we will consider the total information encoded in the population response. It should be noted that, since the spikes detected from each channel have been left unsorted and not resolved into clusters corresponding to individual neurons, this will be a multi-unit analysis,

but only in the sense of neighbouring neurons being detected by the same electrode contact.

2.8.1 *Methods for computing information*

The mutual information between the spiking activity during the presentation of the test stimulus and the identity of that stimulus was computed using the *Information Breakdown Toolbox* for MATLAB (Magri et al., 2009). Bias correction was performed using the PT method (see Section 1.3) unless indicated otherwise.

To test the significance of changes in information over time, we used a paired Student's t-test to compare the difference in information values in **A** and **B** against the null-hypothesis of no change between points A and B. Although the distribution of information values is evidently non-Gaussian (it is bounded below at 0 bits), the distribution in differences in information is close to Gaussian. We could instead have used the Mann–Whitney U test to compare the two distributions **A** and **B**. This test does not assume the two distributions are Gaussian, but makes the additional assumption that all samples are independent. Since we record from the same set of channels for both **A** and **B**, we are violating the independence assumption, and so the paired Student's t-test is a more appropriate choice.

We show the Gaussian kernel estimation of the distribution of information over channels (a "violin plot", right-hand panel of Figure 2.10a, for instance) at the start (A) and end (B) of training. These were found using the same method as described in Section 2.6.1. Again, the kernel bandwidth was selected as $H = \min(h_A, h_B)/2$ to ensure sufficient detail was captured and the two density estimates are comparable.

2.8.2 *Initial analysis*

First, we will consider the amount of information about the stimulus contained in a simple firing rate encoding. For each test stimulus presentation, our response is the total number of spikes which were detected from a single channel during the first 527 ms of the stimulus presentation.[3]

For each recording channel, we computed how much information was contained in this overall firing response about the identity of which stimulus had been presented. The results of this initial analysis are shown in Figure 2.10. We found that information in the overall firing rate of V1 channels increased with training for M2 ($(+0.069 \pm 0.017)$ bits, or $(+16 \pm 5)$ % relative change; $p = 0.0004$) but not for M1

3 This duration is chosen because there is slight variation in the stimulus presentation time, and 527 ms slightly shorter than the shortest presentation duration.

$((-0.051 \pm 0.029)$ bits or (-34 ± 19) % relative change; $p = 0.09$). For V4, there was an increase in information for both subjects, however this increase was significant for M2 $((+0.056 \pm 0.013)$ bits or $(+87 \pm 21)$ % relative change; $p = 0.0005$) but was not significant for M1 $((+0.028 \pm 0.020)$ bits or $(+22 \pm 16)$ % relative change; $p = 0.17$).

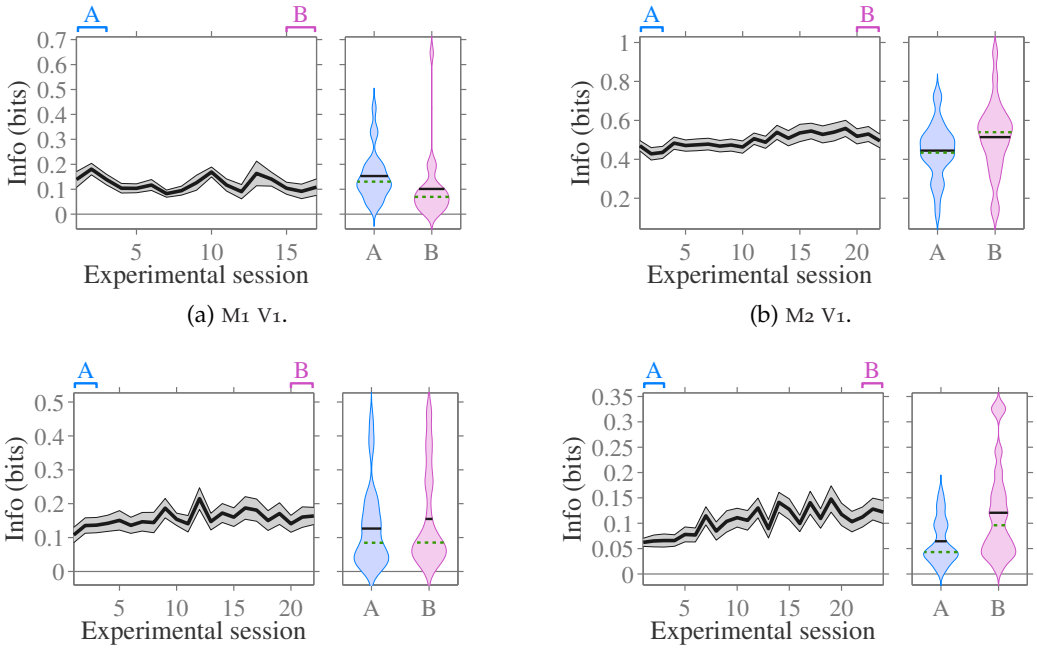

(a) M1 V1. (b) M2 V1.

(c) M1 V4. (d) M2 V4.

FIGURE 2.10. *Information about the test stimulus contained in the firing rate during test presentation and its progression over training sessions.* Main panels: information, averaged over channels ((a) 23 channels, (b) 25 channels, (c) 30 channels, (d) 20 channels), with standard error across channels indicated by the shaded region. Right hand panels: distribution over channels of the information contained in the first three sessions (A) versus last three sessions (B), with mean (solid black line) and median (dashed green line) over channels indicated. The violin plot shows a Gaussian kernel density, using a bandwidth determined as described in Section 2.8.1. The PT bias correction method was used, without further correction to the residual bias.

For some channels, the measured information was a *negative* value. Consequently, the violin plots in Figure 2.10 showing the distribution of information values across channels extend below 0. This is not because these channels contain a negative amount of information about the stimulus — in fact it is mathematically impossible for there to be less than 0 mutual information between two random variables (see Equation 1.3 and its discussion). Instead, this observed negative value is due to the inherent uncertainty of our measurement of mutual information, which we corrected against the finite-sampling upward bias using the PT method. If we were to measure two completely independent events and perfectly correct for the bias due to finite sampling, our measurements of the information would be distributed around 0.

As described in Section 2.6.3, the non-significant reduction of information witnessed for M1 V1 is most likely explained by the unavoidable reduction of recording signal quality over time. However, one channel had a large increase in information content against the trend observed for other channels on this electrode array (see Figure 2.10a, right panel). This channel is one of a minority whose response profile changes completely between consecutive sessions, and so the sudden large increase in information is most likely due to a small movement in the electrode contact changing which neurons are measured in the data. We address this discrepancy next.

2.8.3 *Removing inconsistent channels*

We noted that some channels were moving between sessions. In general, it is just as likely for electrode contacts to move into locations where they are more informative as to move such that they are less informative. However, to make the results more comparable across sessions, we chose to remove channels whose raster profile (such as those shown in Section 2.4) and overall firing rate in response to the 30 % sample stimulus changed clearly and suddenly from one session to the next. We manually selected a small number of channels on this basis, and removed them from the analysis. For each dataset, the number of channels included afterwards is indicated in Table 2.5.

Region	Animal	Channels before	Channels after
V1	M1	23	14
	M2	25	20
V4	M1	30	25
	M2	20	18

TABLE 2.5. *Number of channels before and after restriction on the basis of consistent or smoothly changing firing rates across sessions.*

Besides the channel for M1 V1 with an aberrantly large increase in information mentioned above, there is little impact on the results (Figure 2.11) compared with previously (Figure 2.10). For this dataset, M1 V1, the removal of the outlier means the reduction in information over time is now statistically significant ((-0.049 ± 0.018) bits or (-41 ± 15) %, $p = 0.015$). For the other datasets, there were no notable changes.

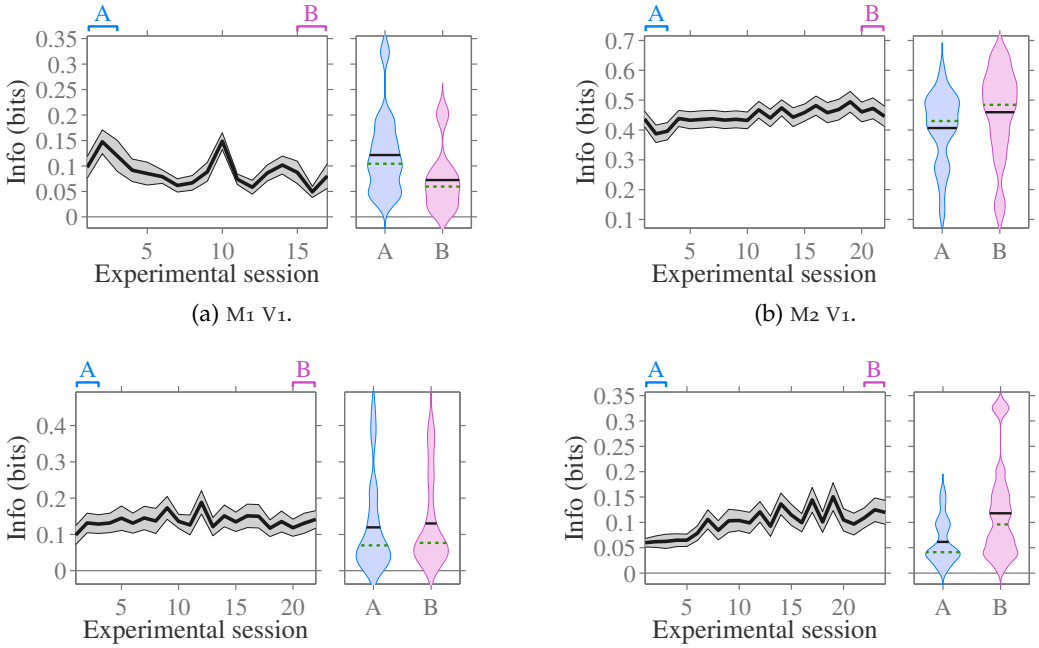

(a) M1 V1. (b) M2 V1.

(c) M1 V4. (d) M2 V4.

FIGURE 2.11. *Information, after removing inconsistent channels, about the test stimulus contained in the firing rate during test presentation and its progression over training sessions.* Main panels: the average over channels ((a) 14 channels, (b) 20 channels, (c) 25 channels, (d) 18 channels) with standard error across channels indicated by the shaded region. Right hand panels: distribution over channels of the information contained in the first three sessions (A) versus last three sessions (B), with mean (solid black line) and median (dashed green line) over channels indicated. The PT bias correction method was used, without further correction to the residual bias.

2.8.4 *Correcting stimulus class imbalance*

As mentioned in Section 2.2.6, the stimulus presentation procedure was to include a fixed number of repetitions of each stimulus in a block of trials and present them in a random order. At the end of each block, additional trials were presented for stimuli which the subject responded to incorrectly. Since stimuli with a contrast far from the pedestal contrast of 30 % are much easier for the subject, trials which were repeated at the end of the block were not uniformly distributed across the stimuli. Overall, this means that harder stimuli close to 30 % contrast are presented more often than the easier stimuli, as depicted in Figure 2.12.

To compute the amount of information about the stimulus contained in the animal's response, we do not need to have a uniform distribution across stimuli. However, the subject becomes better at the task with training, and the change in relative performance is necessarily not uniform across sessions. For M1, the proportion of trials which belong to each stimulus class was very similar throughout the experiment, as shown in Figures 2.12a and 2.12c. However for M2, this was not the case. During training with the V1 stimulation protocol, there was a larger increase in performance for the harder contrast stimuli, which were consequently presented less frequently by the end of training — the percentage of stimuli with a contrast in one of the hardest 6 categories (closest to 30 % contrast) fell by 2.5 % in absolute terms. This change in stimulus class distribution may seem small, but the size of this change is comparable to the amount of change in information we previously computed. When training M2 with the V4 stimuli, the overall performance was initially lower. Consequently, the largest increase in performance was that attained for the easier stimuli, and the percentage of trials featuring one of the 6 easiest stimuli (furthest from 30 % contrast) fell by 5.4 % in absolute terms.

Changes in the distribution of classes between sessions can impact our analysis in two ways. Firstly, as described Equation 1.3 the amount of information between stimulus, S, and response, R, is dependent on the entropy of the stimulus, $\mathrm{H}(S)$. As the distribution of stimulus classes moves closer to uniform, the stimulus entropy increases. Since our stimulus distribution generally tends to become flatter after training, this may cause the measured information to be inflated as training progresses. Secondly, as seen for M2 V1, the proportion of trials which are in the easier categories is higher for later sessions. These stimuli will have the most distinguishable responses, and their increasing prevalence in the dataset may also produce an artificial increase in information with training.

We corrected the class imbalance on a session-by-session basis by subsampling the trials for more frequent stimulus classes down to the frequency of the least common

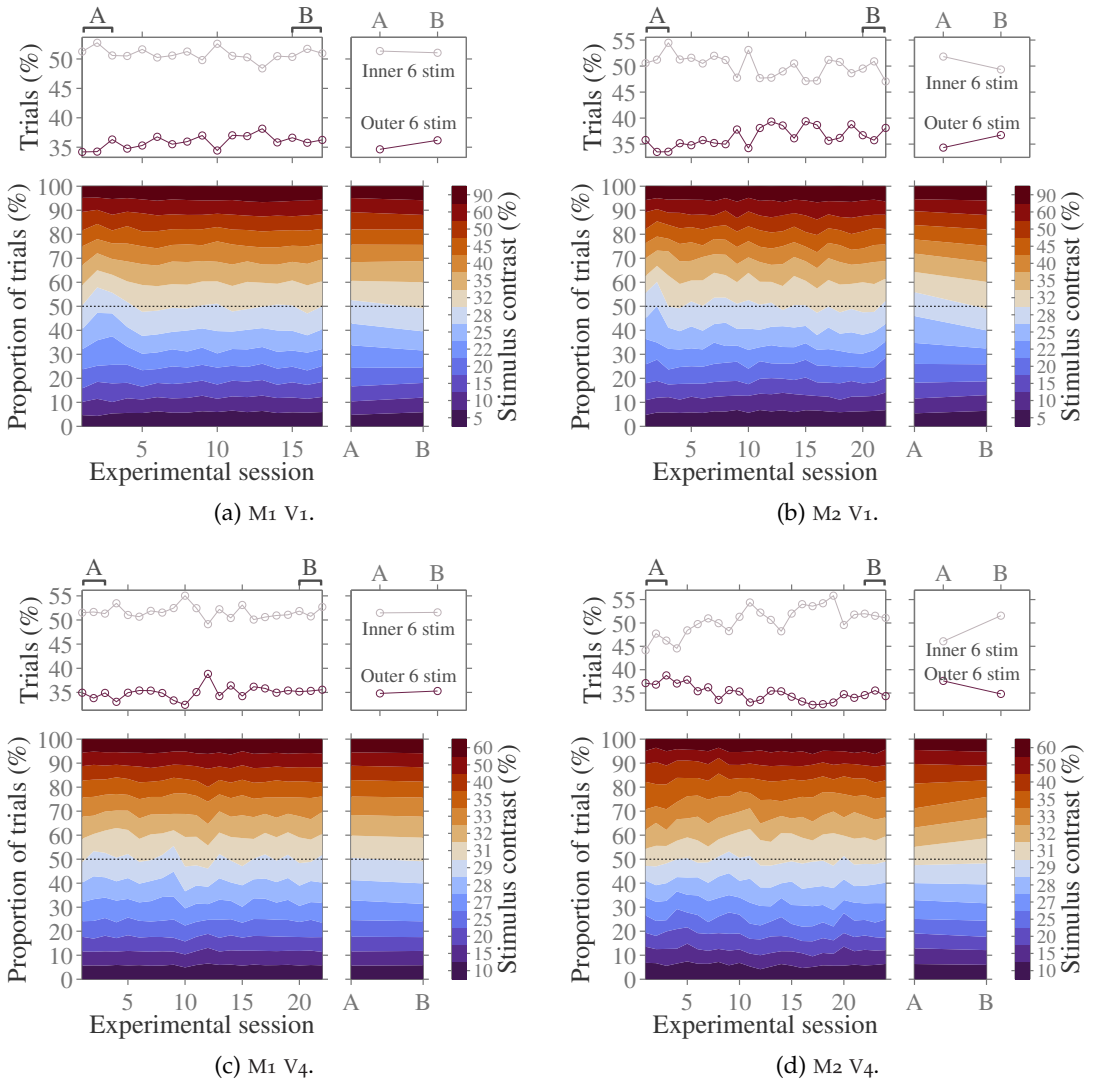

(a) M1 V1.

(b) M2 V1.

(c) M1 V4.

(d) M2 V4.

FIGURE 2.12. *Proportion of trials in each stimulus class.* Main panels: the proportion (%) of trials which belong to each stimulus class, with colours indicated to the right, as a function of experimental session. Above panels: the "inner 6" contrasts closest to 30 % (grey) and "outer 6" contrasts furthest from 30 % (purple). See Table 2.3 for the 6 contrasts in each group by brain region. Right hand panels: proportion of trials presented during the first (*A*) and last (*B*) three sessions.

stimulus class. The trials included in the subsample were selected at random across the set of trials for each stimulus, without replacement.

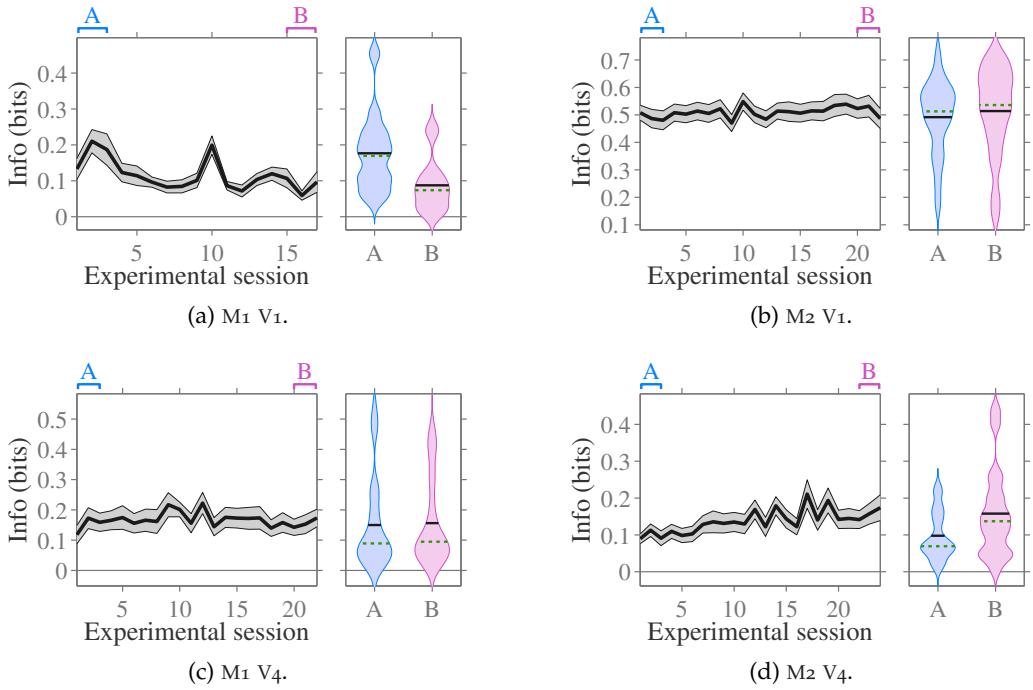

(a) M1 V1. (b) M2 V1.

(c) M1 V4. (d) M2 V4.

FIGURE 2.13. *Information, after correcting for the stimulus class balance in each session, about the test stimulus contained in the firing rate during test presentation and its progression over training sessions.* Subpanels are arranged as per Figure 2.11, with the same number of channels included. The PT bias correction method was used, without further correction to the residual bias.

Overall, we find the amount of information increases when the class imbalance is corrected for (compare the y-scales of Figure 2.13 with those of Figure 2.11). This is because the stimulus entropy, $\mathrm{H}(S)$, has increased when the stimulus distribution became uniform.

As anticipated, correcting for changes in the class balance over time reduces the relative increase in information between the beginning and end of training. For V1, the change in information over training seen in M1 is reduced more ((-0.089 ± 0.023) bits or (-50 ± 13) %, $p = 0.0018$) and the increase in information for M2 is no longer statistically significant ($(+0.022 \pm 0.016)$ bits or $(+4.5 \pm 4.4)$ %, $p = 0.18$). For V4, the outcomes stand unchanged even though the relative change in information is reduced (M1: $(+0.006 \pm 0.022)$ bits or $(+4 \pm 15)$ %, $p = 0.78$; M2: $(+0.060 \pm 0.018)$ bits or $(+61 \pm 19)$ %, $p = 0.004$).

This *post-hoc* class rebalancing was applied throughout the rest of this chapter. Moreover, the subset of trials which was selected was also maintained, to ensure comparability of results across sections.

2.8.5 *Defending against changes in session duration*

A substantial amount of session-to-session variability in the measurements was observed in our results, depicted in the time-course plots of Figure 2.10. A large part of this variability was due to changes in the duration of each session — some sessions contain 5 times as many trials as others.

Although we were utilising the PT bias correction technique, this typically requires 4 trials per response for each stimulus condition to be completely effective (Panzeri et al., 2007). When analysing the amount of information contained in the overall firing rate, the cardinality of the set of spike counts per channel — the number of possible numbers of spikes during the test stimulus presentation — ranges from 3 to 50. The number of trials in one session for an individual stimulus varies from 11 to 191, with the total number of trials per session ranging from 254 to 1889. Consequently, the number of trials per response to a single stimulus varies from 1.2 to 26.5. After correcting for the stimulus class imbalance, the number of trials we are considering from each session falls, ranging from 154 to 1540, exasperating the problem. With this, the number of trials per response ranges from 1.1 to 18.3. Not only is there a 20 fold difference in the number of trials per response, but some sessions have stimuli with only a quarter of the number of repetitions we should be using for the bias correction to be effective (Panzeri et al., 2007).

This shortage of trials per stimulus condition results means the PT bias correction method underestimates the bias for the shorter sessions, leading to an overestimate in the reported information. This is illustrated in Figure 2.14, where we compare the estimated information with the reciprocal number of trials, $1/N$, and find a linear correlation. This is in keeping with the literature, since I_{measured} is known to be proportional to $1/N$ if no bias correction is performed (Treves and Panzeri, 1995).

Without correcting for the bias due to finite sampling, the correlation between $1/N$ and I_{measured} is large and significant. For V1, the Pearson's correlation coefficient (see Equation 2.5) between them was $\rho(I, 1/N) = 0.99$ and $\rho = 0.98$ for M1 and M2 respectively, which was a significant correlation in all cases ($p < 2 \times 10^{-13}$ and $p < 8 \times 10^{-16}$). For V4, $\rho = 0.98$ and $\rho = 0.92$ with p-values $p < 2 \times 10^{-14}$ and $p < 2 \times 10^{-10}$. But even if we correct for the bias with PT or QE, the correlation remains large ($\rho > 0.4$) and significant ($p < 0.04$) for all datasets except M2 V1 with PT, where $\rho = +0.27$ and $p = 0.23$. The correlation is strongest for M1 V1, with $\rho > 0.89$ and $p < 1 \times 10^{-6}$ with either PT or QE bias correction.

There are several potential ways we can correct for the change in bias incurred by the changes in number of trials.

- Subsample all sessions down to the same number of trials (rarefy).

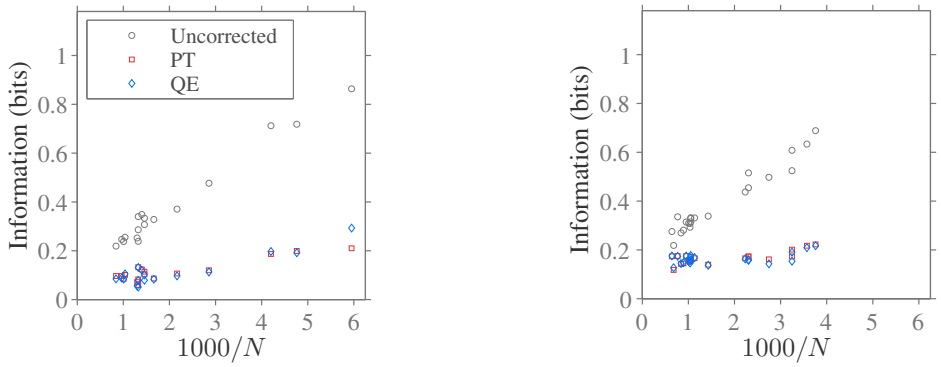

(a) M1 V1.

(b) M2 V1.

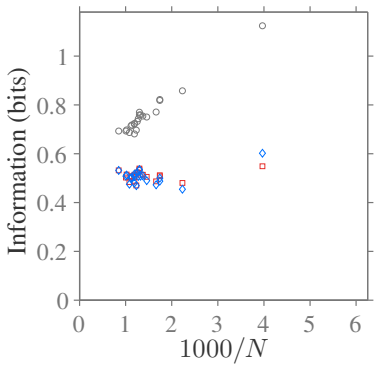

(c) M1 V4.

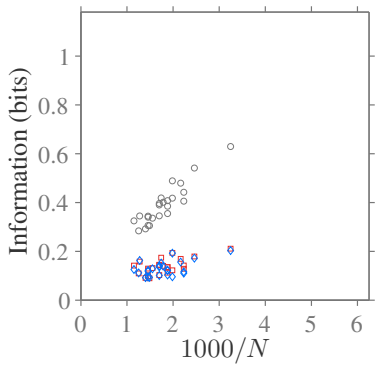

(d) M2 V4.

FIGURE 2.14. *Distribution of measured information as a function of* $1/N$*, where* N *is the number of trials in the session.* Results are shown both without correcting for the finite measurement bias (grey circles), using PT bias correction (red squares), and using QE bias correction (blue diamonds). Information was computed after using subsampling to address the stimulus class imbalance (see Section 2.8.4), and this is reflected in the value of N.

- Use bootstrapping, randomising the mapping between stimulus and response, to estimate the residual bias and subtract this from the reported information.
- Group together stimuli above and below 30 % contrast so we only have two stimulus classes, each with approximately 7 times more trials than before.
- Group together trials across consecutive sessions so we have the same number of trials in each information computation step.

The first method is clearly undesirable, since we would be throwing away most of our data and knowingly operating in the regime where the bias correction method breaks down for all sessions instead of only a few. In such a scenario, the bias on the estimated information would be larger than the actual information and our comparison across sessions would have little validity. Instead, we focus on the three other — more practical — methods, whose outcomes are described below.

2.8.5.1 *Trial-wise analysis*

We now consider what happens if we group together trials from multiple sessions into a single block and analyse them together. Doing so allows us to overcome the difference in bias between sessions, since the same number of trials would be used in each block and this can be set large enough to ensure we are in the correct domain for bias correction to perform adequately. There are typically no more than 25 different firing rates for any single channel, so we grouped together 100 trials of each stimulus condition.

Using this methodology, we focus on the subject's performance as a function of the number of trials which they have completed since the beginning of the experiment, irrespective of how many training sessions these trials are spread across. Therefore, such a technique makes sense if we consider learning to occur during sessions and not to occur between them. However, such a view is in contrast with the hypothesis that one of the important functions of sleep is to facilitate consolidation of memories and learning accumulated during the day. Should this be an important contributor towards perceptual learning, one would expect the breaks between sessions not to be irrelevant but to instead enable an increase in performance even without exposure to the training stimuli.

Since we performed the spike extraction such that the spontaneous firing rate is held constant across sessions for each channel, the firing rate during stimulus presentation is comparable between sessions. This means it is plausible that, when decoding the information, the extracted firing rate corresponding to the stimuli could be similar across consecutive sessions.

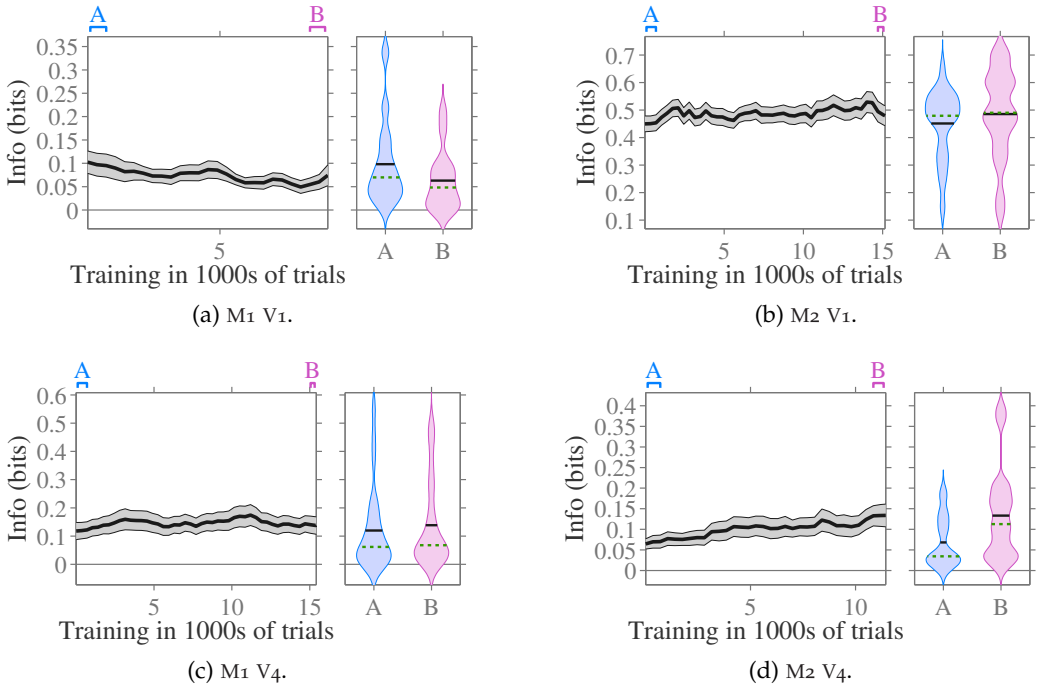

(a) M1 V1.

(b) M2 V1.

(c) M1 V4.

(d) M2 V4.

FIGURE 2.15. *Information about the test stimulus contained in the firing rate during test presentation and its progression over training sessions, estimated across blocks of* 100 *consecutive trials of each stimulus class taken by merging consecutive sessions together to accumulate sufficiently many trials.* Main panels: the average over channels ((a) 14 channels, (b) 20 channels, (c) 25 channels, (d) 18 channels) with standard error across channels indicated by the shaded region. Right hand panels: distribution over channels of the information contained in the first three blocks of 1400 trials (*A*) versus last three blocks (*B*), with mean (solid black line) and median (dashed green line) over channels indicated. The violin plot shows a Gaussian kernel density, using a bandwidth determined as described in Section 2.8.1. The PT bias correction method was used, without further correction to the residual bias. The stimulus class imbalance was addressed on a session-by-session basis by subsampling as described previously (Section 2.8.4) before merging sessions together.

We find that grouping trials together in this way smooths out the problems with inter-session changes in residual bias on the information estimate. But because of both changes in neural connectivity and small movement in the electrode contacts between sessions, the neural code is not guaranteed to be the same between sessions. Indeed, we observed a peak in the estimated information corresponding to longer sessions where the trial sample size is smaller than or a similar size to the number of trials grouped together in each block (not shown[4]). For this reason, it is prudent not to proceed with such a methodology.

2.8.5.2 *Bootstrap correction*

Shuffling the responses across stimuli destroys the information contained in the response about the stimulus. By performing such shuffling and computing the amount of information between the randomly paired labels, we can estimate the bias (Optican et al., 1991). Using this in conjunction with a bias correction technique such as PT (applied both when performing the original and the bootstrapped information calculation) allows us to estimate the residual bias which is unaccounted for by the PT correction. As described in Section 1.3.4 and by Panzeri and Treves (1996), this will typically lead to an overestimate of the bias. However, since our residual bias will be significantly reduced beforehand due to the PT technique, the overestimation is on a much smaller residual bias and impacts the results less.

We find that using bootstrapping for the bias correction does indeed overestimate the bias, resulting in a negative correlation between information and $1/N$. This effect is particularly problematic for the V1 dataset of M2, where the correlation was $\rho < -0.72$ ($p < 2 \times 10^{-4}$; see Figure 2.16b), and the V4 M1 dataset, where the correlation was $\rho < -0.44$ ($p < 0.038$; see Figure 2.16c) even with bias correction with PT or QE in addition to using bootstrapping.

2.8.5.3 *Grouping stimuli together*

During the experiment, the subject is tasked with determining whether the stimulus contrast is higher or lower than the 30 % sample stimulus presented at the start of each trial. As a consequence of this, the subject does not need to learn exactly what stimulus is on screen, only whether the stimulus is in the half above or below 30 % contrast. For instance, since the target output is the same for 31 % and 32 % contrast stimuli, there is no need for the subject to discriminate between them, but there is

4 This phenomena occurred when the analysis was repeated with a smaller number of trials grouped together, and is not present in Figure 2.15 due to the smoothing effect of using such large blocks of 1400 trials.

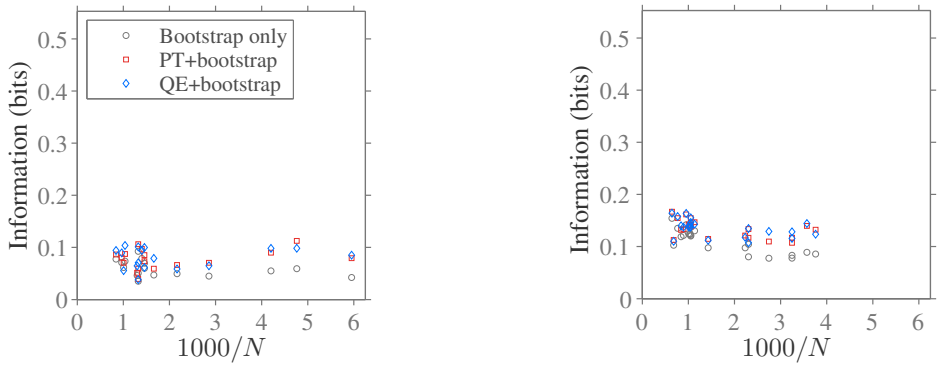

(a) M1 V1.

(b) M2 V1.

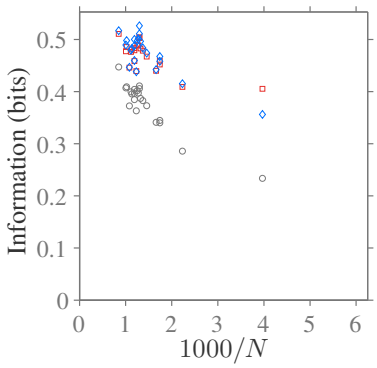

(c) M1 V4.

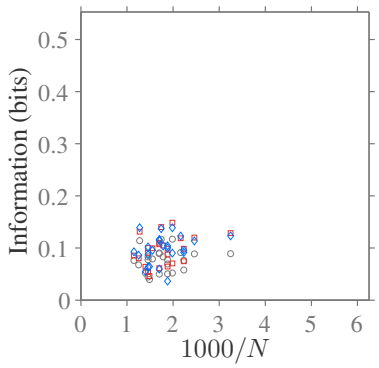

(d) M2 V4.

FIGURE 2.16. *Distribution of measured information, with bootstrap bias correction, as a function of* $1/N$*, where N is the number of trials in the session.* Results are shown with bias correction either achieved solely from subtracting the information contained in response-shuffled copies of the data (bootstraps; grey circles), or by combining this with a more principled bias correction technique (PT, red squares; QE, blue diamonds).

motivation for the subject to learn to discriminate between these and the 29 % contrast stimulus.

We refer to the subset of information which assists in decoding whether the stimulus was higher or lower than the 30 % threshold as the task-pertinent information, and discuss this in Section 2.9. For now, we will only consider the impact on the residual information bias when we restrict ourselves to measuring only the task-pertinent information. In this calculation, we determine how much information the firing rate conveys about which group the stimulus is in (either higher or lower than 30 %) instead of the information about precisely which of the 14 stimuli was on screen. Grouping the stimuli together in this way should reduce the residual bias, since there are only two class labels, and 7 times as many trials per class.

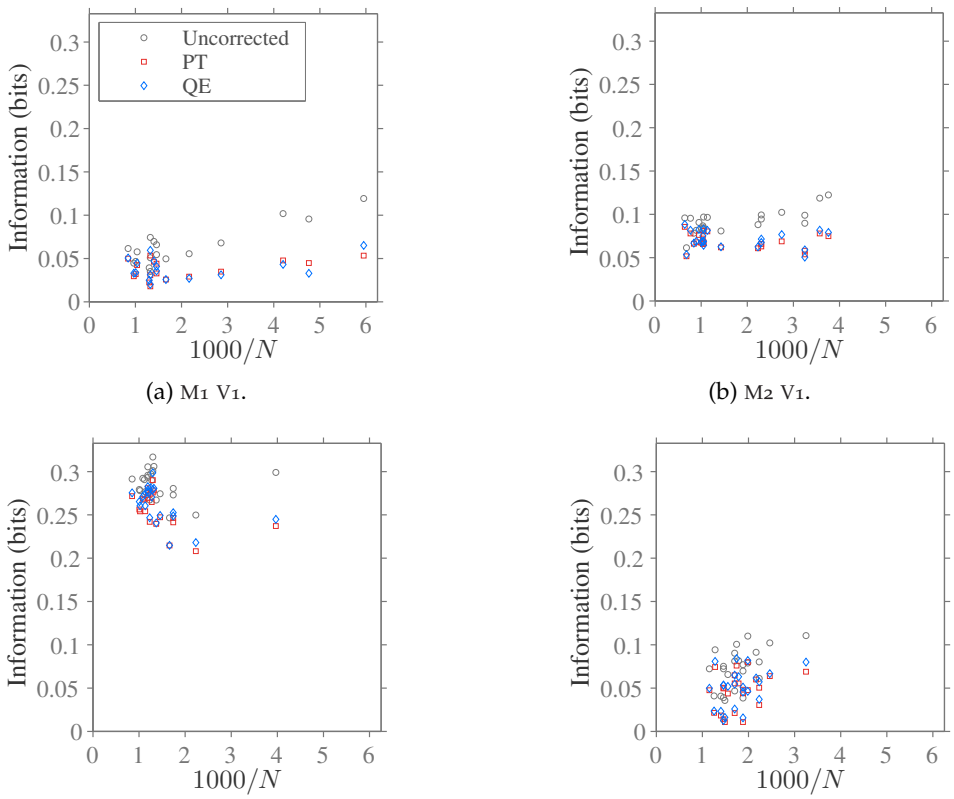

(a) M1 V1. (b) M2 V1.

(c) M1 V4. (d) M2 V4.

FIGURE 2.17. *Distribution of task-pertinent information measured as a function of* $1/N$*, where* N *is the number of trials in the session.* Results are shown both without correcting for the finite measurement bias (grey circles), using PT bias correction (red squares), and using QE bias correction (blue diamonds).

As anticipated, using only two stimulus classes to increase the number of trials per stimulus class greatly reduces the residual bias after PT bias correction. This is witnessed in the reduced correlation between estimated information and $1/N$ seen in Figure 2.17. Here we find the magnitude of the correlations between $1/N$ and I_{measured}

are reduced and no longer significant, with the exception of M2 V1, where $\rho < -0.47$ for both PT and QE ($p < 0.027$).

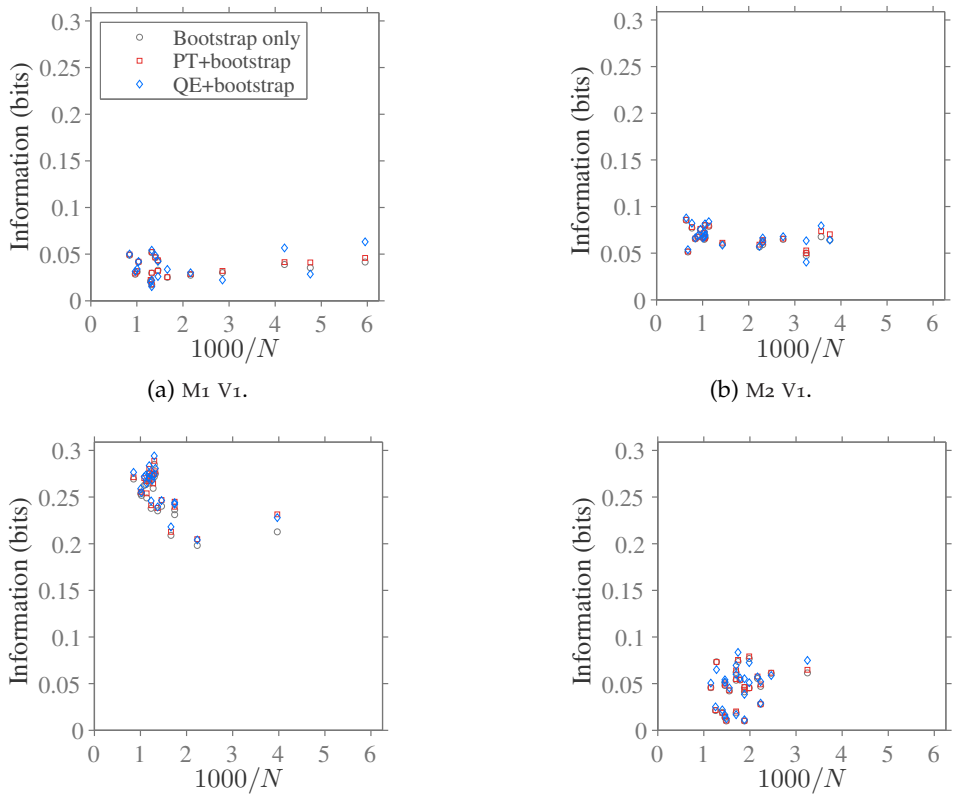

(a) M1 V1. (b) M2 V1.

(c) M1 V4. (d) M2 V4.

FIGURE 2.18. *Distribution of task-pertinent information measured with bootstrap correction as a function of $1/N$, where N is the number of trials in the session.* Results are shown both without correcting for the finite measurement bias (grey circles), using PT bias correction (red squares), and using QE bias correction (blue diamonds).

We can also consider applying the bootstrap correction from Section 2.8.5.2 in addition to reducing the number of stimulus labels to the two groups, shown in Figure 2.18. Using all three bias reduction techniques (including either PT or QE), the correlation for M2 V1 was still significant ($p < 0.008$), with $\rho < -0.54$. We believe this correlation, which only causes a small change in magnitude of the measured information, is because subject M2 had a tendency to train for longer as the sessions progressed, but only with the stimulus in the retinotopic location for V1. For this dataset, there was a correlation between the number of sessions elapsed and the number of trials in the session of $\rho = +0.42$, which was noteworthy but did not exceed our criteria for significance ($p = 0.053$). None of the other datasets had a comparable level of correlation between the number of the session and how many trials were collected ($|\rho| < 0.22$ with $p > 0.4$).

Using bootstrapping to correct for residual bias, the correlations between $1/N$ and $I_{measured}$ are slightly smaller for PT than QE, though the values are very similar and no claim can justifiably be made about which technique gives superior bias correction. Since the PT method is faster to compute, we chose to use this for the rest of our analysis.

2.8.6 *Final results*

After removing channels with sudden changes in firing rate between consecutive sessions, correcting for the change in stimulus class balance by subsampling, restricting our analysis to only consider task-pertinent information about the grouping of the stimulus (whether it exceeds 30 % contrast), and using both the PT method and bootstrapping to correct for the finite sampling bias on the measured information, we can present our results concerning the amount of information contained in the firing rate collected during stimulus presentation from one channel at a time. These results are shown in Figure 2.19.

We found there was no significant change during training (comparing the first with the last three experimental sessions) in the information conveyed by the recording channels of V1 for M1 ($p = 0.30$). However there was for M2 ($p < 6 \times 10^{-5}$), with an increase of $(+0.054 \pm 0.010)$ bits from A to B. For brain region V4, there was also no significant change during training for M1 ($p = 0.31$), but there was an increase of $(+0.052 \pm 0.012)$ bits for M2 ($p = 0.00056$).

2.9 TASK-PERTINENT AND NONPERTINENT INFORMATION

Previously, we were computing the amount of information in the neural response (the firing rate over the stimulus presentation period) about the identity of the presented stimulus. Computing the mutual information between these two tells us how much information we gain about which stimulus was presented when we are told how many spikes were detected on a given electrode contact. However, the objective the subject is tasked with — to identify whether the presented stimulus has a contrast higher or lower than the pedestal contrast — is somewhat different. To achieve this goal, it is not necessary to distinguish exactly which stimulus was presented.

We can separate the information given by the neural response into two parts: task-pertinent and task-nonpertinent information. The task-pertinent information helps one tell whether the stimulus was in the half above or below the pedestal contrast of 30 %. However we also gain information about exactly which stimuli within the upper and lower half of the set of contrasts is more likely to have been presented.

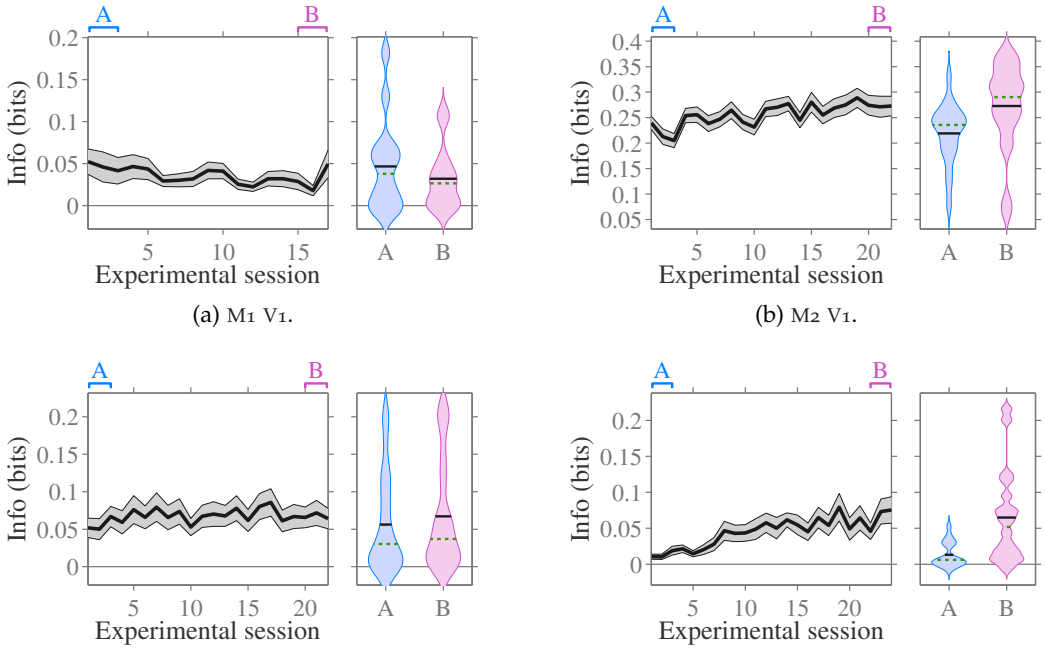

(a) M1 V1. (b) M2 V1.

(c) M1 V4. (d) M2 V4.

FIGURE 2.19. *Task-pertinent information about the stimulus contained in the firing rate during* 527 ms *of stimulus presentation.* Only task-pertinent information (whether the stimulus was higher or lower than 30 % contrast) was included. The finite sampling bias was corrected for by using both the PT method and by subtracting the average of 20 bootstrapped information measurements obtained by randomly pairing responses and stimulus labels. Main panels: the average over channels ((a) 14 channels, (b) 20 channels, (c) 25 channels, (d) 18 channels) with standard error across channels indicated by the shaded region. Right hand panels: distribution over channels of the information contained in the first three sessions (*A*) versus last three sessions (*B*), with mean (solid black line) and median (dashed green line) over channels indicated. The stimulus class imbalance was corrected using subsampling, as described in Section 2.8.4.

Although this information helps one distinguish which stimulus was presented (and hence presumably helps the subject perceive the stimuli more accurately), it is not pertinent to the subject's task.

For instance, any information which helps one discriminate between whether a 29 % or 31 % contrast stimulus was more likely to have been presented is pertinent to the task. Whereas if we gain information about the stimulus which updates the probability of it having a 28 % versus a 29 % contrast without changing the probability that it was one of 28 % or 29 % contrast, this is not pertinent to the task.

Although it is only a binary response (a choice of one of two saccade targets), it is still possible for the behavioural response to encode both task-pertinent and task-nonpertinent information. For instance, let us assume that the subject performs the task at a rate higher than chance. Then, a behavioural response of "*test contrast is lower*" tells us a contrast in the lower half was more likely to have been presented, providing task-pertinent information. Additionally, since contrasts further from the 30 % threshold are easier for the subject, we can empirically observe that a response of "*test contrast is lower*" is more likely to be elicited if the contrast was further below the threshold than if it was close to the threshold.[5] This difference in relative likelihood supplies us with additional, task-nonpertinent, information about which stimulus was presented.

2.9.1 *Methods for decomposing task-pertinent information*

First, we computed the total information contained in the neural response as before, using the total spikes recorded by a single channel over 527 ms of stimulus presentation as the response on each trial. The finite sampling bias on the estimated information was corrected for using the PT method, and further residual bias removed using bootstrapping (see Section 2.8.5.2). Stimulus class imbalance was corrected for using subsampling, as described in Section 2.8.4.

The amount of task-pertinent information contained in the response was estimated by shuffling the stimulus labels against the responses, whilst preserving which side of 30 % contrast the stimulus label was on. This destroys any information about the stimulus beyond that pertinent to the task — choosing whether the stimulus was above or below 30 % contrast — but maintains the number of class labels and samples per class. Consequently, the bias on the information will be similar to that when computing the total information, and the results will be more directly comparable.[6]

5 This trivially follows using Bayes' rule.

6 However, the bias will not be the same for the two information values because after shuffling the range of possible values for the response will have increased. Consequently, it is still necessary to do individual bias correction with PT and bootstrapping on each of the information computations.

We repeated this with 20 permutations, each with their own set of 20 bootstraps, and took the average over them. The amount of task-nonpertinent information was estimated by subtracting the task-pertinent information (found with shuffling) from the total information (found without shuffling).

To compute the proportion of information in the response which was pertinent to the task, we divided the estimated task-pertinent information by the total information (after correcting for the bias on each estimate). To prevent channels whose responses contain negligible information about the stimulus contaminating the results with anomalously large (or small) outliers after the division, we excluded any channels whose total information was less than 1.5 times the standard deviation across the bootstrapped information values. This threshold was determined empirically; 3 standard deviations unnecessarily removed too many channels, whereas 1 standard deviation retained channels with too little information whose task-pertinence proportion was unstable (at or beyond 0 and 1), which increased the overall variance. Approximately half the channels were removed with this step (M1 V1: 14 $\rightarrow$ 4, M2 V1: 20 $\rightarrow$ 20, M1 V4: 25 $\rightarrow$ 13, M2 V4: 18 $\rightarrow$ 7). Additionally, the proportional information reported for each channel was capped at 0 and 1 before taking the average over channels. Although it is impossible for the proportion of information which is task-pertinent to fall outside the range $[0, 1]$, our measurements of the information are fuzzy. In particular, this can arise from subtracting the average over bootstraps, since the bootstraps are stochastic samples and we subtract different bootstraps from the total and task-pertinent information. With the 1.5 standard deviation threshold, we observed that only a single channel fell outside this cap.

To quantify the change over time, we again compared the information averaged over the first three sessions (A) with the information over the last three sessions (B). For the relative information, only channels which had a significant amount of total information (exceeding 1.5 times the standard deviation over bootstraps) for both the average over A and also over B were included. This step was included to ensure A and B were directly comparable; a paired t-test was used to compare the information at A with B.

Similarly, we considered the amount of information about the stimulus contained in the behavioural response of the animal — a saccade to one of two targets indicating whether the subject believed the contrast to be higher or lower than 30 % (two forced-choice). The same procedure was used to decompose the total information in this response into task-pertinent and nonpertinent components, and find the proportion of the information which was task-pertinent.

2.9.2 *Results for V1 information pertinence*

We separated the total information about the stimulus contained in the neural response into task-pertinent and task-nonpertinent components as described in Section 2.9.1. For M1, there was a non-significant decrease in the total information, task-pertinent information, and the task-nonpertinent information between A and B (paired Student's t-test; $p = 0.20$, $p = 0.38$, and $p = 0.13$ respectively), as shown in Figure 2.20a. Correspondingly, there was no significant change in the fraction of the total information which was task-pertinent either ($p = 0.60$; see Figure 2.20c).

For M2, there was a small, non-significant, decrease in the task-nonpertinent information between A and B ((-0.010 ± 0.007) bits, $p = 0.16$), but there was a significant increase in the task-pertinent information ($(+0.060 \pm 0.011)$ bits, $p = 2 \times 10^{-5}$; see Figure 2.20b). Together, these give a combined increase in the total information of $(+0.050 \pm 0.015)$ bits ($p = 0.004$). Since the task-nonpertinent information was stable while the task-pertinent information increased with training, the proportion of encoded information which was task-pertinent increased by $(+7.0 \pm 1.3)$ % ($p = 4 \times 10^{-5}$), as shown in Figure 2.20d.

Over the same period of training, we examined the decomposition of the information contained in the behavioural response of the experimental subject. Similar trends were found for M1 and M2, as shown in Figure 2.21. There was a vast increase in the amount of task-pertinent information between A and B of $+0.32$ bits and $+0.34$ bits respectively, which more than tripled the amount of task-pertinent information given in the subject's response between the beginning and end of the experiment. The task-nonpertinent information in the response increased by a modest $+0.06$ bits and $+0.03$ bits respectively, which is a relative increase of 71 % and 32 % from A to B. Collectively, this meant the proportion of information which was task-pertinent increased from near 60 % to near 80 % for both subjects, as shown in Figure 2.21c and (d).

2.9.3 *Results for V4 information pertinence*

For M1, we found no significant change in the total, task-pertinent, or task-nonpertinent information about the stimulus encoded in V4 channels ($p = 0.48$, $p = 0.19$, and $p = 0.94$ respectively; see Figure 2.22a). There was a small, but non-significant, increase of $(+0.014 \pm 0.010)$ bits in the average task-pertinent information between A and B. Correspondingly, there was no significant change in the fraction of information which was task-pertinent either ($p = 0.61$; see Figure 2.22c).

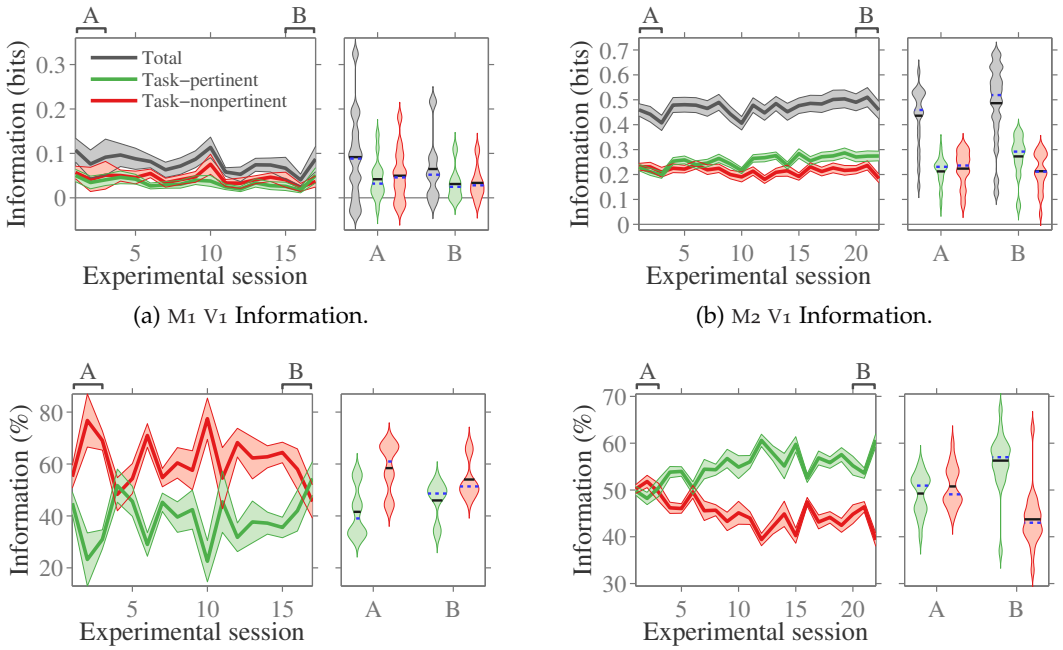

(a) M1 V1 Information.

(b) M2 V1 Information.

(c) M1 V1 Relative information.

(d) M2 V1 Relative information.

FIGURE 2.20. *Breakdown of task-pertinent and nonpertinent information contained in V1 recording channels.* In (a) and (b), the total information about the stimulus (grey), task-pertinent information (green), and task-nonpertinent (red) contained in each of 14 and 20 channels respectively. In (c) and (d), the relative information about the stimulus which is task-pertinent (green) and task-nonpertinent (red) contained in channels with a significant amount of total information (4 and 20 respectively). Main panels: across training sessions, the average information over channels, with standard error across channels indicated by the shaded region. Right hand panels: distribution over channels of the information (or relative information) in the first three sessions (*A*) versus last three sessions (*B*), with mean (solid black line) and median (dashed blue line) over channels indicated. The violin plot shows a Gaussian kernel density, using a bandwidth determined as described in Section 2.8.1. The PT bias correction method was used, with the residual bias further reduced using bootstrapping (see Section 2.8.5.2). The stimulus class imbalance was corrected using subsampling, as described in Section 2.8.4.

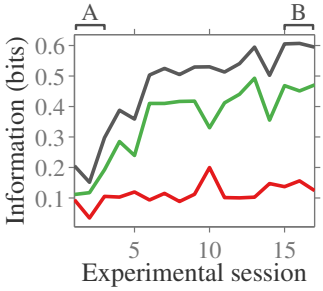

(a) M1 V1 Information.

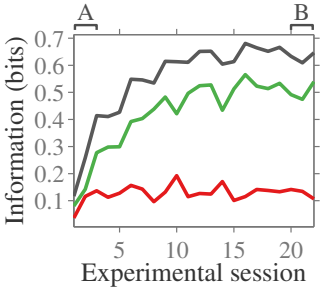

(b) M2 V1 Information.

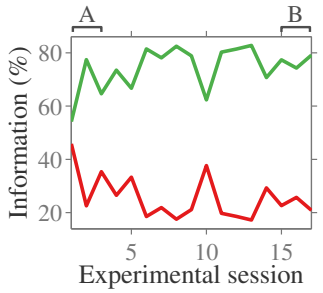

(c) M1 V1 Relative information.

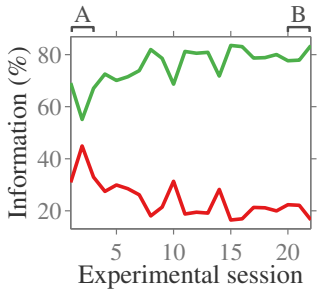

(d) M2 V1 Relative information.

FIGURE 2.21. *Breakdown of task-pertinent and nonpertinent information contained in behavioural responses during V1 recording.* In (a) and (b), the total information about the stimulus (grey), task-pertinent information (green), and task-nonpertinent (red) contained the behavioural response on each trial. In (c) and (d), the relative information about the stimulus which is task-pertinent (green) and task-nonpertinent (red). The PT bias correction method was used, with the residual bias further reduced using bootstrapping (see Section 2.8.5.2). The stimulus class imbalance was corrected using subsampling, as described in Section 2.8.4.

On the other hand, for M2 there was a significant ($p = 0.0005$) increase in task-pertinent information from A to B, increasing by $(+0.054 \pm 0.013)$ bits, which is approximately 5 times its initial value. Meanwhile, the amount of task-nonpertinent information did not notably change ($(+0.008 \pm 0.008)$ bits, $p = 0.32$). Accumulatively, these effects produced an increase in the total information of $(+0.062 \pm 0.018)$ bits, which was significant ($p = 0.003$). As a consequence of this, the proportion of information which is task-pertinent increased from under 20 % to around 50 %, with a swing from A to B of $(+33 \pm 3)$ % ($p = 5 \times 10^{-5}$).

Most information is initially not pertinent to the task, which may relate to most channels initially being inhibited by sample stimulus, as described in Section 2.6.2 (Figure 2.7d). The largest increase in task-pertinent information occurs on the 5th experimental session. This corresponds to a session where several channels changed from stimulus-inhibited (negative d') to stimulus-excited (positive d').

The behavioural information for V4 training sessions shows a similar trend to the behavioural information during V1 training sessions. Namely, there is a larger increase in task-pertinent information and a smaller increase in task-nonpertinent information.

For M1, the subject began training with a decent initial performance, and correspondingly a decent amount of task-pertinent information is given by the behavioural response, as shown in Figure 2.23a. Indeed, for M1 around 75 % of the information contained in the behavioural response is task-pertinent at the beginning of training, and this percentage does not notably change throughout training (see Figure 2.23c). The total information encoded in the neural response does increase with training, but most of this arises from an increase in task-pertinent information (+0.128 bits) as opposed to nonpertinent information (+0.034 bits).

Compared to M1, subject M2 began training with very poor performance on the task. Correspondingly, the behavioural response initially provides less information about which stimulus was presented (see Figure 2.23b) — and over 80 % of that is not pertinent to the task (see Figure 2.23d). The amount of task-pertinent information given by the behavioural response increases by 0.238 bits from A to B (a 26-fold increase), whilst the task-nonpertinent information doubles, only increasing by 0.057 bits. Consequently, there is a massive swing of +54 % in the fraction of information encoded in the behavioural response which is task-pertinent.

2.9.4 *Discussion of task-pertinence of encoded information*

We decomposed the information encoded in the firing rate detected by V1 and V4 recording channels into task-pertinent information and task-nonpertinent informa-

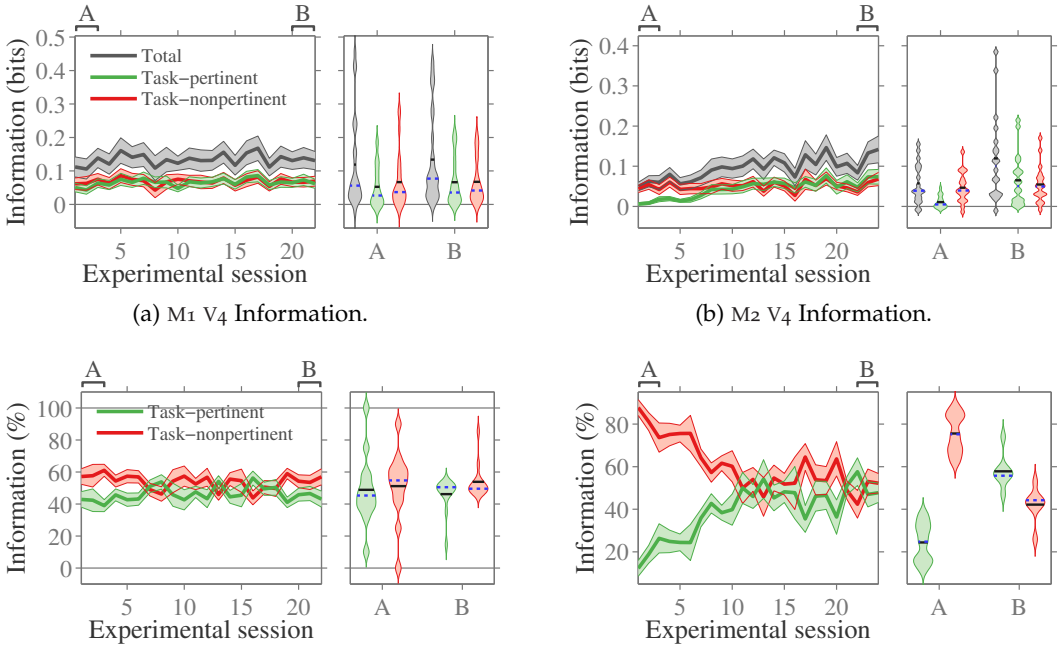

(a) M1 V4 Information.

(b) M2 V4 Information.

(c) M1 V4 Relative information.

(d) M2 V4 Relative information.

FIGURE 2.22. *Breakdown of task-pertinent and nonpertinent information contained in V4 recording channels.* In (a) and (b), the total information about the stimulus (grey), task-pertinent information (green), and task-nonpertinent (red) contained in each of 25 and 18 channels respectively. In (c) and (d), the relative information about the stimulus which is task-pertinent (green) and task-nonpertinent (red) contained in channels with a significant amount of total information (13 and 7 respectively). Main panels: across training sessions, the average information over channels, with standard error across channels indicated by the shaded region. Right hand panels: distribution over channels of the information (or relative information) in the first three sessions (*A*) versus last three sessions (*B*), with mean (solid black line) and median (dashed blue line) over channels indicated. The violin plot shows a Gaussian kernel density, using a bandwidth determined as described in Section 2.8.1. The PT bias correction method was used, with the residual bias further reduced using bootstrapping (see Section 2.8.5.2). The stimulus class imbalance was corrected using subsampling, as described in Section 2.8.4.

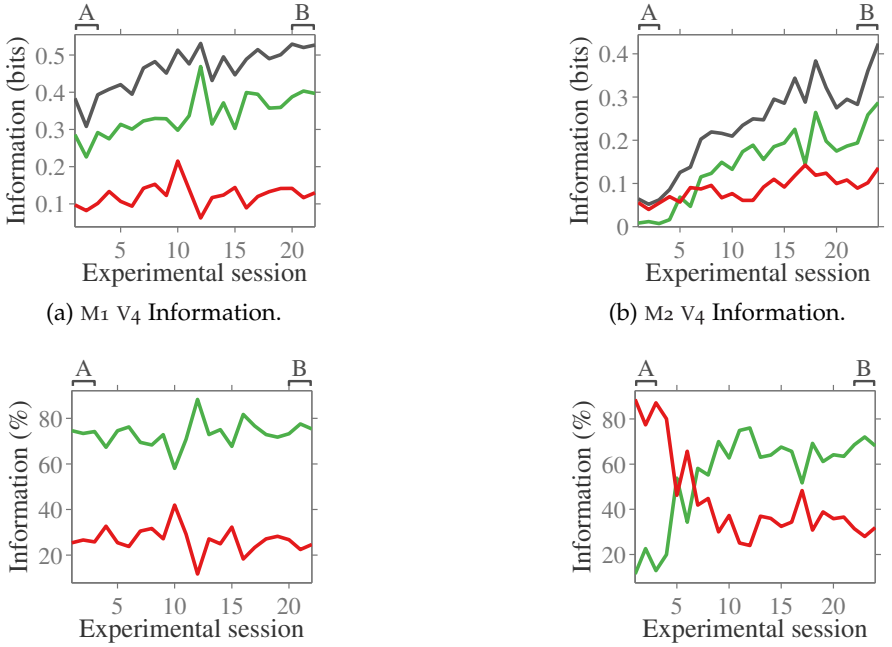

(a) M1 V4 Information.

(b) M2 V4 Information.

(c) M1 V4 Relative information.

(d) M2 V4 Relative information.

FIGURE 2.23. *Breakdown of task-pertinent and nonpertinent information contained in behavioural responses during V4 recording.* In (a) and (b), the total information about the stimulus (grey), task-pertinent information (green), and task-nonpertinent (red) contained the behavioural response on each trial. In (c) and (d), the relative information about the stimulus which is task-pertinent (green) and task-nonpertinent (red). The PT bias correction method was used, with the residual bias further reduced using bootstrapping (see Section 2.8.5.2). The stimulus class imbalance was corrected using subsampling, as described in Section 2.8.4.

tion. The task-pertinent information is that which would help an observer to classify whether the stimulus was in the upper or lower half of all stimulus contrasts. Task-nonpertinent information, which is also encoded in the firing rate, is that which would help an observer to narrow down which of the stimuli within the upper or lower half was more likely. Although the task-nonpertinent information is useful when trying to decode exactly which stimulus was presented, it is not useful for the behavioural task which the subject needs to perform. Consequently, there is an incentive for the subject's neocortex to increase the amount of task-pertinent information which is encoded so that the task can be completed more accurately, but no direct incentive to increase the amount of task-nonpertinent information.

We applied the same procedure whilst considering the subject's behavioural response. Although the behavioural response is binary, differences in the success rate for each specific stimulus mean we gain task-nonpertinent information about the stimulus when observing the behavioural response.

Across V1 and V4 firing rates for both subjects, there was never a significant change in the amount of task-nonpertinent information between the beginning (A) and end (B) of training. For M2, the firing rate from both V1 and V4 channels showed a significant increase in the task-pertinent information between beginning and end of training. Consequently, the total information encoded also increased significantly, and the proportion of information which was task-pertinent increased significantly. For M1, the firing rate from V1 and V4 channels did not show a significant increase in task-pertinent information. Similarly, there was no significant change in the total information, nor in the proportion of information which was task-pertinent. These results are consistent with the neocortex learning to optimise the reward signal given from the behavioural task — the encoded information which is not pertinent to the task is held constant throughout training whilst the task-pertinent information increases with training.

There was an increase in both task-pertinent and task-nonpertinent information contained in the behavioural response for both subjects during training with both V1 and V4 recordings. However, the increase in task-pertinent information was always larger than the increase in task-nonpertinent information.

Arguably, changes in amount of task-pertinent information are more interesting to consider than the amount of task-nonpertinent information, since this directly relates to the performance of the subject. But even if this were not the case, there is no significant change in the task-nonpertinent information; consequently, for the rest of this chapter we will only consider the amount of information about the stimulus which is task-pertinent. We will do so by collapsing the stimulus labels together into two groups which, as described in Section 2.8.5.3, reduces the residual bias on the

computed information since having 2 classes instead of 14 provides us with 7 times more samples per class.

2.10 INFORMATION LATENCY

So far, we have only been considering the amount of information about the stimulus encoded in the firing rate during the entire stimulation period. But is it truly best to use the entire 527 ms period of stimulation? Due to environmental pressures such as predation, perception occurs in notably less than half a second. It is possible that the signal encoding which stimulus is on screen is only transiently emitted by visually responsive neurons, in which case a shorter window will give just as much information about the stimulus. In this section, we investigate when the firing rate of the neurons is most informative about the stimulus.

2.10.1 *Methods and results for information latency*

We considered the firing rate of each multi-unit channel as measured within windows of varying lengths, logarithmically spaced from 2.5 ms to 501 ms. Since we are using windows shorter than the stimulation period, we also varied the latency of the window with respect to the time of the stimulus onset. For each window duration, we varied the latency of the window from the very start to the very end of the stimulus presentation period, at linear intervals equal to either 10 ms or one quarter of the window duration (whichever was shorter).

First, we consider the question of which window duration provides the most information about the stimulus. Since a longer window duration means a more accurate sample of the firing rate and therefore a higher SNR, we would expect longer windows to provide more task-pertinent information about the stimulus. Taking the maximum information across all latencies, as shown in Figure 2.24, we find that longer windows are not always more informative.

For V1 (Figure 2.24a and Figure 2.24b), shorter windows with a duration around 50 ms can capture the most informative firing rate. Measuring the firing rate with windows around 250 ms yields the least information, with an increase as windows become longer than this. For both subjects, there is no notable change between the start and end of training (*A* and *B*) in the amount of information encoded in windows shorter than 250 ms, but there does seem to be a change for longer windows. However, this change is different for the two subjects, with information measured for longer windows decreasing after training for M1 but increasing for M2.

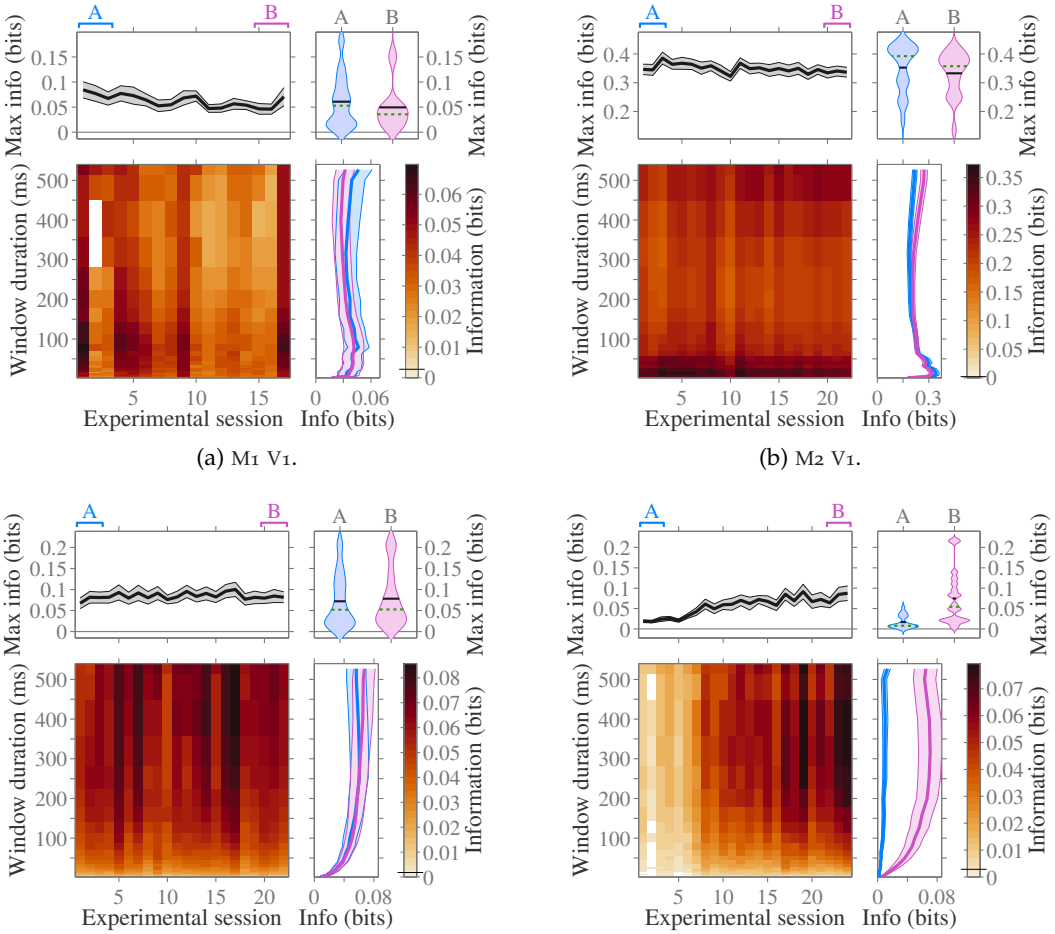

(a) M1 V1.

(b) M2 V1.

(c) M1 V4.

(d) M2 V4.

FIGURE 2.24. *Duration of the window over which firing rate is measured influences the measured information.* For each recording channel and window duration, we took the maximum information over all latencies, then averaged the information over channels. Main panels: heatmap showing information against experimental session and window duration. For each information value, we took 20 bootstrapped information values by randomly pairing stimuli and responses. After taking the maximum over latencies, the mean of the bootstraps was subtracted from the reported information, and if the value did not exceed 3 standard deviations over the bootstrapped information values it was deemed insignificant (shown in white; median significance threshold indicated by a line across the colour bar). Above: maximum information over all window durations. The average over channels is shown (black line), along with the standard error over channels (grey shaded region). Right: for each window duration, the average information over the first (*A*; blue) and last (*B*; purple) three sessions. The average over channels is shown, along with the standard error over channels (shaded region). Above right: violin plots for *A* and *B* showing the Gaussian kernel density estimate over channels of the maximum information. Note that window durations were sampled logarithmically, but are shown here on a linear scale.

For V4 (Figure 2.24c and Figure 2.24d), using a longer window to measure the firing rate is always more informative. There seems to be an increase in information after training for all window durations for M2, but only when the firing rate window is longer than 350 ms for M1.

Our results are parametrised in three dimensions — experimental session (number of days of training), window duration, and window latency — which is too many to portray at once in a single figure. The results in Figure 2.24 are a summary over two of these dimensions, collapsing the window latency dimension by taking the maximum. To understand the results better, we next collapse along the "session" dimension instead.

As the set of window latencies considered is necessarily different for each window duration,[7] we cannot simply average the data over the experimental session dimension. Since we wish to understand *when* the firing rate is most informative about the stimulus, we reparametrised the results over latencies with a very high sampling frequency and, for each window duration, took the average over all information measurements containing this latency. These steps were repeated for bootstrapped information values, and their average was subtracted from the information estimate. Information values less than 3 times the standard deviation of the bootstraps were considered non-significant (indicated in white in Figure 2.25).

These results, shown in Figure 2.25, corroborate the findings discussed for Figure 2.24. Namely, firing rates evaluated over longer durations always give more information about the stimulus for V4, but not V1.

Examining the data as a function of latency, we can see *when* it is possible to estimate the V1 firing rate using only a very short window and still gain a large amount of information about the stimulus. As shown in Figure 2.25a and Figure 2.25b, short windows of 40 ms and below are only transitively informative, with a narrow peak at 50 ms latency after the onset of the stimulus. This temporally localised period of high information content coincides with the elevated firing rate of the stimulus-onset response, as shown in the rastergrams of Section 2.4, which also occurs with a latency around 50 ms. To directly compare the temporal profile of the information with the average firing rate, we plotted the average firing rate as a function of the latency and experimental session, shown in Figure 2.26. This was evaluated using windows 5 ms in duration, and Figure 2.27 shows the amount of information contained in the firing rate using the same windows.

For both subjects, the sharp peak in the information contained in V1 coincides precisely with the maxima of the average firing rate, with a latency of approximately

7 One cannot reasonably examine the information encoded in the 400 ms of stimulus-driven activity starting from a 200 ms latency, since the stimulus presentation has finished within 530 ms.

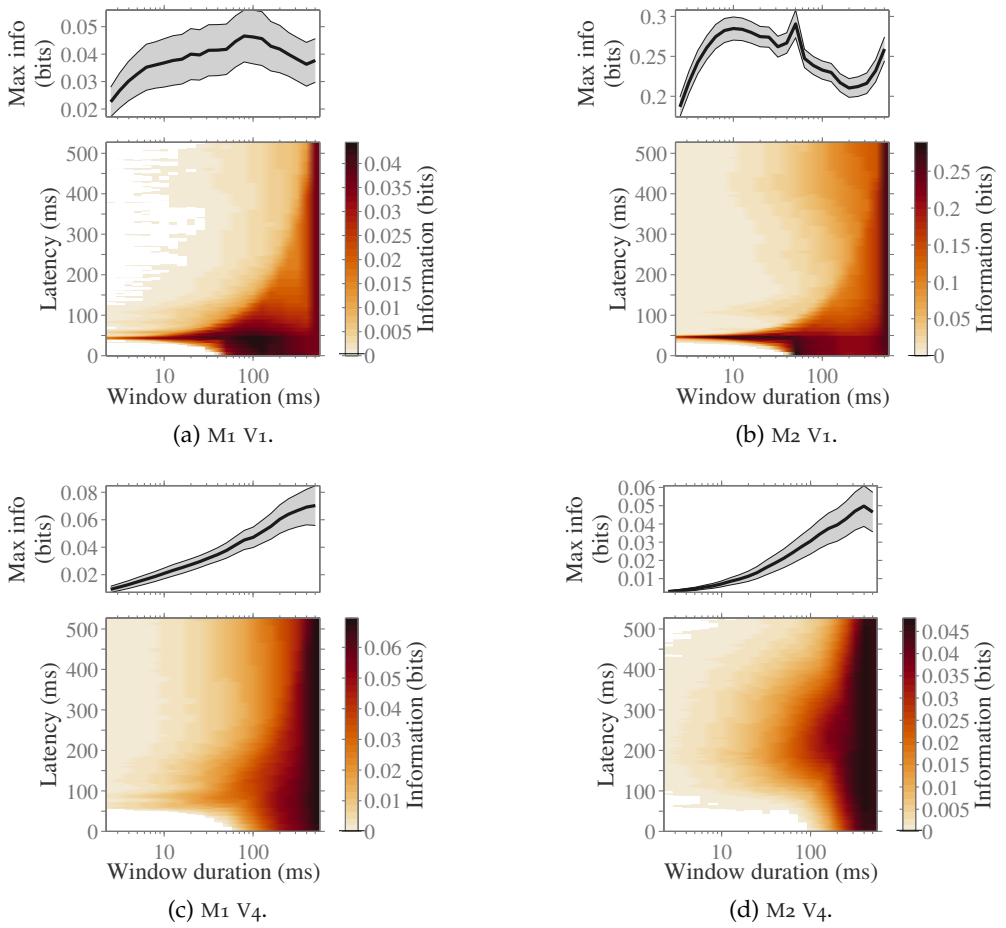

(a) M1 V1. (b) M2 V1.

(c) M1 V4. (d) M2 V4.

FIGURE 2.25. *Information, encoded as firing rate, as a function of window latency.* For a given latency and window duration, the information value reported is the average over all windows of this duration which include that latency (see text for more details). Results are averaged over experimental sessions ((a): 17, (b): 22, (c): 22, (d): 24). Values which are not significant (defined as 3 standard deviations of the bootstrapped information measurements) are shown in white, with a typical threshold for significance indicated by a black line across the colour bar. Note that the scale for the window durations is logarithmic, differing from Figure 2.24. Above: maximum over all latencies, with standard error over channels indicated by the shaded region. This curve is different from those shown in Figure 2.24 due to the smoothing effect of averaging across coincident windows before taking the maximum value.

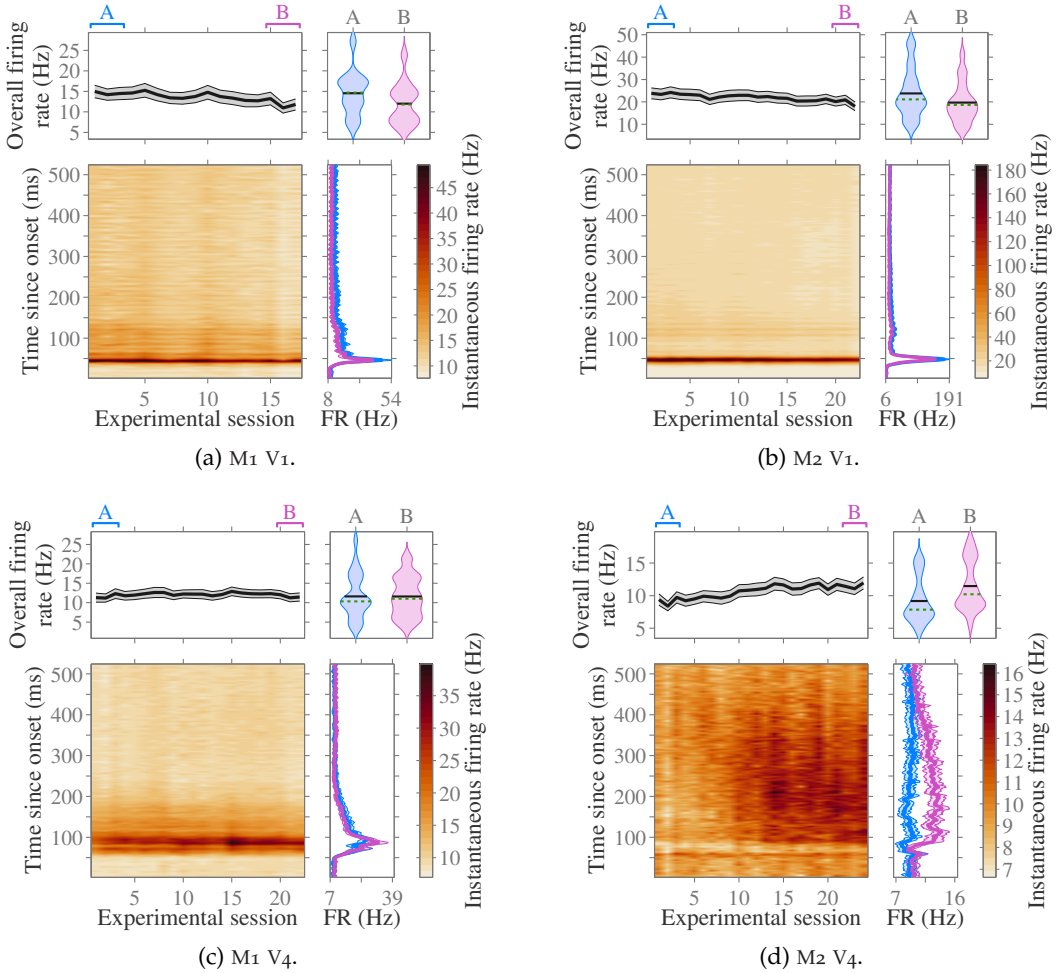

(a) M1 V1.

(b) M2 V1.

(c) M1 V4.

(d) M2 V4.

FIGURE 2.26. *Average firing rate over* 5 ms *windows.* Windows were sampled at 1.25 ms intervals, shown with a latency corresponding to the middle of each window. Information values which did not exceed 3 standard deviations over the corresponding bootstraps were deemed insignificant (shown in white; median significance threshold indicated by a line across the colour bar). Above: overall firing rate during 527 ms of stimulus presentation, averaged over channels (black line), with standard error over channels shown (grey region). Right: average over the first (*A*; blue) and last (*B*; purple) three sessions, averaged over channels with standard error indicated (shaded region). Above right: distribution over channels of overall firing rate for *A* and *B*.

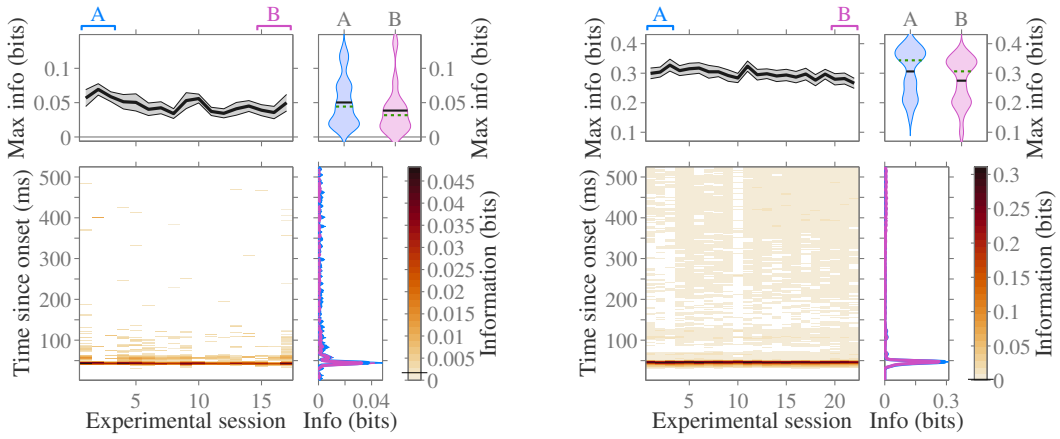

(a) M1 V1. (b) M2 V1.

FIGURE 2.27. *Information encoded as firing rate over windows with* 5 ms *duration.* Main panels: heatmap showing information in each experimental session with latencies, in 1.25 ms intervals, ranging from the start to end of the stimulus presentation. The y-axis value corresponds to the centre of each window. Above: maximum over all latencies and average over channels (black line), with standard error over channels shown (grey region). Right: average over the first (A; blue) and last (B; purple) three sessions, averaged over channels, with standard error indicated (shaded region). Above-right: for A and B, the distribution over channels of the maximum information over all latencies.

50 ms. The firing rate for V4 shows a large stimulus-onset response with 100 ms latency for M1 (see Figure 2.26c), but this is not present for M2 (see Figure 2.26d). However, for M2 the overall firing rate increased significantly ($p < 5 \times 10^{-6}$) with training by (2.30 ± 0.35) Hz. These observations correspond to our sensitivity analysis (see Section 2.6), where we observed almost all recording channels for M2 V4 were initially not tuned to the stimulus class. The firing rate showed no change over training for M2 ($p = 0.97$). For V1, the overall firing rate fell significantly during training for both subjects (M1: (-2.54 ± 0.42) Hz, $p < 4 \times 10^{-5}$; M2 (-4.13 ± 0.69) Hz, $p < 1 \times 10^{-6}$). As mentioned previously, we believe this effect is caused by a decline in signal quality for the recording electrodes over time.

Windows of only 5 ms were not informative enough to depict the distribution of information over latency for V4. Instead, we present results using 50 ms windows, depicted in Figure 2.28. Here, we can again see a close correspondence between the average firing rate and encoded information against the time since the onset of the stimulus.

In Figure 2.28b, we can see an increase in the amount of information encoded in the V1 firing rate towards the end of the stimulation presentation duration. This observation is mirrored in Figure 2.25b, and a similar result for V4 in Figure 2.25c, where (looking from top to bottom of the heatmaps) we find windows of duration 50 ms

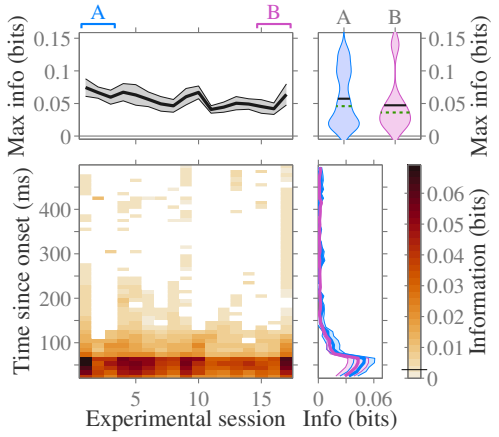

(a) M1 V1.

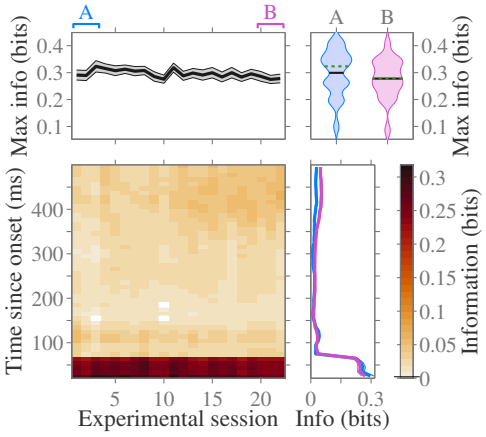

(b) M2 V1.

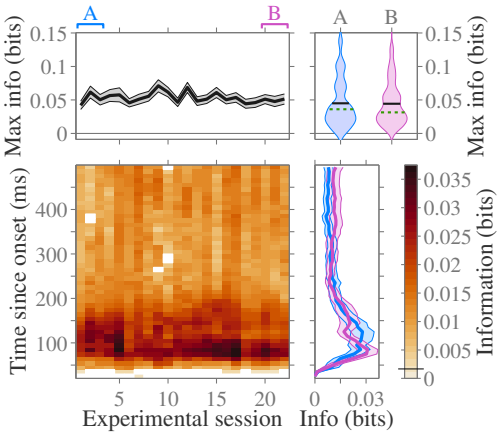

(c) M1 V4.

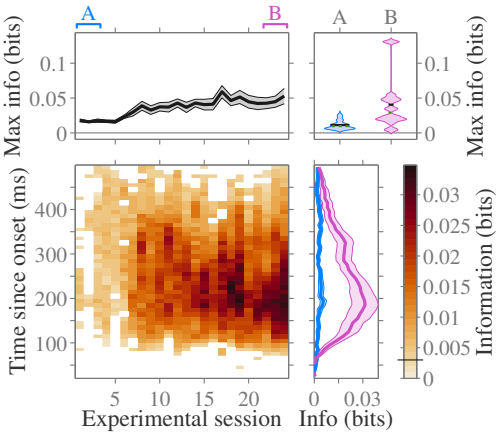

(d) M2 V4.

FIGURE 2.28. *Information encoded in the firing rate measured over* 50 ms *windows.* Plots are arranged as per Figure 2.27, but with 50 ms windows sampled at latencies with intervals of 10 ms.

to 150 ms yield a double-peak in the information as a function of latency. The firing rate is most informative when sampled with low latency, but a second peak occurs for late latencies toward the end of the stimulus presentation. However, Figure 2.25 only shows the average information over all sessions and we can not conclude from it whether the information changes with training.

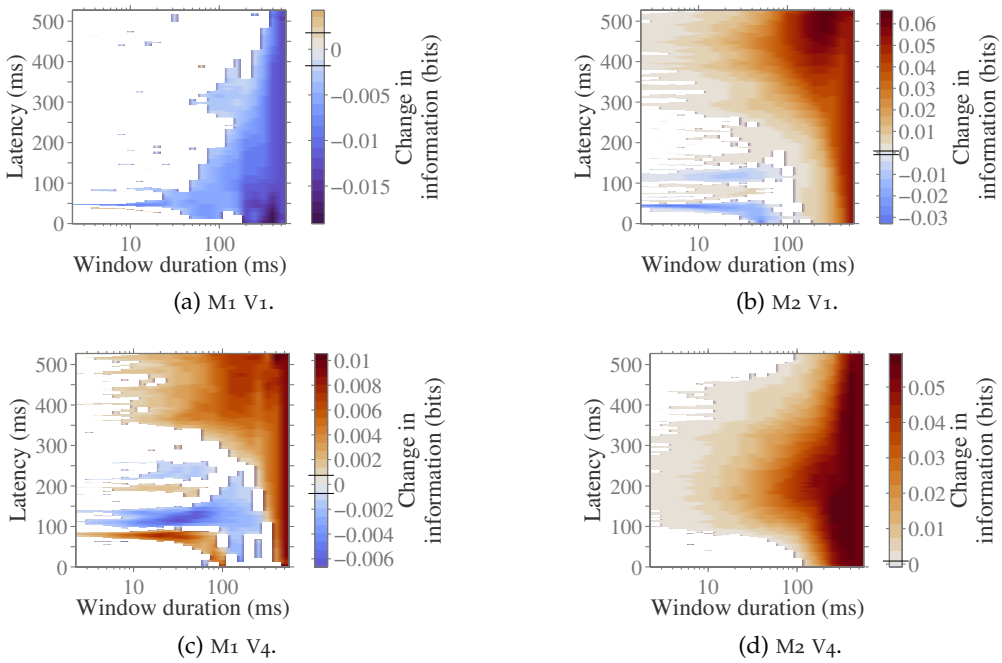

(a) M1 V1. (b) M2 V1.

(c) M1 V4. (d) M2 V4.

FIGURE 2.29. *Change in information with training, as a function of window latency.* Similar to Figure 2.25, here we show the difference in the average during the final and first three sessions. For a given latency and window duration, the information value reported is the difference in the average over all windows of this duration which include that latency (see text for more details). Information values with no significant change between the start and end of training (determined by 3 times the standard deviation over the difference in bootstrapped information values) are shown in white, with a typical threshold for significance indicated by two black lines across the colour bar.

To investigate what properties of the response profile change with training, we repeated the methodology used for Figure 2.25, but took the difference between the average over the first and last three sessions. The results are shown in Figure 2.29. We found there was a significant increase in information in the final 150 ms for both M2 V1 and M1 V4, with magnitude 0.06 bits and 0.009 bits (see Figure 2.29b and Figure 2.29c).

For both subjects, we do not find an increase in the most informative part of the stimulus response profile for V1. On the contrary, we find a significant reduction in the information encoded by the narrow, sharp, peak in firing rate with 50 ms latency (of approximately 0.01 bits and 0.03 bits), which we had previously noted was the most

informative part of the response to the stimulus. This corresponds to the reduction in firing rate between the start and end of training.

For M2 V4, there is an increase in information, primarily with a latency from 150 ms to 250 ms. Again, this corresponds to the increase in firing rate seen for this set of recordings.

2.10.2 *Discussion of information latency*

In this section, we have seen that almost all the information contained in the firing rate of V1 is provided in the first 5 ms at the start of a short burst of rapid firing in response to the onset of the stimulus. With such a short window, we will only be able to detect one or possibly two spikes, yet the change in probability of this single spike is able to convey 0.4 bits of information about the stimulus on a single recording channel of M2. Over the course of training, the stimulus-induced firing rate recorded in V1 fell for both subjects. We believe this reduction in observed firing rate is not due to the firing rate actually falling, but is due to the deterioration in signal quality in the electrode array. Since our spike detection threshold was set to have a consistent spontaneous firing rate (using the methodology and rationale described in Section 2.3.4) an increase in noise can result in an increased detection threshold, subsequently reducing the stimulus modulated activity. The amount of information encoded in the peak response also falls for both subjects, which is well explained by the reduction in firing rate.

We found that the amount of information encoded in the V1 firing rate fell as the duration of the window used to summate the neural activity increased above 100 ms. This ran counter to our expectations, since a longer window duration should intuitively integrate over more signal, resulting in an increase in information. However, this follows naturally from the fact that the sharp burst of activity triggered by the onset of the stimulus contains so much more information than the activity which subsequently follows it. The activity later in the stimulus presentation period has an SNR much lower than the preceding activity, so including this in the window will reduce the overall SNR and hence the total information.

Despite this, there was an increase in the information encoded in V1 with longer windows for M1, due to another increase in the amount of information about the stimulus contained in the firing rate during the final 200 ms of stimulus presentation (Figure 2.29b). This signal increased in information over training despite the firing rate at this latency after the onset of the stimulus remaining the same during training (Figure 2.26b). The same result — an increase in late-presentation information without an increase in firing rate — was found in V4 for M1 (Figure 2.29c).

There are several possible explanations for this result. It could be that V1 and V4 become better at encoding the contrast of the stimuli so that the subject can extract the information to perform the task. However, this seems unlikely since the amount of information encoded remains small when compared to the information contained in the activity of the large burst of stimulus-onset activity. The subject would seem to do better if they were to remember the intensity of the initial response instead of interpreting the activity later in the stimulus presentation. Alternatively, the activity in V1 and V4 could become more informative due to top-down influences. If the subject is thinking about their planned response, information about the contrast of the stimulus may be leaking back to the visual cortex from higher cortical regions. This result leads us to ask whether there is information about the stimulus encoded in the activity after the stimulus is removed, since in this case there is no bottom-up stimulation and we are left only with the effects of internal activity.

2.11 INFORMATION SUSTAINED IN POST-STIMULATION ACTIVITY

In Section 2.10, we described an increase in information late in the stimulus presentation for both M2 V1 and M1 V4, which could hypothetically be caused by information projected back to the visual cortex from higher cortical regions. Following on from this, we will next consider how much task-pertinent information about the stimulus is maintained in the neural activity after the stimulus is removed, to determine how much information about the stimulus is present in the visual cortex without the influence of the visual stimulation.

2.11.1 *Post-stimulation information about the stimulus*

We noted in Section 2.4 that there was a large increase in firing rate triggered by the onset of the stimulus, which is also shown in Figure 2.26, with a latency of around 50 ms, corresponding to the latency of the signal from the cones of the retina to reach the visual cortex. A similar burst of activity is triggered by the removal (or offset) of the stimulus. The change in the visual stimulation over time is the negative of the stimulus, which is just as powerful a stimulant as the stimulus itself. The offset-response also has a latency, occurring in V1 50 ms after the stimulus is removed. This offset-response will contain substantial information about the stimulus, driven by the change in visual stimulation.

In this section, we want to remove as much visually driven activity as possible, which includes the offset-response with its 50 ms delay to V1. Consequently, we ignored the first 220 ms of activity after the stimulus offset and restricted ourselves to

studying the information encoded in the subsequent 200 ms. These 200 ms were immediately followed by the removal of the fixation point and the appearance of the black and white targets with which the subject recorded their response by means of a saccade to the corresponding target. We computed the amount of task-pertinent information encoded in the firing rate, correcting for the change in class balance (see Section 2.8.4), using the PT bias correction, with further correction by subtracting the mean of 20 bootstrapped information values (see Section 2.8.5.2).

For both V1 and V4, we detected information about the stimulus encoded after it was removed with a small effect size, around a tenth of the amount of information present during the stimulus presentation (shown in Figures 2.30a, 2.30b, 2.31a, and 2.31b; amount of information can be compared with that present in Figure 2.25). To illustrate the effect size in comparison with the noise when measuring information for a non-informative event, we also computed the amount of information about the stimulus encoded in the firing rate during the 200 ms *before* the onset of the stimulus. Since stimuli were presented in a random order, it is not possible for the activity before the onset of the stimulus to contain any information about it, and we find that, with bias correction, the measured information is very close to 0 (see Figures 2.30e, 2.30f, 2.31e, and 2.31f).

For V1, subject M1, there was, across channels, a significant amount of information about the stimulus encoded in the post-stimulation firing rate ($p = 0.023$), but the increase in information between the first (A) and last (B) three sessions of (0.0027 ± 0.0059) bits was not significant ($p = 0.66$). For subject M2, the increase over training of (0.0044 ± 0.0011) bits of information encoded post-stimulus was significant ($p = 0.00070$).

For V4, M1 again had, across channels, a significant amount of information encoded in the post-stimulus firing rate ($p = 0.0032$) without a significant increase between the start and end of training ($(+0.0030 \pm 0.0017)$ bits, $p = 0.087$). With subject M2, the amount of information was not significant ($p = 0.091$) and did not increase significantly either ($(+0.0032 \pm 0.0019)$ bits, $p = 0.11$).

Regarding *how* information about the stimulus could be encoded after it is removed, three potential causes for this are readily apparent: bottom-up effects driven by the retina, residual effects within the visual cortex itself, and top-down effects driven by feedback from higher cortical regions.

First, let us consider bottom-up effects driven by the retina. During the experimental trial, the subject must keep their gaze fixated on the central target whilst the sample and test stimuli appear and disappear (see Section 2.2.6 for details of the experimental set-up). Such unnatural fixation will mean the same rods and cones are exposed to the test stimulus whilst it is presented, and this will partially deplete their

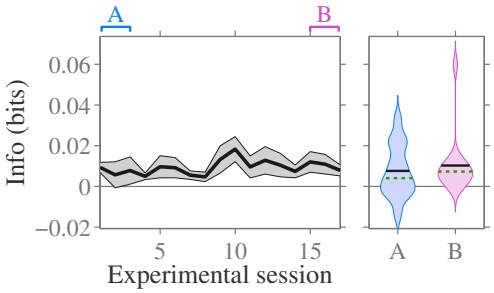

(a) M1 V1, post-stimulus information about stimulus.

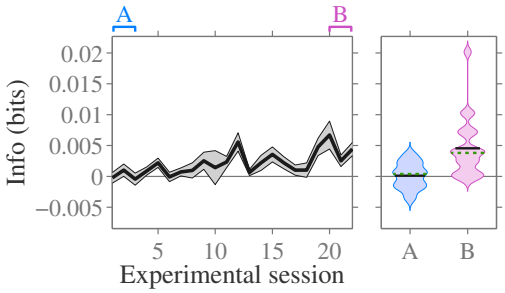

(b) M2 V1, post-stimulus information about stimulus.

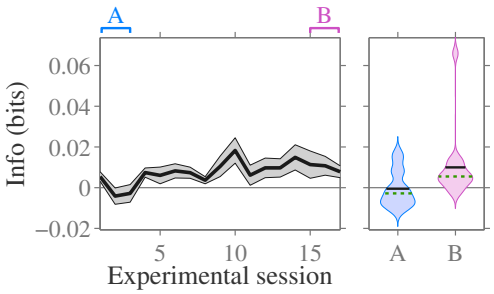

(c) M1 V1, post-stimulus information about response.

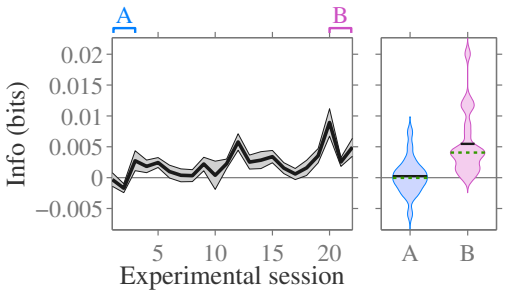

(d) M2 V1, post-stimulus information about response.

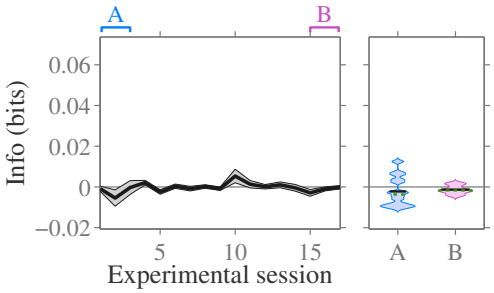

(e) M1 V1, pre-stimulus information about stimulus.

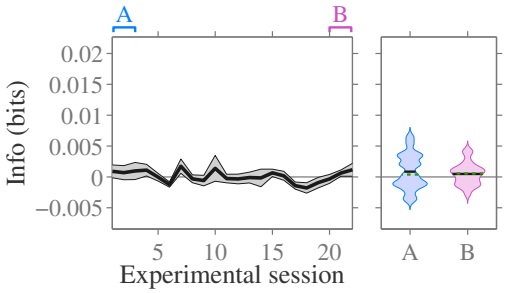

(f) M2 V1, pre-stimulus information about stimulus.

FIGURE 2.30. *Information about the stimulus encoded in V1 after stimulus is removed.* In (a) and (b), the amount of information about whether the contrast of the stimulus exceeded 30 % encoded in the firing rate during the window 220 ms to 420 ms after the stimulus was removed. In (c) and (d), the amount of information about the behavioural response given by the subject encoded in the firing rate during the window 220 ms to 420 ms after the stimulus was removed. In (e) and (f), the information about the stimulus encoded in the 200 ms before the stimulus was presented, shown here for comparison purposes only.

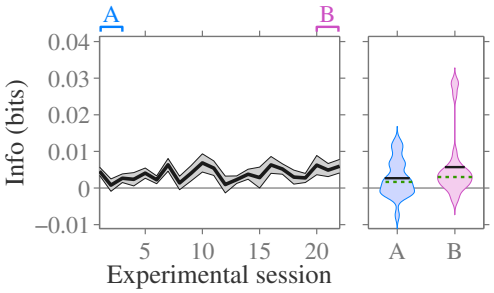

(a) M1 V4, post-stimulus information about stimulus.

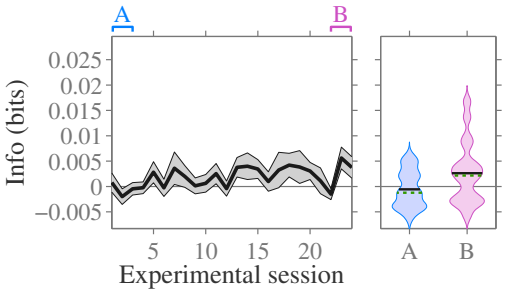

(b) M2 V4, post-stimulus information about stimulus.

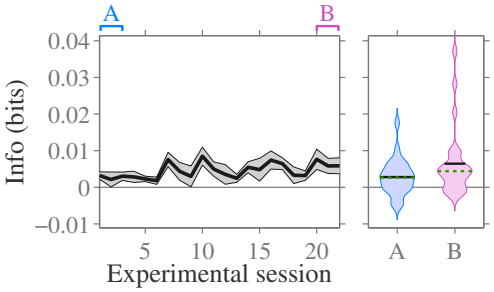

(c) M1 V4, post-stimulus information about response.

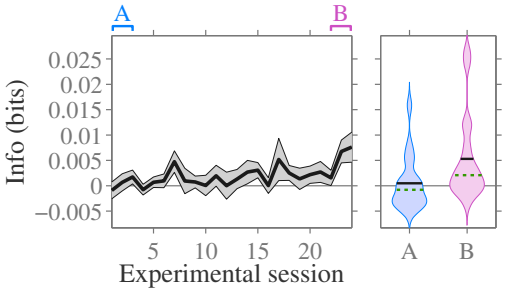

(d) M2 V4, post-stimulus information about response.

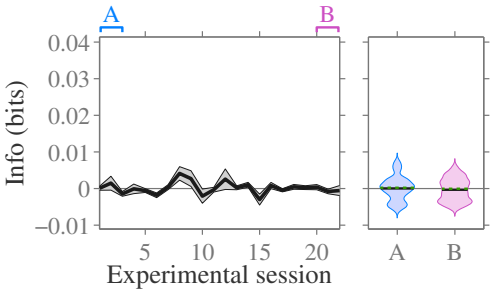

(e) M1 V4, pre-stimulus information about stimulus.

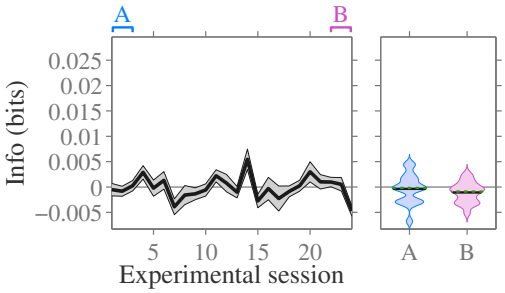

(f) M2 V4, pre-stimulus information about stimulus.

FIGURE 2.31. *Information about the stimulus encoded in V4 after stimulus is removed.* In (a) and (b), the amount of information about whether the contrast of the stimulus exceeded 30 % encoded in the firing rate during the window 220 ms to 420 ms after the stimulus was removed. In (c) and (d), the amount of information about the behavioural response given by the subject encoded in the firing rate during the window 220 ms to 420 ms after the stimulus was removed. In (e) and (f), the information about the stimulus encoded in the 200 ms before the stimulus was presented, shown here for comparison purposes only.

supply of photopigment. This depletion of photopigment results in a negative afterimage, wherein the subject sees an internally generated inverse of the over-exposed stimulus at the same location of the visual field. Such negative afterimages can be induced readily in humans, although for the effect to be clearly perceived the subject must fixate on the stimulus for some tens of seconds, in order fully deplete the photopigment. Since our test stimulus is only presented for 530 ms, the amount of depleted photopigment will be much smaller, resulting a much less intense afterimage (potentially imperceivable), but it is still possible that there is an effect of the conditioning of the retina during the stimulus presentation which manifests itself as a change in retinal activity (triggering a change in the visual cortex upstream) after it is removed.

Secondly, there could be a residual effect residing in the visual cortex itself. Possible mechanisms include activity patterns sustained in recurrent activity, delayed responses to the stimulus due to slow, long-range lateral connections, and desensitisation through depletion, which could result in effects either positively or negatively correlated with the contrast of the preceding stimulus.

Thirdly, there could be top-down effects driven by feedback from higher cortical regions. The experimental paradigm we are using requires the subject to remember the stimulus, or properties of it, for 425 ms before they can give their response. Consequently, the stimulus must remain in working memory in higher cortical regions involved with planning. Since there are as many backward cortical projections as forward connections within the neocortex, it is possible for the memory of the stimulus residing in the higher regions to excite neurons in the visual cortex even after it is no longer present.

2.11.2 *Difference in post-stimulation firing rate*

To assist in distinguishing between these explanations, we investigated the difference in post-stimulation firing rate between stimuli with contrast above and below 30 %. If the effects providing information about the stimulus after its removal are due to the suppression of activity in the visual cortex from depletion of neurotransmitters, this will mean higher contrast stimuli reduce the subsequent activity by more than lower contrast stimuli. Whereas if the effect is caused by feedback, we would expect to find the memory of the stimulus recreates the activity induced by the stimulus, with more actively responded stimuli also inducing more activity after the stimulus is removed.

For each test stimulus, we measured the average firing rate during the 200 ms window starting 220 ms after the stimulus presentation ended. The change in stimulus class balance during training was not addressed using subsampling, as described in

Section 2.8.4. Instead, we took the average firing rate for each stimulus class, then took the average over the 7 stimulus classes below and above 30 % contrast. Next we took the difference between these two averages (referred to as "Difference in firing rate" along the y-axis in Figure 2.32 and Figure 2.33). Finally, we averaged the difference in firing rate over the first (A) and last (B) three sessions, taking a Student's t-test between the distribution over channels of each, and a paired Student's t-test between A and B.

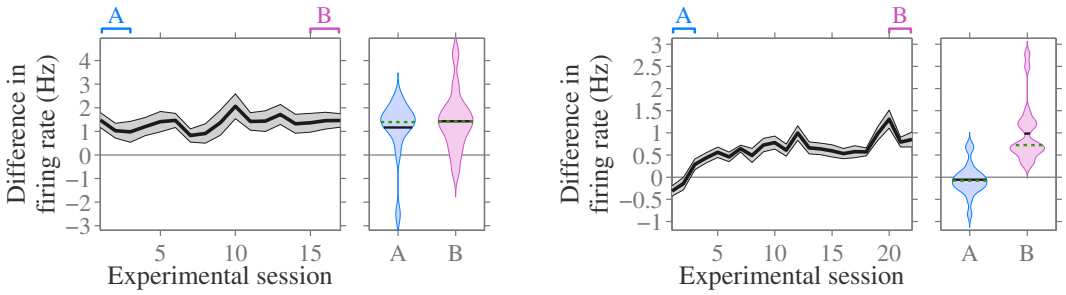

(a) M1 V1. (b) M2 V1.

FIGURE 2.32. *For V1, difference in post-stimulus firing rate between contrasts above and below* 30 %.

Broadly speaking, both V1 and V4 brain regions have higher neural activity following presentation of a higher contrast, and the difference in activity between contrasts above and below 30 % increases with training. However, these results, shown in Figure 2.32 and Figure 2.33, were not significant for both animals.

Considering V1, M1 (see Figure 2.32a) has a significantly non-zero difference in firing rate both before (A; $p = 0.003$) and after (B; $p = 0.0008$) training, which rises from $(+1.16 \pm 0.32)$ Hz to $(+1.43 \pm 0.33)$ Hz. However the increase in firing rate difference between A and B of $(+0.26 \pm 0.28)$ Hz is not significant. Subject M2 (see Figure 2.32b) has a lower initial difference in firing rate for the two groups of stimuli, which does not show significant tuning ($p = 0.48$). From this lower starting point, there is a significant ($p < 3 \times 10^{-6}$) increase in difference in firing rate of $(+1.04 \pm 0.16)$ Hz during training.

For V4, M1 (see Figure 2.33a) does not have significantly different post-stimulation firing rates for the two stimulus groups either before (A; $p = 0.49$) or after (B; $p = 0.34$) training. Correspondingly, the small change in firing rate difference of $(+0.08 \pm 0.15)$ Hz was not significant either. With M2 (see Figure 2.33b), the difference in firing rate of $(+0.18 \pm 0.10)$ Hz was not initially significant (A; $p = 0.072$) but was after training (B; $p = 0.01$). The change between A and B in firing rate difference was $(+0.52 \pm 0.22)$ Hz, also significant ($p = 0.032$).

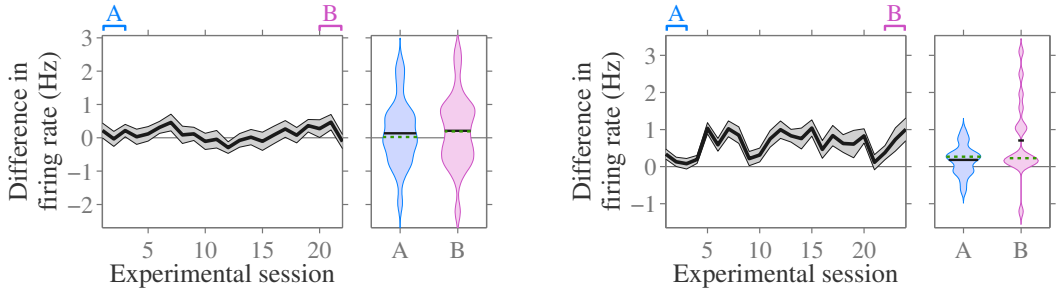

(a) M1 V4. (b) M2 V4.

FIGURE 2.33. *For V4, difference in post-stimulus firing rate between contrasts above and below 30 %.*

2.11.3 *Post-stimulation information about behavioural response*

In a similar manner to how we computed the amount of information about the group of the stimulus (higher or lower than 30 % contrast), we can also compute the amount of information the neural activity contains about the behavioural response the animal is about to provide at the end of the trial. Taking the firing rate during the activity 220 ms to 420 ms after the stimulus was removed, we computed the amount of information about the behavioural response provided by the subject.

The results, shown in Figures 2.30c, 2.30d, 2.31c, and 2.31d, indicate the amount of information encoded about the behavioural response is comparable to that of the stimulus group. This is inevitable: since the performance of the subjects is much higher than chance, exceeding 85 % after training, the behavioural responses contain a lot of information about whether the contrast of the stimulus exceeds 30 %.

Before training, V1 post-stimulus activity did not contain a significant amount of information about the behavioural response for either subject (M1: $p = 0.84$; M2: $p = 0.72$). But after training, there was a significant information about the animal's behaviour for both subjects (M1: $p = 0.045$; M2: $p < 0.0002$), even though the change in information with training was only significant for M2 (M1: $(+0.0105 \pm 0.0050)$ bits, $p = 0.055$; M2: $(+0.0052 \pm 0.0011)$ bits, $p < 0.0002$). There was not significantly more or less information about the behavioural response than the stimulus group (M1: (-0.0003 ± 0.0010) bits, $p = 0.76$; M2: $(+0.0009 \pm 0.0005)$ bits, $p = 0.062$).

For V4, M1 showed a significant amount of information about the behavioural response both before ($p = 0.009$) and after ($p = 0.002$) training, without a significant change between the two ($(+0.0037 \pm 0.0020)$ bits, $p = 0.077$). Meanwhile M2 showed a significant amount only after training ($p = 0.016$), without showing a significant difference after training compared to before ($(+0.0048 \pm 0.0026)$ bits, $p = 0.077$). There was significantly more information about the behavioural response for M2, but this

is not true for M1 (M1: $(+0.0007 \pm 0.0006)$ bits, $p = 0.26$; M2: $(+0.0027 \pm 0.0011)$ bits, $p = 0.024$).

2.11.4 *Discussion of post-stimulus information*

In this section, we investigated the amount of information about the stimulus and about the behavioural response of the subject encoded in the post-stimulus activity within V1 and V4. We found that, after training, there was a significant amount of information about the behavioural response in both brain regions for both subjects. The amount of information about the stimulus group was also significant in V1 for both subjects, and in V4 for M1. During training, there was an increase in information about both the stimulus and behavioural response in both V1 and V4 for both subjects, although the increase was only significant with M2 V1.

For M2 V4, there was significantly more information about the behavioural response than the actual group of the stimulus, and a non-significant increase was also seen for M1 in both V1 and V4. In addition to this, we found there was a higher post-stimulation firing rate following the presentation of higher contrast stimuli, which are associated with a higher firing rate during the stimulus presentation, though this phenomenon was not observed in V4 for M1.

This information present after the stimulus presentation has ended can be explained either as an artifact from the activity from the recent stimulation which persists in affecting the visual cortex from the bottom-up, or a feedback signal indicating the memory of the stimulus while the subject waits to give their response. It is hard to make strong conclusions about which scenario is most likely from our results in this section, since the magnitude of the information we are considering is small and its changes even smaller. Since the difference in post-stimulus activity following higher and lower contrast stimuli increased with training, the effect is unlikely to be caused by forward connections from the retina. As there is more information about the behavioural response than the group of the stimulus, it is tempting to conclude that the post-stimulus activity is modulated by feedback affects instead of conditioning to the preceding stimulus. However, the difference between the two was small, and may be confounded by the fact that the subject's perception of the stimulus is provided by the neural activity in the visual cortex during stimulus presentation. A change in the magnitude of this activity would simultaneously alter the probability of the behavioural response, and the conditioning within the visual cortex itself.

So far, we have only considered the amount of information encoded in the spikes collected by a single electrode contact — that is to say, the spikes from neurons surrounding a single electrode contact. However, when the subject's brain is deciding how to respond to the stimulus on each trial, it potentially has available to it the spikes from every neuron in the brain simultaneously. Consequently, it is more pertinent for us to consider how much information is encoded at the population level — the firing measured from many neurons simultaneously.

Whilst we cannot simultaneously measure the firing rate of every neuron in the visual cortex, we can consider the firing rates simultaneously observed on all our 20 to 30 multi-unit recording channels (for exact values for each dataset, see Table 2.5). Computing the amount of information encoded in the vector of simultaneous responses across all the recording channels allows us to investigate how the encoded information scales as the number of neurons increases. Since the neurons in a neighbouring region of cortex will encode the stimulus in a similar manner, there will be a reasonable amount of redundancy between the neurons. Consequently, the total amount of information will rise sublinearly with respect to the number of channels included in the response vector. However, even if the neurons are encoding visual stimulation using identical response functions, there is still a benefit to knowing the response across multiple channels since each will have an independent sample for (some of) the noise on each recording channel.

The noise on the sampling of the neurons will not be completely independent, since their inputs are correlated and they are connected to each other either directly or indirectly via other neurons in the network. As discussed in Section 1.4.2, the presence of correlated noise within a population of neurons is generally thought to hinder the amount of information encoded in the population. This is certainly the case for a homogeneous population, since the correlated noise will cause neurons with the same tuning response to the stimulus to have the same, or similar, bias for any given sample. In this case, we could do better by having decorrelated noise, so that the noise from each neuron cancels out when we average the response over the population. However, for a heterogeneous population, it is possible for noise correlations to increase the amount of information encoded at the population level, if the noise correlations are in direction which helps disambiguate between potential responses (Averbeck et al., 2006; Moreno-Bote et al., 2014).

We could compute the amount of information in the vector of simultaneously recorded responses from all our electrode channels from the differential entropy, Equation 1.3, as before. However, the number of possible response vectors rises ex-

ponentially with its dimensionality, and, as discussed in Section 1.3.4, the available bias correction techniques will not be able to match this. Consequently, directly computing the amount of information encoded in such a large response vector will not yield any meaningful results. Instead, we trained a classification model on the high-dimensional responses. The performance of the model — the proportion of samples which it correctly classifies — provides a lower-bound on the amount of information present in the data (Quiroga and Panzeri, 2009).

In line with our findings about task-pertinent information in Section 2.9, we will group together all the contrasts on one side of the 30 % contrast task separation line. This means objective function for the classification model we will train on the data will match the objective function which the subject was tasked with during the experiments.

2.12.1 *Methods for decoding population activity*

Our input to the model is the vector of multi-unit firing rates recorded from each electrode contact over the initial 527 ms of test-stimulus presentation.

2.12.1.1 *Linear discriminant classifier*

To evaluate the amount of information contained in the data, we trained a Fisher linear discriminant classifier to distinguish between the two groups of stimuli. Given a training dataset of labelled data-points with m-dimensions for each training sample, the linear classifier fits an $(m-1)$-dimensional hyperplane to separate the classes of the training samples optimally, under the assumption that the two clusters to be separated are multivariate normal distributions.

The vector normal to the hyperplane is

$$\vec{w} = \Sigma^{-1} \left(\vec{\mu_1} - \vec{\mu_0} \right) \tag{2.6}$$

where Σ is the covariance matrix between the two populations, as determined from the labelled training data, and $\vec{\mu_0}$ and $\vec{\mu_1}$ are the means of the two distributions, for class 0 (for our data, contrast $<30\,\%$) and class 1 (contrast $>30\,\%$).

After training the model to define a separating hyperplane, test data-points can be classified by inspecting which side of the hyperplane they fall upon. For a new data point, $\vec{x}$, we classify $\vec{x}$ as group 1 if

$$\vec{w} \cdot \vec{x} > c, \tag{2.7}$$

otherwise we classify it as the group labelled 0.

Example linear classifiers are shown in Figures 2.34 and 2.35. Note that for illustrative purposes, these figures show classifiers which were trained using only two recording channels, but for the results discussed later in this section our classifiers were trained on all recording channels. In these preliminary figures, we can see that the separating plane fit by the linear model does a good job at separating the two classes, given the observed dataset. After the animal has been trained on the task and the changes due to perceptual learning have saturated, the samples with contrast $<30\,\%$ and $>30\,\%$ are more easily separable.

The linear discriminant model was fit using MATLAB's `classify` function (with type 'linear'). We also tested a quadratic model, and using Mahalanobis distances for the discrimination (not shown). However, neither of these models resulted in better performance than the linear model.

Restricting ourselves to a linear model of the data imposes the assumption that the contrast response tuning curves are monotonic for all neurons under observation. This is a gross reduction of the space of possible encoding schemes and will prevent many theoretically possible stimulus codes from giving any information about the stimuli. For instance if the firing rate is 10 Hz for 0 % to 20 % contrast, 30 Hz for 20 % to 30 % contrast, and 20 Hz for $>30\,\%$ contrast: this would give considerable task-pertinent information about the stimulus but it is entirely lost when we are restricted to using a linear decoder. However, in practice our neurons nearly all have monotonically increasing response curves (as discussed in Section 2.5) and thus making such an imposition on the model does not appear to hinder its performance, as demonstrated by the similarity of performance for linear and quadratic decoder models.

2.12.1.2 *Performance evaluation*

To investigate the performance of the classifier on the data from a single session, we used leave-one-out cross-validation. Under leave-one-out cross-validation, given a dataset with n samples, the decoder is trained on the labelled data from $(n-1)$ samples and we then check whether the decoder classifies the remaining trial correctly. This is repeated, so that each of the n samples takes a turn at being the singular test sample, and then the performance is defined as the proportion of trials which are identified correctly.

In the machine learning literature, leave-one-out is regarded as a poor method of cross-validation in order to evaluate and compare models against one another. This is because the models trained in each leave-one-out fold of the data will have almost identical sets of training data. Consequently each classifier will be almost identical — with a linear classifier, the learned hyperplane will be almost exactly the same for

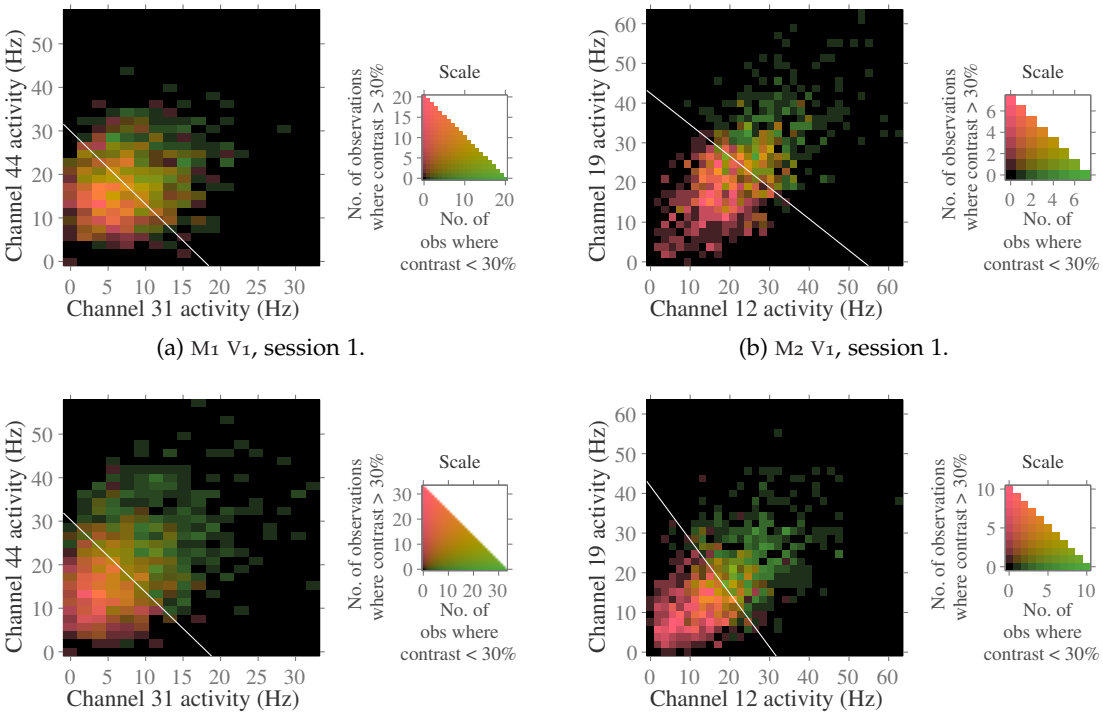

(a) M1 V1, session 1.

(b) M2 V1, session 1.

(c) M1 V1, session 17.

(d) M2 V1, session 22.

FIGURE 2.34. *Exemplar linear discriminators for pairs of V1 channels.* The number of paired observations of firing rates for two channels is shown on a two-dimensional colour bar scale. The hue of each pixel indicates the fraction of observations of the firing rate pair (x, y) which were recorded with a stimulus above or below 30 % contrast (red: below; green above). Lightness and chroma (saturation) indicate the total number of observations of (x, y) using a logarithmic scaling (a doubling of the number of samples results in the same absolute change in lightness and chroma). Pairs of firing rates which were never observed to co-occurr are shown in black. The separating hyperplane fit by the model is superimposed in white. In each case, the model was trained on the data from only two recording channels, for illustrative purposes. For each subject, each pair of channels was evaluated and we selected the pair which gave the highest classification performance during the final recording session. For M1 V1, this pair of channels permitted 64.2 % training accuracy for the naïve animal and 73.4 % during the final experimental session, shown in (a) and (c) respectively. For M2 V1, this pair of channels permitted 78.5 % training accuracy for the naïve animal and 83.8 % during the final experimental session, shown in (b) and (d) respectively.

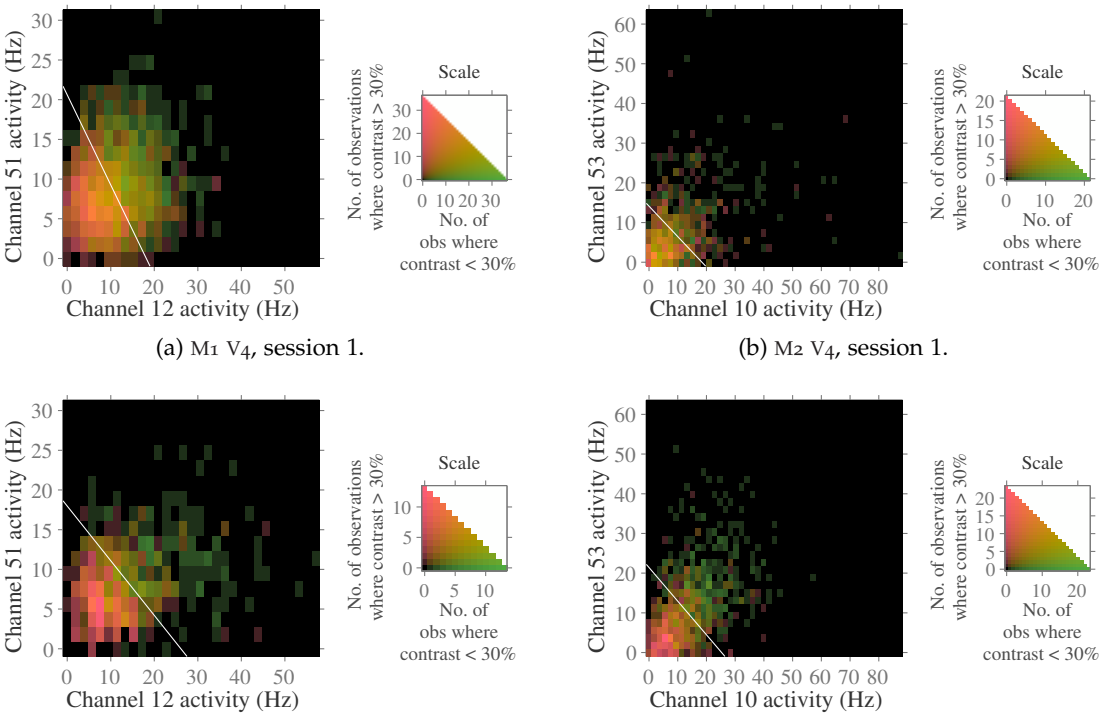

(a) M1 V4, session 1.

(b) M2 V4, session 1.

(c) M1 V4, session 35.

(d) M2 V4, session 25.

FIGURE 2.35. *Exemplar linear discriminators for pairs of V4 channels.* The number of paired observations of firing rates for two channels is shown on a two-dimensional colour bar scale, as per Figure 2.34. The separating hyperplane fit by the model is superimposed in white. We selected the pair of channels which provided the highest classifier performance during the final recording session. For M1 V4, this pair of channels permitted 65.4 % training accuracy for the naïve animal and 74.1 % during the final experimental session, shown in (a) and (c) respectively. For M2 V4, this pair of channels permitted 54.1 % training accuracy for the naïve animal and 73.4 % during the final experimental session, shown in (b) and (d) respectively.

each test-step — and the evaluation will not indicate the variance of performance which would be expected across a diversity of sample sets. Such problems result in suboptimal model selection criteria, however these need not concern us since our task is to most accurately estimate the performance of the model. For this, leave-one-out has low bias and variance (Zhang and Yang, 2015), which is most appropriate to us since we are interested in how the data changes over training.

However, we also need to address the change in class balance over training, as described in Section 2.8.4. Instead of using the same balanced subsample we randomly selected and used across previous sections, we randomly subsampled the data (such that the same number of each stimulus contrast was included) independently on every fold of the leave-one-out validation.[8] To ensure the measured performance was robust against changes in the class balance, we determined the classification accuracy for each of the 14 stimulus classes and then reported the performance as the average of these 14 accuracies.

2.12.1.3 *Information estimate*

We also computed the amount of information about the target response encoded in the decoded response. As with the overall model performance measurement, the class balance was corrected *post hoc* by weighting each stimulus class equally while deriving the probability of the response to each stimulus group. That is to say, the probability of each response given the stimulus was in the lower (or higher) group was set to be equal to the average over all stimuli conditions within the group. The mutual information between the response and the true label of the group was then derived using Equation 1.3. Since we only have 2 stimulus and 2 response conditions, the bias correction routine to account for the finite-sampling is simpler than the full PT method. We estimated the bias using Equation 7 of Panzeri and Treves (1996), which we restate here as

$$I_{\text{bias}} = \frac{1}{2N \ln 2}, \tag{2.8}$$

where N is the total number of samples, under the assumption that each of the 4 stimulus-response pairs can occur in practice. This estimate of the bias was subtracted from our information calculations.

8 We also tried training the model using leave-one-out validation without subsampling and our findings were not notably different.

2.12.1.4 *Shuffling to destroy noise correlations*

We wanted to investigate whether correlations in the noise between the neurons which we recorded helped or hindered the total information across the population. In order to do this, we first measured the performance of the decoder with the original data recorded simultaneously from each channel, and then measured the performance again using a copy of the data where the responses from each channel were shuffled between trials. Our shuffling was conditioned on the contrast of the test stimulus, so that responses from each channel still corresponded to the same stimulus (and the stimulus correlations were preserved), but any correlations in the noise of the recorded neurons were destroyed. We repeated the analysis of decoder performance for 20 different shuffles of the data and report the overall average accuracy. Finally, we compared the average accuracy of the decoders trained on shuffled responses with the decoder trained on the original responses using a paired Student's t-test across experimental sessions.

2.12.2 *Results of decoding population activity*

For V1, there is a decline in the performance of the M1 decoder over time and a small increase in the performance for M2, shown in Figure 2.36. Our results from the population-level decoder correspond to our findings about the information encoded in 527 ms activity, taken for individual channels and then averaged across them, depicted in Figure 2.19.

The change in performance of the decoder over time does not correspond to the change in subject's performance in either case. For M2 (see Figure 2.36b), the subject's behavioural performance increases rapidly initially for the first few sessions and after that it increases steadily until reaching a plateau after around 12 recording sessions, rising from 67 % accuracy at the beginning to 89 % accuracy after training. In comparison, the decoder performance rises from an initial 83 % accuracy only to 88 %. When expressed in terms of information, the increase is larger, from 0.33 bits to 0.46 bits. The behavioural performance increases similarly for M1 (rising from 69 % to 87 %, shown in Figure 2.36a), whilst the performance of the decoder declines slightly over time (falling from 74 % to 72 %). As stated previously, we expect this decline in performance is due to a decline in signal quality over time and is not due to a reduction of information encoded within the cortex.

Destroying the noise correlations between the responses from each channel increased the performance of the decoder significantly for both subjects (M1: $p = 0.0006$; M2: $p < 4 \times 10^{-17}$). However this effect was larger for M2 (an improvement in perfor-

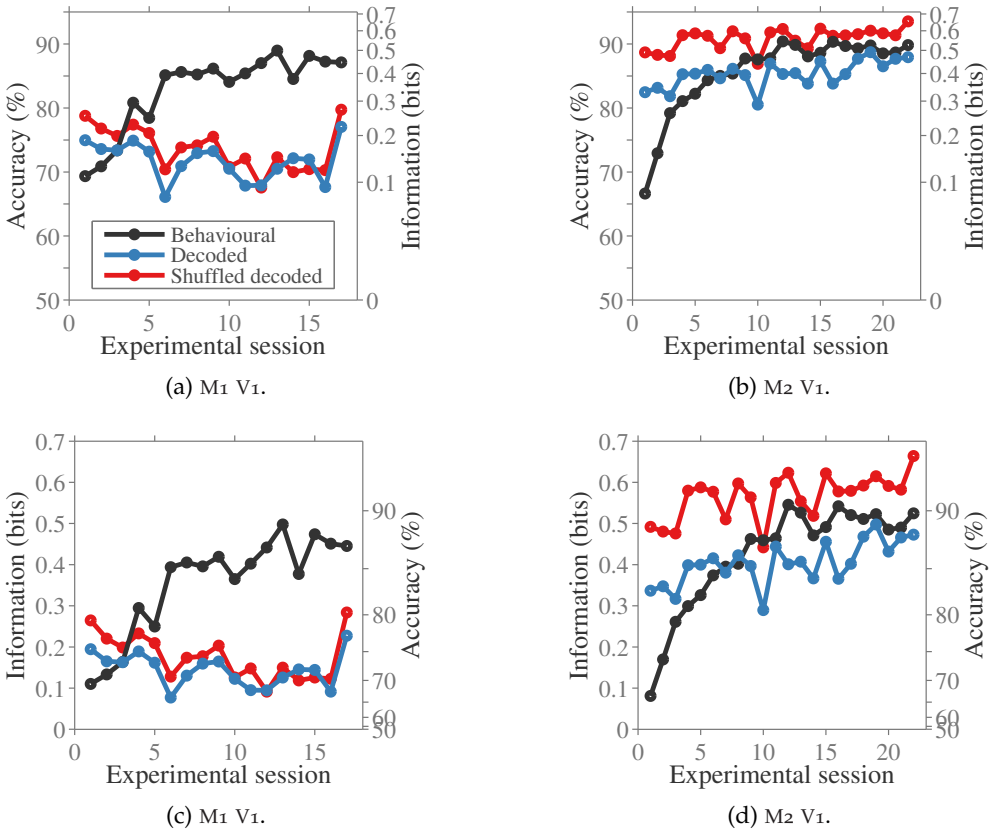

(a) M1 V1. (b) M2 V1.

(c) M1 V1. (d) M2 V1.

FIGURE 2.36. *Classifying the stimulus using V1 population activity.* We report the accuracy of the linear decoder at classifying the group of each stimulus (greater or less than 30 % contrast) after training on the population activity (blue; (a) M1, 14 channels; (b) M2, 20 channels). In (a) and (b), performance was evaluated as the average accuracy across each of the 14 stimulus classes (main y-axis, left-side). A second y-axis (right-side) shows the corresponding amount of information about the stimulus group which would be attained if the average accuracy for stimuli lower than 30 % contrast and the accuracy for stimuli higher than 30 % contrast were equal. We also report the accuracy of the linear decoder when trained on a copy of the data with responses recorded from each channel matched at random such that noise correlations are removed (red; see Section 2.12.1.4). For comparison, the behavioural performance of the subject is also shown for each recording session (black). In (c) and (d), we show the information about the stimulus group (higher or lower than 30 % contrast) contained in the responses from the behaviour and decoders (main y-axis, left-side). A second y-axis (right-side) shows the overall accuracy which would illicit this information (assuming the same accuracy for every stimulus).

mance of (5.4 ± 0.2) %) than M1 ($(+1.9 \pm 0.5)$ %). Additionally, the effect of removing noise correlations on M1 declined as experimental training progressed, falling from 3.1 % to 1.3 % (average of first and last three sessions respectively). This corroborates our notion that the decline in information and hence performance for the decoder is due to a gradual degradation of signal quality in the apparatus. For M2, the performance advantage for a decoder trained without noise correlations also fell, but only not as much, decreasing from 5.9 % to 4.8 % (average of first and last three sessions). However, this marginal decrease seems to be due to saturation of the model performance. The decoder trained on data with noise correlations removed attains 94 % accuracy by the final session, which leaves little room for improvement, and the difference in the amount of information encoded by the two decoders is stable at 0.15 bits through training.

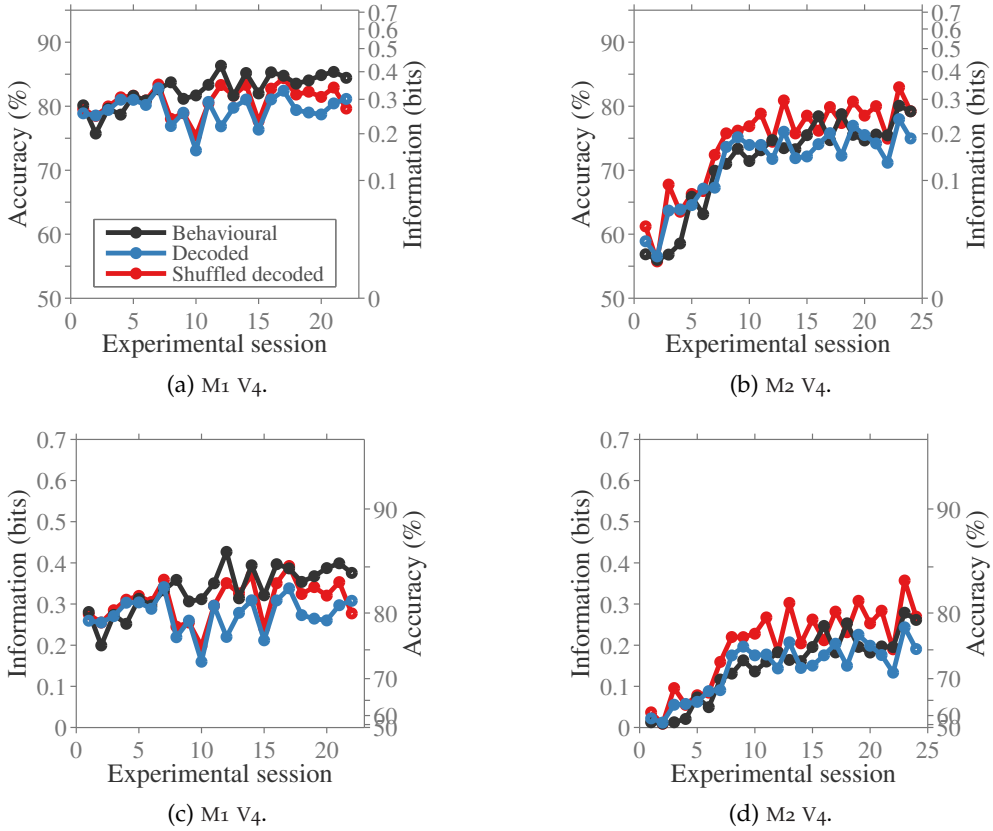

(a) M1 V4.

(b) M2 V4.

(c) M1 V4.

(d) M2 V4.

FIGURE 2.37. *Classifying the stimulus group from V4 population activity.* We report the accuracy of the linear decoder classifying the group of each stimulus (greater or less than 30 % contrast) after training on the population activity (blue; (a) M1, 25 channels; (b) M2, 18 channels). For details, see caption of Figure 2.36.

For both subjects, the decoder trained on the V4 population activity yielded a surprisingly similar level of accuracy as the subject's behavioural responses across all experimental sessions (shown in Figure 2.37b, blue and black lines). However, for M1

the decoder performance increased less than the subject's performance — a negligible increase from 79 % to 81 % whilst the subject's responses improved from 79 % to 85 % accuracy. For M2 the trends with learning were well matched, with the decoder's accuracy increasing from 59 % to 75 % whilst the subject's behavioural accuracy increased from 57 % to 79 %.

Again, destroying the noise correlations between channels by shuffling the responses across trials improved the accuracy attained with the decoder. For both subjects the effect was statistically significant ($p = 0.0004$ and $p < 4 \times 10^{-8}$, respectively), with a larger difference of $(+3.2 \pm 0.4)$ % accuracy for M2 than for M1 ($(+1.4 \pm 0.3)$ %). Over time, the advantage for the decoder trained on data with the noise correlations removed increased for both subjects, increasing marginally from 0.4 % to 1.2 % for M1 and more notably for M2 from 1.9 % to 4.3 %.

2.12.3 *Discussion on decoding population activity*

By training a linear discriminator to classify the stimuli, we investigated the task-pertinent information about the stimulus encoded in the population-level activity. Our results here corroborated our findings about the amount of information encoded on average in each channel, described in Section 2.8.6.

With V4, our decoder gives a surprisingly similar performance to the subject's behavioural response. If the subject is deciding how to respond based solely on the activity in its V4, this means the information contained in the neurons of V4 are highly redundant since the information encoded at the population level must saturate when fewer than 30 neurons are considered. We will test how closely the classifications of the decoder match the behavioural responses given by the subject next, in Section 2.13.

With V1 M2, the performance of the decoder starts high and does not make much improvement over time, whilst the performance of the subject improves to match the accuracy of the decoder. This means that the information needed to complete the task accurately was present in the primary visual cortex from the start, but the subject needed to rewire higher cortical regions in order to access this information when making its decision about the stimulus.

The performance of the decoder always *increased* when we removed noise correlations between channels by shuffling the data across trials. This suggests that noise correlations hinder the ability of the brain to perceive the contrast of the stimulus correctly, and the subject's performance would potentially improve if the visual cortex learnt to decouple the noise for its neurons (Cohen and Newsome, 2008). However, there was no particular decline in the difference between the decoder trained on the

original data and the decoder trained on shuffled data. The decline in difference with and without noise correlations in V1 for M1 is most likely due to a decline in recording signal quality since the accuracy of the model falls over time. For M2, the marginal decrease in difference is most likely due to saturation of the model performance — the decoder trained on data with noise correlations removed attains 94 % accuracy by the final session, which leaves little room for improvement, and there was no notable decrease in the difference when we considered the amount of information encoded. The dataset which shows the largest improvement in decoder accuracy is M2 V4, which also has an *increase* in the gap between decoders trained without and with noise correlations, so a reduction in noise correlation over time is certainly not the cause for the improved behavioural performance.

2.13 AGREEMENT BETWEEN DECODER AND BEHAVIOURAL RESPONSES

Previously, we speculated about the possibility of the subject's responses on each trial being mediated by the activity in V4. Should this hypothesis be correct, the classifications made by a decoder trained on the activity within V4 should, right or wrong, be the same as the responses given by the subject. We tested this by evaluating the response coincidence (agreement) between the classifications made by the decoder and the behavioural responses of the subject.

The response coincidence, ξ, was defined as the proportion of trials on which the two responses matched. However, to avoid changes in the response coincidence over time due to changes in the class balance, we measured the response coincidence for each stimulus class individually and then averaged over all the classes to find the overall response coincidence rate. If we express the behavioural response to a trial t as y_t, and the decoder response x_t, then the response coincidence is given by

$$\xi = \frac{1}{|\mathbf{C}|} \sum_{c \in \mathbf{C}} \left(\frac{1}{|\mathbf{T_c}|} \sum_{t \in \mathbf{T_c}} \delta(x_t - y_t) \right), \tag{2.9}$$

where $\mathbf{C}$ is the set of all stimulus classes, and $\mathbf{T_c}$ is the set of trials where stimulus c was presented. This methodology is similar to how the response accuracy was reported in the previous section.

2.13.1 *Methods for comparing decoding and behavioural responses*

In order to evaluate whether the response coincidence was significant, we must first construct a null hypothesis (NH) model. This is important because the expected re-

sponse coincidence rate is highly dependent on the accuracy of the two classifiers under consideration. For instance, if the behaviour and decoder are both 50 % accurate, we naïvely expect them to agree with each other 50 % of the time. But if both are 100 % accurate, by construction they must agree with each other 100 % of the time as well. If we take an intermediate accuracy, the expected rate of agreement between the two classifiers will also be intermediate. For instance, if both are 75 % accurate, they will both agree on the correct classification $0.75 \times 0.75 = 0.5625$ of the time and agree on the incorrect classification $0.25 \times 0.25 = 0.0625$, yielding a total expected response coincidence rate of 62.5 %.

In order to construct our NH model, we assumed that the classifications made by the subject's behaviour and our decoder are sampled from a Bernoulli distribution, each with a fixed probability of being correct. (This assumption was implicitly made in the statements of the previous paragraph.) More specifically, we used 14 Bernoulli distributions, one for each stimulus class, since we know the accuracy for either decoder or behaviour varies depending on the stimulus class.

Let the probability that the behavioural response is correct when a stimulus from class c is presented by p_c, and the probability that the decoder trained on the population activity is correct by q_c. It then follows that the expected agreement rate under this null hypothesis (NH) is given by

$$\xi_{\mathrm{NH}} = \frac{1}{|\mathbf{C}|} \sum_{c \in \mathbf{C}} \left(p_c \, q_c + (1 - p_c) \, (1 - q_c) \right), \tag{2.10}$$

where $\mathbf{C}$ is the set of all stimulus classes, and $|\mathbf{C}|$ is the number of stimulus classes. We determined p_c and q_c empirically by measuring the accuracy of the subject's behavioural and decoder responses for each condition. The expected agreement ξ_{NH} was then determined from these values using Equation 2.10.

In order to test for significance whether the observed agreement deviated significantly from the NH, we used bootstrapping. For each bootstrap, we generated a synthetic classification from both the behaviour and decoder for every trial of the experiment. The response for an individual trial was generated by randomly sampling two Bernoulli distributions with probabilities p_c and q_c respectively. Having generated synthetic responses for every trial, the bootstrapped agreement was found using Equation 2.9. We repeated this for 100 000 bootstraps, and extracted the 5th percentile of the bootstraps as the one-sided $p < 0.05$ confidence interval.

To evaluate whether the level of agreement was significant at the beginning and the end of the experiment, we took the average response agreement over the first and last three sessions respectively. Correspondingly, to find the confidence interval under the NH, we averaged the bootstraps also (one bootstrap from each of the sessions at once),

then we identified the significance threshold as the 5th percentile over the distribution of 100 000 bootstrapped average agreement rates.

2.13.1.1 *Conditional information*

Measuring the response coincidence rate alone is problematic, because the rate at which the decoder and behavioural responses agree with each other trivially increases as their individual accuracies increase. In Section 2.13.1, we described how to test whether the response coincidence rate is significantly more than expected under a null-hypothesis assuming independent responses conditioned on the class of the stimulus. An alternative solution to this is to measure the mutual information between the behaviour and decoder responses conditioned on the class of the stimulus.

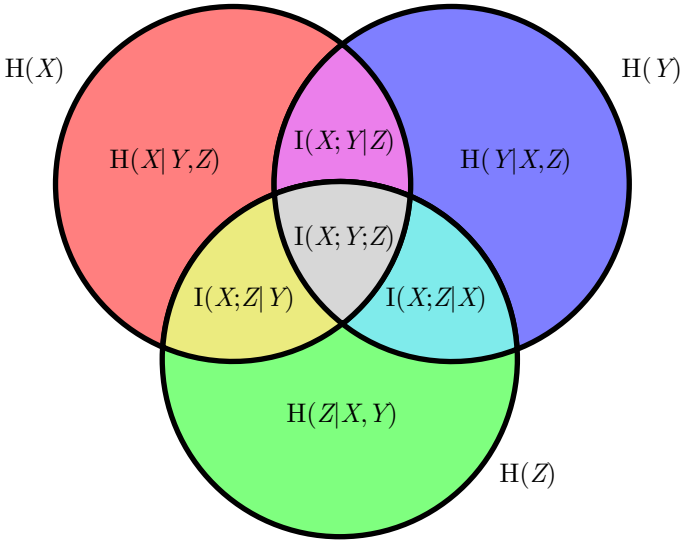

FIGURE 2.38. *Venn diagram of the mutual information between three random variables, X, Y, and Z.* The three black circles represent the entropies of X, Y, and Z ($\mathrm{H}(X)$, $\mathrm{H}(Y)$, and $\mathrm{H}(Z)$); their total area is the joint uncertainty over all three variables, $\mathrm{H}(X,Y,Z)$. The intersection between all three circles (grey region) is $\mathrm{I}(X;Y;Z)$, the entropy (or information) mutually shared by all three variables. The area covered only by a single circle (red, blue, or green regions) represents the entropy unique to a single variable. Of particular interest to us is the area covered by precisely two circles, which denotes the entropy shared exclusively by two variables, such as the magenta region (and similarly also yellow and cyan). This is equivalent to the mutual information between two random variables (X and Y) conditioned on the simultaneous observation of a third, Z, and is given by $\mathrm{I}(X;Y|Z)$ as described in Equation 2.11. Similar to Figure 1.4, in this diagram all regions are non-empty and as such all three variables are partially but incompletely redundant.

Conditional mutual information is the expected mutual information between two variables conditioned on a third,

$$\begin{aligned} \mathrm{I}(X;Y|Z) &= \mathbb{E}_{z\sim Z}\left[I(X;Y|Z)\right] \\ &= \mathop{\mathbb{E}}_{x\sim X, y\sim Y, z\sim Z}\left[\log_2 \frac{p(x,y|z)}{p(x|z)p(y|z)}\right] \\ &= \sum_{z\in\mathbf{Z}} p(z) \sum_{x\in\mathbf{X}, y\in\mathbf{Y}} p(x,y|z)\ \log_2 \frac{p(x,y|z)}{p(x|z)p(y|z)}. \end{aligned} \tag{2.11}$$

This relationship between the three variables and the associated joint entropies is conceptually illustrated in Figure 2.38. We computed the amount of information about the behavioural response encoded in the decoder classifications, conditioned on the correct response to the stimulus using Equation 2.11. The methodology was the same as described in Section 2.12.1.3, but we measured the amount of information about the behavioural response contained in the decoder responses for each of the two stimulus groups and then combined the two values with equal weighting.

2.13.2 *Results for response agreement rate*

The response coincidence rate and conditional information were not statistically significant at the start or the end of training for M1 V1 (Figure 2.39a and Figure 2.39c). The conditional information fell from 0.0065 bits above baseline to equal the baseline NH after training. However for M2, shown in Figure 2.39b and Figure 2.39d, the information about the behaviour conditioned on the stimulus was not initially different from the NH and rose to 0.0137 bits, which was significantly different from the NH.

For V4, there was an increase in agreement between the behaviour and decoder responses during training for both subjects. With M1, the conditional information between the two was not initially significant at 0.0045 bits above the expected level, but increased to 0.0190 bits which was significant. For M2, the conditional information was significant throughout training and also increased from 0.0072 bits to 0.0477 bits.

2.13.3 *Discussion of response agreement rate*

For all our data except V1 in M1, there was an increase in the amount of information about the behavioural responses contained in the responses of the decoder of Section 2.12 trained on the firing rate from all simultaneously recorded channels. Furthermore, this increase was not explained by an increase in performance of the two classifiers. We controlled for this by conditioning our information calculation on the

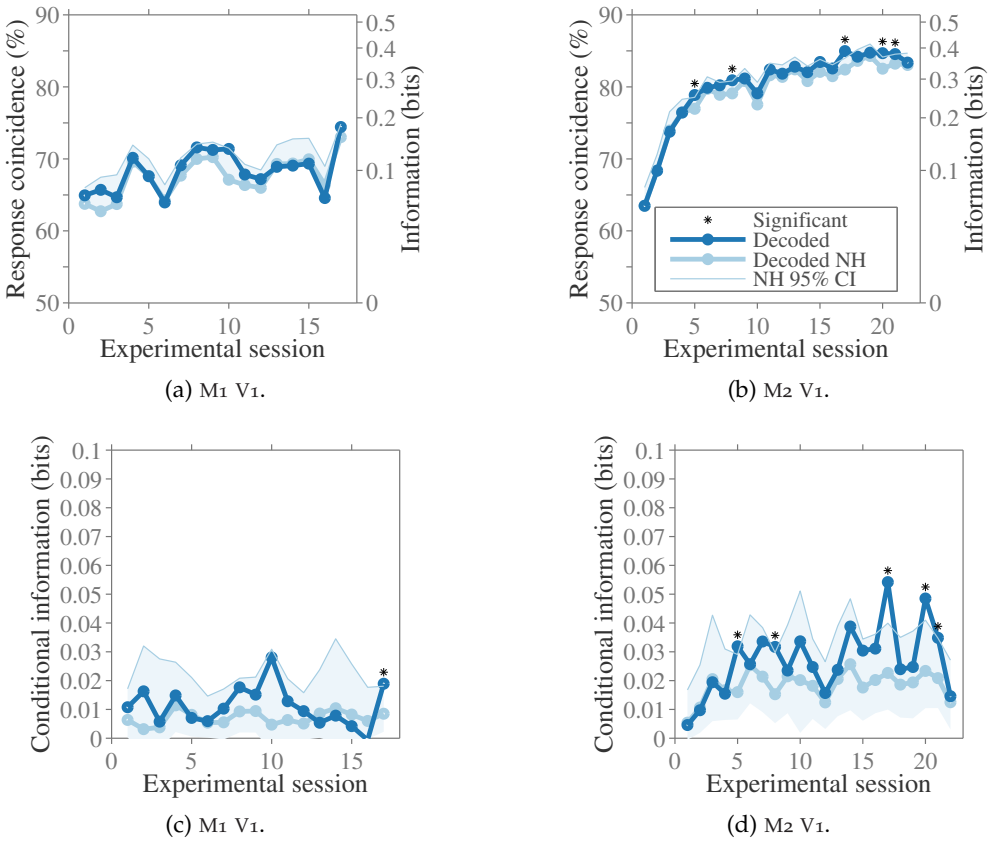

(a) M1 V1.

(b) M2 V1.

(c) M1 V1.

(d) M2 V1.

FIGURE 2.39. *Response coincidence rate for V1.* In (a) and (b), the response coincidence rate, ξ, is the average probability that the classifications given by the model trained on the population activity will match those given by the subject's behavioural response (main y-axis, left-side). A second y-axis (right-side) shows the corresponding amount of information about the stimulus group which would be attained if the average accuracy for stimuli lower than 30 % contrast and the accuracy for stimuli higher than 30 % contrast were equal. The shaded region indicates the 95 % confidence interval (CI) of the null hypothesis (NH) constructed for each session (see Section 2.13.1 for details). In (c) and (d), the amount of information about the behavioural response given by the decoder, conditioned on the correct experimental response to the stimulus.

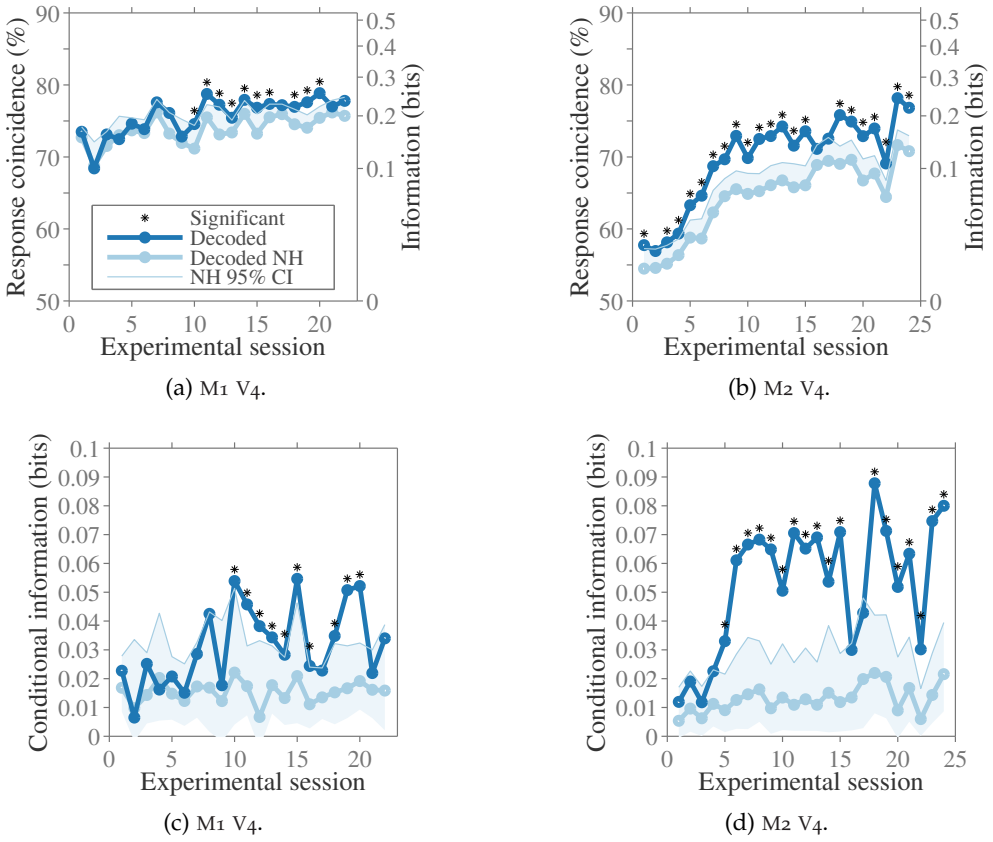

(a) M1 V4.

(b) M2 V4.

(c) M1 V4.

(d) M2 V4.

FIGURE 2.40. *Response coincidence rate for V4.* Same as Figure 2.39, but for V4.

target response and by comparing with the distribution of samples under a NH model of conditional independence.

The increase in response coincidence rate over the course of training could be explained by the higher cortical regions in the subject's brain getting better at interpreting the information encoded in the visual cortex, and hence becoming more reliant on the signals which we recorded to construct our linear classifier. Alternatively, feedback from the higher cortical regions could increase, causing information about the subject's response to propagate into the visual cortical regions after the decision has been made (but before it is given). The increase in agreement was larger for V4 than V1.

2.14 CONCLUSIONS

In this chapter, we used information theoretic techniques to evaluate how the neural activity in V1 and V4 changed during repeated training on a visual domain-specific classification task. Over the course of the training regime, the subject's ability to discriminate whether the Gabor and sinusoidal grating presented had higher or lower contrast than a 30 % contrast sample stimulus improved. We were interested in studying the neural correlates of this phenomenon, referred to as perceptual learning. The experimental process was performed for two macaques (M1 and M2), and we analysed the amount of information encoded in the spike trains elicited in response to the test stimulus, whose contrast was selected within a range of 5 % to 90 %.

2.14.1 *Task-pertinent information*

We decomposed the information about the stimulus contained in the neural activity into task-pertinent information, that helps an observer distinguish whether the presented stimulus had a contrast higher or lower than 30 %, and task-nonpertinent information, that only helps distinguish which of the 7 stimuli in each of the two categories was more likely. From this, we found the amount of information which was not pertinent to the experimental task remained the same throughout training, whereas the amount of information which was pertinent to the task increased (this increase was statistically significant for M2 but not M1). These observations are compatible with the hypothesis that the cortex is rewiring itself with training in a way which is directed towards optimising the target objective provided by the experimental protocol, which might be provided to visual regions in the form of feedback from higher cortical regions involved with decision making. It also suggests that the neurons in the visual cortex are restricted to encoding information in a certain manner,

such that they can not increase the task-pertinent information at the expense of the information encoded about the stimulus which is not relevant to the behavioural task. One possible explanation for this is that the contrast tuning curves of the cortical neurons become sharper with training, but the tuning curves are constrained such that they cannot mimic the step-function. In a previous study analysing the same dataset, Chen et al. (2013) found that exponential functions corresponding to the psychometric performance of the subject became steeper with training, in corroboration with this idea.

2.14.2 *Timing of information*

Within V1, the most informative neural activity was the transient response to the onset of the stimulus, an observation supported by previous literature (Müller et al., 2001). This is the first cortical response to the stimulus after it is presented, occurring with a latency of approximately 50 ms, in which the firing rate increases sharply, but briefly. More information can be obtained by observing the neural activity during a short slice of only 10 ms than the overall firing rate for the entire 530 ms stimulus presentation period, provided the timing of the 10 ms window is chosen appropriately. Furthermore, the most informative part of the stimulus onset response is the beginning. We previously reported (Lowe, 2012) that splitting 20 ms windows into 5 bins each with duration 4 ms to capture spike timing information only yielded an increase in information above a rate code for the timing of the onset response. This is most likely because higher contrast stimuli elicit spikes sooner within the retina, and as a consequence the cortical response for higher contrast stimuli has lower latency (Albrecht et al., 2002). However, the amount of information encoded in the stimulus-onset response did not increase with training. In fact, for both subjects, it *declined* with training. This is most likely explained by a decline in quality of the recording electrodes — in Section 2.6 we demonstrated the sensitivity of the electrodes in V1 declined over time. The lack of improvement in the most informative V1 activity could be because the brain is not able to use this activity in the regions making the decision of how to respond behaviourally. However, this seems unlikely as V1 is the largest cortical region and appears to play an essential part of visual processing in mammals.[9] Throwing away information from by far the most informative component of the response does not seem a likely coding strategy employed by the brain, but since changes in lighting and contrast are hurdles to be overcome when identifying a stimulus it is possible that this is the case. Usually the visual system needs to know what

9 There are direct connections from LGN to V2 and visual area 3 (V3), but V1 also makes projections to both of these cortices.

an object is in spite of its contrast, not to identify the contrast itself, and later stages in the visual processing hierarchy are less sensitive to changes in contrast (Sclar et al., 1990). Because of this, it would be useful to see the results if this experiment were repeated with fine grained classification on a different stimulus property, such as orientation or spatial frequency.

Although the information in the onset-response did not increase with training, the overall firing rate for the whole stimulus presentation did rise, for M2 at least. This was due to an increase in information in the late stages of stimulus presentation — the final 200 ms. Since the neural activity present after the stimulus was removed contained more information about the behavioural response than the target label of the stimulus, and the decoder trained on data from later sessions showed a significant correlation with the behavioural responses, we believe this information is indicative of latent representation of the stimulus feedback sustained after the removal of the stimulus through feedback from higher cortical regions.

2.14.3 *Information at the population level*

As evidenced by our results with the linear decoder, V4 activity during the stimulus presentation is indicative of the behavioural response of the subject. We trained the linear decoder to classify the group of the stimulus, giving us a reflection of the information about the stimulus contained in the cortical activity. We did not train the decoder to predict the behavioural choices made by the subject, and yet its responses coincided with the subject's behaviour more often than expected by chance. This phenomenon of elevated response agreement occurred after training but not before.

There also was information about both the stimulus group and the behavioural response given by the subject in the sustained activity within the visual cortex after the stimulus was removed. This increased with training for both subjects and both brain regions. As discussed in Section 2.11.4, this could be due to information reaching the visual cortex from the higher brain regions within the cortex associated with decision making. Previous analysis of the same dataset found the response time of the subject fell with training (Chen, 2013; Chen et al., 2013), which could be related to this result.

Using a decoder to classify the stimuli based on the population activity, we found that before training the subject there was more information about the stimulus in the small population of V1 neurons that we recorded than in the behavioural responses of the subject. As training progressed, the information encoded in the V1 neurons of M2 rose, but not as quickly as the behavioural performance rose, such that after training the behavioural performance was higher than the decoder trained on V1 activity. In contrast, the V4 population contained a similar amount of information about the stim-

ulus as the behavioural response, and though both rose with training, this remained true throughout the experiment. These results suggest a large amount of redundancy in the neural activity, since decision processes of the subject in principle have access to all the neurons of the brain, but perform at a level comparable with a decoder train on the activity of only around 20 neurons.[10] However this is not so surprising, since it has long been known that single neurons can convey a large fraction of the information present in the behavioural response (Britten et al., 1992). The information contained in a pooled set of neural responses saturates quickly as the size of the pool grows due to the correlations of the responses within the population (Zohary et al., 1994). But further to this, the performance we could attain with only a handful of V1 neurons[11] was *higher* than the initial performance of the individual. This indicates the information needed to complete the task is available before training begins, but that neural pathways must be rewired for such information to propagate to the higher cortical regions which decide what behavioural response to provide.

By shuffling responses from recording channels across trials, we measured the impact of noise correlations on the decoder trained on either V1 or V4 activity. We found that the impact of noise correlations on the population-level information did not fall with training, even when the pairwise noise correlations declined over the same period. However, we note that this interpretation of the results was not obvious when we measured the accuracy of the decoder instead of the information it contained, due to the non-linear relationship between information and accuracy. In a study of the macaque dorsal medial superior temporal area (MSTd), Gu et al. (2011) found similar results: pairwise noise correlations between neurons are reduced with training, but this does not yield an increase in performance in a decoder trained on the population activity.

2.14.4 *Correlations with behaviour*

Previous analysis of the same dataset using area under receiver operating characteristic curve (AUROC) found that, on average, the probability of agreement between the spiking activity from individual recording channels in V4 and the behavioural response rose with training, and the agreement between V1 and behaviour rose for M2, but not M1 (Chen, 2013). In this new work (Section 2.13.1), we controlled for the change in behavioural performance with training, and computed the conditional mu-

10 In fact, the situation is more extreme than this. We used greedy feature selection to investigate the performance of the decoder as a function of the number of channels available to it, and found the decoder performance saturated with only 8 recording channels (not shown).

11 The decoder trained on V1 activity also saturated with the 8 best recording channels (see Footnote 10).

tual information between decoded population activity and behaviour (conditioning on the identity of the stimulus).

For both animals, we find that knowing the result of the decoder trained on the V4 population activity did not provide as much information about the behavioural response (beyond the information contained in the identity of the stimulus) before training began, but did yield a significant amount of information after training. There was also an increase in information about the behavioural response contained in the activity of the V1 population for M2 (but not M1), though the effect size was smaller than for V4. There are two interpretations to this result: either the subject becomes more dependent on the activity of its V1 and V4 neurons when making its decision,[12] or that information pertaining to the subject's decision is fed back into V1 and V4 from higher cortical regions. However, both of these interpretations are problematic. Since we already showed that the performance of the V4 decoder and the subject's behaviour are similar throughout training, it would make more sense for the subject's decision process to be equally reliant on its V4 activity throughout training. But similarly, there is no reason to suspect that feedback from higher cortical regions involved in the decision making process to the visual cortex should increase with training. Furthermore, the decision of which behavioural response to provide is not necessarily finalised during the stimulus presentation period — the subject has another 400 ms of fixation after the stimulus is removed before they are able to respond, and even then they do not necessarily respond immediately. However, the response time does decline with training (Chen, 2013; Chen et al., 2013), so it may be that decisions made by the subject are initially made after the stimulus is removed, but with training the subject becomes more decisive and feedback pertaining to this decision can consequently be witnessed in the visual areas during the stimulus presentation. This seems the more likely conclusion to draw from the analysis. In particular, we suspect that the rise in information in M1 V1 about the behavioural response is restricted to the final 200 ms of activity, which is where we see increases in information about the stimulus. Although the primary visual cortex has long been believed to process visual information only, recent studies have shown that mouse V1 responds to locomotion, even in the dark (Keller et al., 2012; Pakan et al., 2016; Saleem et al., 2013). This finding lends support to the idea of projections to macaque V1 from motor planning regions, which could be triggered once the subject has decided on its response to the stimulus and is planning its saccade to the response stimuli.

12 Since we only record a small number of cortical neurons, we would here assume that the activity of the neurons which we record are representative of the cortical region as a whole.

3

POWER OF CORTICAL OSCILLATIONS WITHIN V1 LAMINAE

In Chapter 2, we considered the amount of information encoded in the spiking activity of a population of cortical neurons in both the primary visual cortex (V1) and visual area 4 (V4). In this chapter, we will consider the population activity encoded in the CSD, the distribution of flows of current within the cortex. We examine the CSD within V1 across the depth of a single cortical column, and decompose the signal into oscillations at different frequency ranges, examining the amount of information the power of the oscillations contain about a naturalistic video stimulus.

3.1 BACKGROUND

The aggregate population activity generates oscillations in the medium within which neurons reside. These oscillations in the LFPs arise through rhythmic or correlated activity within the local population. The LFP is believed to consist of various components, principally generated by synaptic input currents and their return currents, however there is also contribution from slow calcium-mediated spiking activity and even from fast sodium-mediated action potentials (Einevoll et al., 2013). In particular, pyramidal neurons contribute more to the creation of LFPs than any other type of neuron. This is due to their large dendritic trees, which result in a large spatial separation between synaptic inputs and return currents. LFPs are diffuse, with uncorrelated synaptic activity inducing changes in potential at a range of 200 µm, whilst the effects of correlated activity can be seen at recording sites millimetres away from the source. Since LFPs are generated by localised synaptic currents, it is often more useful to construct a model of the current source density (CSD) which underlies the observed potentials. Furthermore, lower frequency components of the LFP have larger spatial extent than high frequency components (Łęski et al., 2013).

Many brain functions have been tied to cortical oscillations (Buzsáki and Draguhn, 2004; Colgin, 2016; Einevoll et al., 2013), including sensory processing (Henrie and Shapley, 2005; Kreiman et al., 2006; Mazzoni et al., 2011; Szymanski et al., 2011), motor function (Rickert et al., 2005; Scherberger et al., 2005), planning (Buzsáki, 2015), attention (Fries et al., 2001; Jensen et al., 2007; Klimesch, 2012), perception (Fries et al., 1997; Gross et al., 2007; Grossberg and Somers, 1991), memory (Jensen et al., 2002,0; Klimesch, 1999; Liebe et al., 2012; Pesaran et al., 2002; Raghavachari et al.,

2001), even stimulating microglia to reduce the plaque associated with Alzheimer's disease (Iaccarino et al., 2016) and coupling of the brain to the gastric system (Monto et al., 2008; Richter et al., 2017). In addition to this, theoretical research hypothesises that cortical oscillations gate the transfer of information between cortices (Ahissar and Oram, 2015), enable consciousness (Llinás et al., 1998), and facilitate predictive coding (Arnal and Giraud, 2012), speech (Giraud and Poeppel, 2012), and working memory (Dipoppa and Gutkin, 2013).

In particular, previous work has demonstrated that in the macaque V1 there are two LFP frequency bands, 1 Hz to 8 Hz and 60 Hz to 100 Hz, which encode independent information in the macaque V1 about natural stimuli (Belitski et al., 2008). We hypothesised that the two frequency bands are generated through different cortical processes. In this study, we investigated where within the cortical depth these frequency bands are most informative. Under the hypothesis of two independent cortical circuits generating the two bands, we expect to observe that the two frequency bands are generated at different cortical depths.

3.2 METHODS

The experimental data analysed in this chapter was acquired by Daniel Zaldivar and Yusuke Murayama, under the supervision of Nikos Logothetis at the Max Plank Institute for Biological Cybernetics. Data was collected from V1 in four healthy rhesus monkeys (Macaca mulatta; four males 8 kg to 11 kg; 10 years to 12 years). All the experimental procedures were approved by the local authorities (Regierungspräsidium, Baden-Württemberg, Tübingen, Germany; Project Number KY4/09) and were in full compliance with the guidelines of the European Community (EUVD 86/609/EEC) and were in concordance with the recommendation of the Weatherall report for the care and use of non-human primates (Weatherall, 2006). The animals were group-housed in an enriched environment, under daily veterinarian care. Weight, food and water intake were carefully monitored on a daily basis.

3.2.1 *Anesthesia for neurophysiology*

The anesthesia protocol for all the experimental procedures have been described previously (Logothetis et al., 1999, 2001). Briefly, glycopyrrolate (0.01 mg kg^{-1}) and ketamine (15 mg kg^{-1}), were used previous to general anesthesia. Induction with fentanyl (3 mg kg^{-1}), thiopental (5 mg kg^{-1}) and succinylcholine chloride (3 mg kg^{-1}), animals were intubated and ventilated using a Servo Ventilator 900C (Siemens, Ger-

many) maintaining an end-tidal CO_2 of 33 mm Hg to 35 mm Hg and oxygen saturation above 95 %.

The anesthesia was maintained with remifentanil (0.5 µg kg^{-1} min to 2 µg kg^{-1} min) and mivacurium chloride (2 mg kg^{-1} h to 6 mg kg^{-1} h) which ensured no eye movement during electrophygiological recordings. The anesthetics dosage were established by measuring stress hormones and were selected to ensure unaffected physiological response at normal catecholamine concentrations (Logothetis et al., 1999). In addition, it has been shown that using remifentanil has no significant effect on the neurovascular and neural activity of brain areas that do not belong to the pain matrix (Goense and Logothetis, 2008; Zappe et al., 2008). In particular, visual cortex does not bind remifentanil. We monitored the physiological state of the monkey continuously and kept within normal limits. Body temperature was tightly maintained at 38 °C to 39 °C. Throughout the experiment lactate Ringer's (Jonosteril, Fresenius Kabi, Germany) with 2.5 % glucose was continuously infused at a rate of 10 ml kg^{-1} h^{-1} in order to maintain an adequate acid-base balance and intravascular volume and blood pressure were maintained by the administration of hydroxyethyl starch as needed (Volulyte, Fresenius Kabi, Germany).

We used anesthetised animals as it allows for a longer data acquisition for each session, and lets us associate the neural activity to specific features of the stimulus without the effects of the animal's cognitive state, including effects of attention and arousal. Such phenomena would introduce additional signals, complicating the interpretation of the results.

3.2.2 *Visual stimulation*

A few drops of 1 % cyclopentolate hydrochloride were used in each eye to achieve mydriasis. Animals were wearing hard contact lenses (Wöhlk-Contact-Linsen, Schönkirchen, Germany) to focus the eyes on the stimulus plane. The visual stimulation in all experimental sessions was presented to the eye for which the recording sites had the stronger ocular preference. The stimulus was presented using either an in-house custom-built projector (SVGA fibre-optic system with a resolution of 800 × 600 pixels, a frame rate of 30 Hz), or a CRT monitor (Iiyama MA203DT Vision Master Pro 513, frame rate 118 Hz) placed at eye level, 50 cm in front of the eye. We found the same results with both display devices, except that when using a monitor refresh of 30 Hz the stimulus induced cortical oscillations at 30 Hz not seen otherwise. Since this is the result of using an artificial stimulus with a low refresh rate (a well-known issue at this stimulus frequency), we removed this from the data (see Section 3.2.5) and pooled the results across all sessions. The visual stimulus consisted of high contrast

(100 %), gamma corrected, fast-moving, colourful movie clips (no soundtrack) from a commercially available movie. Stimulus timings were controlled by a computer running a real-time OS (QNX, Ottawa, Canada). Stimulus-on periods of 120 s (5 sessions; 1 session: 40 s) were interleaved with stimulus-off periods (isoluminant grey screen) of 30 s.

3.2.3 *Luminosity function*

In order to best approximate the luminosity perceived by macaques, we relied on analogies with the human visual system. Research in humans suggests the luminosity function is linearly related to the L- and M-cone activation, and independent of the S-cone activation (Stockman et al., 2008). Furthermore, the weighting of L and M activations towards perceived luminance is believed to be similar to the L : M ratio in the individual (Stockman et al., 2008). Old world monkeys such as macaques have an L : M ratio which is approximately 1 : 1 (Dobkins et al., 2000), so we assumed a luminosity function equally weighed between the L and M cone activations, $Y(f) = L(f) + M(f)$. The 10° cone fundamentals[1] of Stockman and Sharpe (2000) were used[2] since the cone fundamentals of old world monkeys are known to be very similar to humans (Dobkins et al., 2000). We recorded the emission spectra for both our display devices with a light-spectrometer. By taking the product of the emission spectra for pure red, green and blue with the luminosity function, integrating over wavelength and normalising, we obtained the relative luminance in terms of pixel intensity for the two devices used in the experiment,

$$Y_{\text{projector}} = 0.2171 \cdot R + 0.6531 \cdot G + 0.1298 \cdot B \tag{3.1}$$

$$Y_{\text{CRT}} = 0.1487 \cdot R + 0.6822 \cdot G + 0.1691 \cdot B. \tag{3.2}$$

Here, R, G, and B denote the fractional pixel intensity in the movie file.

3.2.4 *Neurophysiology data collection*

The electrophysiological recordings were performed by doing a small skull trepanation, after which the dura was visualised with a microscope (Zeiss Opmi MDU/S5, Germany) and carefully dissected. The electrodes were slowly advanced into the visual areas under visual and auditory guidance using manual micromanipulator

1 The cone fundamentals are similar to the pigment response curves shown in Figure 1.2, but account for the non-linear relationship between the changes in the pigment and the response produced by the cone.

2 Tabulated in CSV format by the Colour & Vision Research Laboratory of University College London, http://www.cvrl.org/cones.htm.

(Narashige Group, Japan). Electrodes consisted of laminar probes (NeuroNexus Technologies, Ann Arbor, USA). These electrodes contained 16 contacts on a single shank 3 mm long and 150 µm thick. The electrode sites were spaced at 150 µm apart, with a recording area of 413 μm^2 each. We used a flattened silver wire, which was positioned under the skin, as reference electrode (Murayama et al., 2010). The recording access was filed with a mixture of 0.6 % agar dissolved in NaCl 0.9 %, pH 7.4 solution which guaranteed good electrical connection between the ground contact and the animal (Oeltermann et al., 2007). The impedance of the contact points was measured during the experiments and ranged from 480 kΩ to 800 kΩ. The signals were amplified and filtered into a broadband of 1 Hz to 8000 Hz (Alpha-Omega Engineering, Nazareth, Israel) and then digitised at 20.833 kHz with 16 bit resolution (PCI-6052E; National Instruments, Austin, TX).

Session	Display	Video frame rate (fps)	Artefact Frequencies Removed (Hz)	Eccentricity	Stimulus size
E07nm1	CRT	118.089	50, 150	$(4.8 \pm 3.0)°$	$17.9° \times 13.5°$
F10nm1	Projector	30.015	30, 60	$(2.7 \pm 1.0)°$	$15.0° \times 11.3°$
H05391	Projector	30.015	30	$(7.7 \pm 1.0)°$	$20.0° \times 15.0°$
H05nm7	Projector	30.015	30, 60	$(4.2 \pm 1.0)°$	$15.0° \times 11.3°$
H05nm9	CRT	118.089		$(4.0 \pm 3.0)°$	$18.0° \times 13.4°$
J10nm1	CRT	118.089		$(2.6 \pm 3.0)°$	$17.9° \times 13.4°$

TABLE 3.1. *Metadata for recording sessions.* Stimuli were presented using either an in-house custom-built projector (SVGA fibre-optic system with a resolution of 800×600 pixels; "Projector"), or a cathode ray tube monitor (Iiyama MA203DT Vision Master Pro 513; "CRT") placed at eye level, 50 cm in front of the eye. Videos presented at 118 Hz were up-sampled versions of the original 30 Hz video, which was achieved by repeating each frame four times. For artefact removal methodology, see Section 3.2.5.

3.2.5 *Artefact removal*

An artefact removal procedure was performed to reduce the effects of line noise (one session) and phase locking to the refresh rate of the stimulus (the three sessions with 30 Hz stimulus). Artefact frequencies (see Table 3.1) were identified by large, localised peaks in the power spectral density, which was computed with the periodogram method. In each case, the average artefact waveform was found and subtracted from the recorded signal. To correct for phase shifts of the artefact, the averaging and

subsequent subtraction were performed in blocks of 50 artefact periods with a phase chosen to maximise the cross-covariance of the signal with the artefact waveform.

3.2.6 *Current source density*

The CSD was derived from the LFP using the inverse CSD method (Pettersen et al., 2006). To compute this, we used a δ-source model of local field generation, in which the cortical column is approximated by a finite set of infinitely thin discs (one for each recording site). We used a diameter of 500 µm, chosen to correspond to the effective size of columnar activity (Horton and Adams, 2005; Lund et al., 2003). Since this method requires an even spacing between voltage measurements, gaps caused by faulty recording contacts in the electrode were filled in with a local average (Wójcik and Łęski, 2010). A homogeneous cortical conductivity of $0.4\,\mathrm{S\,m^{-1}}$ was assumed (Logothetis et al., 2007). The agar solution placed on top of the recording access point had an NaCl concentration of $9\,\mathrm{mg\,mL^{-1}}$, and the conductivity of this was estimated to be $2.2\,\mathrm{S\,m^{-1}}$ (Kandadai et al., 2012). The CSD was spatially smoothed with a three-point Hamming filter.

3.2.7 *Multi-unit activity*

The MUA was calculated by downsampling the raw signal by a factor of 3, band-passing the voltage recording between 900 Hz to 3000 Hz with a zero-phase sixth-order infinite impulse response (IIR) Butterworth filter, taking the absolute value, and then downsampling by a further factor of 12.

3.2.8 *Receptive field locations*

The spatial RFs were found by reverse correlating the MUA and the pixel-by-pixel Z-scored frame-by-frame difference in luminance with an assumed latency of 66.7 ms. The rate of change in luminance was used because it is known to correlate well with thalamic drive. For each session, the RF centre was manually located using the average of the reverse correlation score across all cortical channels such that the centre was near the point with maximum reverse correlation and the region with highest correlation fell within 1° of the RF centre.

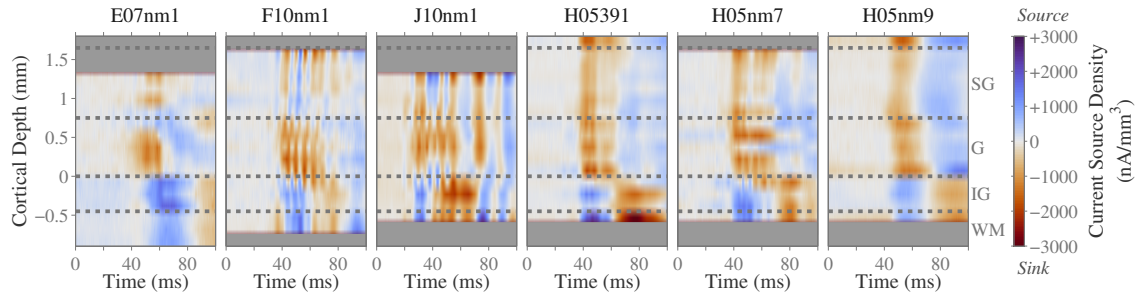

(a) Alignment of CSD across sessions.

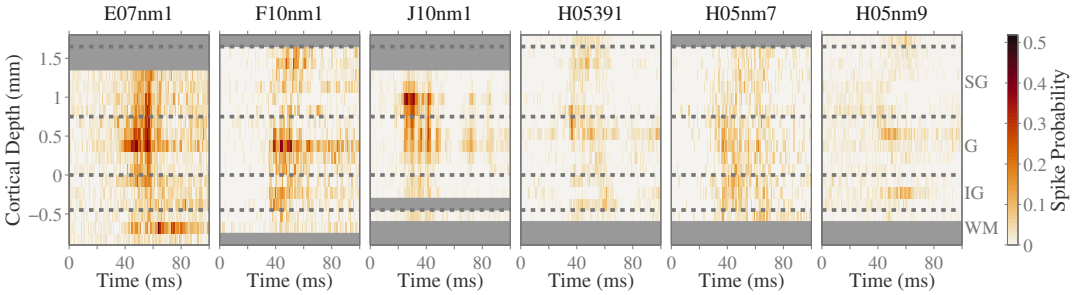

(b) Alignment of MUA across sessions.

FIGURE 3.1. *Electrode alignment.* (a): Stimulus triggered average CSD responses, post-alignment. For sessions H05391, H05nm7, H05nm9 and E07nm1, the average response to onset of the movie stimulus is shown, whereas for sessions F10nm1 and J10nm1 the response to a full-field flash is shown. (b): Corresponding spike densities for the responses in panel (a) (1 ms window duration).

3.2.9 *Aligning electrode penetrations*

For each recording session, the electrode was implanted in V1 at the recording site. For each penetration, we endeavoured to align the electrode such that the most shallow electrode contact was at the boundary between cortical matter and the dura (near layer 1; L1). However, this *ad-hoc* method of alignment is unreliable, in part due to variation in cortical and laminar thickness both within and between subjects. Therefore, we performed *post-hoc* realignment of the electrode contacts using the same methodology as Self et al. (2013) and van Kerkoerle et al. (2014), described below.

To identify the depth of each electrode contact, we measured the potential evoked in response to the onset of the movie clip, and in response to full-screen maximum-luminance 100 ms flash stimuli with 6 s intervals. From the measured potentials, we identified the boundary between the granular (G) and infragranular (IG) compartments as the source-sink reversal in the evoked CSD (Mitzdorf, 1985; Mitzdorf and Singer, 1979). For this measurement, the CSD was computed from the LFP as described in Section 3.2.6, but without applying the Hamming filter to spatially smooth the signal. The data from each electrode was re-aligned such that the source-sink reversal

for each recording session was at a depth of 0 mm, as shown in Figure 3.1a. We estimated the location of the boundary between the G and supragranular (SG) compartments by cross-referencing literature describing the average thickness of cortical laminae in Macaca mulatta, area 17 (Lund, 1973; O'Kusky and Colonnier, 1982).

The majority of thalamic afferents in V1 stimulate layer 4 (L4) (though some argue the connection is indirect; Hansen et al., 2012), and studies have found the first cortical response to the onset of stimuli is at L4Cα, in the middle of the G compartment (Callaway, 1998). Consequently, we also extracted spikes from the broadband recordings, and investigated the spatiotemporal distribution of the spiking response to the onset of the stimulus. For this purpose, we extracted spikes by first high-pass filtering the raw signal above 500 Hz with a zero-phase eighth-order IIR Butterworth filter. We classified any points more than 3.5 standard deviations above the mean signal during inter-stimulus periods as a spike, under the restriction of a minimum inter-spike-interval of 1 ms. Finally, we binned the spikes in intervals of 1 ms and took the average count over all stimulus presentations to find the instantaneous spike probability. As shown in Figure 3.1b, there is a strong and early response near the middle of G across all recording sessions, indicating the electrode alignment is correct.

3.2.10 *Power as a function of depth and frequency*

To derive the power as a function of temporal frequency, the cortical data (LFP and CSD) was filtered in a series of bands each with a fractional bandwidth of 50 %. We held the fractional bandwidth constant instead of the actual bandwidth because cortical power falls off rapidly with frequency, approximately following a power law. Each successive band we considered begins and ends with frequencies 1.291 times higher than the last, so that each band has 0 % overlap with bands further away than its immediate neighbours and a 44 % and 56 % overlap with its preceding and succeeding bands respectively. The data was filtered with a zero-phase sixth-order IIR Butterworth filter, after which the instantaneous power was estimated by taking the squared absolute value of the Hilbert transform. The power in each band was integrated over a series of 50 ms windows, centred at the time of each frame change in the movie (once every 33 ms, leading to a 50 % overlap of neighbouring windows). The power in the 4 Hz to 16 Hz and 60 Hz to 170 Hz bands was extracted in the same manner. In Figures 3.4a and 3.4b, the average power over all frame presentations is shown, expressed in decibels relative to the average broadband 1.5 Hz to 248 Hz power (estimated by summing the power in alternate bands of 50 % fractional bandwidth). Note that in Figures 3.4 and 3.5, datapoints are shown at the band centres, identified as the arithmetic mean between the cutoff frequencies.

3.2.11 *Information as a function of depth and frequency*

Power in each band was computed as described in Section 3.2.10. Then, for each frequency band and depth, we took a 10-bin histogram over the set of measured powers across all frame stimuli and repetitions, with the bin edges chosen such that 10 % of the distribution fell into each bin. We say that the power of the oscillation in a given frequency band is the **response** to the current frame on screen (the **stimulus**). The **binned response** is then the identity of the bin within which the response (power) fell for the histogram. The probability distribution of cortical power differs depending on which frame was presented.

We found the mutual information between the response and the stimulus (Equation 1.1) using the *Information Breakdown Toolbox* for MATLAB (Magri et al., 2009). Bias in the estimated mutual information due to undersampling, described in Section 1.3.4, was corrected for using the PT method (Treves and Panzeri, 1995). Each information calculation was also bootstrapped 20 times with a randomly shuffled mapping from stimulus to response (each also bias-corrected using PT). To ensure the amount of information was statistically significant, we checked each information estimate exceeded the bootstrap mean by more than 3 standard deviations of the bootstrap values. The bootstrap mean was then subtracted from the estimated information, to counter any residual bias.

3.2.12 *Cortical distribution of power*

For each session, the distribution of power across the cortical depth (Figures 3.4a and 3.4b, right-hand insets) was determined by normalising the power at each depth by the summed power across all cortical depths for that band. We then took an average across sessions, weighted by the number of cortical recording sites in each session to prevent faulty (omitted) electrode contact sites from distorting the result.

3.2.13 *Information redundancy*

Information redundancy was computed with the same stimuli and response powers as described above in Section 3.2.11. However, when computing the information redundancy we instead used 3 bins for the cortical response, with each histogram bin containing a third of the power datapoints across all repetitions of the movie stimulus.

First let us define S, to denote the set of stimuli, and X and Y, two different responses (either different frequency bands or the same frequency bands but measured at different depths). The information about the stimulus which is contained in each is $\mathrm{I}(X;S)$ and $\mathrm{I}(Y;S)$, which we computed using the methodology of Section 3.2.11. Additionally, we can consider the information in the joint distribution of simultaneously observed X and Y values, $\mathrm{I}(\{X,Y\};S)$. To compute this value, we considered each combination of the pre-binned X and Y values as a different response, yielding a total of 9 different responses for $\{X,Y\}$.

Using this, we can derive the relative redundancy, which we define as

$$\text{Redundancy}(X,Y;S) = \frac{\mathrm{I}(X;S) + \mathrm{I}(Y;S) - \mathrm{I}(\{X,Y\};S)}{\mathrm{I}(\{X,Y\};S)}. \tag{3.3}$$

If $\text{Redundancy}(X,Y;S) > 0$, this implies that X and Y contain redundant information about S. If $\text{Redundancy}(X,Y;S) < 0$, then X and Y are synergistic, such that knowing the paired state of X and Y simultaneously contains more information about S than one would expect from the information just contained in X and Y individually.[3]

Additionally, we define the relative information gain as

$$\text{InfoGain}(Y \to \{X,Y\};S) = \frac{\mathrm{I}(\{X,Y\};S) - \mathrm{I}(Y;S)}{\mathrm{I}(X;S)}, \tag{3.4}$$

which is the amount of information gained about the stimulus when we already know Y and X is revealed to us, relative to the total amount of information about the stimulus contained in X. InfoGain is an asymmetric measure, unlike Redundancy. If X contains no more information about S than is already contained in Y, then $\mathrm{I}(\{X,Y\};S) = \mathrm{I}(Y;S)$ and we therefore have $\text{InfoGain}(Y \to \{X,Y\};S) = 0$, which makes intuitive sense in line with the concept of information gain. However, if $\mathrm{I}(X;S) = 0$, meaning X contains no information about the stimulus, this would be divergent, so we instead choose to define $\text{InfoGain}(Y \to \{X,Y\};S) = 0$ for this case. If X and Y contain independent information about the stimulus, $\mathrm{I}(\{X,Y\};S) = \mathrm{I}(X;S) + \mathrm{I}(Y;S)$, then we find[4] that $\text{InfoGain}(Y \to \{X,Y\};S) = 1 = 100\%$.

3 Unfortunately, since redundant and synergistic information co-occur when transitioning from knowing either X or Y to knowing their joint state X,Y, it is not possible to quantify the redundancy and synergy in isolation (Averbeck et al., 2006; Banerjee and Griffith, 2015; Griffith and Koch, 2014; Latham and Nirenberg, 2005; Williams and Beer, 2010). The term which we refer to as "Redundancy" in Equation 3.3, is in reality the difference of the true (but unobservable) redundancy and synergy about S in X and Y. Consequently, we can only conclude how much more redundancy than synergy there is, and when redundancy exceeds synergy that there is at least some redundancy. For instance, in the case $\text{Redundancy}(X,Y;S) = 0$, we can only conclude that there is the same amount of synergy as redundancy; it is not necessarily the case that X and Y contain exclusively independent information about S.

4 However, as stated above in Footnote 3, $\text{InfoGain} = 1$ is necessary but insufficient to conclude that X and Y contain exclusively independent information about S, since the same result can be achieved provided their synergy and redundancy effects cancel each other out. Should X and Y contain more

3.2.14 *Signal and noise correlations*

We also computed the signal and noise correlation between pairs of unbinned responses to the movie stimulus. The power was extracted as described in Section 3.2.10.

For the signal correlation, the power in response to each stimulus was averaged over repetitions, producing a single mean response to each frame. Then, for a given frequency band and recording depth, we correlated the average frame responses against the average responses elicited by another frequency band or depth using the Pearson correlation coefficient (defined in Equation 2.5).

The noise correlation was computed by considering the power elicited during a single frame over all repetitions of the movie stimulus. We then computed the Pearson correlation coefficient between responses X and Y over presentations of the same stimulus. This was repeated for each pair of frames, and we took the average over all pairs as the noise correlation between X and Y.

For both the signal and the noise correlation, we produced 20 bootstrap correlations by repeating the procedure for randomly paired responses by shuffling over either stimuli (signal) or repetitions (noise). After averaging over sessions, correlation coefficients which were less than three standard deviations of the bootstraps from the bootstrap mean were deemed not significantly correlated (shown in white in Figures 3.7 and 3.9).

3.2.15 *Information about scene changes*

To compute the amount of information encoded in the cortical activity about scene changes in the stimulus, we used the same procedure as described in Section 3.2.11. However, instead of computing the amount of information encoded about the unique identity of each frame in the movie stimulus, we labelled our stimuli as the number of frames since the last scene cut in the movie — except for frames occurring more than T_{sc} seconds after a scene cut which were instead all labelled as -1. The parameter T_{sc} was varied over the range $[0, 0.5]$. This stimulus relabelling scheme meant that all frames following a scene cut were identified as the same stimulus condition, and frames not involved in a scene cut were labelled as another stimulus.

For this to provide a different quantification of information than labelling each individual frame with a unique ID, it is important that the number of collisions provided by the non-injective label remapping is sufficiently large. Of the 96 scenes in the presented movie stimulus, only 5 had a duration shorter than 0.5 s, and all of

synergistic than redundant information about S, we will observe a relative information gain exceeding $1 = 100\%$.

these were at least 0.4 s long. Consequently, when we chose $T_{sc} <= 0.4$, this encoding of the stimulus preserves information about the occurrence of a scene cut but all the information about which scene begins or its contents is removed.

For this part of the analysis, we did not integrate the power over 50 ms but instead used the instantaneous power as the cortical response. We expressed the information about scene changes as a percentage of the total information present in the instantaneous CSD power.

3.2.16 *Information about spatial components*

To extract a measure of change in the movie at different spatial scales, we followed the procedure illustrated in Figure 3.2 and described below. First, we took the two-dimensional fast-Fourier transform of a 224 px square from the luminance of the movie (with luminance determined as described in Section 3.2.3). We applied a fourth-order IIR Butterworth filter with a width of one octave by means of a mask in the Fourier domain, and then projected the output back to the spatial domain. We then took the pixel-wise difference between each spatially-filtered pair of consecutive frames. We integrated the absolute magnitude of the rate-of-change of spatially filtered luminance within a 2° diameter circular window centred at the receptive field location (determined as described in Section 3.2.8).

Applying this to the entire movie provided a temporal sequence of luminance changes in each spatial range. Similar to how the cortical response was binned, for each spatial range we took a 10-bin histogram and labelled each frame according to the identity of the bin in which its rate-of-change of luminance fell. The mutual information between this labelling of the stimulus and the neural response — the power within 4 Hz to 16 Hz and 60 Hz to 170 Hz frequency bands — was computed with a 67 ms lag between stimulus and response.

3.2.17 *Information about fine and coarse luminance changes*

Coarse and fine luminance changes in the stimulus were extracted using the methodology of Section 3.2.16, but instead of a bandpass filter we used a low-pass (<0.3 cpd) and high-pass (>1 cpd) fourth-order IIR Butterworth filter respectively. For both the 4 Hz to 16 Hz and 60 Hz to 170 Hz CSD powers, we computed the correlation with and information about the coarse and fine luminance changes.

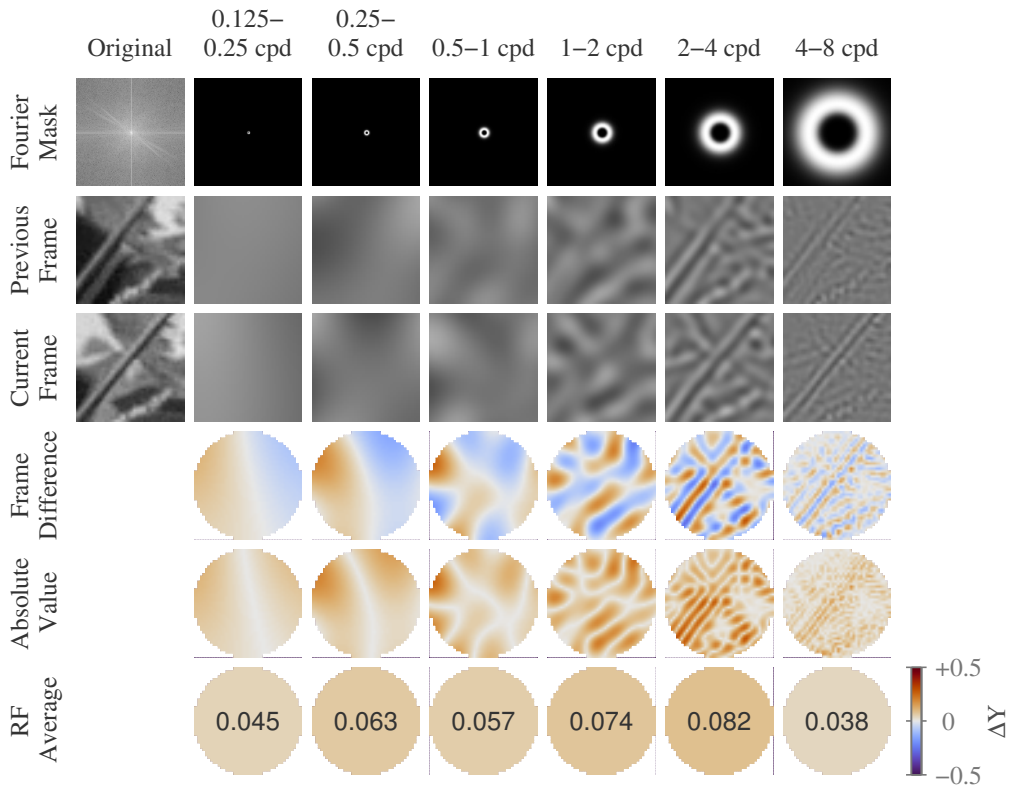

FIGURE 3.2. *Extraction of spatially filtered luminance components.* The luminance of the original video (left) is fast-Fourier transformed in a 224 px × 224 px square for each frame (top-left: FFT of "current frame"). The mask isolates bands of spatial frequencies that are one octave wide (Row 1), yielding the spatially filtered frames (Rows 2 and 3). The stimulus magnitude at each spatial frequency band was obtained by taking the luminance difference of successive frames (Row 4), taking its absolute value (Row 5), and averaging this within the receptive field (Row 6).

3.2.18 *Information latency between granular and infragranular compartments*

The information about fine and coarse stimuli contained in 4 Hz to 16 Hz and 60 Hz to 170 Hz neural frequency bands was computed as a function of the lag between stimulus and response, in steps of 1.73 ms. For each cortical recording depth, we determined the latency of the response as the lag which gave the maximum amount of information about the stimulus. This step was performed for each session individually. Then, for each pair of electrode recording depths, we took the difference in their peak latencies (ΔLatency), and performed a t-test over the 6 sessions to test for statistical significance. In Figure 3.13, the insignificant ($p > 0.05$) latency differences are shown in white.

3.2.19 *Information about spatiotemporal stimulus components*

We extended the methodology of Section 3.2.16, to extract specific temporal components (as well as spatial components) of the movie stimulus. To achieve this, we inserted an additional step, and applied a fourth-order IIR Butterworth filter across the temporal dimension whilst in the Fourier domain. There were many points in the processing pipeline where we could add the temporal filter step, and we chose to apply the temporal filter after temporally differentiating the signal. However further investigations demonstrated that the ordering of these steps in the analysis did not impact our results (not shown). The full procedure was thus as follows.

1. Apply spatial filter.
2. Measure rate of change over time.
3. Apply temporal filter.
4. Take absolute value.
5. Integrate over receptive field location.
6. Compute information with 67 ms lag between stimulus and response.

3.3 RESULTS

To understand how oscillatory activity at different layers of primary visual cortex (V1) encodes naturalistic visual information, we recorded neural activity in cortical area V1 with a multi-contact laminar electrode array in four monkeys (Macaca mulatta), anaesthetised with opiates. The animals were presented with a clip from a Hollywood

movie which lasted 40 s (1 session) or 120 s (5 sessions) and was repeated 40 to 150 times (see Section 3.2).

Each electrode housed 16 equally spaced (150 µm) contacts spanning a total depth of 2250 µm, and was inserted perpendicular to the cortical surface (Figure 3.3a). We recorded broadband LFPs from each electrode contact, and used the LFPs to compute at each electrode location the CSD, a measure of the local flow of charge at any given point (Einevoll et al., 2013). To align the depth of the electrodes across recording sessions, we identified the border between Layer 4 and 5 as the inversion of the CSD from sink to source in response to the onset of visual stimulation (see Schroeder et al., 1991, and Figure 3.1). We then divided the cortical depth into granular (G), supragranular (SG), and infragranular (IG) compartments (see Section 3.2.9 for details).

In order to identify the spatial area of the movie stimulus that modulated the neural activity that we recorded, we estimated the spatial RF of the MUA recorded in each electrode contact site by reverse-correlating the rate of change of luminance of each pixel in the movie with the MUA. The spatial-RF locations that we identified (see Figure 3.3b for an example session) did not vary with depth, confirming the angle of the electrode penetration was perpendicular and that all electrode contacts were recording from the same cortical column.

3.3.1 *Distribution of information across depth and frequency*

We considered how neural activity in different frequency bands changed in response to the movie. To visually convey how information is encoded into different frequency bands (Figure 3.3c), we filtered the CSD at three cortical depths in three spectral bands during eight presentations of a portion of the movie clip. Within this small sample of the overall dataset, one can observe that large, low-frequency deflections in the activity are consistent across trials within G and IG depths, and the envelope-amplitude of activity in the 60 Hz to 170 Hz band is also consistent across trials, most clearly for the SG compartment. Activity in the 28 Hz to 44 Hz range was more variable across trials, and did not seem to be stimulus modulated.

We quantified these observations by computing how much information the spectral power of the LFP and CSD contain about the identity of which movie frame is currently on screen (see Section 3.2.11). Despite the fact that the power is distributed evenly across depth and decays smoothly as frequency increases (Figures 3.4a and 3.4b), we found that information in the spectral power was localised around particular depths and frequencies (Figures 3.4c and 3.4d).

For both LFP and CSD, information about the movie is highest in the 4 Hz to 16 Hz range at the top of the granular (G) compartment (layer 4A/B), and >60 Hz near the

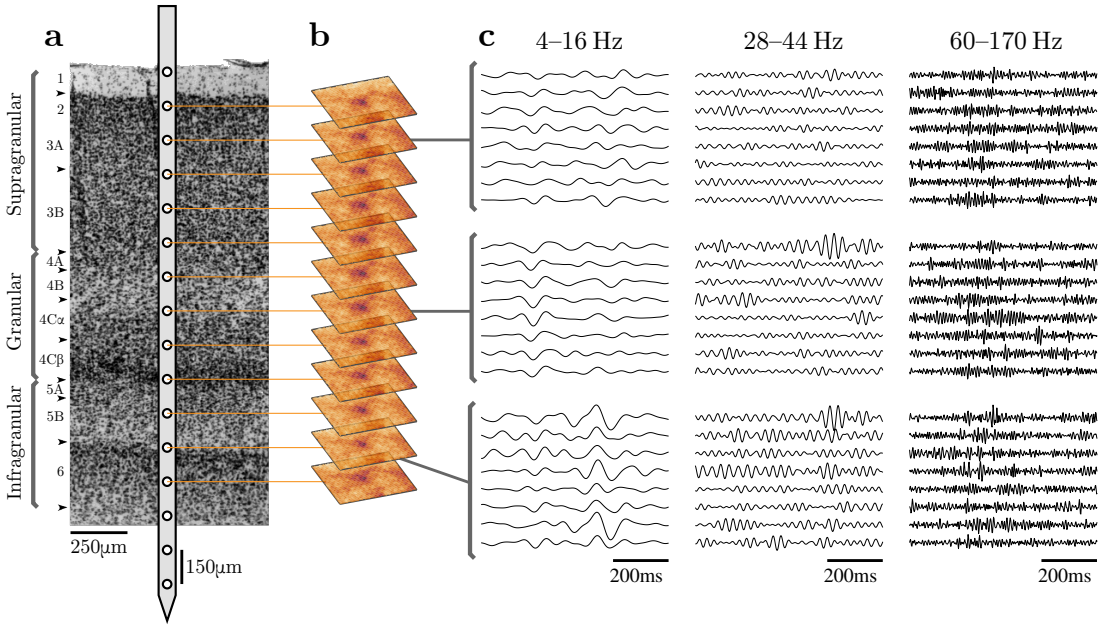

FIGURE 3.3. *Overview of data collection and example data.* (a): Illustration of experimental recording setup, showing approximate locations of electrode contacts in relation to a Nissl stained section of macaque V1 cortex. Boundaries between cortical laminae are indicated with arrowheads. Stain reprinted from Tyler et al. (1998), with permission (Copyright © 1998 Wiley-Liss, Inc). (b): Receptive field locations were consistent across the cortical depth. Location of receptive field for each cortical recording site was identified by reverse correlating the MUA with the luminance changes of each pixel in the movie (session E07nm1). (c): Example CSD traces from simultaneous recordings at three cortical depths for eight repetitions of a movie fragment (session H05nm7). The data is split into three temporal frequency bands (4 Hz to 16 Hz, 28 Hz to 44 Hz, and 60 Hz to 170 Hz).

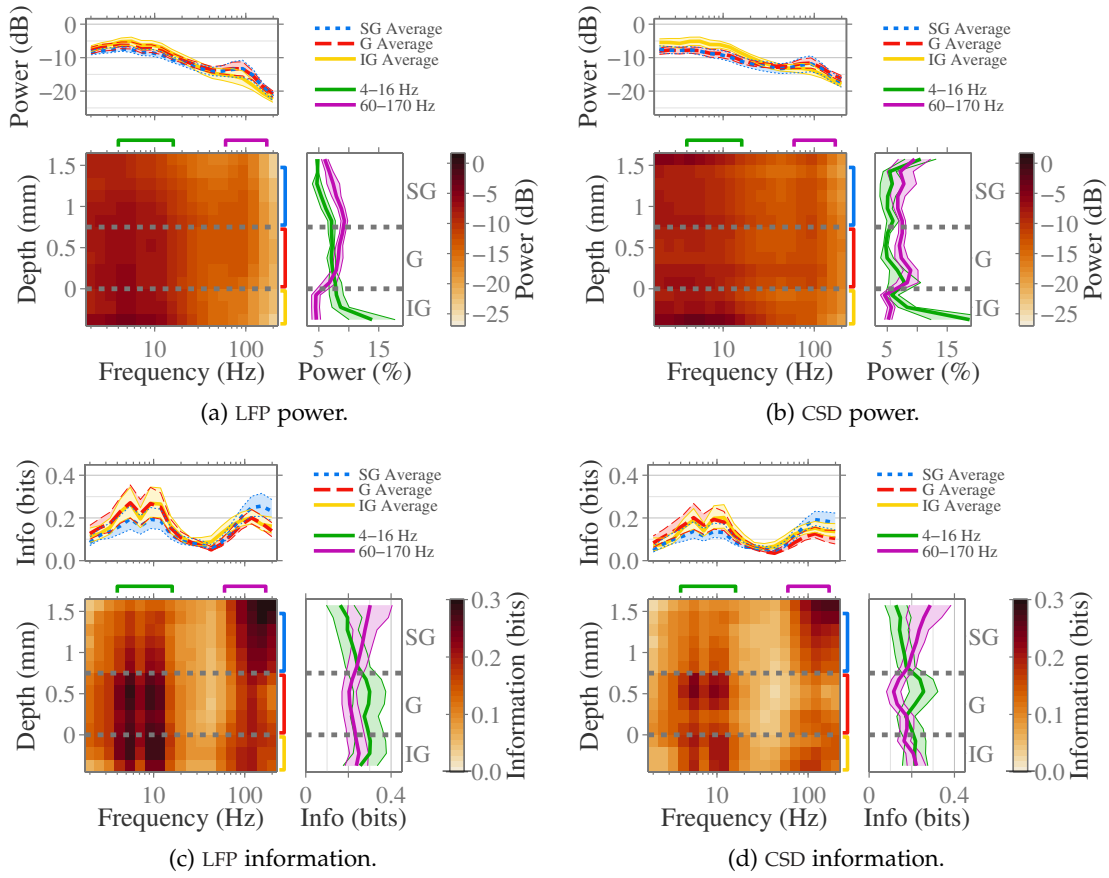

(a) LFP power.

(b) CSD power.

(c) LFP information.

(d) CSD information.

FIGURE 3.4. *Distribution of visual stimulus information across both cortical depth and frequency.* (a): Distribution of LFP power during stimulus presentation. Plot shows the geometric mean power over 6 sessions. Above, mean power within SG, G and IG compartments. Right, laminar distribution of LFP power in 4 Hz to 16 Hz and 60 Hz to 170 Hz frequency bands. (b): Same as (a), but distribution of CSD power instead of LFP power. (c): Distribution of information about the stimulus contained in LFP power. Plot shows the mean information over 6 sessions. Above, mean information within SG, G and IG compartments. Right, cortical distribution of information in the power in 4 Hz to 16 Hz and 60 Hz to 170 Hz frequency bands. (d): Same as (c), but for information in CSD power instead of LFP power. Note that the information, (c) and (d), is distributed very differently from the LFP and CSD power, (a) and (b). Each datapoint in (c) and (d) was tested for statistical significance using bootstrapping, and each datapoint was found to be significant.

top of the SG compartment (layer 2). Additionally, there are secondary local maxima in IG for both the 4 Hz to 16 Hz and 60 Hz to 150 Hz ranges. These results are consistent across all individual recording sessions (Figure 3.5). Since LFP and CSD have the same distribution of information, but the CSD has better spatial localisation than the LFP (Einevoll et al., 2013; Kajikawa and Schroeder, 2011), we will restrict ourselves to only studying the CSD for the remainder of the chapter.

These results suggest that within a single neocortical column there are two frequency bands which act as stimulus-encoding channels, which are approximately the 4 Hz to 16 Hz and 60 Hz to 170 Hz frequency ranges.

3.3.2 *Information redundancy between frequencies*

These results raise the question whether the two frequency ranges (4 Hz to 16 Hz and 60 Hz to 170 Hz) encode the same or different information about the stimulus, and whether the same information is encoded within a given frequency band across the entire cortical depth. To answer this, we computed the redundancy between pairs of frequency bands of the information about the stimulus which they encode (see Section 3.2.13). Computing information redundancy allows us to quantify how similar the information about the stimulus is for a given pair of frequency bands and depths — high redundancy shows the information about the stimulus is mostly the same in the two bands, low redundancy means the two bands contain independent information about the stimulus.

As shown in Figure 3.6, we found there are two frequency domains within which information is redundant: 4 Hz to 40 Hz and >40 Hz. Furthermore, the information contained in neural frequencies <40 Hz is different to the information contained in frequencies >40 Hz, since we measured these to be independent (redundancy $\leq$0 %, information gain $\geq$100 %. Additionally, we note that the same <40 Hz and >40 Hz division is observed for the signal correlation (Figure 3.7), and our results corroborate earlier findings (Belitski et al., 2008). Taken together, our results thus show that the two bands (4 Hz to 16 Hz and 60 Hz to 170 Hz) contain the most information about the stimulus and encode different information about the stimulus.

3.3.3 *Information redundancy across depth*

Next, we investigated whether the information contained in these frequency bands was the same across the cortical depths. To this end, we computed the redundancy of the information about the stimulus contained in oscillations at different cortical

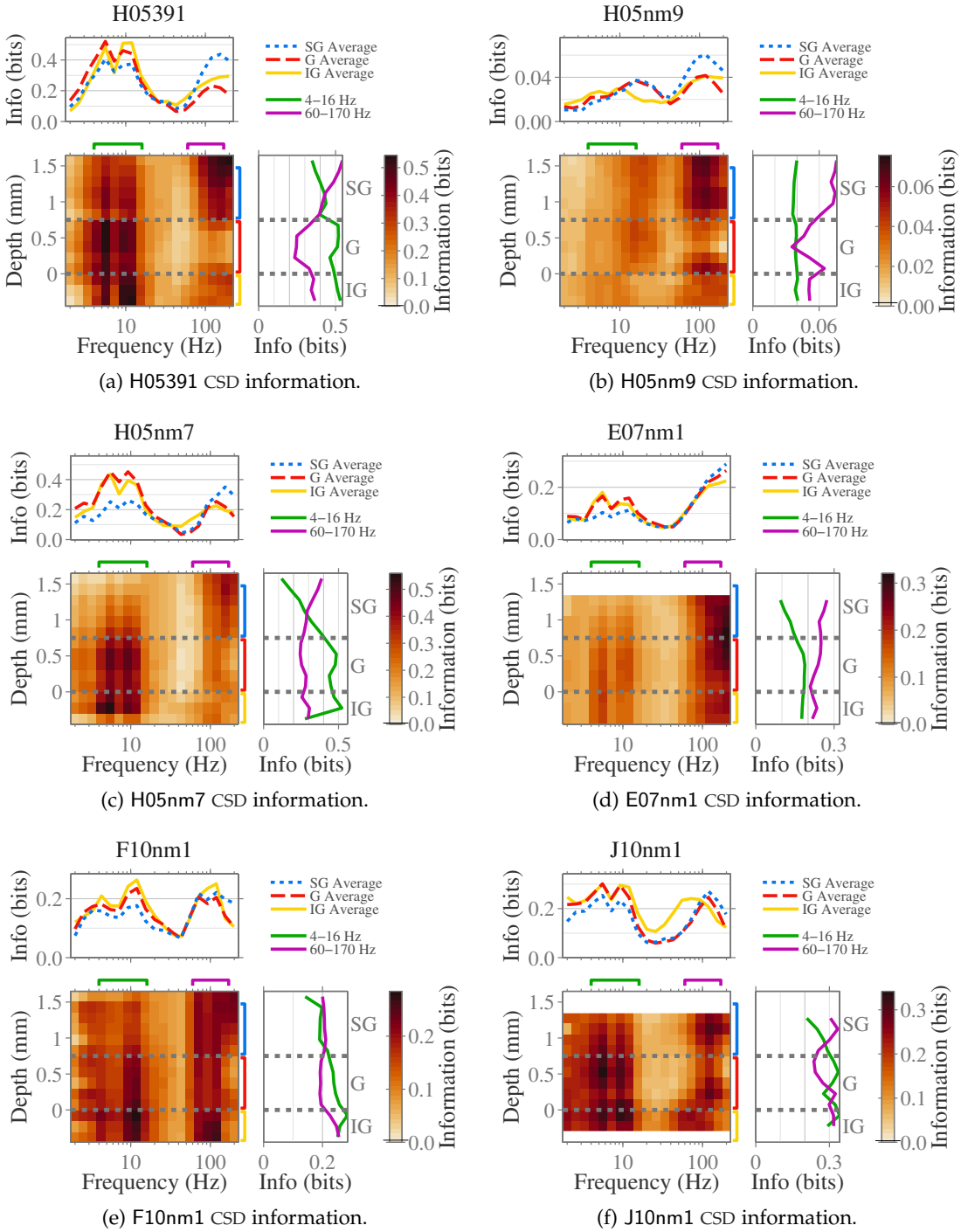

(a) H05391 CSD information.

(b) H05nm9 CSD information.

(c) H05nm7 CSD information.

(d) E07nm1 CSD information.

(e) F10nm1 CSD information.

(f) J10nm1 CSD information.

FIGURE 3.5. *Distribution of information about the movie across both cortical depth and frequency for individual sessions* Same as Figure 3.4d, but shown for each recording session individually.

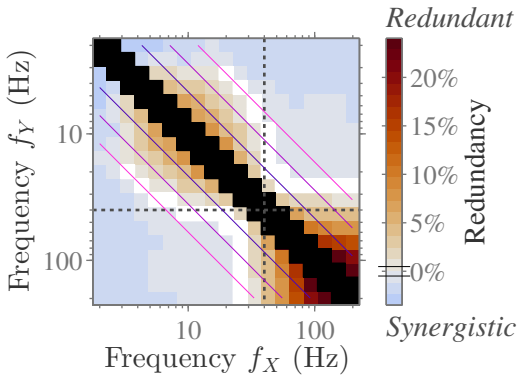

(a) Redundancy between frequencies.

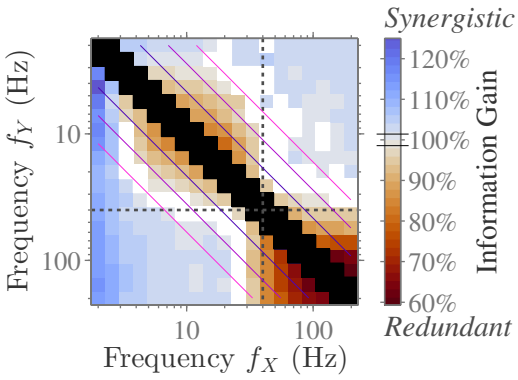

(b) Information gain between frequencies.

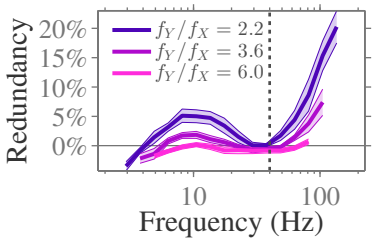

(c) Redundancy cross-section.

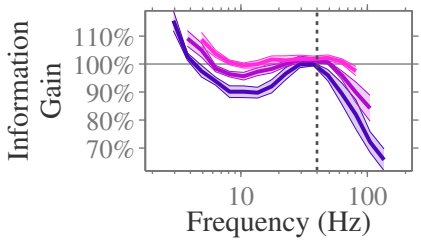

(d) Information gain cross-section.

FIGURE 3.6. *Information redundancy between CSD frequency components.* (a): Redundancy (as defined in Equation 3.3) between pairs of frequencies, averaged over all cortical recording depths, then averaged over 6 sessions. Each datapoint was tested for statistical significance using bootstrapping, and non-significant values are shown in white (the median threshold for statistical significance is shown as a line across the colour bar). The leading diagonal, which is trivially redundant, and second diagonal, which is highly redundant due to the 50 % overlap between neighbouring frequency bands, are removed (black). (b): Same as (a), but for the asymmetric information gain InfoGain $(Y \to \{X, Y\}; S)$ (defined in Equation 3.4). (c): Redundancy between pairs of bands with a fixed ratio between their frequencies, plotted against the geometric mean of their band centres. The shaded region indicates the standard error on the mean over 6 sessions. (d): Same as (c), but for the information gain. We averaged over both $Y \to \{X, Y\}$ and $X \to \{X, Y\}$ for each pair of frequencies when tracing the information gain between pairs of channels with constant frequency ratio.

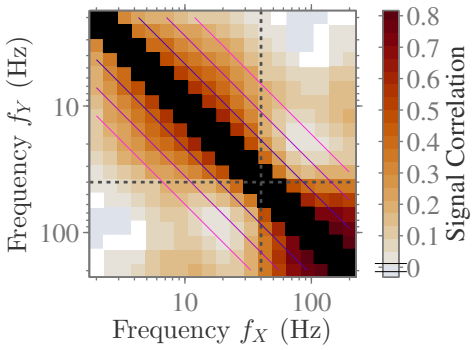

(a) Signal correlation between frequencies.

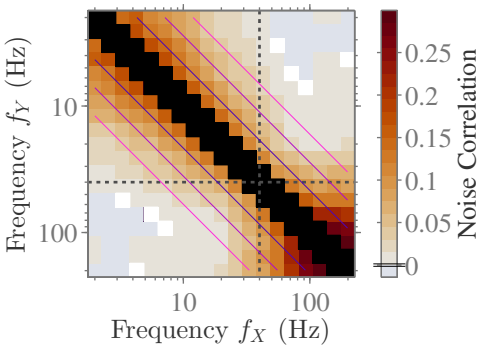

(b) Noise correlation between frequencies.

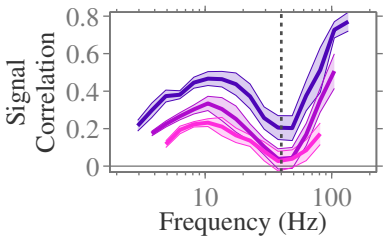

(c) Signal correlation cross-section.

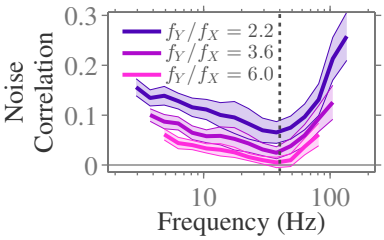

(d) Noise correlation cross-section.

FIGURE 3.7. *Correlation between CSD frequency bands.* (a): Signal correlation between the power in pairs of frequencies, median across 12 to 14 cortical recording sites, mean over 6 sessions. The leading diagonal, which is trivially perfectly correlated, and second diagonal, which is highly correlated due to the 50 % overlap between neighbouring frequency bands, are removed (black). (b): Noise correlation between the power in pairs of frequencies, median across 12 to 14 cortical recording sites, mean over 6 sessions. (c): As per Figure 3.6c, the signal correlation between pair of frequencies with a fixed ratio between their frequencies, plotted against the geometric mean of their band centres. (d): Same as (c), but for noise correlation.

depths, both within the same band at each depth, and between different bands (Figure 3.8; see Section 3.2.13).

Within the 4 Hz to 16 Hz frequency range, there is redundancy across the entire cortical depth, but there are two distinct cortical compartments (above and below the CSD reversal, marked as 0 mm depth) within which there is increased redundancy. These findings are in agreement with Maier et al. (2010), who found a transition corresponding to the G/IG boundary which isolated two cortical compartments with high coherence for LFP oscillations <100 Hz. We also find that gamma oscillations (60 Hz to 170 Hz) have substantial redundancy across the cortical depth.

We investigated the redundancy between cortical oscillations and spiking activity by extracting the power of the 900 Hz to 3000 Hz frequency range which indicates the aggregate multi-unit activity (MUA). The information in the MUA is redundant with the 60 Hz to 170 Hz frequency band (Figure 3.8, right-hand panels). This indicates that the population spiking activity contains the same information as the gamma range, which is in agreement with previous findings (Belitski et al., 2008).

Comparing the 4 Hz to 16 Hz band with either higher frequency bands, we found the lower frequency range contains information which is not expressed in the higher frequencies at any cortical depth. It consequently follows that the two localised regions of high information content from Figure 3.4d (granular 4 Hz to 16 Hz and supragranular >60 Hz) are not redundant to each other and contain complementary information about the stimulus.

We also evaluated the signal and noise correlation between pairs of channels across these frequency bands. As shown in Figure 3.9, the signal and noise correlation both follow the same distribution as the redundancy.

These findings prompted us to investigate which properties of the stimulus were encoded by the two frequencies bands. Since their powers contain independent information about the stimulus, we want to find two orthogonal properties of the stimulus which are encoded by these two complementary spectral bands.

3.3.4 *Information about scene cuts*

Flash stimuli and the onset of the movie both induce large depolarisations in the cortex, with characteristic waveform profiles. Indeed, we used the characteristic CSD response to align our electrode penetrations between sessions (see Section 3.2.9). Similarly, transitions between movie scenes cause discontinuities in the content of the stimulus, which may involve a similarly large change in the gross luminance of the stimulus. The sudden transitions associated with scene cuts can be considered analogous to the discontinuities in visual stimulation associated with saccades during

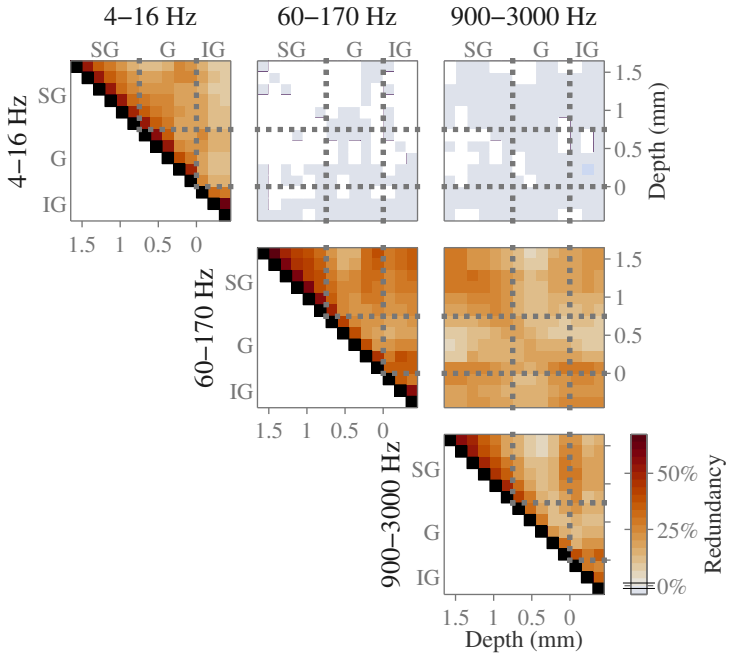

(a) Redundancy.

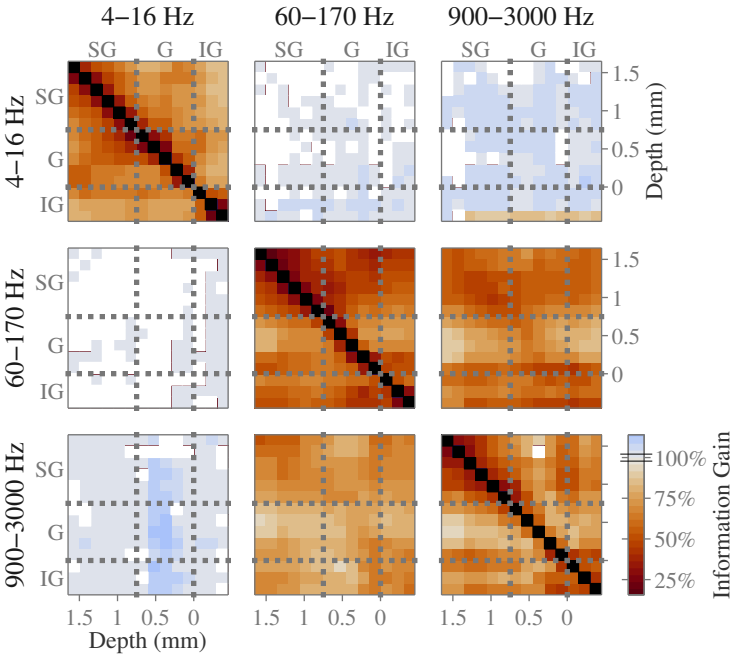

(b) Information gain.

FIGURE 3.8. *Redundancy of information contained in pairs of cortical laminae, for isolated CSD frequency bands and MUA.* We show both the redundancy, (a), and the information gain, InfoGain $(Y \to \{X, Y\}; S)$, (b). Since redundancy, as we define in Equation 3.3, is symmetric, the lower triangle (removed) is a mirror image of the upper triangle. Information gain is an asymmetric measure, and we show the gain from knowing the y-axis datapoint to knowing both x and y datapoints. Non-significant datapoints are shown in white, with the median upper and lower thresholds for significance indicated by the black lines across each colour bar.

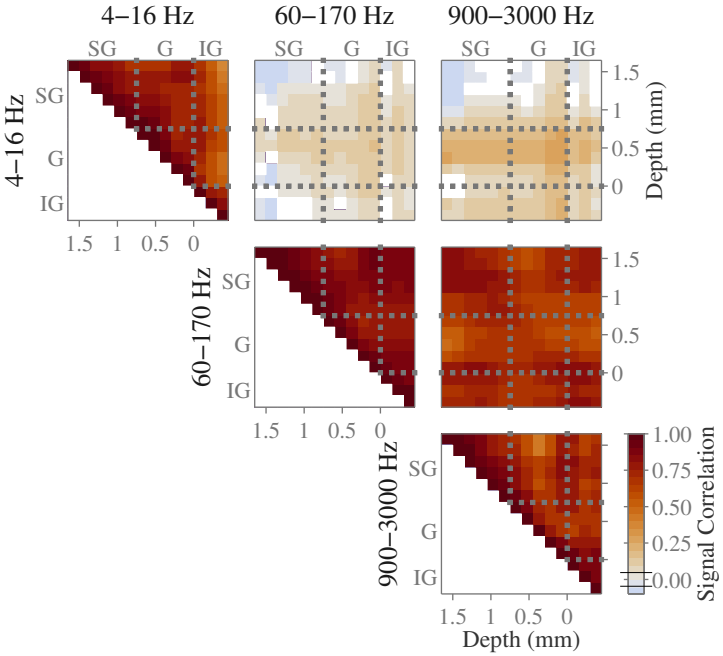

(a) Signal correlation.

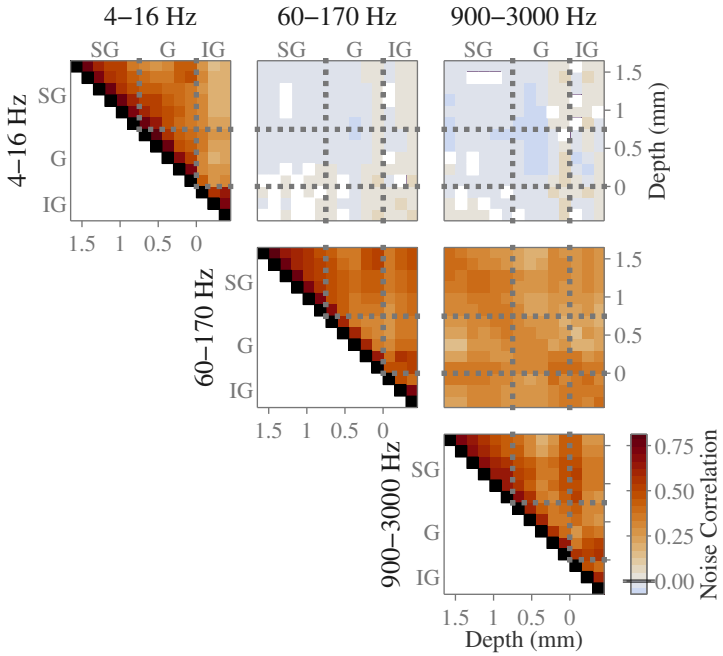

(b) Noise correlation.

FIGURE 3.9. *Correlation across cortical laminae of power in CSD frequency bands and MUA.* Since correlation is symmetric, the lower triangle (removed) is a mirror image of the upper triangle. Non-significant datapoints are shown in white, with minimum and maximum significance thresholds indicated by the black lines across the colour bar.

natural behaviour. Consequently, we investigated how much information the cortical response contained about scene cuts in the stimulus.

This was achieved by relabelling the frames in the stimulus to encode only the length of time since the last scene cut, up to a certain threshold duration. Information about which scene cut was presented was destroyed by ensuring the stimulus labels following each of the 96 scene cuts collided with each other. Information about frames past the scene cut horizon threshold was destroyed by labelling all remaining frames as identical (see Section 3.2.15 for more details).

We found that approximately a quarter of the information in the 4 Hz to 16 Hz range pertained to the activity immediately following scene cuts, as shown in Figure 3.10a. In contrast, only about a tenth as much (2.5 %) of the information contained in both the 60 Hz to 170 Hz power and the MUA was explained by the timing of scene cuts. Consequently, we conclude that scene changes (or saccades in natural behaviour) is one property of the visual feed which is encoded differently between the 4 Hz to 16 Hz and 60 Hz to 170 Hz bands.

After a short delay, due to the latency of the visual system, the amount of information about scene cuts rises and saturates quickly. Consequently, we can conclude that 4 Hz to 16 Hz power only has information about scene cuts transitively, lasting for approximately 100 ms after the response to the scene cut begins. Also noteworthy, the fraction of the 4 Hz to 16 Hz information which is about scene changes is not homogeneous: 5 % to 10 % more of the information encoded in upper-G and upper-IG was explained by scene cuts than in lower-G and lower-IG.

Using a static scene cut horizon of 200 ms, we investigated the fraction of information explained by scene cuts in the cortical power as a function of frequency (see Figure 3.10b). The amount of information explained by scene cuts is highest for the 7 Hz to 20 Hz range.

These results demonstrate one property of the movie stimulus which is strongly encoded by one frequency range — namely the fast, global, changes in luminance associated with scene cuts. Next we generalised this property to consider different spatial and then temporal scales of change in the movie.

3.3.5 *Information about spatial frequency components of visual stimulus*

We next considered the amount of information about different spatial scales of the movie stimulus. Since neurons in the primary visual cortex are known to respond strongly to moving sinusoidal gratings with specific spatial frequencies, it is intuitive to consider how much information the frequency bands contained about changes in luminance as a function of spatial frequency.

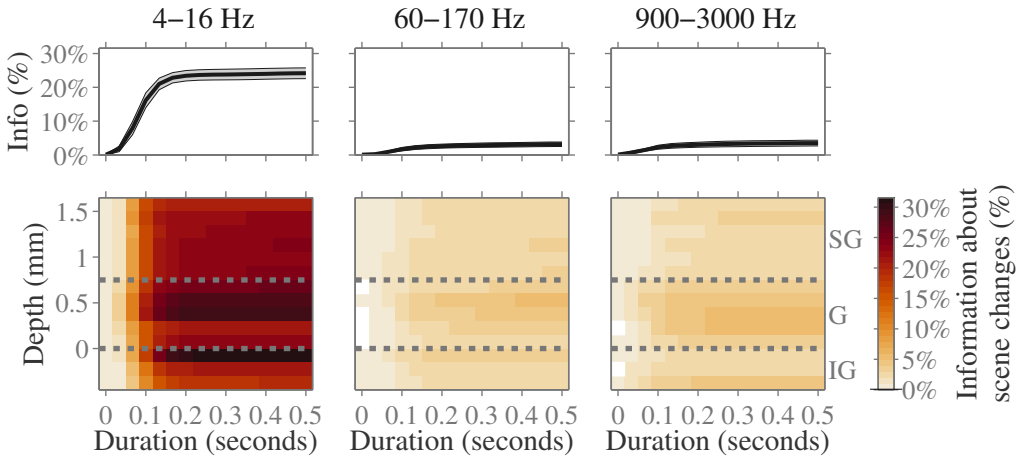

(a) As a function the duration after the scene cut horizon threshold.

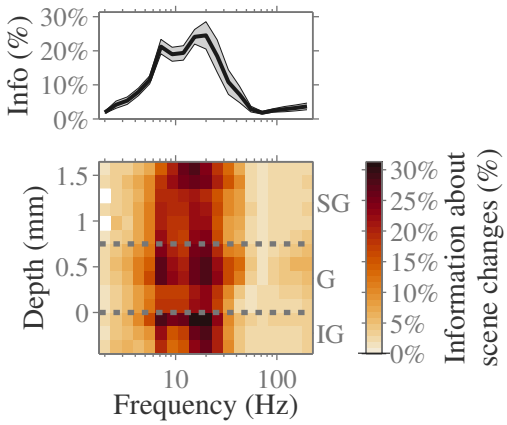

(b) Across a range of cortical frequencies.

FIGURE 3.10. *Information about the presence of scene cuts.* We computed the information about scene cuts as described in Section 3.2.15, and for each session expressed this as a proportion of the total information present (indicated in Figure 3.5) before averaging across recording sessions. (a): Information in the power across the cortical depth for the 4 Hz to 16 Hz (left) and 60 Hz to 170 Hz (middle) frequency bands, and MUA (900 Hz to 3000 Hz; right), averaged over 6 sessions. Information values which were not significantly different from the bootstrap distribution are shown in white, with the median threshold for significance indicated by a black line across the colour bar. Above, the average percentage of information explained by scene cuts over all cortical recording sites is shown, with the standard error across sessions indicated by the shaded region. (b): Information about scene cuts contained in a range of CSD frequencies, in which we only considered the time since the last scene cut for the 0.2 s immediately following each cut.

We decomposed the series of frames in the movie into set of spatial frequency components by finding the rate of change of luminance within a given set of spatial frequency bands (as described in Section 3.2.16 and Figure 3.2), and then computed the amount of information about this series contained in the neural activity.

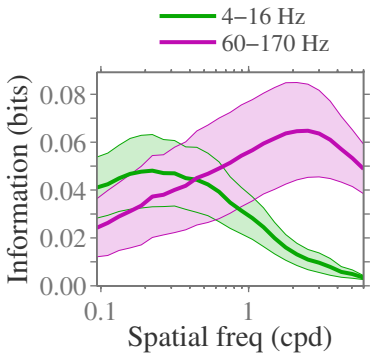

(a) Information about spatial components.

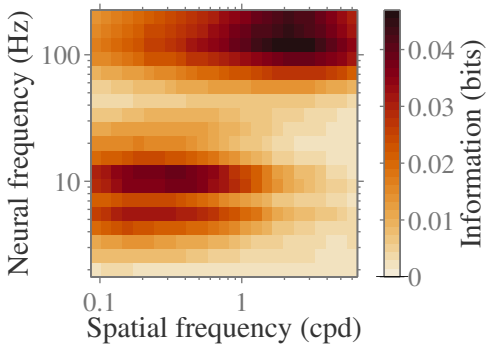

(b) Information about spatial components in different neural frequency bands.

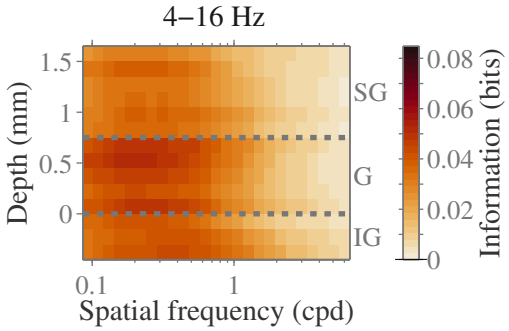

(c) Information about spatial components in 4 Hz to 16 Hz CSD across cortical depth.

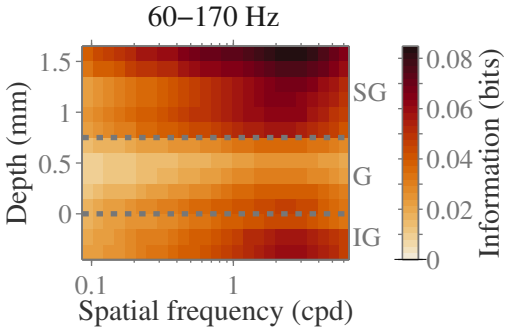

(d) Information about spatial components in 60 Hz to 170 Hz CSD across cortical depth.

FIGURE 3.11. *Information about different spatial components across laminae and frequency bands.* (a): Information about spatial components of the stimulus contained in low frequency CSD power (4 Hz to 16 Hz, average of information within G compartment; green) and high frequency CSD power (60 Hz to 170 Hz, average of information within SG compartment; purple). Shaded area: standard error across 6 sessions. (b): Information about visual spatial components contained in a range of CSD frequencies, median over 12 recording sites. (c) and (d): Information in low (4 Hz to 16 Hz) and high (60 Hz to 170 Hz) CSD frequency bands across cortical laminae. In each plot, the mean over 6 sessions is indicated.

The results are summarised in Figure 3.11a, which shows the information encoded in the two frequency bands, averaged across the whole cortical depth. We found the low frequency CSD bands (<40 Hz) contained more information about low spatial frequencies (0.1 cpd to 0.6 cpd), whereas the higher spectral frequencies (>40 Hz) contained more information about high spatial frequencies (0.6 cpd to 5.0 cpd). Importantly, there was no continuous transition between these two; as shown in Figure 3.11b, we instead observe an abrupt change at 40 Hz, with lower and higher

neural oscillation frequencies tuned to stimulus features with different spatial frequencies. Neural oscillations at intermediate frequencies do not encode intermediate spatial components of the stimulus — they do not encode any spatial aspect of the stimulus.

These observations held true across the entire cortical depth (Figure 3.11c and Figure 3.11d), with the two frequency bands (4 Hz to 16 Hz and 60 Hz to 170 Hz) containing information about opposing spatial frequencies.

Since information theoretic measures capture any possible relationship between stimulus and response, we cannot use it to determine the nature of how changes in luminance lead to changes in cortical power. To resolve this question, we investigated the correlation between the CSD power and both coarse (<0.3 cpd, low-pass spatial filter) and fine (>1 cpd, high-pass spatial filter) spatial components of the movie stimulus, illustrative example traces of which are shown above Figure 3.12. These two spatial components have a relatively low coefficient of correlation with each other ($r = 0.18$), indicating that although these aspects of the movie stimulus do covary, most of their behaviour is independent.

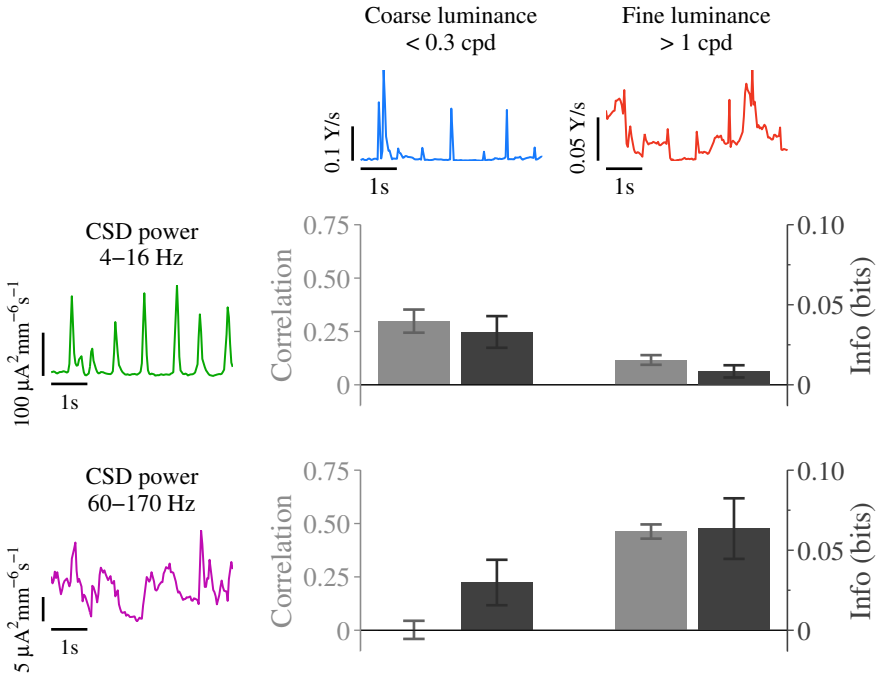

FIGURE 3.12. *Overview of information components.* Relationship between Coarse/Fine changes in luminance and Low/High frequency neural activity. Left: Instantaneous power in 4 Hz to 16 Hz band (averaged over trials and SG layers) and 60 Hz to 170 Hz band (averaged over trials and G layers) for an example session (H05nm7). Above: Coarse (<0.3 cpd) and fine (>1 cpd) rate of change in luminance over the same time period. The barchart shows, for each pair of stimulus and response, Pearson's correlation coefficient (pale grey; left-hand axis) and mutual information (dark grey; right-hand axis).

We found (Figure 3.12) the low frequency CSD power is positively correlated with the coarse changes in luminance, and high frequency CSD power is positively correlated with the finer changes in luminance — in both cases an increase in luminance of the stimulus yields an increase in power as a response. Example CSD traces are shown for two electrode contacts (Figure 3.12, left side) over same time period as the luminance example traces. By visual inspection, one can observe that peaks and troughs in the luminance signals are coincident with peaks and troughs in the CSD power of the appropriate frequency range.

3.3.6 *Information latency*

We also investigated the latency at which information about the movie was expressed across the cortical depth. To do so, we measured the amount of information about fine and coarse changes in luminance encoded in the CSD power, whilst varying assumed lag between stimulus and response. The latency between stimulus and response was defined as the lag which optimised their mutual information (see Section 3.2.18 for details).

Then, for each session, we compared the latency pairwise between different depths Figure 3.13. We checked whether the difference in latency was consistent across sessions. We found there was no consistent pattern to the latency between the power of 60 Hz to 170 Hz oscillations with respect to changes in luminance in the >1.0 cpd range. However, there was a reliable difference in latency for the information in the 4 Hz to 16 Hz power (with respect to coarse changes in luminance, <0.3 cpd). The channels within the G compartment consistently had the shortest response latency, with a lead of 10 ms over SG and upper IG (L5).

3.3.7 *Information about spatiotemporal components of visual stimulus*

Next, we considered the information about different temporal components of the movie. We extracted specific temporal frequency bands of the luminance signal in the movie using the same method as the spatial components, but with a temporal filter after taking the derivative of the spatially filtered luminance (see Section 3.2.19 for more details).

First, we considered two spatial frequency bands, 0.16 cpd to 0.32 cpd and 1.6 cpd to 3.2 cpd, each of which was one octave in width and corresponded (see Figure 3.11) to the peak information in one of the two CSD frequency bands, either 4 Hz to 16 Hz or 60 Hz to 170 Hz. We extracted temporal components of these two spatial signals using a series of bandpass filters whose lower cutoff frequencies ranged linearly from

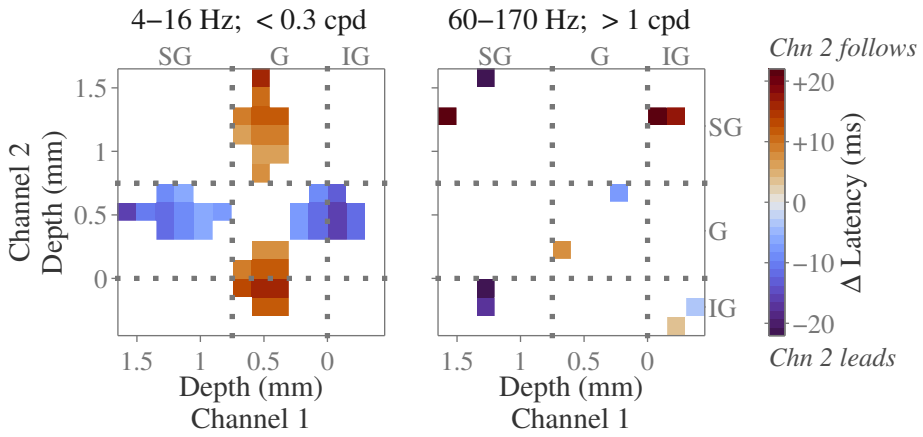

FIGURE 3.13. *Difference in peak information latency between recording depths.* We present the difference in latency between pairs of recording channels, from Channel 1 to Channel 2; if Δ is positive, Channel 1 precedes Channel 2. Left: difference in the latency of peak information between channels, for information about coarse luminance changes (<0.3 cpd) encoded in the power of 4 Hz to 16 Hz oscillations. Right: information in the 60 Hz to 170 Hz power range about finer scaled, >1.0 cpd, luminance changes. Both plots show the average over 6 sessions, with non-significant differences in latency (Student's *t*-test) shown in white.

0 Hz to 14 Hz and upper cutoff frequencies ranged from 1 Hz to 15 Hz (the Nyquist frequency of the movie stimulus).

The 4 Hz to 16 Hz CSD power contains most information about high temporal frequency components of the low spatial frequency changes in the movie (Figure 3.14, left-most column). These components include scene cuts and similar stimuli, where there is a sudden gross change in the stimulus. In contrast, the information about coarse, 0.16 cpd to 0.32 cpd, stimuli which is encoded in the 60 Hz to 170 Hz CSD frequency range is preferentially about the slow temporal components instead of fast. The information peaks with a lowpass filter (shown as 0 Hz lower cutoff in Figure 3.14), indicating that the information contained in this aspect of the cortical response is closely tied to the absolute magnitude of the change in luminance.

We had already identified that the 60 Hz to 170 Hz CSD range contained most information about the finer spatial scales in the movie. Now we also observe that a broad range of temporal components contribute to this signal, with a peak for the 3 Hz to 15 Hz temporal range of the stimulus (Figure 3.14, right-most column).

We wanted to consider the information about spatiotemporal components of the movie as a continuous function of both spatial and temporal frequency ranges. For this, we fixed the temporal bandwidth as 6 Hz and again fixed the spatial bandwidth as one octave. As shown in Figure 3.15, the two CSD frequency ranges contain information about entirely complementary spatiotemporal components of the stimulus, and the MUA contains information about the same spatiotemporal range as the 60 Hz to 170 Hz power.

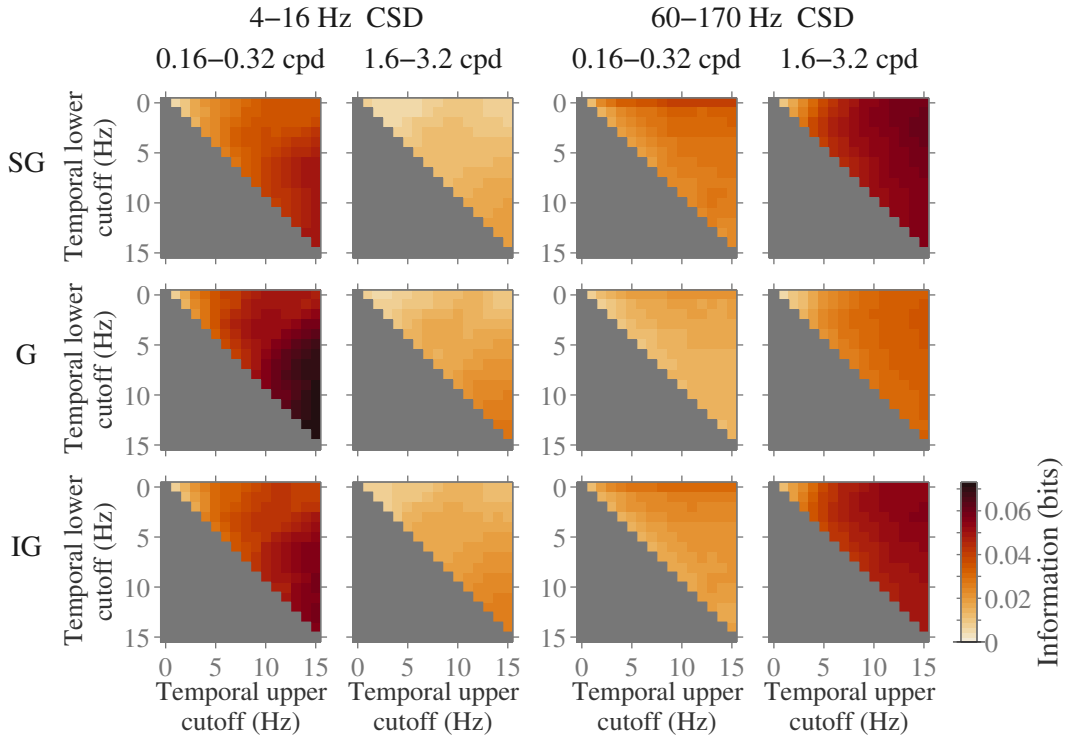

FIGURE 3.14. *Information about different temporal components of the stimulus.* The amount of information about the rate of change of luminance encoded in 4 Hz to 16 Hz (left two columns) and 60 Hz to 170 Hz (right two columns) frequency bands of the neural CSD activity, subject to either a low or high spatial filter (width of one octave) and a temporal filter. We applied temporal filters (6th-order IIR Butterworth filter) with lower cutoff f_{low} from 0Hz to 14Hz (y-axes) and upper cutoff f_{up} from f_{low} to 15Hz (x-axes). (In the case $f_{\text{low}} = 0$, a lowpass filter was used instead of a bandpass.) The lower triangle of each panel, where $f_{\text{up}} < f_{\text{low}}$, is omitted. Each row of panels corresponds to a different cortical depth, averaging over SG, G and IG compartments, respectively. Throughout all panels, the mean over 6 sessions is indicated. Statistical significance thresholds were computed for each datapoint individually, and a typical significance threshold is shown by the black line across the colour bar, near 0.

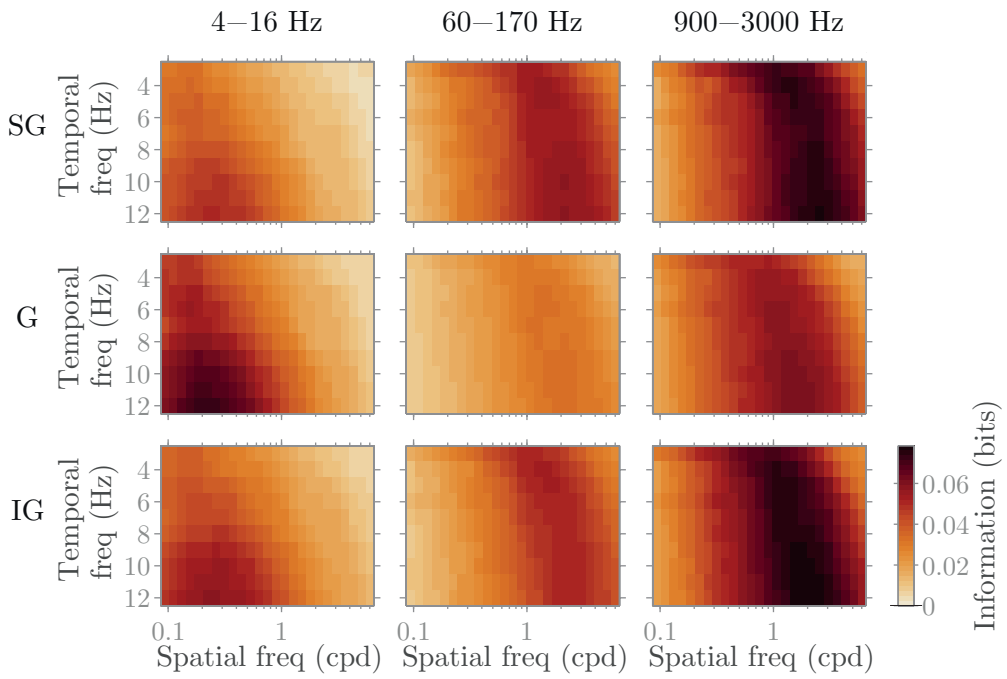

FIGURE 3.15. *Information about different spatiotemporal components.* The luminance of the movie was filtered in the spatial domain with using bandpass filters each with width one octave, and in the temporal domain with bandpass filters each with width 6 Hz. Datapoints are shown against the middle of the band on both x and y axes. We show the amount of information about the rate of change of filtered luminance encoded in the 4 Hz to 16 Hz frequency range of the CSD (left column), information in 60 Hz to 170 Hz power (middle), and information in the MUA (right). Each row of panels corresponds to a different cortical depth, averaging over SG, G and IG compartments, respectively. Throughout all panels, the mean over 6 sessions is indicated. Statistical significance thresholds were computed for each datapoint individually, and a typical significance threshold is shown by the black line across the colour bar, near 0.

In summary, we find that while the average power of cortical oscillations is distributed similarly across the entire cortical depth, the strength of these oscillations at particular frequencies are tuned to the stimulus at certain depths (Figure 3.4). Previous work by Belitski et al. (2008) demonstrated there are two cortical frequency bands (<40 Hz and >40 Hz) within V1 which encode independent information about the natural visual scenes. We discovered that these frequency bands are partially redundant within themselves across the whole cortical depth, but the information contained within them is localised at specific cortical laminae. In particular, the 4 Hz to 16 Hz frequency band is informative in the upper granular and mid-infragranular compartments, and the 60 Hz to 170 Hz range at upper supragranular and mid-infragranular regions.

We investigated which unique properties of the stimulus may be encoded by each frequency band. The occurrence of scene cuts in the movie, whose effects can be considered analogous to saccades in natural behaviour, accounted for a quarter of the information in the 7 Hz to 20 Hz band, but a negligible fraction of the information present in other frequencies.

Subsequently, we examined whether changes in luminance at different spatial frequencies induced differential changes in the cortex as a function of neural frequency and depth. In corroboration with the results for scene cuts, we found that a similar frequency range, 4 Hz to 16 Hz, encoded information about changes in the low spatial frequency aspects of the stimulus. The high frequency components of the neural activity, >60 Hz, encoded information about the high spatial frequency components of the stimulus, shown in Figure 3.11b.

Extending our decomposition of the natural stimulus into the temporal domain, we found our two neural frequency bands encoded information about different spatiotemporal aspects of the stimulus. The 4 Hz to 16 Hz band of neural oscillations conveyed most information about sudden, coarse, changes in the stimulus — such as would be induced by scene transitions in the movie presented and saccades in natural behaviour. The 60 Hz to 170 Hz band of neural activity conveyed information about complementary spatiotemporal components at higher spatial frequency spanning across all temporal ranges. The peak spatial range encoded by this band was dependent on the temporal frequency range considered, with shorter temporal frequencies corresponding to broader changes in the stimulus.

Our results suggest there is multiplexing in the cortex, with low frequency and high frequency oscillations of the same population activity simultaneously encoding low and high spatial frequency components of the stimulus respectively. This finding

corroborates previous results studying EEG: Smith et al. (2006) found that two bands of oscillations — theta (4 Hz to 8 Hz) and beta (12 Hz to 25 Hz) — correspond to the conscious perception of low and high spatial frequency aspects (respectively) of a bistable image.

As L4 is generally regarded as the principal layer of V1 receiving afferent inputs from the LGN (see Section 1.2.3; Callaway, 1998; Harris and Mrsic-Flogel, 2013; Horton and Adams, 2005; Nassi and Callaway, 2009), this begs the question of how information in the gamma band has "arisen" in SG layers without passing through G. Of course, since axons from the LGN target specific sites within L4 of V1, it is reasonable to assume that fine-resolution information about the visual stimulus arrives from the LGN into L4 of V1, with the information encoded in the pattern of V1 neurons activated by these afferent connections. Such information is not detectable from the population level activity. From there, fine-scale information can be redirected to SG, where it is encoded in oscillations of activity in the 60 Hz to 170 Hz.

As we discussed in Section 1.2, the most important visual pathways from the retina to V1 are the P- and M-pathways. The M-pathway is encoded by parasol ganglion cells in the retina, which are responsive to low spatial and high temporal frequencies. This pathway terminates in L4Cα of V1. The P-pathway originates with midget ganglion cells, encoding low temporal, high spatial frequencies of the stimulus and terminating in L4Cβ of V1.

The properties of these two pathways are reminiscent of properties of the two frequency bands we have isolated. The 4 Hz to 16 Hz power pertains to changes in the stimulus with high temporal, low spatial frequencies, like the parasol ganglion cells. The 60 Hz to 170 Hz power and MUA pertain to changes in the stimulus with high spatial frequencies, similar to the midget ganglion cells. Consequently, these frequency bands in V1 may be conveying information passed directly through the M- and P-pathways from the retina. The information could, hypothetically, be encoded into these frequency ranges by the LGN, or within V1.

The terminus locations for the M- and P-pathways are mid- and lower-G, which is not the cortical depths for which we identified the origins of the two informative frequency bands. However, this does not disprove the hypothesis, since the dendritic and somatic structures of the cortical neurons in V1 are spatially extended, spanning multiple layers. Even if the feedforward visual information from LGN solely terminated in the G compartment (which it does not), the information could be transferred to other cortical depths before oscillatory population activity is generated.

There are several other possible interpretations of our findings. For instance, the segregation of visual information into two frequency bands may be preparation for the fork in the visual hierarchy into dorsal (motion-sensitive) and ventral (shape-

sensitive) streams. It has previously been hypothesised that the M-pathway steered information to the dorsal stream and the P-pathway to the ventral stream. Studies since have demonstrated that activity in middle temporal cortex (MT) is dependent on both M- and P-pathways (Merigan et al., 1991; Yabuta et al., 2001). Our results may be indicative of two different pathways for transmission of information between cortices, in which V1 integrates both M- and P-pathways together and then separates them out again. However, this seems like an ambitious objective for V1 to achieve.

As discussed in Section 1.2.3, neurons in V1 are known to be tuned to the orientation, spatial frequency, direction of motion, and colour of oriented bars. Functionally, this is similar to edge detection, which requires high spatial frequency contrast in the stimulus. It is therefore possible that the 60 Hz to 170 Hz power reflects the output of the cortical column. Such a hypothesis could be tested by investigating whether cortical power in this frequency range is tuned to orientated bar stimuli.

The information encoded in the 4 Hz to 16 Hz power pertained to coarse, sudden changes in the stimulus, such as scene cuts. When coarse and fast changes occur in the movie, the next frame seen by the cortex is very different from the previous stimuli in an unpredictable manner. Should V1 be utilising predictive coding, a sudden change in the stimulus such as this would violate the expected input predicted by V1. Consequently, it may be that 4 Hz to 16 Hz activity reflects an error signal, either triggering the latent state of V1 neurons to correct for the error or reset ready for a new initialisation.

Recent work by van Kerkoerle et al. (2014) has shown that stimulation in V1 induces gamma (40 Hz to 90 Hz) activity in V4 (feedforward), whilst stimulation in V4 induces alpha (5 Hz to 15 Hz) oscillations in V1 (feedback). These results seem to lend further credence to the interpretation of alpha as a feedback error signal and gamma as a feedforward output of V1. Van Kerkoerle et al. (2014) also found that the gamma waves were initiated at L4, propagating outwards to the top of SG and bottom of IG. Alpha waves propagated in the opposite direction, originating at the top and bottom of the cortex and travelling the middle. Our own analysis demonstrated that the gamma band was most informative at the top and bottom boundaries of the cortical column, and alpha in the middle of L4. These localisations are the terminus of the waves found by van Kerkoerle et al. (2014), not their origins as we would have initially expected. Reconciling these results together, we hypothesise that the cortical waves are gated as they travel through the cortical depth, such that the amplitude of the oscillations is amplified and supressed in a stimulus-dependent manner. However, this is a complex interpretation of the data and more evidence is needed to test its validity.

We discuss possible future work to resolve these issues and questions in Chapter 5.

4

PHASE OF CORTICAL OSCILLATIONS WITHIN V1 LAMINAE

In Chapter 3, we considered the information about a naturalistic video stimulus contained in the power of oscillations in the CSD. In this chapter, we will investigate the information encoded in the phase of the CSD, how this relates to the power or amplitude of the oscillations, and what properties of the stimulus may be encoded by the phase of the oscillations.

4.1 METHODS

Since this dataset is the same as that analysed in Chapter 3, the methodology for data collection and preprocessing are the same as were described in Section 3.2. In this section, we present additional methods specific to the analysis of the oscillation phase.

4.1.1 *Phase across depth and frequencies*

The phase was computed in a similar manner to the power, documented in Section 3.2.10. We filtered both the LFP and CSD using a series of bands each with a fractional bandwidth of 50 %, spaced logarithmically at multiples of 1.291. This spacing ensures each band has 0 % overlap with bands further away than its immediate neighbours and a 44 % and 56 % overlap with its preceding and succeeding bands respectively. The signal was filtered with a zero-phase sixth-order IIR Butterworth filter, after which the instantaneous phase was estimated by taking the angle of the Hilbert transform. This procedure was also used to extract the phase of the 4 Hz to 16 Hz and 60 Hz to 170 Hz frequency bands.

4.1.2 *Information contained in cortical oscillation phase*

The amount of information about the stimulus contained in the phase was computed in the same manner as the information in the power, described in Section 3.2.11. We again used 10 equipopulated bins, with the first bin starting at a phase of 0 radians, and the final bin ending at 2π radians. Due to the smooth, circular nature of phase,

our samples of the phase vary uniformly across the range $[0, 2\pi)$ and hence the 10 bins each have a width of approximately $\pi/5$ radians.

When computing the redundancy, we again used 3 equipopulated bins. Hence for the phase, the bin widths were approximately $2\pi/3$ radians.

4.1.3 *Signal and noise correlation*

For both signal and noise correlation calculations, we used directional statistics (also known as circular statistics) which were computed using the *CircStat* toolbox (Berens, 2009).

The phase–phase correlations were evaluated with the circular-circular correlation coefficient (Jammalamadaka and SenGupta, 2001, page 176), given by

$$\rho_{\circlearrowleft\circlearrowleft}(\alpha, \beta) = \frac{\sum_{j=1,\ldots,N} \sin(\alpha_j - \bar{\alpha}) \sin(\beta_j - \bar{\beta})}{\sqrt{\sum_{j=1,\ldots,N} \sin^2(\alpha_j - \bar{\alpha}) \sin^2(\beta_j - \bar{\beta})}}, \tag{4.1}$$

for N samples of pairs of angles from distributions α and β, whose circular means are empirically determined to be $\bar{\alpha}$ and $\bar{\beta}$ respectively.

To find the phase–power correlations, we used the circular-linear correlation (Zar, 1999, Equation 27.47), which is defined in terms of the linear-linear Pearson correlation coefficient, $\rho(X, Y)$, which we described in Equation 2.5. We define $r_{sx} = \rho(\sin(\alpha), X)$, $r_{cx} = \rho(\cos(\alpha), X)$, and $r_{sc} = \rho(\sin(\alpha), \cos(\alpha))$ for a circular variable α and linear variable X, each using the Pearson correlation coefficient. From this, the circular-linear correlation coefficient is given by

$$\rho_{\circlearrowleft\rightarrow}(\alpha, X) = \sqrt{\frac{r_{sx}^2 + r_{cx}^2 - 2\, r_{sx}\, r_{cx}\, r_{sc}}{1 - r_{sc}^2}}. \tag{4.2}$$

To determine the statistical significance of our results, we also computed bootstrapped phase–phase and phase–power correlation coefficients. We performed the correlation coefficient calculation with randomly paired α_j and β_j values (for phase–phase) and α_j and X_j values (for phase–power). This was repeated for 20 shuffled copies of the time series data.[1] After averaging over sessions, correlation coefficients which were less than three standard deviations of the bootstraps from the bootstrap mean were deemed not significantly correlated (shown in white in Figures 4.3 and 4.5).

1 Which was shuffled after extracting phase and power values.

4.1.4 *Phase synchrony*

We defined the phase synchronization as the absolute magnitude of the vector average of the difference in phase (Kreuz, 2011). Let us consider two random variables, X and Y, whose phases, α and β respectively, are simultaneously observed on N occassions. The vector average of the phase difference between X and Y is given by the complex number

$$z_{\alpha,\beta} = \frac{1}{N} \sum_{j=1,\ldots,N} \exp(\mathrm{i}(\alpha_j - \beta_j)), \tag{4.3}$$

where i is the imaginary unit, $\mathrm{i} = \sqrt{-1}$. From this, we determined the average phase difference as

$$\langle \Delta\phi \rangle = \arg(z_{\alpha,\beta}) = \mathrm{atan2}(\mathrm{Re}(z_{\alpha,\beta}), \mathrm{Im}(z_{\alpha,\beta})), \tag{4.4}$$

and the phase synchrony as

$$R_{\alpha,\beta} = |z_{\alpha,\beta}| = \mathrm{abs}(z_{\alpha,\beta}). \tag{4.5}$$

4.1.5 *Cross-frequency phase–amplitude coupling*

Strength of cross-frequency coupling was measured using the modulation index (Tort et al., 2010). CSD data was filtered for two bands, 4 Hz to 16 Hz and 60 Hz to 170 Hz, using a zero-phase sixth-order Butterworth filter, and the instantaneous phase of 4 Hz to 16 Hz and envelope amplitude of 60 Hz to 170 Hz were each estimated using a Hilbert transform. We took a histogram of the 4 Hz to 16 Hz phase datapoints with $M = 16$ bins each of width $\pi/8$ radians, and for each bin took the average of the 60 Hz to 170 Hz amplitudes simultaneously co-occurring with each of the phases in that bin. This provides the expected amplitude, $a(j)$, at one depth as a function of phase, $\phi(j)$, at another depth, indexed by the bin index, j.

We then normalise a against the total over all bins, $a'(j) = a(j) / \sum_k a(k)$, such that a' has the properties of a discrete probability density function.

Next, we utilise the Kullback-Leibler (KL) divergence, in general given by

$$D_{\mathrm{KL}}(P \| Q) = \sum_k P(k) \log_2 \frac{P(k)}{Q(k)} \tag{4.6}$$

for two discrete probability distributions P and Q. The **modulation index** is defined as the normalised KL divergence of the distribution a' from a uniform distribution (Tort et al., 2010), which is given by

$$\mathrm{MI} = \frac{\log_2(M) + \sum_{j=1,\ldots,M} a'_j \log_2(a'_j)}{\log_2(M)}. \tag{4.7}$$

4.2 RESULTS

4.2.1 *Information contained in phase of cortical oscillations*

We computed the amount of information about the movie encoded in the phase of oscillations in both cortical LFP and CSD, as a function of cortical depth and oscillation frequency. As shown in Figure 4.1, we find that there is more information in the phase than the power of oscillations (see Figure 3.4) for all frequencies lower than 40 Hz. The phase contains much less information for higher frequencies, and the power contains more information than the phase for all frequencies above 40 Hz. Intuitively, this is because the phase of high frequency oscillations changes more rapidly and hence it is harder for it to be well aligned across trials than the phase of lower frequency oscillations. In contrast, power of an oscillation fluctuates with the envelope amplitude of the oscillation, which can change much slower than the frequency of the oscillations. Hence the power of fast oscillations can be stable enough to demonstrate repeatability across trials.

Similar to the results for power, we find that the phase of oscillations in the LFP and CSD produce similar results, but the CSD provides superior spatial localisation (although the information in the CSD is reduced compared with the LFP). For brevity, we therefore only consider the information in the CSD for the remainder of the chapter.

4.2.2 *Phase–phase redundancy*

These results prompt us to consider the redundancy of the phase of oscillations. Do the phases of oscillations at different frequencies convey information about the same aspects of the stimulus, as we found for the information in the power of the same oscillations? Furthermore, how is the information in the phase related to the information in the power?

First, we consider the relationship between the phases of the frequency bands (50 % bandwidth) occurring at the same cortical depths as one another. As shown in Figure 4.2, we find that pairs of frequency bands $<$40 Hz contain synergistic information

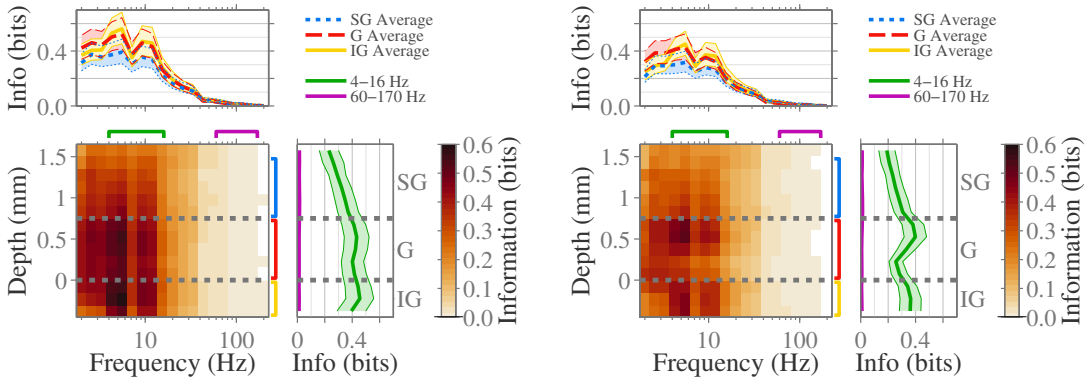

(a) LFP phase information.

(b) CSD phase information.

FIGURE 4.1. Information about the stimulus contained in the phase of the extracellular neural signal, as a function of frequency. Mean of 6 sessions. (a): LFP. (b): CSD.

about the stimulus, except for overlapping frequency bands which show redundancy. This means that knowing the phase of two such frequency bands provides more information about the stimulus than the information in the two of them individually. The observed synergy is similar across all pairs of frequencies <40 Hz, which suggests the cause is intrinsic to the Fourier transform and its phase in general, and not specific to the cortical oscillation data we are considering. In particular, peaks and troughs in the overall CSD signal occur when multiple frequency components reach 0 and π radians, respectively. As we already demonstrated in Section 3.3.4 for the information in the power (and will demonstrate for the phase in Section 4.2.5), scene transitions provide an important stimulation drive for low frequency oscillations. In particular, scene cuts induce similar oscillation waveforms on each of their occurrences (not shown, but similar to the stimulus-onset stereotyped response shown in Figure 3.1a). Since the distribution over phase for any single frequency component is uniform, coincident phases for a pair of frequencies are much more informative about peaks and troughs in the signal.

For frequencies above 40 Hz, the redundancy of the phase with other frequency bands was not significant, due to the low amount of information in this frequency range.

We also computed the signal and noise correlation, using the methodology described in Section 4.1.3. Beyond the trivially positively correlated signal correlation of neighbouring frequency bands, as shown in Figure 4.3a we find there are some pairs of frequencies which are positively correlated (phase of 10 Hz and 30 Hz) and negatively correlated (phase of 3 Hz and 30 Hz). The level of signal correlation is lower than we observed for the power–power correlation across frequency (see Figure 3.7).

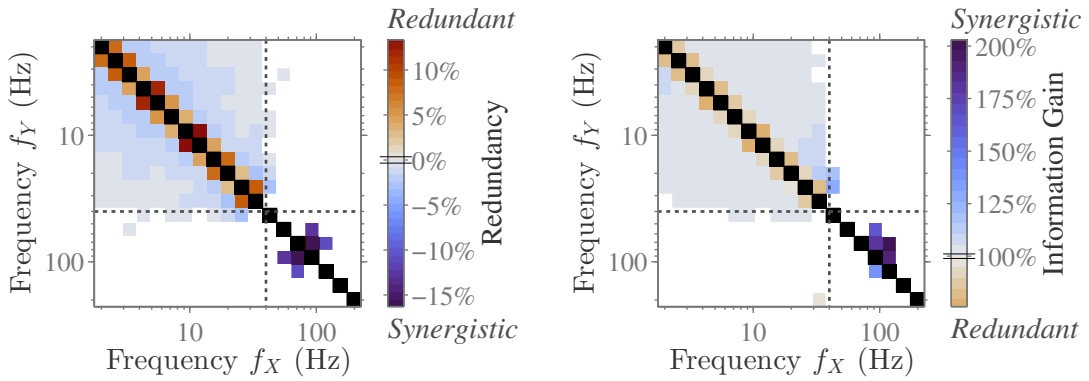

(a) Redundancy.

(b) Information gain.

FIGURE 4.2. *Information redundancy between the phase of CSD frequency components.* (a): Redundancy (as defined in Equation 3.3) between pairs of frequencies, averaged over all cortical recording depths, then averaged over 6 sessions. Each datapoint was tested for statistical significance using bootstrapping, and non-significant values are shown in white (the median threshold for statistical significance is shown as a line across the colour bar). The leading diagonal, which is trivially redundant, is removed (black). (b): Same as (a), but for the asymmetric information gain $\mathrm{InfoGain}\left(Y \to \{X, Y\}; S\right)$ (defined in Equation 3.4).

The noise correlation was small and positive for all pairs of phases considered, shown in Figure 4.3b.

Unlike when we considered the information in the cortical power, neither the redundancy between phases of frequencies, nor signal and noise correlation structure, provided us with sufficient motivation to chose any particular frequency bands to isolate. Therefore, we continue to examine the 4 Hz to 16 Hz and 60 Hz to 170 Hz frequency bands which we arrived at from our analysis of the information encoded in cortical power. This allows us to compare the information in the phase and power of the same bands.

4.2.3 *Phase–power redundancy*

Similar to the above, we can also consider the redundancy between information in the power and phase as a function of their frequencies. As shown in Figure 4.4, we find that some pairs of power and phase have redundant information about the stimulus, some synergistic, and others approximately independent.

There is significant redundancy between the 5 Hz to 15 Hz phase and 10 Hz to 20 Hz power, though the effect size is small. Synergy is found between the phase (across all frequencies) and the power of oscillations below 10 Hz, with a notable gain relative to the amount of information in the power of these frequencies (see Figure 4.4b). We also see synergy between the phase of frequencies below 20 Hz with the power in

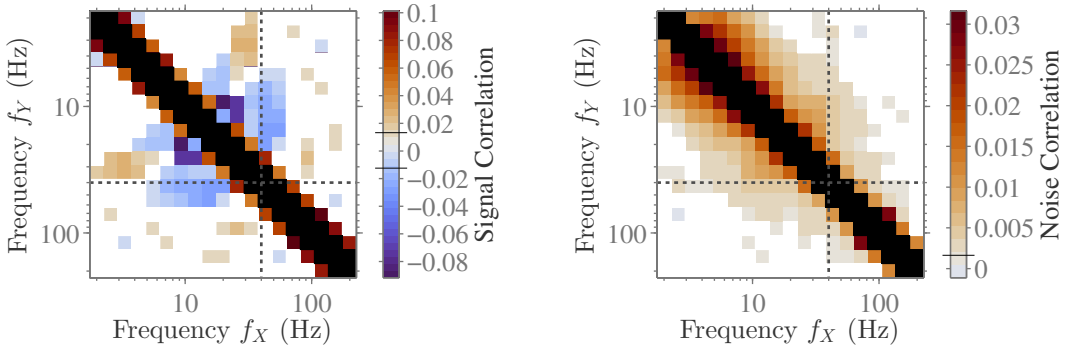

(a) Signal correlation

(b) Noise correlation

FIGURE 4.3. *Correlation between phase of different* CSD *frequency components.* (a): Signal correlation between the phase in pairs of frequencies, median across 12 to 14 cortical recording sites, mean across 6 sessions. The leading diagonal, which is trivially perfectly correlated, and second diagonal, which is highly correlated due to the 50 % overlap between neighbouring frequency bands, are removed (black). (b): Noise correlation between the phase in pairs of frequencies, median across 12 to 14 cortical recording sites, mean across 6 sessions. Non-significant datapoints are shown in white, with minimum and maximum significance thresholds indicated by the black lines across the colour bar.

higher frequencies (>60 Hz). These findings could be caused by a coupling of the envelope amplitude of the power for oscillations in one frequency band with the phase of oscillations in another band, which we consider in Section 4.2.8.

4.2.4 *Cross-channel, cross-depth redundancy*

Next, we consider how the information in the cortical phase is related to the information in the power and MUA across the cortical depth. We computed the redundancy between the 4 Hz to 16 Hz phase and the 4 Hz to 16 Hz power, 60 Hz to 170 Hz power and MUA (see figure Figure 4.5a).

We found the 4 Hz to 16 Hz phase at G and SG depths was redundant with the phase at other G and SG cortical depths, but mostly independent of the phase in IG. The phase in IG is redundant to the phase at other IG depths. This suggests compartmentalisation of the 4 Hz to 16 Hz frequency band, with two independent cortical oscillations occurring in this band but generated at (and localised in) two different cortical depths. The results for signal (Figure 4.5b) and noise (Figure 4.5c) correlation support this view, as there is less correlation between G or SG phase and IG phase than there is within either compartment.

The information about the stimulus in the 4 Hz to 16 Hz phase was synergistic with the 4 Hz to 16 Hz power. Our explanation for this ties in with our explanation of the phase–phase synergy discussed above. Since phase is uniformly instead of

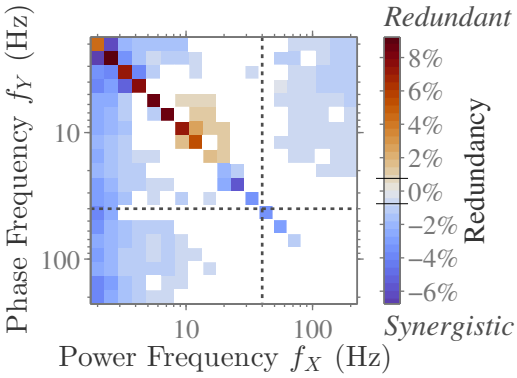

(a) Redundancy.

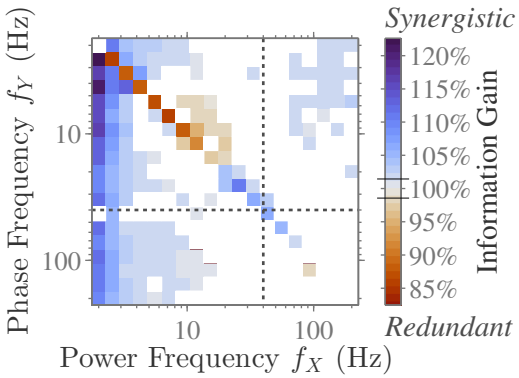

(b) InfoGain (Phase → {Phase, Power} ; S).

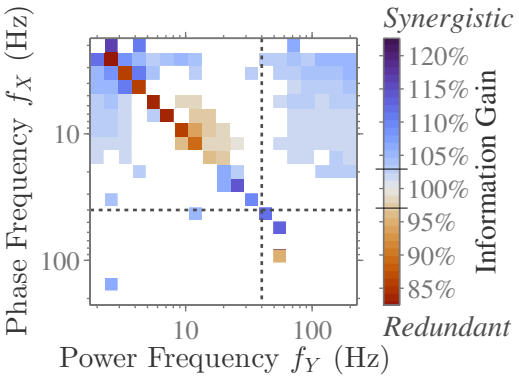

(c) InfoGain (Power → {Phase, Power} ; S).

FIGURE 4.4. *Information redundancy between the phase and power of CSD frequency components.* (a): Redundancy (as defined in Equation 3.3) between phase and power, averaged over all cortical recording depths, then averaged over 6 sessions. Each datapoint was tested for statistical significance using bootstrapping, and non-significant values are shown in white (the median threshold for statistical significance is shown as a line across the colour bar). (b): Same as (a), but for the asymmetric information gain when Phase is already known and Power is revealed (see Equation 3.4). (c): Same as (b), but for the information gain when Power is already known and Phase is revealed.

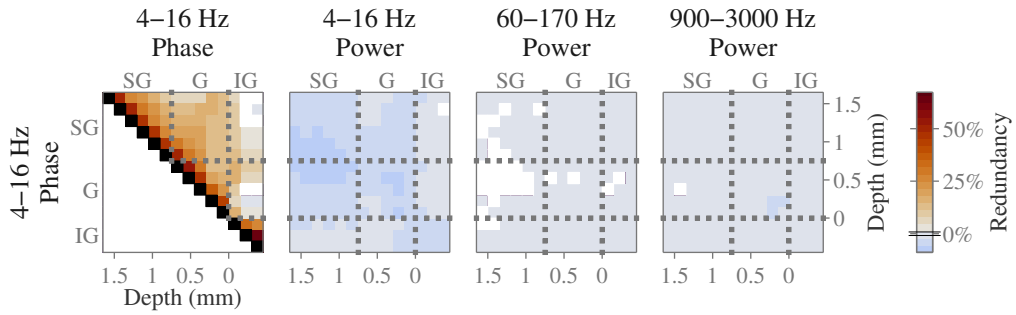

(a) Redundancy.

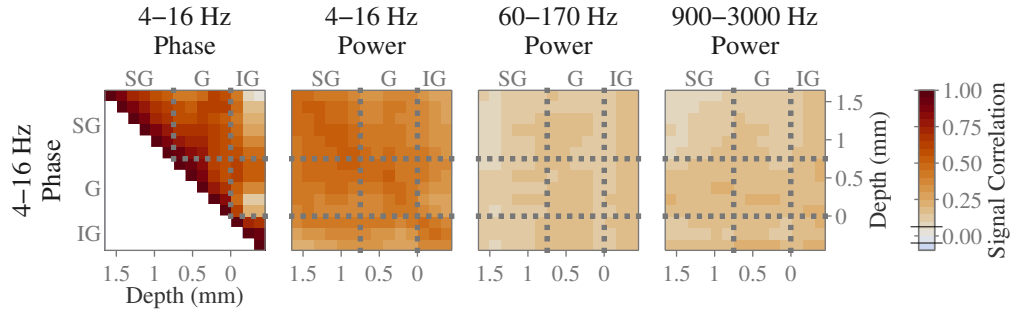

(b) Signal correlation.

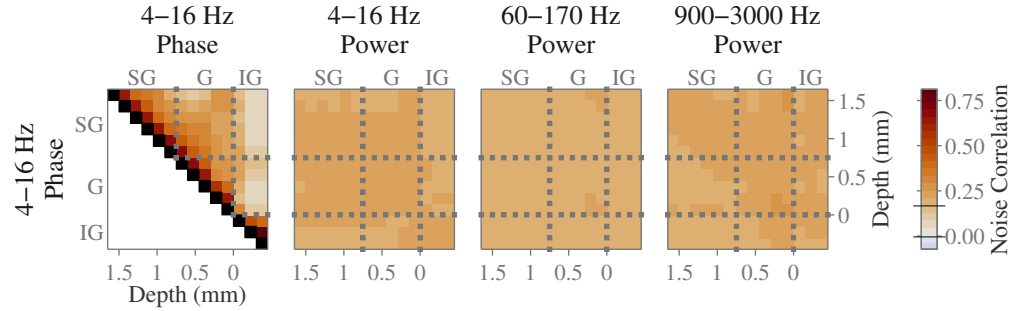

(c) Noise correlation.

FIGURE 4.5. *Redundancy of* 4 Hz *to* 16 Hz *CSD phase with* 4 Hz *to* 16 Hz *power,* 60 Hz *to* 170 Hz *power and MUA (*900 Hz *to* 3000 Hz *power).* (a): Redundancy (as defined in Equation 3.3) between phase and power. Non-significant datapoints are shown in white, with median significance threshold (positive and negative) indicated by the black lines across the colour bar. (b): Signal correlation, reported as circular-circular correlation coefficient between phases and the circular-linear correlation coefficient between phase and power (see Section 4.1.3). Non-significant datapoints are shown in white, with minimum and maximum significance thresholds indicated by the black lines across the colour bar. (c): Same as (b), but for noise correlation instead of signal correlation.

sparsely distributed, a secondary signal about the CSD helps disambiguate whether the phase occurs during most, lower power, time points or during well-stereotyped waveform events or responses to the stimulus, which have higher power. We note that the correlation with the 4 Hz to 16 Hz phase is higher for the 4 Hz to 16 Hz power than the higher frequency bands, whilst the noise is constant across all three, which supports this interpretation.

The information about the stimulus encoded in the 4 Hz to 16 Hz phase appears to be different to the information encoded in the 60 Hz to 170 Hz power and MUA activity, which have balanced synergy and redundancy as shown in Figure 4.5a.

4.2.5 *Information about scene cuts*

We computed the amount of information in the CSD phase about scene transitions in the movie (agnostic about which of the scene transitions was occurring) in the same manner as described in Section 3.2.15.

In terms of number of bits encoded, the phase and power contain the same amount of information about the presence of scene cuts. The fraction of information contained in the CSD phase which is explained by scene transitions is smaller than we observed for the power (see Figure 4.6; Figure 3.10 for comparison), since the total amount of information encoded in the $<$40 Hz phase is larger than that encoded in the power. This indicates that the phase encodes more properties of the stimulus than the power of cortical oscillations.

In Section 3.3.4, we found that scene transitions explained more of the information in the cortical power for oscillations in the range 7 Hz to 20 Hz. For the phase of oscillations, the peak frequency range best explained by scene cuts is similar again, though the curve is flatter.

4.2.6 *Information about spatiotemporal components*

We computed the amount of information about changes in luminance at different spatiotemporal scales contained in the CSD phase, the methodology for which is described in Section 3.2.19.

The amount of information encoded in the CSD phase is only around 10 % of the information encoded in the power (Figure 4.7; see Section 3.3.7 for comparison). This result is surprising, since we observed in Section 4.2.5 that the CSD contains a significant amount of information about scene cuts in the movie — around 0.06 bits, which is ten times more than we observe here. These two results appear to be contradictory, since scene transitions typically involve sudden, coarse changes in the luminance of

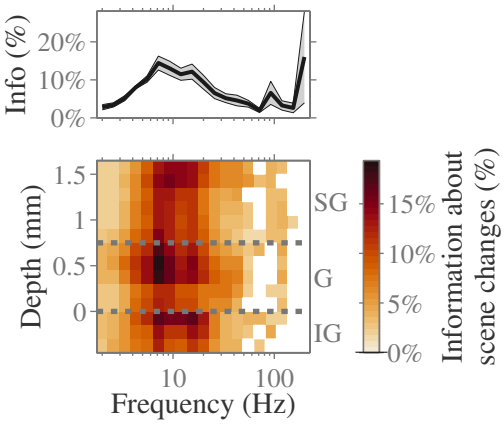

FIGURE 4.6. *Information about the presence of scene cuts.* We computed the information about scene cuts as described in Section 3.2.15, and for each session expressed this as a proportion of the total information present before averaging across recording sessions. Information values which were not significantly different from the bootstrap distribution are shown in white, with the median threshold for significance indicated by a black line across the colour bar. Above, the average percentage of information explained by scene cuts over all cortical recording sites is shown, with the standard error across sessions indicated by the shaded region. Information about scene cuts contained in a range of CSD frequencies, in which we only considered the time since the last scene cut for the 0.2 s immediately following each.

the stimulus. But we note that the spatiotemporal distribution of information contained in the 4 Hz to 16 Hz phase is the same as the distribution for the 4 Hz to 16 Hz power, though the distribution over depth is skewed towards deeper, IG, cortical layers.

How does this behaviour arise, when the CSD power was observed to give similar results for both scene transitions and spatiotemporal changes? Unlike the power, the phase is always changing rapidly — it must change at a rate similar to the frequency of the filtered band — whereas the envelope amplitude describing how the power changes over time can vary much more slowly. Consequently, the power of the CSD has a long autocorrelation duration and the phase does not. This means that small perturbations in the differences between recorded and actual presentation times of the stimuli will not have much effect on the measured information in the power but will for the phase. Consequently, the relationship between the spatiotemporal changes in the movie and the CSD phase may not be well aligned across trials.

4.2.7 *Phase synchrony*

We determined the average phase difference and the phase synchrony between oscillations in the 4 Hz to 16 Hz band across the cortical depth, for both stimulus driven and spontaneous activity. As shown in Figure 4.8, there is high phase synchrony

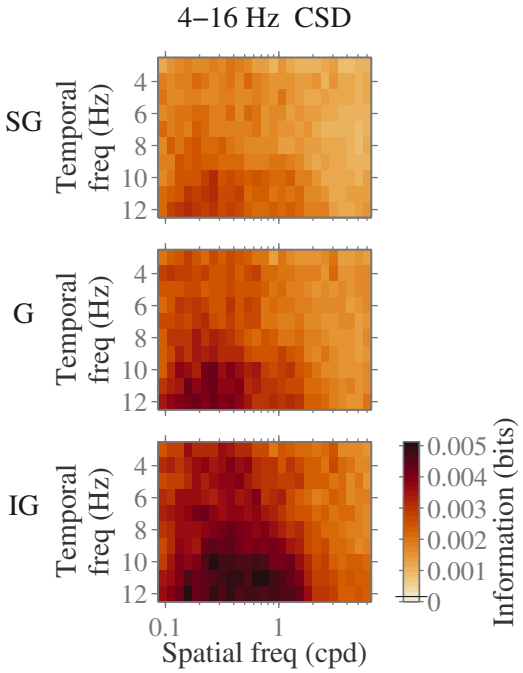

FIGURE 4.7. *Information contained in the* 4 Hz *to* 16 Hz *CSD phase about different spatiotemporal components.* The luminance of the movie was filtered in the spatial domain with using bandpass filters each with width one octave, and in the temporal domain with bandpass filters each with width 6 Hz. Datapoints are shown against the middle of the band on both x and y axes. Each row of panels corresponds to a different cortical depth, averaging over SG, G and IG compartments, respectively. Throughout all panels, the mean over 6 sessions is indicated. Statistical significance thresholds were computed for each datapoint individually, and a typical significance threshold is shown by the black line across the colour bar.

within G and SG, and synchrony within IG, but low synchrony between these compartments. Furthermore, the average phase difference between channels was always near 0 (wherever there was synchrony). These results were similar for stimulus driven and spontaneous activity.

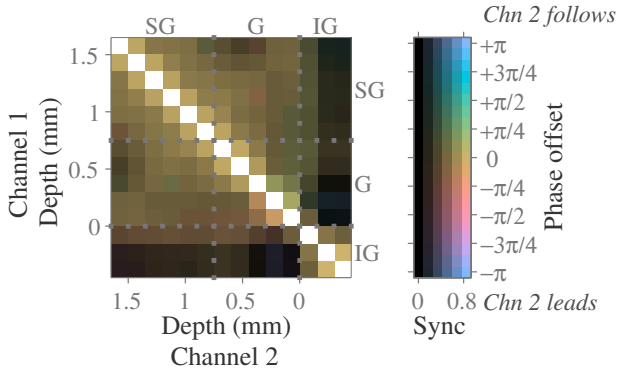

(a) Stimulus driven.

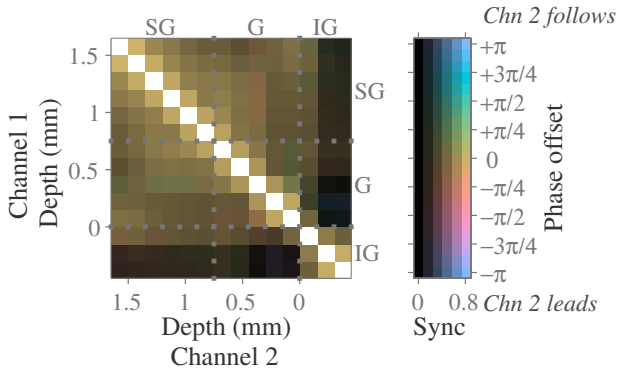

(b) Spontaneous.

FIGURE 4.8. 4 Hz *to* 16 Hz *phase synchrony between cortical depths.* The two-dimensional colour scale shows both average phase offset (hue) and phase synchrony (lightness). Positive phase differences (green) correspond to the phase of channel 1 (y-axis) leading that of channel 2 (x-axis). Negative phase differences (red) correspond to the phase of channel 2 (x-axis) leading channel 1 (y-axis). Similar phases are shown in yellow and opposing phases in blue. The phase synchrony is shown for stimulus driven (a) and spontaneous (b) activity.

We determined the phase difference and synchrony for the 60 Hz to 170 Hz oscillations in the CSD in the same manner as for the 4 Hz to 16 Hz frequency range. As shown in Figure 4.9, the phase of lower-G is typically opposed to that of IG. This may correspond to the source-sink reversal associated with the stimulus onset which we discussed in Section 3.2.9. There is also a gradient in phase across SG and G, with the middle of G leading the response.

We observed there is less synchrony in the spontaneous activity than the stimulus driven activity, but the relationship in the phase across the cortex is the same in both cases.

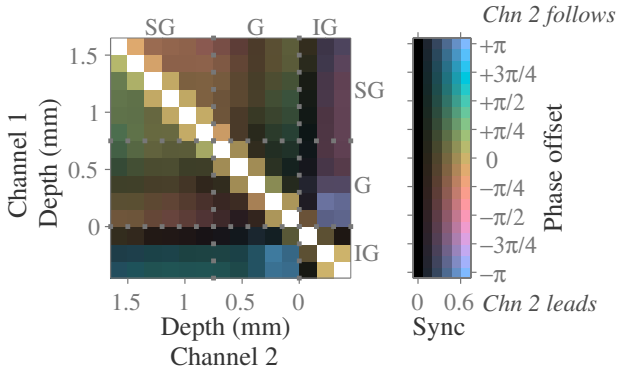

(a) Stimulus driven.

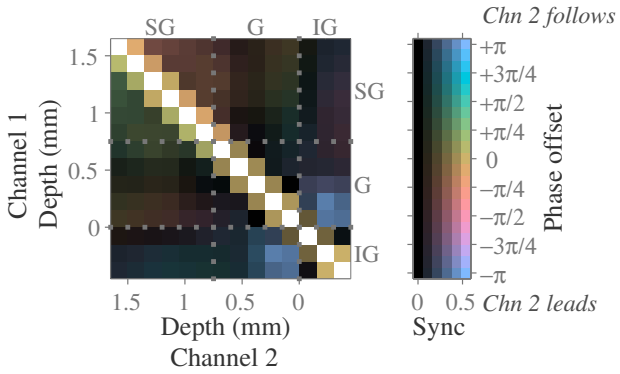

(b) Spontaneous.

FIGURE 4.9. 60 Hz *to* 170 Hz *phase synchrony between cortical depths.* The two-dimensional colour scale shows both average phase offset (hue) and phase synchrony (lightness). Positive phase differences (green) correspond to the phase of channel 1 (y-axis) leading that of channel 2 (x-axis). Negative phase differences (red) correspond to the phase of channel 2 (x-axis) leading channel 1 (y-axis). Similar phases are shown in yellow and opposing phases in blue. The phase synchrony is shown for stimulus driven (a) and spontaneous (b) activity.

4.2.8 *Cross-frequency phase–amplitude coupling*

Another manner in which we can investigate the relationship between phase and power is cross-frequency coupling. Cross-frequency coupling occurs when the phase of one frequency band is correlated with the envelope amplitude for another frequency band. We investigated the cross-frequency coupling between the 4 Hz to 16 Hz phase and the 60 Hz to 170 Hz envelope amplitude using the modulation index, described in Section 4.1.5.

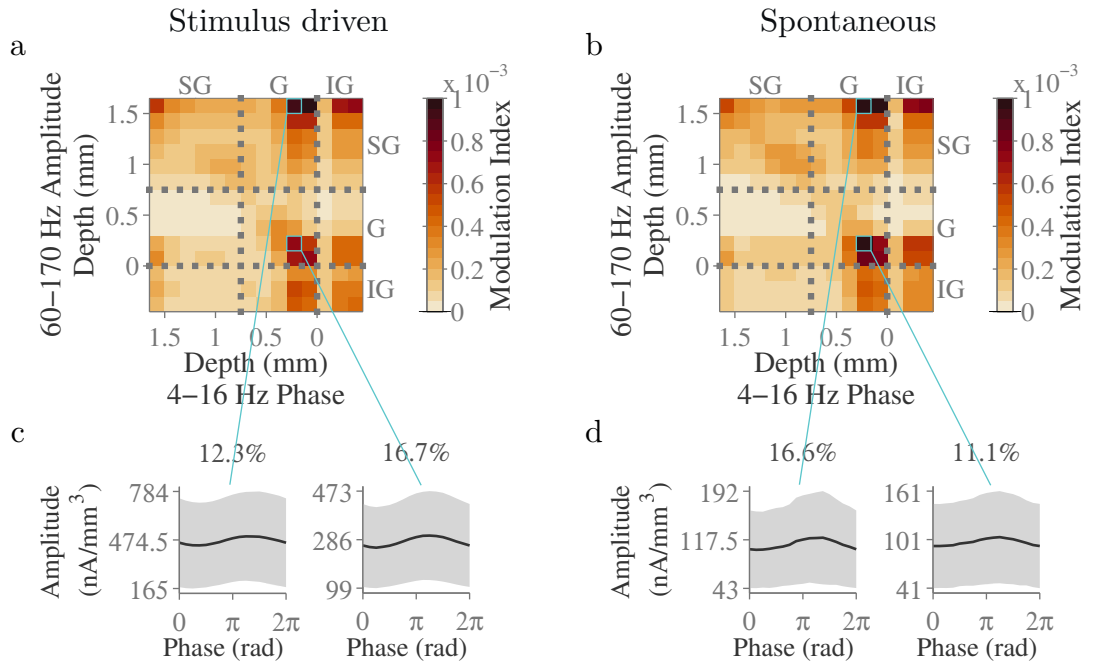

FIGURE 4.10. *Cross-frequency phase–amplitude coupling.* Phase–amplitude modulation index between low frequency (4 Hz to 16 Hz) phase and high frequency (60 Hz to 170 Hz) amplitude ((a): movie driven activity; (b): spontaneous activity). Mean of 5 sessions. (c) and (d): Amplitude as a function of binned phase for a typical example session (F10nm1), for IG→IG coupling (left) and IG→SG coupling (right).

We observed a spatially localised coupling between the 4 Hz to 16 Hz phase of both lower-G and mid-IG with the amplitude of 60 Hz to 170 Hz oscillations in upper-SG (Figure 4.10). Additionally, in both G and IG there is a coupling between the local 4 Hz to 16 Hz phase and the local 60 Hz to 170 Hz amplitude. The same relationship was discovered to hold both for spontaneous activity and stimulus-driven recordings, and our findings are in agreement with previous work (Spaak et al., 2012).

We considered the amount of information encoded in the phase of cortical oscillations. For low frequency oscillations (<40 Hz) we found there was around 50 % more information in the phase than there was in the power. Higher frequency oscillations have phases which vary too quickly to reliably correspond to the same parts of the stimulus, and hence we do not find they convey much information about the stimulus.

We found that the information in the phase of any pair of oscillation frequencies less than 40 Hz (recorded within the same cortical depth as each other) were synergistic (except for overlapping bands). Furthermore, we found a substantial amount of information about the timing of scene cuts in the CSD phase. The occurrence of each scene cut produces a stereotypical waveform in response in the cortex (not shown), similar to the stimulus-onset response shown in Figure 3.1a. Consequently, we believe the synergy between the phase of non-overlapping cortical frequency bands is because maxima and minima of the overall CSD occur when all frequencies strike phase 0 and π simultaneously, and these maxima and minima events are repeatably triggered by the stimulus.

Though we found the phase encodes more information about the stimulus than the power, we were not able to relate it to the rate of change of luminance of the movie at any particular spatiotemporal scales. Other than scene transitions, it is still not clear what information about the stimulus is encoded in the phase.

The information in the phase appears to be compartmentalised, with the SG and G depths (layers 1–4) encoding independent information to IG (layers 5 and 6). This finding suggests that there are two different cortical oscillations active in this frequency range, driven by different cortical process and, consequently, arising at different depths in the cortical microcircuit. Our investigation of the phase synchrony across the cortical depth supports this observation, showing that 4 Hz to 16 Hz oscillations across SG and G have near-simultaneous phase, which is not synchronised with that of IG. However, we did observe that both of these compartmentalised oscillations, sited higher and lower up the cortical depth, are informative about scene transitions in the movie. Whichever aspects they encode remain unknown.

In agreement with previous work (Spaak et al., 2012), we found there was cross-frequency coupling between the stimulus-encoding power of gamma oscillations in L1 and the phase of alpha oscillations in lower L4. Anatomically, we believe this is related to the pyramidal cell bodies in L5A, which have apical dendritic tufts in L1 (Hill et al., 2013; Zhu and Zhu, 2004). This cross-frequency coupling could be one mechanism through which the L1 gamma oscillations containing high levels of infor-

mation about the stimulus is converted into an alpha oscillation for feedback into a hierarchically lower cortical region. Such a mechanism would be support the feedback/feedforward hypothesis of van Kerkoerle et al. (2014) which we discussed in Section 3.4. However, the direction of causality for the cross-frequency coupling is unknown, so the observed results could instead be manifested by alpha oscillations in L4 modulating the gamma power in L1. Neurons in L5 are known to be related to long-range cortical output (Hill et al., 2013), and inputs into L1 are known to be predominantly inputs from higher-order cortices, so this cross-frequency coupling may provide a system for low-frequency feedback to be translated into higher frequency oscillations within V1.

5

DISCUSSION

In this thesis, we have applied information theoretic techniques to study the activity of populations of neurons within visual cortices V1 and V4. Here, we summarise and discuss our findings, and propose future research directions.

5.1 PERCEPTUAL LEARNING

5.1.1 *Summary*

In Chapter 2, we investigated the neural correlates of a perceptual learning task in which monkeys had to discriminate between stimuli of varying contrast. Together, our results show the most informative signal about the contrast of the stimulus within the cortex is contained in the initial response to the stimulus onset within V1, and this does not rise with training. The lack of increase in this information may be because it is not a trainable property of the adult visual system.

The population activity in V4 rises with training, in line with the rise in behavioural performance of the subject. This indicates that V4 is trained to be better at reading out the information in V1 relevant to the task, and information from V4 may subsequently be read out by higher-order cortices involved in decision making. If the higher cortex must read information from V4 without direct access to V1, this presents an information bottleneck, since V4 contains fewer neurons than V1. Our results also indicate that feedback signals from higher cortical regions into both V1 and V4 become more pronounced with training.

5.1.2 *Open directions for future research*

We identified the narrow beginning of the V1 stimulus-onset response as the most informative cortical signal conveying information about the contrast of the stimulus, and concluded this was perhaps because the latency of the signal reaching the cortex was sensitive to the contrast of the stimulus presented (Albrecht et al., 2002). Consequently, it would be useful to investigate the amount of information encoded in the latency of the first spike in response to the stimulus onset. This would help us determine whether the latency of the signal to V1 is truly the most informative aspect

of the response, and not the total number of spikes in the onset-response. That said, the spontaneous firing rate before the stimulus is around 7 Hz (shown in Figure 2.26), which implies a spontaneously generated spike will occur in the first 50 ms around 35% of the time. With this in mind, the time of the second spike after stimulus onset may prove even more informative.

Typical spontaneous firing rates for pyramid neurons in L2/3 are around 0.03 Hz (Chen et al., 2015). Consequently, the spontaneous firing rate of 7 Hz which we report for our recording channels may be erroneously high, considering our MUA contains spikes from around 5 neurons neighbouring the site of the recording contact. That said, other neuronal cell types within V1 such as stellate cells (Iurilli et al., 2012; Iurilli et al., 2013) and even pyramid neurons in other layers (Dani et al., 2005; Hromádka et al., 2008; Maffei et al., 2006; Manns et al., 2004), do have higher rates of spontaneous activity, typically around 0.5 Hz to 3 Hz, and the distribution of spontaneous firing rates is approximately lognormal (Mizuseki and Buzsáki, 2017). Furthermore, fast-spiking basket neurons (Chadderton et al., 2009) and various types of interneurons (Chen et al., 2015; Hanganu et al., 2009) can have even higher spontaneous firing rates of around 8 Hz.[1] However, pyramidal neurons are the most common neuronal cell type within the cortical microcircuit, constituting around 60 % by cell count within V1 (Binzegger et al., 2004), and L2/3 pyramids the most common of these. Consequently, it is possible that our spike detection thresholds are too low, yielding an erroneously high spontaneously firing rate, and this could be re-evaluated.

As described in Section 2.3.4, spike extraction thresholds were first selected manually for each session, and then a single session was selected to define a target spontaneous activity rate for each recording channel. Then, for each session, we determined the threshold (for each channel) which would yield the same spontaneous activity as the target. This technique provides greater consistency in the firing rate across recording sessions, which would otherwise vary greatly session to session. However, due to a decline in recording quality over time, as evidenced by our sensitivity analysis in Section 2.6, the firing rate which we extracted during stimulus presentation periods consistently declined over the course of the experiment for V1 recordings, as shown in Figure 2.26. For V4, this decline is not observed, either because these recordings (which were completed sooner after the electrode array was implanted than the V1 recordings) had a more consistent recording quality, or because an increase in selectivity of the cortical response outweighed a decline in recording signal.

Another potential side-effect of the spontaneous activity normalisation is a change in the set of neurons which are included in the measured MUA over the course of

1 Many interneurons have their activity suppressed instead of enhanced by stimulation, hence their high spontaneous firing rate.

the experiment. As the SNR falls, the spike extraction threshold rises relative to the measured voltage of spiking events. Consequently, more distal neurons which had signals strong enough to be recorded at the start of the experiment may no longer exceed the detection threshold in later experimental sessions.

Some, but not all, of these issues could be alleviated through a different choice of extraction threshold. For instance, we could select one of the final recording sessions, with the lowest instead of an intermediate SNR, to define the spontaneous activity rate. From this, the threshold should be high enough to eliminate the incorrect detection of background noise as spiking activity throughout all sessions, and more distal neurons which could not be recorded at end of the experiment may be removed from all sessions. Essentially, the amount of signal extracted would be capped at the worst level throughout all sessions, yielding consistency through forced degradation. Alternatively, these issues could be addressed by using a more sophisticated action potential extraction procedure. If we applied cell sorting techniques, we could remove noise-derived events falsely detected as spikes based on their (lack of) spiking waveform. In the ideal scenario, we would cross-reference the spike waveforms between sessions and restrict our analysis to only consider the neurons which could be consistently detected and isolated throughout the experiment. Unfortunately, any small movement of the recording apparatus will change the set of neurons neighbouring the electrode contacts from which recordings are taken; as such it is impossible to guarantee that the same neurons are recorded from over multiple days, even if their action potential waveforms are similar.

We used a Fisher linear discriminant classifier to decode information in the population activity, and alternatives to this could be explored. Linear models, such as linear regression or support vector machines would likely give similar performance to the Fisher linear discriminant which we employed. Non-linear models such as a multi-layered perceptron neural network may be able to capture information in the population activity which was lost when we made the assumption of monotonic tuning curves, however the difference in effect which would result is not likely to be very large. If using a non-linear model to decode the activity does increase the performance, this would show that non-linearities in the tuning curves are much more important than we currently believe.

In our study, we trained the classifier on trials originating during an individual session, and evaluated it against the performance from held out trials from the same session. Consequently, it is possible for the model which we construct to deviate between sessions — if the structure of the population activity changes over time the classifier built for the final session might be quite different from the classifier trained on the data from the first session. Allowing the model built by the classifier to change

over time corresponds with the implicit assumption that the higher-cortical areas can, at will, change the mapping they employ to decode the results of lower-cortical areas. Instead, we could consider the implications of a fixed mapping from low to high cortical regions, for instance by training a decoder on data from the initial sessions, then fixing the decoder when evaluating the amount of information present in the later sessions. If there is little difference in performance between the two methods, this would suggest that the cortical region under consideration is directed to improve its encoding of the data by higher cortical regions, or is under the constraint of a certain decoding model employed by higher-cortical regions.

Instead of training a decoder to classify the stimulus and investigating the agreement between the output of this classifier and the behavioural response, we could train a decoder to predict the behavioural response directly. Such a procedure would be similar to that used for a brain-machine interface. This would be useful because there could be information in the population activity pertaining to the behavioural response which we are not currently seeing due to the decoder ignoring this information. Such a scenario is quite plausible, since the decoder is not directly trained to optimise the amount of information about the behavioural response.

The decoder-based population analysis from Section 2.12 and Section 2.13 could also be applied to the population activity collected over shorter windows, such as the few tens of milliseconds surrounding stimulus onset response. In doing so, we could repeat the results of our information latency breakdown from Section 2.10, but for the information encoded in the population activity instead of the average information encoded by individual channels. The final outcome of this would be a heatmap similar to Figure 2.29 showing when the population activity becomes more or less informative over time. However, we anticipate that the results would be similar to the ones we already have, just with a larger effect size (since the population is more informative than any individual channel) and without statistics (since we have many channels but only one neural population), and would not yield any more insight into the neural changes relating to perceptual learning.

Similarly, we could apply the population activity decoder to the activity during the stimulus-off period, as we performed in Section 2.11 for individual channels. Again, we expect this would corroborate the results we have already reported. But since the effect size for post-stimulus information about the stimulus contained in individual channels was low, it would be useful to repeat this analysis using the population activity. This section of the analysis could also benefit from computing the conditional mutual information between the neural activity and the behavioural response, conditioned on the true stimulus group.

We could compute the redundancy between pairs of channels for the information they encode about the stimulus, and see how the redundancy changes with training. The methodology would be similar to that used in later chapters to analyse the redundancy between different CSD frequencies across the cortical depth (in Section 3.3.2, for instance). This would have to be reported with care, since the absolute amount of information encoded in the channels changes (typically increasing, but not always) with training. For instance, if the information encoded in each channel increases and some of the increase is the same information for each channel, this will cause the redundancy to rise. Consequently, it may be more interesting to consider the relative redundancy, normalised against the total information encoded in one or both of the channels, instead. Measuring the pairwise redundancy and how it changes with training would help us understand how changes in the noise structure relate to changes in the information content. We already found that shuffling the responses over trials gave a similar increase in performance of the decoder throughout training, suggesting that the redundancy at the population level remains the same. However the pairwise redundancy could decrease (or increase) from changes in the pairwise correlation structure even while the population-level redundancy is unchanged.

In this study, we only have data from two individuals. To be more confident in our conclusions, it would be useful to collect and analyse the neural correlates of perceptual learning for more subjects, especially since the measured effect size differed between our two subjects. It would be particularly beneficial if we could record from V1 and V4 simultaneously, from neurons with the same RF location in each brain region. With such a dataset, we could test our hypothesis about V4 reading out information from V1.

5.2 LAMINAR DISTRIBUTION OF INFORMATION

5.2.1 *Summary*

In Chapters 3 and 4, we investigated the distribution, over cortical depth and frequency, of visual information encoded in the power and phase of cortical oscillations of the CSD in V1. Our results show there are two independent frequency bands, 4 Hz to 16 Hz and 60 Hz to 170 Hz, whose power encodes information about the visual stimulus. The 4 Hz to 16 Hz power is most informative in G and IG, and its phase is also informative. These encode information about scene cuts and other fast and coarse changes in the stimulus. The 60 Hz to 170 Hz power is redundant with the MUA, both of which encode information about higher spatial frequency components of the stimulus, complementary to that encoded in 4 Hz to 16 Hz. Importantly, the re-

lationship between the frequency of cortical oscillations and the spatial scale which it encodes is not smooth. We observed a discontinuity at 40 Hz, with lower frequencies encoding information about the stimulus at a coarse 0.2 cpd resolution and higher frequencies encoding information about a resolution one order of magnitude finer (2.0 cpd).

In Section 3.4, we speculated that these signals could correspond to the M- and P-pathways of visual information which originate in the retina, since these pathways are known to contain information about similar spatiotemporal frequencies. Alternatively, these frequency ranges could correspond to the feedforward output of V1 (for the 60 Hz to 170 Hz band) and a feedback signal from higher visual cortices including V4 (for the 4 Hz to 16 Hz band), which would corroborate related research (van Kerkoerle et al., 2014).

In Chapter 4, we discovered that different information about the stimulus was encoded in the 4 Hz to 16 Hz phase for laminae below and above the layer 4/5 boundary. Furthermore, the phase of the oscillations either side of this division was not synchronised (but was well phase-locked for laminae within a single compartment). The most likely explanation for this is two independently generated 4 Hz to 16 Hz oscillations. This opens up the possibility of an additional frequency band at the same frequency, one encoding feedback from V4 and another encoding a feedforward signal from LGN, corresponding to the M-pathway.

5.2.2 *Open directions for future research*

Firstly, multi-unit spiking activity has frequency components extending into the high-gamma range at around 100 Hz (Einevoll et al., 2013). In addition to this, recent work by Zanos et al. (2011) has indicated that low-frequency components of the sharp changes in voltage in the broadband signal which associated with spikes are retained in LFP extracted from the broadband signal. As a consequence, there are spurious correlations between the LFP and MUA. These spurious correlations may impact our results, and it would be prudent to remove the waveforms of the spikes from the broadband signal before extracting the power of LFP and CSD oscillations (Zanos et al., 2011) and confirm that the information about the stimulus in the 60 Hz to 170 Hz power is still redundant with that of the MUA.

We determined the CSD from the LFP using the inverse CSD method (iCSD; Pettersen et al., 2006). However, the authors have since detailed a more advanced procedure for estimating the CSD from LFPs. This, the kernel current source density method (kCSD; Potworowski et al., 2012), is non-parametric and uses Gaussian kernels with regularisation to estimate the ground truth CSD. In particular, kCSD provides a native

handling for unevenly spaced signal samples, which is useful since we had a small number of faulty electrode contacts, leaving holes in our sampling grid. Re-extracting the CSD using kCSD would be more accurate, but is unlikely to perturb our results by a large amount.

When discussing the results for information encoded in the power of cortical oscillations, we speculated that the power of the 60 Hz to 170 Hz range may encode the output of the cortical column. Typically, neurons in V1 are tuned to respond to the movement of oriented bars with specific properties, such as orientation, spatial frequency, direction of motion, and colour. We could test this hypothesis by computing the spatiotemporal receptive field of the power of cortical oscillations by reverse correlating it with the movie frames (Theunissen et al., 2001). If the spatiotemporal receptive field corresponds to such a stimulus, and in particular if it is similar to that of the MUA, that would be evidence in support of the hypothesis.

Across our experimental sessions, we recorded from neurons whose RF locations varied in eccentricity, from 2.6°, which is at the inner edge of the parafovea, to 7.7°, in the outer half of the perifoveal ring (see Table 3.1 for a full list of RF eccentricities). Eccentricities across this range vary in visual acuity and cortical magnification, and as such it is reasonable to expect variability between the sessions, especially in the recorded spatial frequency preferences. We reported the average across all sessions, and since there were broad similarities across them it was suitable to do so. However, there was some variability across the individual sessions, particularly in the preferred spatial scale of luminance changes for the 60 Hz to 170 Hz power. For most sessions, the cortical power was most informative about the spatial frequencies of around 2.4 cpd. However, there were two outliers. Session H05391, with the most peripheral RF at $(7.7 \pm 1.0)°$ eccentricity, was tuned to coarser spatial frequencies with a peak around 1.6 cpd. Session F10nm1, with one of the two most central RF locations at $(2.7 \pm 1.0)°$ eccentricity, encoded finer details about the stimulus, peaking at a spatial frequency of at least 5 cpd (its response information curve peaked for the highest spatial frequencies we analysed). These findings speculatively indicate there is a relationship between the RF eccentricity and the spatial resolution of the information in the gamma power and MUA. Such a finding would fit with the changes in visual acuity and cortical magnification as a function of eccentricity. However, more recording sessions with a variety of (more precisely determined) RF locations are needed to confirm this tentative observation.

When determining which spatiotemporal components of the stimulus corresponded to the changes in cortical power and phase, we focused on the rate of change of luminance. However, we did not find information about any spatiotemporal scales present in the phase of oscillations. Consequently, it would be prudent to widen our search

and consider colour-opponent changes in the stimulus, as is provided to the visual cortex through the P-pathway and K-pathway. One could even go so far as to model the transformations to the raw visual input performed by each of the RGC types. In doing so, we would simulate the full effects of processing in the retina and be able to investigate the structure of information in V1 with respect to its actual input. However, such an undertaking would be quite significant, since our understanding of the computational processing within the retina remains incomplete and is actively researched.

We hypothesised that the phase of multiple cortical frequency components encoded synergistic information about the stimulus because scene changes induce stereotypical, transient waveforms and pairs of phase enable the determination of maxima and minima in such shapes. To investigate this hypothesis further, there are several directions we could consider. Firstly, we filtered signal using an IIR Butterworth filter before using the Hilbert transform to determine the instantaneous power and phase. Since such events are temporally isolated, it would be more prudent to use a finite impulse response (FIR) filter instead, so that transient waveforms remain isolated and do not have effects on the reported power and phase across all time, into both the past and future. Alternatively, we could use a wavelet transform to decompose the CSD signal into frequency components each considering isolated temporal periods. Secondly, we could use the characteristic shape of the stimulus-onset response to search for similar events throughout the stimulus presentation. From this, we can investigate how such waveforms relate to scene changes and other aspects of the visual stimulus.

For this project, we principally investigated the population activity by considering the LFP and CSD. However, the process through which each of the different types of neuron within V1 manifest CSDs and how each frequency component in the signal is generated is not yet well understood. Compartmental models of the morphology of cortical neurons can be used to fill in such gaps of understanding (Łęski et al., 2013). If we were to reconstruct the morphology of each cell type within V1 and derive the CSD generated by each, we would be much better equipped to understand which neurons generate the information-encoding oscillations which we have described and localised in this thesis.

BIBLIOGRAPHY

Adini, Y., Sagi, D., and Tsodyks, M. (2002). Context-enabled learning in the human visual system. *Nature*, 415(6873):790–3. doi:10.1038/415790a. (Cited on page 29.)

Ahissar, E. and Oram, T. (2015). Thalamic Relay or Cortico-Thalamic Processing? Old Question, New Answers. *Cerebral Cortex*, 25(4):845. doi:10.1093/cercor/bht296. (Cited on page 120.)

Ahissar, M. and Hochstein, S. (2004). The reverse hierarchy theory of visual perceptual learning. *Trends in Cognitive Sciences*, 8(10):457–64. doi:10.1016/j.tics.2004.08.011. (Cited on page 29.)

Albrecht, D. G., Geisler, W. S., Frazor, R. A., and Crane, A. M. (2002). Visual Cortex Neurons of Monkeys and Cats: Temporal Dynamics of the Contrast Response Function. *Journal of Neurophysiology*, 88(2):888–913. (Cited on pages 115 and 173.)

Arabzadeh, E., Panzeri, S., and Diamond, M. E. (2006). Deciphering the spike train of a sensory neuron: counts and temporal patterns in the rat whisker pathway. *Journal of Neuroscience*, 26(36):9216–26. doi:10.1523/JNEUROSCI.1491-06.2006. (Cited on page 30.)

Arnal, L. H. and Giraud, A.-L. (2012). Cortical oscillations and sensory predictions. *Trends in Cognitive Sciences*, 16(7):390–8. doi:10.1016/j.tics.2012.05.003. (Cited on page 120.)

Averbeck, B. B., Latham, P. E., and Pouget, A. (2006). Neural correlations, population coding and computation. *Nature Reviews Neuroscience*, 7(5):358–366. doi:10.1038/nrn1888. (Cited on pages 23, 98, and 128.)

Ball, K. and Sekuler, R. (1987). Direction-specific improvement in motion discrimination. *Vision Research*, 27(6):953–965. doi:10.1016/0042-6989(87)90011-3. (Cited on page 28.)

Banerjee, P. K. and Griffith, V. (2015). Synergy, Redundancy and Common Information. *CoRR*. arXiv:1509.03706. (Cited on page 128.)

Barlow, P. W. (2008). Reflections on 'plant neurobiology'. *BioSystems*, 92(2):132–147. doi:10.1016/j.biosystems.2008.01.004. (Cited on page 1.)

Belitski, A., Gretton, A., Magri, C., Murayama, Y., Montemurro, M. A., Logothetis, N. K., and Panzeri, S. (2008). Low-frequency local field potentials and spikes in primary visual cortex convey independent visual information. *Journal of Neuroscience*, 28(22):5696–709. doi:10.1523/JNEUROSCI.0009-08.2008. (Cited on pages 120, 136, 140, and 151.)

Berardi, N., Bisti, S., and Maffei, L. (1987). The transfer of visual information across the corpus callosum: spatial and temporal properties in the cat. *The Journal of Physiology*, 384(1):619–632. doi:10.1113/jphysiol.1987.sp016473. (Cited on page 28.)

Berens, P. (2009). CircStat: A MATLAB Toolbox for Circular Statistics. *Journal of Statistical Software*, 31(10). doi:10.18637/jss.v031.i10. (Cited on page 156.)

Berson, D. M., Dunn, F. A., and Takao, M. (2002). Phototransduction by Retinal Ganglion Cells That Set the Circadian Clock. *Science*, 295(5557):1070–1073. doi:10.1126/science.1067262. (Cited on page 3.)

Binzegger, T., Douglas, R. J., and Martin, K. A. C. (2004). A quantitative map of the circuit of cat primary visual cortex. *Journal of Neuroscience*, 24(39):8441–53. doi:10.1523/JNEUROSCI.1400-04.2004. (Cited on page 174.)

Binzegger, T., Douglas, R. J., and Martin, K. A. C. (2009). Topology and dynamics of the canonical circuit of cat V1. *Neural networks*, 22(8):1071–8. doi:10.1016/j.neunet.2009.07.011. (Cited on page 9.)

Bompas, A., Kendall, G., and Sumner, P. (2013). Spotting Fruit versus Picking Fruit as the Selective Advantage of Human Colour Vision. *i-Perception*, 4(2):84–94. doi:10.1068/i0564. (Cited on page 6.)

Bowmaker, J. K. and Dartnall, H. J. (1980). Visual pigments of rods and cones in a human retina. *The Journal of Physiology*, 298:501–511. doi:10.1113/jphysiol.1980.sp013097. (Cited on page 4.)

Brenner, E. D., Stahlberg, R., Mancuso, S., Vivanco, J., Baluška, F., and Van Volkenburgh, E. (2006). Plant neurobiology: an integrated view of plant signaling. *Trends in Plant Science*, 11(8):413–419. doi:10.1016/j.tplants.2006.06.009. (Cited on page 1.)

Britten, K. H., Shadlen, M. N., Newsome, W. T., and Movshon, J. A. (1992). The analysis of visual motion: a comparison of neuronal and psychophysical performance. *Journal of Neuroscience*, 12(12):4745–4765. (Cited on page 117.)

Buzsáki, G. (2015). Hippocampal sharp wave-ripple: A cognitive biomarker for episodic memory and planning. *Hippocampus*, 25(10):1073–1188. doi:10.1002/hipo.22488. (Cited on page 119.)

Buzsáki, G. and Draguhn, A. (2004). Neuronal Oscillations in Cortical Networks. *Science*, 304(5679):1926–1929. doi:10.1126/science.1099745. (Cited on page 119.)

Callaway, E. M. (1998). Local circuits in primary visual cortex of the macaque monkey. *Annual Review of Neuroscience*, 21(1):47–74. doi:10.1146/annurev.neuro.21.1.47. (Cited on pages 126 and 152.)

Carcagno, S. and Plack, C. J. (2011). Subcortical Plasticity Following Perceptual Learning in a Pitch Discrimination Task. *Journal of the Association for Research in Otolaryngology*, 12(1):89–100. doi:10.1007/s10162-010-0236-1. (Cited on page 28.)

Chadderton, P., Agapiou, J. P., McAlpine, D., and Margrie, T. W. (2009). The Synaptic Representation of Sound Source Location in Auditory Cortex. *Journal of Neuroscience*, 29(45):14127–14135. doi:10.1523/JNEUROSCI.2061-09.2009. (Cited on page 174.)

Chen, I.-W., Helmchen, F., and Lütcke, H. (2015). Specific Early and Late Oddball-Evoked Responses in Excitatory and Inhibitory Neurons of Mouse Auditory Cortex. *Journal of Neuroscience*, 35(36):12560–12573. doi:10.1523/JNEUROSCI.2240-15.2015. (Cited on page 174.)

Chen, X. (2013). *Perceptual learning of contrast discrimination and its neural correlates in macaque V4 & V1*. Doctor of philosophy, Newcastle University. (Cited on

pages 30, 116, 117, and 118.)

Chen, X., Sanayei, M., and Thiele, A. (2013). Perceptual learning of contrast discrimination in macaca mulatta. *Journal of Vision*, 13(13):1–15. doi:10.1167/13.13.22. (Cited on pages 30, 32, 115, 116, and 118.)

Chen, X., Sanayei, M., and Thiele, A. (2014). Stimulus roving and flankers affect perceptual learning of contrast discrimination in Macaca mulatta. *PLoS ONE*, 9(10):13–15. doi:10.1371/journal.pone.0109604. (Cited on page 30.)

Cohen, M. R. and Newsome, W. T. (2008). Context-Dependent Changes in Functional Circuitry in Visual Area MT. *Neuron*, 60(1):162–173. doi:10.1016/j.neuron.2008.08.007. (Cited on page 107.)

Colgin, L. L. (2016). Rhythms of the hippocampal network. *Nature Reviews Neuroscience*, 17(4):239–249. doi:10.1038/nrn.2016.21. (Cited on page 119.)

Dani, V. S., Chang, Q., Maffei, A., Turrigiano, G. G., Jaenisch, R., and Nelson, S. B. (2005). Reduced cortical activity due to a shift in the balance between excitation and inhibition in a mouse model of Rett Syndrome. *Proceedings of the National Academy of Sciences*, 102(35):12560–12565. doi:10.1073/pnas.0506071102. (Cited on page 174.)

Dayan, P. and Abbott, L. F. (2001). *Theoretical Neuroscience*. MIT Press. ISBN 978-0-262-54185-5. (Cited on page 2.)

Demany, L. (1985). Perceptual learning in frequency discrimination. *The Journal of the Acoustical Society of America*, 78(3):1118–1120. doi:10.1121/1.393034. (Cited on page 28.)

Dinse, H. R., Ragert, P., Pleger, B., Schwenkreis, P., and Tegenthoff, M. (2003). Pharmacological modulation of perceptual learning and associated cortical reorganization. *Science*, 301(5629):91–4. doi:10.1126/science.1085423. (Cited on pages 28 and 29.)

Dipoppa, M. and Gutkin, B. S. (2013). Flexible frequency control of cortical oscillations enables computations required for working memory. *Proceedings of the National Academy of Sciences*. doi:10.1073/pnas.1303270110. (Cited on page 120.)

Dobkins, K. R., Thiele, A., and Albright, T. D. (2000). Comparison of red-green equiluminance points in humans and macaques: evidence for different L:M cone ratios between species. *Optical Society of America*, 17(3):545–556. doi:10.1364/JOSAA.17.000545. (Cited on page 122.)

Douglas, R. J. and Martin, K. A. C. (1991). A functional microcircuit for cat visual cortex. *The Journal of Physiology*, 440(1):735–769. doi:10.1113/jphysiol.1991.sp018733. (Cited on page 9.)

Douglas, R. J. and Martin, K. A. C. (2004). Neuronal circuits of the neocortex. *Annual review of neuroscience*, 27:419–51. doi:10.1146/annurev.neuro.27.070203.144152. (Cited on page 9.)

Douglas, R. J., Martin, K. A. C., and Whitteridge, D. (1989). A Canonical Microcircuit for Neocortex. *Neural Computation*, 1(4):480–488. doi:10.1162/neco.1989.1.4.480. (Cited on page 9.)

Ecker, J. L., Dumitrescu, O. N., Wong, K. Y., Alam, N. M., Chen, S.-K., LeGates, T., Renna, J. M., Prusky, G. T., Berson, D. M., and Hattar, S. (2010). Melanopsin-Expressing Retinal Ganglion-Cell Photoreceptors: Cellular Diversity and Role

in Pattern Vision. *Neuron*, 67(1):49–60. doi:10.1016/j.neuron.2010.05.023. (Cited on page 3.)

Einevoll, G. T., Kayser, C., Logothetis, N. K., and Panzeri, S. (2013). Modelling and analysis of local field potentials for studying the function of cortical circuits. *Nature Reviews Neuroscience*, 14(11):770–85. doi:10.1038/nrn3599. (Cited on pages 119, 133, 136, and 178.)

Fahle, M. (2005). Perceptual learning: specificity versus generalization. *Current Opinion in Neurobiology*, 15(2):154–60. doi:10.1016/j.conb.2005.03.010. (Cited on page 29.)

Fendick, M. and Westheimer, G. (1983). Effects of practice and the separation of test targets on foveal and peripheral stereoacuity. *Vision Research*, 23(2):145–150. doi:10.1016/0042-6989(83)90137-2. (Cited on page 28.)

Fiorentini, A. and Berardi, N. (1980). Perceptual learning specific for orientation and spatial frequency. *Nature*. doi:10.1038/287043a0. (Cited on pages 28 and 32.)

Fiorentini, A. and Berardi, N. (1981). Learning in grating waveform discrimination: Specificity for orientation and spatial frequency. *Vision Research*, 21(7):1149–1158. doi:10.1016/0042-6989(81)90017-1. (Cited on pages 28 and 32.)

Franke, F., Fiscella, M., Sevelev, M., Roska, B., Hierlemann, A., and da Silveira, R. A. (2016). Structures of Neural Correlation and How They Favor Coding. *Neuron*, 89(2):409–422. doi:10.1016/j.neuron.2015.12.037. (Cited on pages 22 and 25.)

Fries, P., Reynolds, J. H., Rorie, A. E., and Desimone, R. (2001). Modulation of Oscillatory Neuronal Synchronization by Selective Visual Attention. *Science*, 291(5508):1560–1563. doi:10.1126/science.1055465. (Cited on page 119.)

Fries, P., Roelfsema, P. R., Engel, A. K., König, P., and Singer, W. (1997). Synchronization of oscillatory responses in visual cortex correlates with perception in interocular rivalry. *Proceedings of the National Academy of Sciences*, 94(23):12699–12704. doi:10.1073/pnas.94.23.12699. (Cited on page 119.)

Ghose, G. M., Yang, T., and Maunsell, J. H. R. (2002). Physiological correlates of perceptual learning in monkey V1 and V2. *Journal of Neurophysiology*, 87(4):1867–88. doi:10.1152/jn.00690.2001. (Cited on page 29.)

Gibson, J. J. and Gibson, E. J. (1955). Perceptual learning; differentiation or enrichment? *Psychological review*, 62(1):32–41. doi:10.1037/h0048826. (Cited on page 28.)

Gilbert, C. (1994). Early perceptual learning. *Proceedings of the National Academy of Sciences*, 91(February):1195–1197. doi:10.1073/pnas.91.4.1195. (Cited on page 28.)

Gilbert, C. D., Sigman, M., and Crist, R. E. (2001). The Neural Basis of Perceptual Learning. *Neuron*, 31:681–697. doi:10.1016/s0896-6273(01)00424-x. (Cited on pages 28 and 29.)

Giraud, A.-L. and Poeppel, D. (2012). Cortical oscillations and speech processing: emerging computational principles and operations. *Nature Neuroscience*, 15(4):511–517. doi:10.1038/nn.3063. (Cited on page 120.)

Godde, B., Stauffenberg, B., Spengler, F., and Dinse, H. R. (2000). Tactile Coactivation-Induced Changes in Spatial Discrimination Performance. *Journal of Neuroscience*, 20(4):1597–1604. (Cited on page 28.)

Goense, J. B. M. and Logothetis, N. K. (2008). Neurophysiology of the BOLD fMRI Signal in Awake Monkeys. *Current Biology*, 18(9):631–640. doi:10.1016/j.cub.2008.03.054. (Cited on page 121.)

Goodale, M. A. and Milner, A. (1992). Separate visual pathways for perception and action. *Trends in Neurosciences*, 15(1):20–25. doi:10.1016/0166-2236(92)90344-8. (Cited on page 10.)

Griffith, V. and Koch, C. (2014). Quantifying Synergistic Mutual Information. In Prokopenko, M., editor, *Guided Self-Organization: Inception*, pages 159–190. Springer, Berlin. ISBN 978-3-642-53734-9. arXiv:1205.4265v6. doi:10.1007/978-3-642-53734-9_6. (Cited on page 128.)

Gross, J., Schnitzler, A., Timmermann, L., and Ploner, M. (2007). Gamma Oscillations in Human Primary Somatosensory Cortex Reflect Pain Perception. *PLoS Biology*, 5(5):1–6. doi:10.1371/journal.pbio.0050133. (Cited on page 119.)

Grossberg, S. and Somers, D. (1991). Synchronized oscillations during cooperative feature linking in a cortical model of visual perception. *Neural Networks*, 4(4):453–466. doi:10.1016/0893-6080(91)90041-3. (Cited on page 119.)

Gu, Y., Liu, S., Fetsch, C. R., Yang, Y., Fok, S., Sunkara, A., DeAngelis, G. C., and Angelaki, D. E. (2011). Perceptual learning reduces interneuronal correlations in macaque visual cortex. *Neuron*, 71(4):750–61. doi:10.1016/j.neuron.2011.06.015. (Cited on page 117.)

Hanganu, I. L., Okabe, A., Lessmann, V., and Luhmann, H. J. (2009). Cellular Mechanisms of Subplate-Driven and Cholinergic Input-Dependent Network Activity in the Neonatal Rat Somatosensory Cortex. *Cerebral Cortex*, 19(1):89–105. doi:10.1093/cercor/bhn061. (Cited on page 174.)

Hansen, B., Chelaru, M., and Dragoi, V. (2012). Correlated Variability in Laminar Cortical Circuits. *Neuron*, 76(3):590–602. doi:10.1016/j.neuron.2012.08.029. (Cited on page 126.)

Harris, K. D. and Mrsic-Flogel, T. D. (2013). Cortical connectivity and sensory coding. *Nature*, 503(7474):51–8. doi:10.1038/nature12654. (Cited on pages 9 and 152.)

Hecht, S., Shlaer, S., and Pirenne, M. H. (1942). Energy, quanta, and vision. *The Journal of General Physiology*, 25(6):819–840. doi:10.1085/jgp.25.6.819. (Cited on page 5.)

Hendrickson, A. (2005). Organization of the Adult Primate Fovea. In Penfold, P. L. and Provis, J. M., editors, *Macular Degeneration*, pages 1–23. Springer, Heidelberg. ISBN 978-3-540-26977-9. doi:10.1007/3-540-26977-0_1. (Cited on page 5.)

Henrie, J. A. and Shapley, R. (2005). LFP Power Spectra in V1 Cortex: The Graded Effect of Stimulus Contrast. *Journal of Neurophysiology*, 94(1):479–490. doi:10.1152/jn.00919.2004. (Cited on page 119.)

Hill, D. N., Varga, Z., Jia, H., Sakmann, B., and Konnerth, A. (2013). Multibranch activity in basal and tuft dendrites during firing of layer 5 cortical neurons in vivo. *Proceedings of the National Academy of Sciences*, 110(33):13618–23. doi:10.1073/pnas.1312599110. (Cited on pages 170 and 171.)

Hochstein, S. and Ahissar, M. (2002). View from the Top: Hierarchies and Reverse Hierarchies in the Visual System. *Neuron*, 36(3):791–804. doi:10.1016/S0896-6273(02)01091-7. (Cited on page 29.)

Horton, J. C. and Adams, D. L. (2005). The cortical column: a structure without a function. *Philosophical Transactions of the Royal Society of London B: Biological Sciences*, 360(1456):837–62. doi:10.1098/rstb.2005.1623. (Cited on pages 124 and 152.)

Hromádka, T., DeWeese, M. R., and Zador, A. M. (2008). Sparse Representation of Sounds in the Unanesthetized Auditory Cortex. *PLOS Biology*, 6(1):1–14. doi:10.1371/journal.pbio.0060016. (Cited on page 174.)

Hubel, D. H. and Wiesel, T. N. (1962). Receptive fields, binocular interaction and functional architecture in the cat's visual cortex. *The Journal of Physiology*, 160(1):106–154. doi:10.1113/jphysiol.1962.sp006837. (Cited on page 9.)

Hubel, D. H. and Wiesel, T. N. (1963). Shape and arrangement of columns in cat's striate cortex. *The Journal of Physiology*. doi:10.1113/jphysiol.1963.sp007079. (Cited on page 9.)

Iaccarino, H. F., Singer, A. C., Martorell, A. J., Rudenko, A., Gao, F., Gillingham, T. Z., Mathys, H., Seo, J., Kritskiy, O., Abdurrob, F., Adaikkan, C., Canter, R. G., Rueda, R., Brown, E. N., Boyden, E. S., and Tsai, L.-H. (2016). Gamma frequency entrainment attenuates amyloid load and modifies microglia. *Nature*, 540(7632):230–235. doi:10.1038/nature20587. (Cited on page 120.)

Iurilli, G., Benfenati, F., and Medini, P. (2012). Loss of Visually Driven Synaptic Responses in Layer 4 Regular-Spiking Neurons of Rat Visual Cortex in Absence of Competing Inputs. *Cerebral Cortex*, 22(9):2171–2181. doi:10.1093/cercor/bhr304. (Cited on page 174.)

Iurilli, G., Olcese, U., and Medini, P. (2013). Preserved Excitatory-Inhibitory Balance of Cortical Synaptic Inputs following Deprived Eye Stimulation after a Saturating Period of Monocular Deprivation in Rats. *PLOS ONE*, 8(12):1–14. doi:10.1371/journal.pone.0082044. (Cited on page 174.)

Jameson, K. A., Highnote, S. M., and Wasserman, L. M. (2001). Richer color experience in observers with multiple photopigment opsin genes. *Psychonomic Bulletin & Review*, 8(2):244–261. doi:10.3758/BF03196159. (Cited on page 4.)

Jammalamadaka, S. R. and SenGupta, A. (2001). *Topics in Circular Statistics*. World Scientific, Singapore. ISBN 978-981-02-3778-3. doi:10.1142/9789812779267. (Cited on page 156.)

Jensen, O., Gelfand, J., Kounios, J., and Lisman, J. E. (2002). Oscillations in the Alpha Band (9–12 Hz) Increase with Memory Load during Retention in a Short-term Memory Task. *Cerebral Cortex*, 12(8):877. doi:10.1093/cercor/12.8.877. (Cited on page 119.)

Jensen, O., Kaiser, J., and Lachaux, J. P. (2007). Human gamma-frequency oscillations associated with attention and memory. *Trends in Neurosciences*, 30(7):317–324. doi:10.1016/j.tins.2007.05.001. (Cited on page 119.)

Jordan, G. and Mollon, J. D. (1993). A study of women heterozygous for colour deficiencies. *Vision Research*, 33(11):1495–1508. doi:10.1016/0042-6989(93)90143-K. (Cited on page 4.)

Kajikawa, Y. and Schroeder, C. E. (2011). How local is the local field potential? *Neuron*, 72(5):847–858. doi:10.1016/j.neuron.2011.09.029.How. (Cited on page 136.)

Kandadai, M. A., Raymond, J. L., and Shaw, G. J. (2012). Comparison of electrical conductivities of various brain phantom gels: Developing a 'brain gel model'. *Mate-*

rials Science and Engineering: C, 32(8):2664–2667. doi:10.1016/j.msec.2012.07.024. (Cited on page 124.)

Kanitscheider, I., Coen-Cagli, R., and Pouget, A. (2015). Origin of information-limiting noise correlations. *Proceedings of the National Academy of Sciences*, 112(50):E6973–E6982. doi:10.1073/pnas.1508738112. (Cited on page 22.)

Karni, A. and Sagi, D. (1991). Where practice makes perfect in texture discrimination: evidence for primary visual cortex plasticity. *Proceedings of the National Academy of Sciences*, 88(11):4966–4970. doi:10.1073/pnas.88.11.4966. (Cited on pages 28 and 32.)

Keller, G. B., Bonhoeffer, T., and Hübener, M. (2012). Sensorimotor Mismatch Signals in Primary Visual Cortex of the Behaving Mouse. *Neuron*, 74(5):809–815. doi:10.1016/j.neuron.2012.03.040. (Cited on page 118.)

Klimesch, W. (1999). EEG alpha and theta oscillations reflect cognitive and memory performance: a review and analysis. *Brain Research Reviews*, 29(2–3):169–195. doi:10.1016/S0165-0173(98)00056-3. (Cited on page 119.)

Klimesch, W. (2012). Alpha-band oscillations, attention, and controlled access to stored information. *Trends in Cognitive Sciences*, 16(12):606–617. doi:10.1016/j.tics.2012.10.007. (Cited on page 119.)

Kreiman, G., Hung, C. P., Kraskov, A., Quiroga, R. Q., Poggio, T., and DiCarlo, J. J. (2006). Object Selectivity of Local Field Potentials and Spikes in the Macaque Inferior Temporal Cortex. *Neuron*, 49(3):433–445. doi:10.1016/j.neuron.2005.12.019. (Cited on page 119.)

Kreuz, T. (2011). Measures of neuronal signal synchrony. *Scholarpedia*, 6(12):11922. doi:10.4249/scholarpedia.11922. (Cited on page 157.)

Latham, P. E. and Nirenberg, S. (2005). Synergy, Redundancy, and Independence in Population Codes, Revisited. *Journal of Neuroscience*, 25(21):5195–5206. doi:10.1523/JNEUROSCI.5319-04.2005. (Cited on page 128.)

Laughlin, S. B. (2001). Energy as a constraint on the coding and processing of sensory information. *Current Opinion in Neurobiology*, 11(4):475–480. doi:10.1016/S0959-4388(00)00237-3. (Cited on page 13.)

Łęski, S., Lindén, H., Tetzlaff, T., Pettersen, K. H., and Einevoll, G. T. (2013). Frequency dependence of signal power and spatial reach of the local field potential. *PLoS Computational Biology*, 9(7):e1003137. doi:10.1371/journal.pcbi.1003137. (Cited on pages 119 and 180.)

Li, W., Piëch, V., and Gilbert, C. D. (2004). Perceptual learning and top-down influences in primary visual cortex. *Nature Neuroscience*, 7(6):651–657. doi:10.1038/nn1255. (Cited on page 29.)

Liebe, S., Hoerzer, G. M., Logothetis, N. K., and Rainer, G. (2012). Theta coupling between V4 and prefrontal cortex predicts visual short-term memory performance. *Nature Neuroscience*, 15(3):456–462. doi:10.1038/nn.3038. (Cited on page 119.)

Llinás, R., Ribary, U., Contreras, D., and Pedroarena, C. (1998). The neuronal basis for consciousness. *Philosophical Transactions of the Royal Society B: Biological Sciences*. doi:10.1098/rstb.1998.0336. (Cited on page 120.)

Logothetis, N. K., Guggenberger, H., Peled, S., and Pauls, J. (1999). Functional imaging of the monkey brain. *Nature Neuroscience*, 2(6):555–562. doi:10.1038/9210.

(Cited on pages 120 and 121.)

Logothetis, N. K., Kayser, C., and Oeltermann, A. (2007). In vivo measurement of cortical impedance spectrum in monkeys: implications for signal propagation. *Neuron*, 55(5):809–23. doi:10.1016/j.neuron.2007.07.027. (Cited on page 124.)

Logothetis, N. K., Pauls, J., Augath, M., Trinath, T., and Oeltermann, A. (2001). Neurophysiological investigation of the basis of the fMRI signal. *Nature*, 412(6843):150–157. doi:10.1038/35084005. (Cited on page 120.)

Lowe, S. C. (2012). *An information theoretic analysis of perceptual learning data from macaque V1 and V4*. Master of science by research, University of Edinburgh. (Cited on pages 27 and 115.)

Lumer, E. D., Friston, K. J., and Rees, G. (1998). Neural Correlates of Perceptual Rivalry in the Human Brain. *Science*, 280(5371):1930–1934. doi:10.1126/science.280.5371.1930. (Cited on page 20.)

Lund, J. S. (1973). Organization of neurons in the visual cortex, area 17, of the monkey (Macaca mulatta). *The Journal of Comparative Neurology*, 147(4):455–96. doi:10.1002/cne.901470404. (Cited on page 126.)

Lund, J. S., Angelucci, A., and Bressloff, P. C. (2003). Anatomical substrates for functional columns in macaque monkey primary visual cortex. *Cerebral Cortex*, 13(1):15–24. doi:10.1093/cercor/13.1.15. (Cited on page 124.)

MacKay, D. J. C. (2003). *Information theory, inference and learning algorithms*. Cambridge university press. ISBN 978-0-521-64298-9. (Cited on pages 12 and 21.)

Maffei, A., Nataraj, K., Nelson, S. B., and Turrigiano, G. G. (2006). Potentiation of cortical inhibition by visual deprivation. *Nature*, 443(7107):81–84. doi:10.1038/nature05079. (Cited on page 174.)

Magri, C., Whittingstall, K., Singh, V., Logothetis, N. K., and Panzeri, S. (2009). A toolbox for the fast information analysis of multiple-site LFP, EEG and spike train recordings. *BMC Neuroscience*, 10(81). doi:10.1186/1471-2202-10-81. (Cited on pages 11, 55, and 127.)

Maier, A., Adams, G. K., Aura, C., and Leopold, D. A. (2010). Distinct superficial and deep laminar domains of activity in the visual cortex during rest and stimulation. *Frontiers in Systems Neuroscience*, 4(31). doi:10.3389/fnsys.2010.00031. (Cited on page 140.)

Manns, I. D., Sakmann, B., and Brecht, M. (2004). Sub- and suprathreshold receptive field properties of pyramidal neurones in layers 5A and 5B of rat somatosensory barrel cortex. *The Journal of Physiology*, 556(2):601–622. doi:10.1113/jphysiol.2003.053132. (Cited on page 174.)

Mazzoni, A., Brunel, N., Cavallari, S., Logothetis, N. K., and Panzeri, S. (2011). Cortical dynamics during naturalistic sensory stimulations: Experiments and models. *The Journal of Physiology*, 105(1–3):2–15. doi:10.1016/j.jphysparis.2011.07.014. (Cited on page 119.)

Merigan, W. H., Byrne, C. E., and Maunsell, J. H. (1991). Does primate motion perception depend on the magnocellular pathway? *Journal of Neuroscience*, 11(11):3422–3429. doi:10.1007/0-387-28806-6. (Cited on page 153.)

Miikkulainen, R., Bednar, J. A., Choe, Y., and Sirosh, J. (2005). *Computational Maps in the Visual Cortex*. Springer, New York. ISBN 978-0387220246. (Cited on page 9.)

Miller, G. A. (1955). Note on the bias of information estimates. *Information Theory in Psychology: Problems and Methods*. (Cited on page 18.)

Mishkin, M. and Ungerleider, L. G. (1982). Contribution of striate inputs to the visuospatial functions of parieto-preoccipital cortex in monkeys. *Behavioural Brain Research*, 6(1):57–77. doi:10.1016/0166-4328(82)90081-X. (Cited on page 10.)

Mitzdorf, U. (1985). Current source-density method and application in cat cerebral cortex: investigation of evoked potentials and EEG phenomena. *Physiological reviews*, 65(1):37–100. (Cited on page 125.)

Mitzdorf, U. and Singer, W. (1979). Excitatory synaptic ensemble properties in the visual cortex of the macaque monkey: a current source density analysis of electrically evoked potentials. *The Journal of Comparative Neurology*, 187(1):71–83. doi:10.1002/cne.901870105. (Cited on page 125.)

Mizuseki, K. and Buzsáki, G. (2017). Preconfigured, Skewed Distribution of Firing Rates in the Hippocampus and Entorhinal Cortex. *Cell Reports*, 4(5):1010–1021. doi:10.1016/j.celrep.2013.07.039. (Cited on page 174.)

Montemurro, M. A., Senatore, R., and Panzeri, S. (2007). Tight data-robust bounds to mutual information combining shuffling and model selection techniques. *Neural Computation*, 19(11):2913–57. doi:10.1162/neco.2007.19.11.2913. (Cited on page 18.)

Monto, S., Palva, S., Voipio, J., and Palva, J. M. (2008). Very Slow EEG Fluctuations Predict the Dynamics of Stimulus Detection and Oscillation Amplitudes in Humans. *Journal of Neuroscience*, 28(33):8268–8272. doi:10.1523/JNEUROSCI.1910-08.2008. (Cited on page 120.)

Moreno-Bote, R., Beck, J., Kanitscheider, I., Pitkow, X., Latham, P., and Pouget, A. (2014). Information-limiting correlations. *Nature Neuroscience*, 17(10):1410–1417. doi:10.1038/nn.3807. (Cited on pages 22 and 98.)

Mountcastle, V. B. (1957). Modality and topographic properties of single neurons of cat's somatic sensory cortex. *Journal of Neurophysiology*, 20(4):408–34. doi:10.1146/annurev.ph.20.030158.002351. (Cited on page 9.)

Mountcastle, V. B. (1997). The columnar organization of the neocortex. *Brain*, 120(4):701–22. doi:10.1093/brain/120.4.701. (Cited on page 9.)

Müller, J. R., Metha, A. B., Krauskopf, J., and Lennie, P. (2001). Information conveyed by onset transients in responses of striate cortical neurons. *Journal of Neuroscience*, 21(17):6978–90. (Cited on page 115.)

Murayama, Y., Bieβmann, F., Meinecke, F. C., Müller, K.-R., Augath, M., Oeltermann, A., and Logothetis, N. K. (2010). Relationship between neural and hemodynamic signals during spontaneous activity studied with temporal kernel CCA. *Magnetic Resonance Imaging*, 28(8):1095–1103. doi:10.1016/j.mri.2009.12.016. (Cited on page 123.)

Nagy, A. L., MacLeod, D. I. A., Heyneman, N. E., and Eisner, A. (1981). Four cone pigments in women heterozygous for color deficiency. *Journal of the Optical Society of America*, 71(6):719–722. doi:10.1364/JOSA.71.000719. (Cited on page 4.)

Nassi, J. J. and Callaway, E. M. (2009). Parallel processing strategies of the primate visual system. *Nature Reviews Neuroscience*, 10(5):360–72. doi:10.1038/nrn2619. (Cited on pages 6, 7, 8, and 152.)

Nemenman, I., Bialek, W., and de Ruyter van Steveninck, R. (2004). Entropy and information in neural spike trains: progress on the sampling problem. *Physical review. E, Statistical, nonlinear, and soft matter physics*, 69(5 Pt 2):056111. doi:10.1103/physreve.69.056111. (Cited on page 19.)

Niven, J. E. and Laughlin, S. B. (2008). Energy limitation as a selective pressure on the evolution of sensory systems. *Journal of Experimental Biology*, 211(11):1792–1804. doi:10.1242/jeb.017574. (Cited on page 13.)

Oeltermann, A., Augath, M. A., and Logothetis, N. K. (2007). Simultaneous recording of neuronal signals and functional NMR imaging. *Magnetic Resonance Imaging*, 25(6):760–774. doi:10.1016/j.mri.2007.03.015. (Cited on page 123.)

O'Kusky, J. and Colonnier, M. (1982). A laminar analysis of the number of neurons, glia, and synapses in the adult cortex (area 17) of adult macaque monkeys. *The Journal of Comparative Neurology*, 210(3):278–90. doi:10.1002/cne.902100307. (Cited on page 126.)

Optican, L. M., Gawne, T. J., Richmond, B. J., and Joseph, P. J. (1991). Unbiased measures of transmitted information and channel capacity from multivariate neuronal data. *Biological Cybernetics*, 65(5):305–310. doi:10.1007/BF00216963. (Cited on pages 18 and 66.)

Optican, L. M. and Richmond, B. J. (1987). Temporal encoding of two-dimensional patterns by single units in primate inferior temporal cortex. III. Information theoretic analysis. *Journal of Neurophysiology*, 57(1):162–178. (Cited on page 13.)

Pakan, J. M. P., Lowe, S. C., Dylda, E., Keemink, S. W., Currie, S. P., Coutts, C. A., and Rochefort, N. L. (2016). Behavioral-state modulation of inhibition is context-dependent and cell type specific in mouse visual cortex. *eLife*, 5:e14985. doi:10.7554/eLife.14985. (Cited on page 118.)

Panzeri, S., Senatore, R., Montemurro, M. A., and Petersen, R. S. (2007). Correcting for the sampling bias problem in spike train information measures. *Journal of Neurophysiology*, 98(3):1064–72. doi:10.1152/jn.00559.2007. (Cited on pages 19 and 62.)

Panzeri, S. and Treves, A. (1996). Analytical estimates of limited sampling biases in different information measures. *Network: Computation in Neural Systems*, 7:87–107. doi:10.1088/0954-898X/7/1/006. (Cited on pages 18, 19, 66, and 103.)

Pesaran, B., Pezaris, J. S., Sahani, M., Mitra, P. P., and Andersen, R. A. (2002). Temporal structure in neuronal activity during working memory in macaque parietal cortex. *Nature Neuroscience*, 5(8):805–811. doi:10.1038/nn890. (Cited on page 119.)

Pettersen, K. H., Devor, A., Ulbert, I., Dale, A. M., and Einevoll, G. T. (2006). Current-source density estimation based on inversion of electrostatic forward solution: effects of finite extent of neuronal activity and conductivity discontinuities. *Journal of Neuroscience Methods*, 154(1):116–33. doi:10.1016/j.jneumeth.2005.12.005. (Cited on pages 124 and 178.)

Pleger, B., Dinse, H. R., Ragert, P., Schwenkreis, P., Malin, J. P., and Tegenthoff, M. (2001). Shifts in cortical representations predict human discrimination improvement. *Proceedings of the National Academy of Sciences*, 98(21):12255–12260. doi:10.1073/pnas.191176298. (Cited on page 28.)

Pleger, B., Foerster, A. F., Ragert, P., Dinse, H. R., Schwenkreis, P., Malin, J. P., Nicolas, V., and Tegenthoff, M. (2003). Functional imaging of perceptual learning in human primary and secondary somatosensory cortex. *Neuron*, 40(3):643–53. doi:10.1016/s0896-6273(03)00677-9. (Cited on page 29.)

Poggio, T., Fahle, M., and Edelman, S. (1991). Fast Perceptual Learning in Visual Hyperacuity. Technical report, Massachusetts Institute of Technology Artificial Intelligence Laboratory. (Cited on pages 28 and 32.)

Poggio, T., Fahle, M., and Edelman, S. (1992). Fast Perceptual Learning in Visual Hyperacuity. *Science*, 256(5059):1018–21. doi:10.1126/science.1589770. (Cited on page 28.)

Polley, D. B., Steinberg, E. E., and Merzenich, M. M. (2006). Perceptual learning directs auditory cortical map reorganization through top-down influences. *Journal of Neuroscience*, 26(18):4970–82. doi:10.1523/JNEUROSCI.3771-05.2006. (Cited on page 29.)

Potworowski, J., Jakuczun, W., Łęski, S., and Wójcik, D. (2012). Kernel current source density method. *Neural Computation*, 24(2):541–75. doi:10.1162/NECO_a_00236. (Cited on page 178.)

Purves, D., Augustine, G. J., Fitzpatrick, D., Hall, W. C., LaMantia, A.-S., McNamara, J. O., and White, L. E., editors (2008). *Neuroscience*. Sinauer, 4th edition. ISBN 978-0-87893-697-7. (Cited on pages 1, 2, 3, 5, and 6.)

Quiroga, R. Q. and Panzeri, S. (2009). Extracting information from neuronal populations: information theory and decoding approaches. *Nature Reviews Neuroscience*, 10(3):173–85. doi:10.1038/nrn2578. (Cited on pages 11 and 99.)

Raghavachari, S., Kahana, M. J., Rizzuto, D. S., Caplan, J. B., Kirschen, M. P., Bourgeois, B., Madsen, J. R., and Lisman, J. E. (2001). Gating of Human Theta Oscillations by a Working Memory Task. *Journal of Neuroscience*, 21(9):3175–3183. (Cited on page 119.)

Raiguel, S., Vogels, R., Mysore, S. G., and Orban, G. a. (2006). Learning to see the difference specifically alters the most informative V4 neurons. *Journal of Neuroscience*, 26(24):6589–602. doi:10.1523/JNEUROSCI.0457-06.2006. (Cited on pages 29 and 30.)

Reich, D., Mechler, F., and Victor, J. (2001). Temporal coding of contrast in primary visual cortex: when, what, and why. *Journal of Neurophysiology*, 85:1039–1050. (Cited on page 30.)

Richter, C. G., Babo-Rebelo, M., Schwartz, D., and Tallon-Baudry, C. (2017). Phase-amplitude coupling at the organism level: The amplitude of spontaneous alpha rhythm fluctuations varies with the phase of the infra-slow gastric basal rhythm. *NeuroImage*, 146:951–958. doi:10.1016/j.neuroimage.2016.08.043. (Cited on page 120.)

Rickert, J., Oliveira, S. C. D., Vaadia, E., Aertsen, A., Rotter, S., and Mehring, C. (2005). Encoding of movement direction in different frequency ranges of motor cortical local field potentials. *Journal of Neuroscience*, 25(39):8815–8824. doi:10.1523/JNEUROSCI.0816-05.2005. (Cited on page 119.)

Saleem, A. B., Ayaz, A., Jeffery, K. J., Harris, K. D., and Carandini, M. (2013). Integration of visual motion and locomotion in mouse visual cortex. *Nature Neuroscience*, 16(12):1864–1869. doi:10.1038/nn.3567. (Cited on page 118.)

Scherberger, H., Jarvis, M. R., and Andersen, R. A. (2005). Cortical Local Field Potential Encodes Movement Intentions in the Posterior Parietal Cortex. *Neuron*, 46(2):347–354. doi:10.1016/j.neuron.2005.03.004. (Cited on page 119.)

Schoups, A., Vogels, R., and Qian, N. (2001). Practising orientation identification improves orientation coding in V1 neurons. *Nature*, 412(August):549–553. doi:10.1038/35087601. (Cited on page 29.)

Schroeder, C. E., Tenke, C. E., Givre, S. J., Arezzo, J. C., and Jr, H. G. V. (1991). Striate cortical contribution to the surface-recorded pattern-reversal vep in the alert monkey. *Vision Research*, 31(7-8):1143–1157. doi:10.1016/0042-6989(91)90040-C. (Cited on page 133.)

Sclar, G., Maunsell, J. H. R., and Lennie, P. (1990). Coding of image contrast in central visual pathways of the macaque monkey. *Vision Research*, 30(1):1–10. doi:10.1016/0042-6989(90)90123-3. (Cited on page 116.)

Self, M. W., van Kerkoerle, T., Supèr, H., and Roelfsema, P. R. (2013). Distinct roles of the cortical layers of area V1 in figure-ground segregation. *Current Biology*, 23(21):2121–9. doi:10.1016/j.cub.2013.09.013. (Cited on page 125.)

Shannon, C. E. (1948). A Mathematical Theory of Communication. *Bell System Technical Journal*, 27(3):379–423. doi:10.1002/j.1538-7305.1948.tb01338.x. (Cited on page 14.)

Smith, D. H. (2009). Stretch growth of integrated axon tracts: Extremes and exploitations. *Progress in Neurobiology*. doi:10.1016/j.pneurobio.2009.07.006. (Cited on page 2.)

Smith, M. L., Gosselin, F., and Schyns, P. G. (2006). Perceptual moments of conscious visual experience inferred from oscillatory brain activity. *Proceedings of the National Academy of Sciences*, 103(14):5626–31. doi:10.1073/pnas.0508972103. (Cited on page 152.)

Spaak, E., Bonnefond, M., Maier, A., Leopold, D. A., and Jensen, O. (2012). Layer-Specific Entrainment of Gamma-Band Neural Activity by the Alpha Rhythm in Monkey Visual Cortex. *Current Biology*, 22(24):2313–8. doi:10.1016/j.cub.2012.10.020. (Cited on pages 169 and 170.)

Sterzer, P., Kleinschmidt, A., and Rees, G. (2009). The neural bases of multistable perception. *Trends in Cognitive Sciences*, 13(7):310–318. doi:10.1016/j.tics.2009.04.006. (Cited on page 20.)

Stevens, J.-L. R., Law, J. S., Antolík, J., and Bednar, J. A. (2013). Mechanisms for Stable, Robust, and Adaptive Development of Orientation Maps in the Primary Visual Cortex. *Journal of Neuroscience*, 33(40):15747–15766. doi:10.1523/JNEUROSCI.1037-13.2013. (Cited on page 9.)

Stockman, A., Jägle, H., Pirzer, M., and Sharpe, L. T. (2008). The dependence of luminous efficiency on chromatic adaptation. *Journal of Vision*, 8(2008):1. doi:10.1167/8.16.1.Introduction. (Cited on page 122.)

Stockman, A. and Sharpe, L. T. (2000). The spectral sensitivities of the middle- and long-wavelength-sensitive cones derived from measurements in observers of known genotype. *Vision Research*, 40(13):1711–37. doi:10.1016/S0042-6989(00)00021-3. (Cited on page 122.)

Strasburger, H., Rentschler, I., and Jüttner, M. (2011). Peripheral vision and pattern recognition: A review. *Journal of Vision*, 11(5):13. doi:10.1167/11.5.13. (Cited on page 9.)

Strong, S., Koberle, R., de Ruyter van Steveninck, R., and Bialek, W. (1998). Entropy and Information in Neural Spike Trains. *Physical Review Letters*, 80(1):197–200. doi:10.1103/PhysRevLett.80.197. (Cited on page 19.)

Szymanski, F. D., Rabinowitz, N. C., Magri, C., Panzeri, S., and Schnupp, J. W. H. (2011). The Laminar and Temporal Structure of Stimulus Information in the Phase of Field Potentials of Auditory Cortex. *Journal of Neuroscience*, 31(44):15787–15801. doi:10.1523/JNEUROSCI.1416-11.2011. (Cited on page 119.)

Theunissen, F. E., David, S. V., Singh, N. C., Hsu, A., Vinje, W. E., and Gallant, J. L. (2001). Estimating spatio-temporal receptive fields of auditory and visual neurons from their responses to natural stimuli. *Network: Computation in Neural Systems*, 12(3):289–316. doi:10.1088/0954-898X/12/3/304. (Cited on page 179.)

Thiele, A., Delicato, L. S., Roberts, M. J., and Gieselmann, M. A. (2006). A novel electrode-pipette design for simultaneous recording of extracellular spikes and iontophoretic drug application in awake behaving monkeys. *Journal of Neuroscience Methods*, 158(2):207–11. doi:10.1016/j.jneumeth.2006.05.032. (Cited on page 31.)

Tort, A. B. L., Komorowski, R., Eichenbaum, H., and Kopell, N. (2010). Measuring phase-amplitude coupling between neuronal oscillations of different frequencies. *Journal of Neurophysiology*, 104(2):1195–210. doi:10.1152/jn.00106.2010. (Cited on pages 157 and 158.)

Treves, A. and Panzeri, S. (1995). The Upward Bias in Measures of Information Derived from Limited Data Samples. *Neural Computation*, 7(2):399–407. doi:10.1162/neco.1995.7.2.399. (Cited on pages 18, 19, 62, and 127.)

Tyler, C. J., Dunlop, S. A., Lund, R. D., Harman, A. M., Dann, J. F., Beazley, L. D., and Lund, J. S. (1998). Anatomical comparison of the macaque and marsupial visual cortex: Common features that may reflect retention of essential cortical elements. *The Journal of Comparative Neurology*, 400(4):449–68. doi:10.1002/(SICI)1096-9861(19981102)400:4<449::AID-CNE2>3.0.CO;2-A. (Cited on page 134.)

van Kerkoerle, T., Self, M. W., Dagnino, B., Gariel-Mathis, M.-A., Poort, J., van der Togt, C., and Roelfsema, P. R. (2014). Alpha and gamma oscillations characterize feedback and feedforward processing in monkey visual cortex. *Proceedings of the National Academy of Sciences*, 111(40):14332–14341. doi:10.1073/pnas.1402773111. (Cited on pages 125, 153, 171, and 178.)

Voytek, B. (2012). What is the longest axon in the world? *Quora*. Available from: `https://www.quora.com/What-is-the-longest-axon-in-the-world/answer/Bradley-Voytek`. (Cited on page 2.)

Wässle, H., Grünert, U., Röhrenbeck, J., and Boycott, B. B. (1990). Retinal ganglion cell density and cortical magnification factor in the primate. *Vision Research*, 30(11):1897–1911. doi:10.1016/0042-6989(90)90166-I. (Cited on page 5.)

Watanabe, T., Masuda, N., Megumi, F., Kanai, R., and Rees, G. (2014). Energy landscape and dynamics of brain activity during human bistable perception. *Nature Communications*, 5:4765. arXiv:1011.1669v3. doi:10.1038/ncomms5765. (Cited on page 20.)

Weatherall, D. (2006). The Weatherall report on the use of non-human primates in research. Technical report, The Royal Society, London. (Cited on page 120.)

Westheimer, G. and Truong, T. T. (1988). Target crowding in foveal and peripheral stereoacuity. *American journal of optometry and physiological optics*. doi:10.1097/00006324-198805000-00015. (Cited on page 28.)

Williams, P. L. and Beer, R. D. (2010). Nonnegative Decomposition of Multivariate Information. *CoRR*. arXiv:1004.2515v1. (Cited on page 128.)

Wilson, S. P. and Bednar, J. A. (2015). What, if anything, are topological maps for? *Developmental Neurobiology*, 75(6):667–681. doi:10.1002/dneu.22281. (Cited on page 9.)

Wójcik, D. K. and Łęski, S. (2010). Current source density reconstruction from incomplete data. *Neural Computation*, 22(1):48–60. doi:10.1162/neco.2009.07-08-831. (Cited on page 124.)

Wolpert, D. (2011). The real reason for brains. *TED*. Available from: `https://www.ted.com/talks/daniel_wolpert_the_real_reason_for_brains`. (Cited on page 1.)

Wong, K. Y., Dunn, F. A., and Berson, D. M. (2005). Photoreceptor Adaptation in Intrinsically Photosensitive Retinal Ganglion Cells. *Neuron*, 48(6):1001–1010. doi:10.1016/j.neuron.2005.11.016. (Cited on page 3.)

Yabuta, N. H., Sawatari, A., and Callaway, E. M. (2001). Two Functional Channels from Primary Visual Cortex to Dorsal Visual Cortical Areas. *Science*, 292(5515):297–300. doi:10.1126/science.1057916. (Cited on page 153.)

Yang, T. and Maunsell, J. H. R. (2004). The effect of perceptual learning on neuronal responses in monkey visual area V4. *Journal of Neuroscience*, 24(7):1617–26. doi:10.1523/JNEUROSCI.4442-03.2004. (Cited on page 29.)

Yu, C., Klein, S., and Levi, D. (2004). Perceptual learning in contrast discrimination and the (minimal) role of context. *Journal of Vision*, 4(3):169–182. doi:10.1167/4.3.4. (Cited on page 29.)

Zanos, T. P., Mineault, P. J., and Pack, C. C. (2011). Removal of Spurious Correlations Between Spikes and Local Field Potentials. *Journal of Neurophysiology*, 105(1):474–486. doi:10.1152/jn.00642.2010.Single. (Cited on page 178.)

Zappe, A. C., Pfeuffer, J., Merkle, H., Logothetis, N. K., and Goense, J. B. M. (2008). The Effect of Labeling Parameters on Perfusion-Based fMRI in Nonhuman Primates. *Journal of Cerebral Blood Flow & Metabolism*, 28(3):640–652. doi:10.1038/sj.jcbfm.9600564. (Cited on page 121.)

Zar, J. H. (1999). *Biostatistical Analysis*. Prentice Hall, New Jersey, 4th edition. ISBN 978-0130815422. (Cited on page 156.)

Zhang, Y. and Yang, Y. (2015). Cross-validation for selecting a model selection procedure. *Journal of Econometrics*, 187(1):95–112. doi:10.1016/j.jeconom.2015.02.006. (Cited on page 103.)

Zhu, Y. and Zhu, J. J. (2004). Rapid arrival and integration of ascending sensory information in layer 1 nonpyramidal neurons and tuft dendrites of layer 5 pyramidal neurons of the neocortex. *Journal of Neuroscience*, 24(6):1272–1279. doi:10.1523/JNEUROSCI.4805-03.2004. (Cited on page 170.)

Zohary, E., Shadlen, M. N., and Newsome, W. T. (1994). Correlated neuronal discharge rate and its implications for psychophysical performance. *Nature*,

370(6485):140–143. doi:10.1038/370140a0. (Cited on page 117.)